Titre: Title:	Biofunctionalization of Gold Nanoparticles with Antibodies to Design an Enhanced Immunological Diagnostic Tool for Cancer
Auteur: Author:	Kurt Ebeling
Date:	2020
Type:	Mémoire ou thèse / Dissertation or Thesis
Référence: Citation:	Ebeling, K. (2020). Biofunctionalization of Gold Nanoparticles with Antibodies to Design an Enhanced Immunological Diagnostic Tool for Cancer [Mémoire de maîtrise, Polytechnique Montréal]. PolyPublie. https://publications.polymtl.ca/5496/

URL de PolyPublie: PolyPublie URL:	https://publications.polymtl.ca/5496/
Directeurs de recherche: Advisors:	Gregory De Crescenzo, Michel Meunier, & Dominique Trudel
Programme: Program:	Génie biomédical

POLYTECHNIQUE MONTRÉAL

affiliée à l'Université de Montréal

Biofunctionalization of Gold Nanoparticles with Antibodies to Design an Enhanced Immunological Diagnostic Tool for Cancer

KURT EBELING

Institut de génie biomédical

Mémoire présenté en vue de l'obtention du diplôme de *Maîtrise ès sciences appliquées*

Génie biomédical

Décembre 2020

POLYTECHNIQUE MONTRÉAL

affiliée à l'Université de Montréal

Ce mémoire intitulé :

Biofunctionalization of Gold Nanoparticles with Antibodies to Design an Enhanced Immunological Diagnostic Tool for Cancer

présenté par **Kurt EBELING**

en vue de l'obtention du diplôme de *Maîtrise ès sciences appliquées*

a été dûment accepté par le jury d'examen constitué de :

Olivier HENRY, président
Gregory DE CRESCENZO, membre et directeur de recherche
Michel MEUNIER, membre et codirecteur de recherche
Dominique TRUDEL, membre et codirectrice de recherche
Xavier BANQUY, membre externe

DEDICATION

This thesis is dedicated to my dad, who suffers from a rare sporadic genetic disorder called multiple system atrophy affecting 1 in 100 000 people worldwide. I know you always told me that when the going gets tough, the tough get going and this Master's has taught me that, having to deal with the biggest highs and lows of my life. I know you always wanted me to pursue my dreams in science and medicine, and this Master's helped me get one step closer to that. I hope someday someone will find a cure to this horrible disease thanks to a scientific breakthrough. While I cannot guarantee that it will be me who finds the cure, I know a future connected to science is still my calling, and that you helped foster that passion.

ACKNOWLEDGEMENTS

First of all, I would like to extend my gratitude to my PI Greg De Crescenzo for taking me under his wing as his new “guinea pig” being an Anglophone from Western Canada (something I know he has been excited to brag about to his colleagues). Without his steady guidance and pragmatic advice on research and life, I do not think that my grad school experience would have been the same. I would also like to thank my co-supervisor Michel Meunier for treating me like a part of his family, inviting me out to various social events with his research group that made me feel part of a greater community while at Polytechnique. Despite being far away from home, I felt less isolated. Thank you, Greg and Michel, for welcoming me into your groups. I would also like to thank my other co-supervisor Dominique Trudel, despite having little chance to work with you. I found your perspective in meetings very insightful and it reaffirmed my career aspirations after grad school.

Next, I would like to thank my colleagues for whom I am eternally grateful for their help and patience. Thank you Benoît Liberelle for being my mentor for my research project, providing me with sound advice that I know I will apply to my future career (even if at times it felt like you were probably pulling your hair out trying to understand my perspective). Your patience was greatly appreciated as I slowly got into the hang of things. Thank you Romane Oliveiro for being not only a great colleague providing me with useful tips for research and courses, but a great friend willing to help out even when I felt like my head was going to explode from stress, being so open to talking about anything besides research when I felt like I needed a break from it. Thank you Morteza Kafshgari for lending a helping hand with my research project especially with getting me cells. Thank you Cécile Darviot, Leonidas Agiotis, Isabelle Largillière, Jennyfer Zapata, Paule Marcoux-Valiquette, Lu Wang and Audrey Nsamela for being great resources for research and courses, especially to Cécile and Isabelle for giving me tutorials on those infamous engineering physics courses that I loved to hate, and would not have gotten through without your help and patience. Thank you, Jimmy Gaudreault and Catherine Forest-Nault, for being great colleagues and so willing to help out when I needed it (especially you Jimmy with your uncanny sense of humour).

Lastly, I would like to thank my family (especially my mom). Even though they lived far away from me during this time, whenever I felt like I needed to take my mind off of things, or when real life problems came up, I knew they were always open to a chat.

RÉSUMÉ

Le cancer du sein est à la fois la forme de cancer la plus diagnostiquée et la deuxième cause de mortalité chez les femmes canadiennes. L'immunohistochimie (IHC) est une technique étalon pour la caractérisation en profondeur des tissus et le diagnostic précis de la tumeur du cancer du sein. Cette technique repose sur l'étude immunologique des tissus, par le biais d'anticorps chromogènes générant un signal colorimétrique. Toutefois, cette technique a plusieurs inconvénients, notamment la perte ou la modification d'antigènes ciblés pendant la préparation du tissu ou encore le risque de photoblanchiment. De plus, l'analyse des résultats peut varier grandement selon le pathologiste responsable de l'examen du tissu. Ces éléments peuvent avoir un impact négatif sur la sensibilité et la spécificité du diagnostic, et ainsi augmenter la probabilité de faux positifs et faux négatifs. Ainsi, augmenter la précision des tests de diagnostic du cancer du sein demeure un enjeu important pour une meilleure prise en charge des patients diagnostiqués.

Ce mémoire présente l'utilisation de nanoparticules d'or (AuNPs) immunoplasmoniques comme une alternative à l'IHC pour le diagnostic du cancer du sein. Des anticorps ciblant des biomarqueurs du cancer du sein sont chimiquement conjugués aux AuNPs par l'intermédiaire de polyéthylène glycol (PEG) portant en bout de chaîne des groupes fonctionnels réactifs.

Dans ce mémoire, d'importantes contributions portant sur le développement d'AuNPs fonctionnalisées sont, dans un premier temps, passées en revue, afin de mettre en lumière les enjeux chimiques et physiques qui entourent la conception de formulations stables, robustes, fiables, reproductibles et sensibles capables de cibler et de se lier à des cellules cancéreuses de façon spécifique. Les travaux expérimentaux présentés dans la suite du mémoire ont pour objectif principal la comparaison de trois différentes stratégies de fonctionnalisation covalente des AuNPs avec des anticorps. Ces stratégies portent sur l'orientation des anticorps greffés par rapport à la surface des AuNPs. Pour chacune, les avantages et inconvénients relatifs à la préparation, l'optimisation, et le comportement des AuNPs lorsque mises en présence de cellules cancéreuses sont évalués. Les propriétés chimiques et physiques, ainsi que les rendements et l'activité biologique sont caractérisés. Enfin, sur la base des résultats expérimentaux rapportés, une comparaison critique des trois stratégies de fonctionnalisation est proposée. Les bénéfices de la

conjugaison covalente des anticorps sur les AuNPs, par rapport à leur simple adsorption physique, sont également discutés.

Les travaux présentés dans ce mémoire permettent de mettre en évidence des différences à la fois au niveau des propriétés chimiques, optiques, des rendements et de l'activité lors de la comparaison de deux stratégies de conjugaison covalentes. Des conditions pour un meilleur contrôle de la stabilité, fiabilité et reproductibilité des formulations ont été identifiées. De plus, des différences sont observées dans la capacité des AuNPs à se lier à deux lignées cellulaires cancéreuses, MDA-MB-231 et MDA-MB-453.

Ce mémoire constitue une contribution importante pour le domaine de recherche portant sur la biofonctionnalisation d'AuNPs à des fins diagnostiques, en apportant une caractérisation approfondie de chaque étape de différents protocoles de fonctionnalisation. Des travaux futurs, portant notamment sur la caractérisation de l'activité biologique des anticorps greffés aux AuNPs ainsi que sur l'applications des AuNPs immunoplasmoniques à des systèmes biologiques plus complexes, restent nécessaires. Néanmoins, les travaux présentés dans ce mémoire ont produit des résultats prometteurs permettant d'ouvrir la voie vers la conception d'AuNPs immunoplasmoniques à des fins diagnostiques, avec pour objectif à long terme le développement de techniques diagnostiques alternatives à l'IHC pour le diagnostic du cancer du sein.

ABSTRACT

Breast cancer is the most diagnosed form of cancer in Canadian women, and is the second leading cause of death for them. In a histological setting where breast cancer tissue is examined, immunohistochemistry (IHC) is the go-to technique for providing a more in-depth diagnosis of the breast cancer tumour. The technique relies upon immunological-based staining of the tissue and generation of a colorimetric signal from chromogenic antibodies. However, this technique suffers from several drawbacks, namely loss or modifications of targeted antigens during preparation of the tissue, variations in skill of the examining pathologist, and photobleaching. These can all reduce both the sensitivity and specificity of the diagnosis and increase the likelihood of a misdiagnosis or a failure to detect it. Improving the accuracy of cancer diagnostics is thus an important issue to address, so as to more appropriately proceed to care management of the diagnosed patient.

In this thesis work, functionalized immunoplasmonic gold nanoparticles (AuNPs) are a proposed alternative to IHC for breast cancer diagnosis. Herein, breast cancer-detecting antibodies are chemically conjugated to AuNPs via polyethylene glycol (PEG) linkers containing reactive functional groups located at the ends of their chains. This thesis work will review important contributions discovered in developing these functionalized AuNPs, by elucidating the chemical and physical challenges related to designing stable, robust, reliable, reproducible, and sensitive formulations that can specifically target and bind to cancer cells. The main goals of this thesis work were to compare and contrast different strategies for functionalizing AuNPs with antibodies on the basis of their advantages and disadvantages in preparation, optimization and their ultimate application to cancer cells. Each part of this thesis will review in turn three different strategies that would orient antibodies with respect to AuNPs in different ways, such that both the chemical and physical properties, yield and biological activity could all be characterized. This allowed for a final head-to-head comparison between all three chemical conjugation strategies, alongside a comparison to antibodies physically adsorbed to AuNPs in a non-specific manner.

Overall, differences in chemical and physical properties, yield and activity were all observed for two different chemical conjugation strategies, and various parameters influencing their stability, reliability and reproducibility were optimized. In addition, differences were seen regarding their abilities to bind to two different cancer cell lines, MDA-MB-231 and MDA-MB-

453. This thesis work thus constitutes an important contribution to the research field of AuNP functionalization for diagnostic purposes, by providing a more in-depth characterization of each step of the process of functionalization. It also provides insight on how various parameters could be controlled and ultimately influence the ability of each strategy to produce functionalized AuNPs capable of recognizing and binding to cancer cells. Although further work still needs to be pursued in order to better characterize the biological activity of the antibodies bound to these functionalized AuNPs, as well as applying these formulations to more complex biological systems, this work has produced promising results that should hopefully shed light on designing improved immunoplasmonic AuNPs for diagnostic purposes. This could lead to breakthroughs in the field that would ultimately produce an alternative technique to rival IHC in cancer diagnostics.

TABLE OF CONTENTS

DEDICATION III

ACKNOWLEDGEMENTS IV

RÉSUMÉ V

ABSTRACT VII

TABLE OF CONTENTS IX

LIST OF TABLES XIII

LIST OF FIGURES XVI

LIST OF SYMBOLS AND ABBREVIATIONS XXVI

LIST OF APPENDICES XXX

CHAPTER 1 INTRODUCTION 1

1.1 Background on Cancer Diagnosis 1

1.2 Limitations of Immunohistochemistry as a Cancer Diagnostic Technique 2

1.3 Objectives for Designing an Immunological Diagnostic Tool Able to Address Voids from Immunohistochemistry 3

CHAPTER 2 LITERATURE REVIEW 6

2.1 Immunohistochemistry (IHC) 6

2.2 Gold Nanoparticle Visualization of Cancer Cells 7

2.2.1. Optical Properties of Gold Nanoparticles 7

2.2.2. Physical Properties of Gold Nanoparticles 11

2.3 Functionalization of Gold Nanoparticles with Biological Molecules 14

2.3.1. Decoration of Gold Nanoparticles with Polyethylene Glycol (PEGylation) 15

2.3.2. Characterization of PEGylation 18

2.3.3. Conjugation of PEGylated Gold Nanoparticles to Antibodies 21

a) Randomly Oriented Approach 23
b) Semi-Oriented Aproach 25
c) Oriented Aproach 27
2.3.4. Characterization of Antibodies Conjugated to PEGylated AuNPs 29
a) Quantitative Assays for Characterizing Antibody-Functionalized AuNPs 29
b) Characterization of the Bioactivity of Antibody-Functionalized AuNPs 30
c) Application of Antibody-Functionalized AuNPs to Cells for their Characterization 31
CHAPTER 3 CHEMICAL CONJUGATION OF POLYETHYLENE GLYCOL AND ANTIBODIES TO GOLD NANOPARTICLES 32
3.1 Materials and Methods for Characterization of Biofunctionalized Gold Nanoparticles 33
3.1.1. Materials for Biofunctionalization 33
a) Source of AuNPs 33
b) Sources of PEG 34
c) Source of Antibodies 34
3.1.2. Characterization Methods for Biofunctionalization 34
3.2 PEGylation of Gold Nanoparticles 35
3.2.1. Characterization of the Decoration of Gold Nanoparticles with PEG 36
a) DLS Measurements 36
b) ZP Measurements 38
3.2.2. Stability of PEGylated Gold Nanoparticles 40
3.3 Randomly Oriented Strategy for Antibody Conjugation 46
3.3.1. Characterization of Antibody Conjugation 47
a) DLS Measurements 47
b) ZP Measurements 53

3.3.2. Stability of Antibody-Conjugated, PEGylated Gold Nanoparticles....56
3.4 Semi-Oriented Strategy for Antibody Conjugation....60
3.4.1 Characterization of Antibody Conjugation....61
a) DLS Measurements....61
b) ZP Measurements....65
3.4.2 Stability of Antibody-Conjugated, PEGylated Gold Nanoparticles....67
3.5 Oriented Strategy for Antibody Conjugation....69
3.5.1. Oxidation of Antibodies....70
3.5.2. Characterization of Oxidized Antibodies....70
a) Chromatograms of Oxidized Antibodies Compared to Standards....71
b) UV-VIS Absorbance Measurement of Re-Concentrated Oxidized Antibodies....71
c) Purpald Assay to Quantify Oxidized Antibodies....73
d) SPR Sensorgrams to Evaluate Activity of Oxidized Antibodies....74
3.6 Comparison Between Antibody Conjugation Strategies....75
3.6.1. Functionalized AuNP Concentrations Measured via UV-VIS Absorbance....75
3.6.2. Indirect Quantification of Functionalized NPs via ELISA....77
3.6.3. Direct Quantification of Functionalized NPs via NanoOrange Assay....80
3.6.4. Quantification of Number of Functionalized NPs Bound to Cancer Cells....82
CHAPTER 4 GENERAL DISCUSSION....85
4.1. Summary of Important Results....85
4.2. Comparison to Literature....87
4.3. Evaluation of Thesis Objectives....89
CHAPTER 5 CONCLUSIONS AND RECOMMENDATIONS....90
5.1. Recommendations....90

5.2. Concluding Remarks 92

REFERENCES 93

APPENDICES 110

LIST OF TABLES

Table 2-1 Overview of challenges of IHC as a diagnostic technique for breast cancer 6

Table 2-2 Example of commercially available, heterobifunctional PEG containing a SH group at one end. List of PEG drawn from several vendors labelled as: 1 – Nanocs, 2 – Sigma-Aldrich, 3 – JenKem, 4 – Creative PEGWorks, 5 – Polyscience, 6 – Pure PEG, 7 – Boc Sciences [99]. 17

Table 3-1 Overview of different PEG molecules used during this Master's thesis project. Biofunctionalization strategies are labelled as follows: (1) random, (2) semi-oriented, (3) oriented.....34

Table 3-2 Overview of the techniques used to characterize the biofunctionalization of AuNPs...34

Table 3-3 Overview of different samples tested for DLS characterization of PEGylated AuNPs.36

Table 3-4 List of monofunctional methoxy- and bifunctional NHS-PEGylated AuNP samples and their respective conditions tested during the stability assay. 42

Table 3-5 Overview of different samples tested for DLS characterization of m-PEGylated AuNPs put into contact with antibodies. 47

Table 3-6 Overview of different samples tested for DLS characterization of antibody-conjugated, NHS-PEGylated AuNPs.....50

Table 3-7 List of monofunctional m- and bifunctional NHS-PEGylated AuNP samples incubated with antibodies, with their respective conditions tested during the stability assay.....56

Table 3-8 Overview of different samples tested for DLS characterization of antibody-conjugated, Mal-PEGylated AuNPs. 61

Table 3-9 List of monofunctional methoxy- and bifunctional Mal-PEGylated AuNP samples incubated with their respective antibodies, alongside controls and incubation conditions tested during the stability assay. Please note that all samples were washed with citrate prior to PEGylation. 68

Table 3-10 Concentrations of oxidized TZM recovered calculated either by: (A) linear regression analysis of integrated chromatograms from TZM standard curves in Appendix I (Figure 5-6),

following injection and elution from SEC column, and (B) UV-VIS A280 measurement following re-concentration of the SEC fraction collected. 72

Table 4-1 Overview of the two biofunctionalization strategies explored with a relative comparison of different parameters. 85

Table 5-1 Overview of different PEG molecules (heteromono- and bifunctional) used during this Master's thesis project. 110

Table 5-2 Summary of concentrations of free thiols determined from an Ellman's test performed on each PEG stock. 111

Table 5-3 Overview of 2 mM thiolated PEG freezer stock aliquot volumes required per 600 µL of AuNPs, for PEGylating at different percentages of either NHS-PEG-SH or Hyd-PEG-SH (NHS and Hyd for short, respectively) relative to mPEG-SH, in order to achieve a final total thiolated PEG concentration of 10 µM. 117

Table 5-4 List of heteromonofunctional mPEG-SH and heterobifunctional NHS-PEG-SH or Hyd-PEG-SH AuNP samples and their respective conditions tested during the stability assay. In the interest of simplicity, only mixed PEGylated AuNP samples with a 10% composition are included. 120

Table 5-5 List of heteromonofunctional mPEG-SH and heterobifunctional NHS-PEG-SH, Mal-PEG-SH or Hyd-PEG-SH AuNP samples adsorbed or conjugated to antibodies, and their respective conditions tested during the stability assay. In the interest of simplicity, mixed PEGylated AuNP samples of different percent compositions of each form of PEG are not included. Antibody conjugation approaches are numbered as follows: (1) randomly oriented, (2) semi-oriented, (3) oriented. Controls for all strategies are labelled as such. 121

Table 5-6 Volumes of -80°C freezer stock aliquots of TZM antibodies added to each re-activated NHS-PEGylated AuNP sample for the sake of the antibody-conjugation reaction. 126

Table 5-7 Overview of starting concentrations of antibodies (unmodified and reduced) used during incubation with PEGylated-AuNP samples. 142

Table 5-8 Overview of latest AuNP:cell incubation experiment conducted between antibody-conjugated, PEGylated-AuNP samples and cancer cell lines MDA-MB-231 and MDA-MB-

453 (abbreviated as 231 and 453), with the calculated volumes required to achieve 500 NPs:cell and 150 000 cells, respectively. 150

LIST OF FIGURES

Figure 1-1 Schematic of IHC applied to cancer tissue, with relevant components labelled. In the interest of simplicity, only the blocking (4), staining (5) and visualization (6) steps explained in the above paragraph are shown. Breast cancer stained tissue taken from Novusbio [8]. 2

Figure 1-2 Schematic comparing IHC (*left*) with biofunctionalized IP-AuNPs (*right*) for detecting breast cancer tissue. Image inspired by work of Ciaurriz et. al, 2017 [16] 4

Figure 2-1 Schematic representation of the interactions between incident light (λ) and a spherical NP whose size (d) is small enough to generate LSPs. Image reproduced from Amendola et. al [37]. 8

Figure 2-2 Spectra of different types of AuNPs: a) 15 nm nanospheres, b) 40 nm nanocubes, c-e) nanorods with aspect ratios of 2.4, 3.4 and 4.6, respectively. Image taken from Chen et. al [39]. 9

Figure 2-3 Effects of AuNP Size on A) shape of SPR peak and B) weight contribution of scattering to peak. Images reproduced from nanoComposix [55]. 10

Figure 2-4 Comparison between the UV-VIS spectra of dispersed and aggregated AuNPs. Image reproduced from nanoComposix [55]. 12

Figure 2-5 Difference in TZM avidity for Her2 receptors between IHC (*left*) and functionalized AuNPs (*right*), highlighting the potential increase in avidity resulting from functionalization. Concept of increased avidity of functionalized AuNP conjugates has been demonstrated in past literature [70, 71]. 13

Figure 2-6 Diversity of AuNP shapes and sizes: a) nanospheres, b) nanorods, c) nanodumbbells, d) triangular nanoprisms, e) nanowires, f) nanostars, g) nanodendrites, h) nanocubes. Image reproduced from Elahi et. al [33]. 13

Figure 2-7 Overview of the vocabulary employed to introduce the biofunctionalization of AuNPs with PEG and cancer-targeting antibodies. 15

Figure 2-8 Structure of PEG. Image reproduced from Sigma Aldrich [88].....16

Figure 2-9 Schematic showing how surface defects hamper the PEGylation efficiency of AuNPs by varying the densities of PEG able to pack along irregular surfaces, such as hills and valleys. 17

Figure 2-10 Antibody conjugation strategies: (1) natural amino acids, (2) disulfide bridges, (3) engineered cysteines, (4) non-natural amino acids, (5) glycosylated region, (6) N-termini of heavy and light chains, (7) engineered tags, (8) strong non-covalent interactions via Fc binding domains, (9) nucleotide binding site, (10) receptor-binding region. Image taken from Dennler et. al [125]. 22

Figure 2-11 Schematic of the three main approaches explored in this Master's thesis for covalent conjugation of antibodies: (1) randomly oriented, (2) semi-oriented, (3) oriented.....23

Figure 2-12 Schematic of the randomly oriented approach, whereby NHS/EDC chemistry is employed to conjugate PEGylated AuNPs to antibodies via their amine groups. 24

Figure 2-13 Schematic of the semi-oriented approach, assuming covalent conjugation to maleimide-exposed, PEGylated AuNPs that can react with exposed free thiols. 26

Figure 2-14 Schematic of periodate oxidation of glycosylated antibodies and their ensuing conjugation to hydrazide-exposed, PEGylated AuNPs. Image adapted from Hermanson et. al [97]. 28

Figure 3-1 Effect of NHS- and methoxy-PEGylation (m-PEGylation) on (A) hydrodynamic diameter, (B) dispersion of AuNPs compared to bare AuNPs, and (C) size increase relative to bare AuNPs. Values represent averages of three replicates and error bars show their standard deviation. Asterisks * and ** indicate statistically significant differences of $p<0.05$ and 0.01, respectively, and brackets compare the two samples for which this difference is significant. 37

Figure 3-2 Effect of NHS- and m-PEGylation on ZP (surface charge) of AuNPs, compared to control of bare AuNPs. Abbreviations of samples are the same as those measured for DLS. Values represent averages of three replicates and error bars show standard deviation. Asterisks * and ** indicate statistically significant difference at $p<0.05$ and 0.05, respectively, and brackets compare the two samples for which this difference is significant. 39

Figure 3-3 Illustration of a typical 100 nm AuNP UV-VIS absorbance spectra and its various elements extracted and analyzed from the stability assays. 40

Figure 3-4 Stability curves for controls: (A) normalized percentage of AuNPs remaining, calculated from relative amplitudes of their SPR peaks, and (B) normalized percent change in FWHM of AuNP SPR peaks. Values represent averages of six replicates from two repeats of this experiment (2x3 data points), and error bars show standard deviation. Symbols in legend are depicted as: (+) – positive control, (-) – negative control, N – unwashed, W – washed. 42

Figure 3-5 Stability curves extracted from the relative amplitudes and percent-normalized to the positive control of unwashed, bare AuNPs, for either: (A) 100% mPEG-SH and (B) 10% NHS-PEG-SH and 90% mPEG-SH. Values represent averages of six replicates from two repeats of this experiment (2x3 data points), and error bars represent standard deviation. Symbols in legend are depicted as: (+) – positive control, (-) – negative control, N – unwashed, W – washed, PEG – mPEG-AuNPs, NHS – NHS-PEG-AuNPs, MQ – Milli-Q incubation, PBS – PBS incubation.....44

Figure 3-6 Stability curves extracted from the FWHM and percent-normalized to the positive control of unwashed, bare AuNPs, for either: (A) 100% mPEG-SH and (B) 10% NHS-PEG-SH and 90% mPEG-SH. Values represent averages of six replicates from two repeats of this experiment (2x3 data points), and error bars represent standard deviation. Symbols in legend are depicted as: (+) – positive control, (-) – negative control, N – unwashed, W – washed, PEG – mPEG-AuNPs, NHS – NHS-PEG-AuNPs, MQ – Milli-Q incubation, PBS – PBS incubation. 44

Figure 3-7 Schematic showing a stepwise overview of the chemistry employed to biofunctionalize AuNPs via a randomly oriented strategy.....46

Figure 3-8 DLS results for m-PEGylated AuNP controls: (A) change in size pre- and post-addition of antibodies, (B) change in dispersion pre- and post-addition of antibodies. Values represent averages of three replicates and error bars show standard deviation. Asterisks * and ** indicate statistically significant differences at $p<0.05$ and 0.01, respectively, and brackets compare the two samples for which there is a statistically significant difference. 48

Figure 3-9 Randomly oriented strategy DLS results for: (A) change in size pre- and post-addition of antibodies and re-suspension in PBS+Tween-20, (B) change in dispersion pre- and post-addition of antibodies and re-suspension in PBS+Tween-20, and (C) overall change in size for functionalized AuNPs subtracting post-PEGylation size (pre-block for controls) from post-antibody addition size. Values represent averages of three replicates, and error bars show standard deviation. Asterisks * and ** in (A) and (B) indicate statistically significant differences at $p<0.05$ and 0.01, respectively, and brackets compare the two samples for which there is a statistically significant difference. For (C), # and ^ depict statistically significant differences at $p<0.05$ and 0.01, respectively comparing subtracted size post-PEGylation to final size post-antibody addition. 51

Figure 3-10 ZP results pre- and post-addition of antibodies to m-PEGylated controls in PBS or PBS+Tween-20. Samples are abbreviated as previously during DLS characterization. Values represent averages of three replicates and error bars show standard deviation. Asterisks * and ** indicate statistically significant differences at $p<0.05$ and 0.01, respectively, and brackets compare the two samples for which there is a statistically significant difference. 53

Figure 3-11 Randomly oriented strategy ZP results for: (A) change in surface charge pre- and post-addition of antibodies, and (B) overall change in surface charge for functionalized AuNPs subtracting post-PEGylation size (pre-block for controls) from post-antibody addition size. Samples are abbreviated as previously during DLS characterization. Values represent averages of three replicates and error bars represent show standard deviation. Asterisks * and ** in (A) indicate statistically significant differences at $p<0.05$ and 0.01, respectively, and brackets compare the two samples for which there is a statistically significant difference. For (B), # and ^ depict statistically significant differences at $p<0.05$ and 0.01, respectively comparing subtracted surface charge post-PEGylation to final surface charge post-antibody addition.....55

Figure 3-12 Stability curves of NHS- and m-PEGylated AuNPs bound (conjugated or adsorbed) to antibodies for: (A) normalized percentages of TZM-mPEG-AuNPs remaining relative to positive control, as calculated from the relative amplitudes of SPR peaks, (B) normalized percent changes in FWHM of TZM-mPEG-AuNP SPR peaks relative to positive control, (C)

normalized percentages of TZM-NHS-PEG-AuNPs remaining relative to positive control, as calculated from the relative amplitudes of SPR peaks, and (D) normalized percent changes in FWHM of TZM-NHS-PEG-AuNP SPR peaks relative to positive control. Values represent averages of six replicates from two repeats of this experiment (2x3 replicates each), and error bars show standard deviation. Symbols in legend are depicted as: (+) – positive control, (-) – negative control, N – unwashed, W – washed, PEG – mPEG-AuNPs, NHS – NHS-PEG-AuNPs, MQ – Milli-Q incubation, PBS – PBS incubation, Tween-20 – PBS+Tween-20 incubation. 57

Figure 3-13 Schematic showing a stepwise overview of the chemistry employed to biofunctionalize AuNPs via a semi-oriented strategy. 60

Figure 3-14 Semi-oriented strategy DLS results for: (A) change in size pre- and post-EMCH reaction, (B) change in dispersion pre- and post-EMCH reaction, (C) change in size of EMCH-transformed AuNPs pre- and post-addition of antibodies, (D) change in dispersion of EMCH-transformed AuNPs pre- and post-addition of antibodies, and (E) overall change in size for functionalized AuNPs subtracting post-PEGylation size (pre-EMCH reaction) from post-antibody addition size. All sub-figures have controls of methoxy- and/or Mal-PEGylated AuNPs. Values represent averages of three replicates and error bars show standard deviation. Asterisks * and ** in (A–E) indicate statistically significant differences at $p<0.05$ and 0.01, respectively, and brackets compare the two samples for which there is a statistically significant difference. For (E), ^ depicts statistically significant increases ($p<0.01$) comparing subtracted size post-PEGylation (pre-EMCH reaction) to final size post-antibody addition, and brackets compare final sizes (in C), rather than increases. 62

Figure 3-15 Semi-oriented strategy ZP results for: (A) change in surface charge pre- and post-EMCH reaction, (B) change in surface charge of EMCH-transformed AuNPs pre- and post-addition of antibodies, (C) overall change in surface charge for functionalized AuNPs between post-PEGylation (pre-EMCH) and post-addition of antibodies. Controls of methoxy- and/or Mal-PEGylated AuNPs are included. Samples are labelled as previously. Values represent averages of three replicates and error bars show deviation. Asterisks * and ** in (A–C) indicate statistically significant differences at $p<0.05$ and 0.01, respectively, and brackets

compare the two samples for which the difference is significant. For (C), # and ^ depict statistically significant increases (p<0.05 and 0.01, respectively) comparing subtracted surface charge post-PEGylation (pre-EMCH reaction) to final surface charge post-antibody addition. 66

Figure 3-16 Stability curves of Mal- and m-PEGylated AuNPs conjugated to antibodies for: (A) normalized percentage of AuNPs remaining calculated from the relative amplitudes of their SPR peaks, and (B) normalized percent change in FWHM of AuNP SPR peaks. Values represent averages of six replicates from two repeats (2x3 replicates), and error bars show standard deviation. 68

Figure 3-17 Schematic showing a stepwise overview of the chemistry employed to biofunctionalize AuNPs via an oriented strategy. 70

Figure 3-18 Chromatograms (A280 curves) of collected fractions for TZM standards and oxidized TZM (prepared at 27 μM) that eluted from the SEC column. 71

Figure 3-19 UV-VIS absorbance curves of oxidized TZM SEC fraction re-concentrated with an Amicon™ centrifuge filter (30 kDa MWCO), and compared to stock TZM (27 μM). 72

Figure 3-20 (A) Sensorgrams of antibody standards vs. oxidized antibodies and (B) percent response of oxidized antibodies retained relative to equivalent antibody standard, based on the first 240 s of injection, for SPR experiment injecting antibodies onto Her2 receptors immobilized on a dextran-covered gold surface. Curves in (A) represent average of three separate measurements, with error bars omitted for clarity. Bars in (B) represent average of 2400 data points in 240 s interval, and error bars represent standard deviation of these data points. 74

Figure 3-21 Characterization of the number of antibody-functionalized AuNPs recovered following incubation with antibodies based on their: (A) UV-VIS absorbance spectra and (B) calculated concentrations extracted from their SPR peak maxima and divided relative to a reference standard of bare AuNPs. Abbreviations mean the following: PEG – 100% mPEG-SH, NHS – 30% NHS-PEG-SH and 70% mPEG-SH, Mal – 30% Mal-PEG-SH and 70% mPEG-SH, TZM – incubation with 800 nM TZM antibodies (non-reduced or reduced). Concentration and curve

values represent average of three replicates, and error bars represent standard deviation. Standard deviations for UV-VIS absorbance curves are omitted for clarity.....76

Figure 3-22 Indirectly calculated number of antibodies conjugated and/or adsorbed to various functionalized and PEGylated AuNPs, as obtained through ELISA assays performed on the supernatants collected from functionalized samples incubated overnight. Averages represent triplicates, and error bars represent standard deviation. Asterisks * and ** indicate statistically significant differences at $p<0.05$ and 0.01, respectively, and brackets compare the two samples for which there is a statistically significant difference.....78

Figure 3-23 Estimated ratio of non-specifically adsorbed antibodies to conjugated antibodies based on ELISA-mediated indirect quantification of total number of immobilized antibodies on antibody-functionalized, PEGylated AuNPs. Averages represent triplicates, and error bars represent standard deviation. Asterisk * indicates a statistically significant difference at $p<0.05$ and brackets compare the two samples for which there is a statistically significant difference.....78

Figure 3-24 NanoOrange™ results quantifying the number of antibodies bound to AuNPs via: (1) adsorption onto m-PEGylated AuNPs, (2) conjugation to 30% NHS-PEGylated AuNPs, and (3) conjugation to 30% maleimide-PEGylated AuNPs Values represent averages of three samples each measured in triplicate on a 96-well plate (3x3 data points), and error bars show standard deviation. Asterisk * indicates a statistically significant difference at $p<0.05$ and brackets compare the two samples for which there is a statistically significant difference...81

Figure 3-25 Average number of AuNPs bound per cancer cell for: (A) Her2 (-) (MDA-MB-231), and (B) Her2 (-) vs. Her2 (+) (MDA-MB-453). Averages represent two repeats of same experiment, each with a sample size of 30 imaged cells, and error bars indicate standard deviation. Asterisks * and ** indicate statistically significant differences at $p<0.05$ and 0.01, respectively, and square brackets compare the two samples for which there is a statistically significant difference.....83

Figure 5-1 Schematic illustration depicting the instrumental set-up required for acquiring DLS measurements. Image reproduced from Bhattacharjee et. al, 2016 [173].....113

Figure 5-2 Schematic illustration depicting how the ZP surface charge is acquired. Image reproduced from Bhattacharjee et. al, 2016 [173]. 114

Figure 5-3 Example of AuNPs sedimented in the wells of a 96-well plate, in order to illustrate the importance of re-suspension of AuNPs between absorbance measurements over the course of the stability assays. 122

Figure 5-4 Number of free thiols per TZM over time, as measured from an Ellman's test of the supernatants collected from a TCEP-gel slurry at discrete time intervals. Values represent averages of three 96-well plate measurements per sample, and error bars represent standard deviation. 129

Figure 5-5 Performance of TCEP gel to reduced TZM antibodies over time, as determined by the number of free thiols per TZM detected based on an Ellman's test. Values represent averages of three 96-well plates measurements per sample, and error bars represent standard deviation. 130

Figure 5-6 Standard curves of integrated chromatograms for: (A) area under the curve and (B) peak height for TZM standards injected onto SEC column and recovered at the same elution volume. Values represent average of two replicates, and error bars represent standard deviation. 134

Figure 5-7 Stability curves of Boc-hydrazine- and methoxy-PEGylated AuNPs conjugated to antibodies for: (A) normalized percentage of AuNPs remaining, as calculated from the relative amplitudes of their SPR peaks, and (B) normalized percent change in FWHM of AuNP SPR peaks. Sample abbreviations are labelled as follows: (+) – positive control, (-) – negative control, PEG – mPEG-SH AuNPs, Boc-Hydrazine – 10:1 mPEG-SH:Hyd-PEG-SH AuNPs, MQ – re-suspended in MQ, PBS – re-suspended in PBS. 138

Figure 5-8 ELISA standard curves of: (A) unmodified TZM and (B) TCEP-reduced TZM used to perform linear regression analysis on supernatants of antibody-functionalized AuNP samples. Values represent average of three replicates, and error bars represent standard deviation. . 141

Figure 5-9 Concentrations of antibodies immobilized onto functionalized AuNPs, as obtained indirectly from the ELISA assays performed on the supernatants collected from functionalized

AuNP samples incubated overnight. Concentrations determined via linear regression analysis of either unmodified or reduced TZM standard curves. Values represent averages of three samples acquired in triplicate, with each respective sample measured at two different dilution factors (3x2 data points), and error bars represent standard deviation.....143

Figure 5-10 Antibody:AuNP standard curves for NanoOrange assay for: (A) untransformed data and (B) reciprocal transformation of data (the latter was used to calculate the concentrations of antibodies immobilized on functionalized AuNP samples). Values represent average of three replicates, and error bars represent standard deviation. 145

Figure 5-11 Determination of concentration of antibodies immobilized onto functionalized AuNP samples via the NanoOrange assay from: first (A) reciprocal transformation of reference absorbance data then (B) calculation of antibody concentrations via regression analysis of reciprocally-transformed standard curve (Figure 5-10 B). For the sake of simplicity, the antibody-lacking PEGylated AuNP sample values are omitted and have already been subtracted from each antibody-containing sample. Values represent averages of three samples each measured on 96-well plate in triplicate (3x3 data points), and error bars represent standard deviation. 146

Figure 5-12 Schematic showing a similar optical set-up to the one used to image cells incubated with AuNPs via back scattering under a dark-field microscope. Note that the helium-neon lamp source is not the same as the halogen one used for this experiment, but the same principle for the rest of the set-up still applies. Elements of this optical set-up are abbreviated as follows: HWP – halfway plate to divide path into two, PBS1 and PBS2 – beam splitters 1 and 2, L1, L2 and L3 – focal lengths 1, 2 and 3 to collimate the beam, QWP – quarter-wave plate for circular polarization modulation, RM – small rod mirror used to focus light onto back focal plane of sample, CCD – camera used to take images and record videos, CMOS – sensor of high-speed camera (not used), QPD – quartz polarization device (not used). Image reproduced from Sowa et. al, 2010 [218].....152

Figure 5-13 Example of image captured with optical camera while proceeding via Z-scan of one field of view containing AuNPs attached to cells. AuNPs are circled in white and highlighted

as white dots, while an example of an artefact encountered during visualization is also shown. 153

LIST OF SYMBOLS AND ABBREVIATIONS

A280	Absorbance at 280 nm
AU	Absorbance units
Au	Gold
AuNPs	Gold nanoparticles
BME	β-Mercaptoethanol
BSA	Bovine serum albumin
C	Concentration
CHO	Chinese hamster ovary
COOH	Carboxyl
CV	Column volume
Da	Dalton
DMSO	Dimethyl sulfoxide
DLS	Dynamic light scattering
DTNB	5,5’-Dithio-bis-(2-nitrobenzoic acid)
DTT	Dithiothreitol
ε	Extinction coefficient
EDC	1-Ethyl-3-(3-dimethylaminopropyl)carbodiimide
EDTA	Ethylene diamine tetraacetic acid
EGF	Epidermal growth factor
ELISA	Enzyme-linked immunosorbent assay
EM	Electromagnetic
EMCH	N-ε-maleimidocaproic acid hydrazide
Fab	Fragment antigen-binding

Fc	Fragment crystallizable
FG	Functional group
FPLC	Fast protein liquid chromatography
Func	Biofunctionalized
FWHM	Full width at half-maximum
HABA	4’-Hydroxyazobenzene-2-carboxylic acid
HBF	Heterobifunctional
HCl	Hydrochloric acid
Her2	Human epidermal growth factor receptor 2
HOMO	Highest occupied molecular orbital
HRP	Horseradish peroxidase
Hyd-PEG-SH	Hydrazide-polyethylene glycol-thiol
I_2	Iodine
IgG	Immunoglobulin G
IHC	Immunohistochemistry
IP	Immunoplasmonic
kcal	kilocalorie
kDa	Kilodalton
KI	Potassium iodide
LSPs	Localized surface plasmons
LUMO	Lowest unoccupied molecular orbital
m	Methoxy
Mal	Maleimide
Mal-PEG-SH	Maleimide-polyethylene glycol-thiol

MLC	Multiepitope-ligand cartography
Mob	Electrophoretic mobility
mol	Mole
mPEG-SH	Methoxy-polyethylene glycol-thiol
MQ	Milli-Q water
MRI	Magnetic resonance imaging
MW	Molecular weight
MWCO	Molecular weight cut-off
N_A	Avogadro's number
NaCNBH	Sodium cyanoborohydride
NaCl	Sodium chloride
$NaIO_4$	Sodium periodate
NaOH	Sodium hydroxide
NH3	Amine
NHS	N-hydroxysuccinimide
NHS-PEG-SH	N-hydroxysuccinimide-polyethyleneglycol-thiol
NIR	Near-infrared
NPs	Nanoparticles
NSA	Non-specific adsorption
NUV	Near-ultraviolet
OD	Optical density
OH	Hydroxyl
OPSS-PEG-NHS	Orthopyridyldisulfide-polyethyleneglycol-N-hydroxysuccinimide
PBS	Phosphate-buffered saline

PDI	Polydispersion index
PEG	Polyethylene glycol
QDs	Quantum dots
SEC	Size-exclusion chromatography
SH	Thiol
SIMPLE	Sequential immunoperoxidase labelling and erasing
SNR	Signal-to-noise ratio
SOP	Standard operating procedure
SPA	Succinimidyl propionate
SPR	Surface plasmon resonance
TCEP	Tris(2-carboxyethyl)phosphine hydrochloride
TEM	Transmission electron microscopy
TNBS	Trinitrobenzenesulfonic acid
TZM	Trastuzumab
UV-VIS	Ultraviolet to visible
ZP	Zeta potential

LIST OF APPENDICES

Appendix A – Materials 110

Appendix B – Dynamic Light Scattering and Zeta Potential 112

Appendix C – UV-VIS Absorbance 115

Appendix D – Ellman's Test 116

Appendix E – PEGylation of Gold Nanoparticles 117

Appendix F – Stability Assay Details for Experimental Set-Up and Data Analysis Procedure 119

Appendix G – Randomly Oriented Strategy Methods 125

Appendix H – Semi-Oriented Strategy Methods 127

Appendix I – Oriented Strategy Methods 131

Appendix J – Methods for Indirect Quantification of Functionalized Antibodies 139

Appendix K – Methods for Direct Quantification of Functionalized Antibodies 144

Appendix L – Methods for Quantification of Funtionalized Gold Nanoparticles Bound to Cancer Cells 148

Appendix M – Review of Multiplexing for Imaging Cancer Cells 155

CHAPTER 1 INTRODUCTION

1.1 Background on Cancer Diagnosis

Over their lifetimes, nearly 50% of Canadians will be diagnosed with cancer, 50% of whom will lose their lives [1]. Cancer remains one of the most difficult healthcare problems in our world to solve. Due to the complexity of treating cancer, with many forms being refractory to any treatment, diagnosis is one of the key steps in determining the fate of cancer patients. Ideally, an earlier detection of cancer would increase the chances of survival of the patient, as progression to treating earlier, less complex stages of cancer would happen sooner. The longer the time between the onset of cancer and its diagnosis, the more it resists treatment. Due to the rapid deterioration of cancer as begins to metastasize in Stages III and IV, a prompter diagnosis is desirable, as later stage diagnoses have a poorer prognosis. Any delays in diagnosis could be fatal to patients. Thus, being able to diagnose the earlier, more treatable stages of cancer is an attractive area of research.

Breast cancer is the most common cancer diagnosed in Canadian women, and is the second most frequent cause of their death by cancer [2]. Mammography is considered the gold standard for early breast cancer screening, and takes an X-ray image of the breast tissue [3]. However, it has one limitation of having a high false negative rate of 15 to 20% [4]. Breast cancer screening will thus often require follow-up histological diagnostic tests to substantiate any findings from a mammography, and more closely examine the deeper molecular structure of the tissue, in order to pinpoint the subtype of breast cancer and determine the best course of treatment for the patient [5].

The main histological test used to further examine the molecular structure of breast tissue is called immunohistochemistry (IHC) [6]. An explanation of the steps undertaken for performing IHC are as follows, and an overview of the experimental set up is illustrated in Figure 1-1:

(1) Extraction of the tissue by fine-needle aspiration and fixation with formalin®, rendering this technique *ex vivo*, as opposed to *in vivo*.[1]

(2) Freezing of tissue prior to use, for storage purposes.

---

[1] *ex vivo:* biological tissue is examined outside the body; *in vivo:* biological tissue is examined inside the body

(3) Retrieval of breast cancer antigens residing in the frozen tissue via heat-induction.

(4) Blocking of background proteins / receptors that adsorb in a non-specific manner to either the primary or secondary antibodies employed during the staining step (5). Bovine serum albumin (BSA) is usually employed as a blocking agent [7].

(5) Staining of tissue, which is performed by adding a cocktail of primary antibodies able to recognize and bind to the cancer receptors (antigens), and secondary antibodies conjugated to enzymatic chromogens that can interact with the immobilized primary antibodies. A commonly employed chromogen is horseradish peroxidase (HRP).

(6) Visualization of the stained tissue under a microscope, with an examining pathologist making the diagnosis.

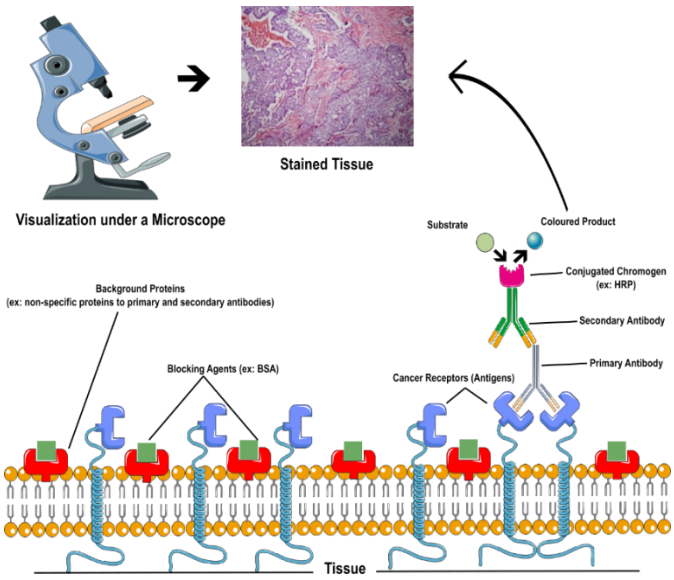

Figure 1-1 Schematic of IHC applied to cancer tissue, with relevant components labelled. In the interest of simplicity, only the blocking (4), staining (5) and visualization (6) steps explained in the above paragraph are shown. Breast cancer stained tissue taken from Novusbio [8].

1.2 Limitations of Immunohistochemistry as a Cancer Diagnostic Technique

Despite the power of this technique in detecting overexpressed cancer antigens in breast tissue, like the human epidermal growth factor receptor 2 (Her2), it suffers from a few notable drawbacks:

(1) The targeted antigens can be inadvertently lost when the tissue is extracted from the patient, or if it is not adequately fixed. This can result in them solubilizing and diffusing away from the examined area during either the epitope retrieval or blocking steps, leading to a decrease in the sensitivity of the assay [9].

(2) Variations in the duration of the fixation step, as well as the threshold staining signal used to define a positive test result and distinguish it from background signals, can also be challenges in terms of reproducibility [10].

(3) Reliance on the skill and experience of the examining pathologist during analysis of the stained tissue, which can result in a statistical bias known as interobserver variability [11].

(4) The fluorescent chromogens employed in IHC are susceptible to a phenomenon called photobleaching [12]. This can cause the quality of a tissue's luminescent signal to degrade over time, meaning that analysis of the stained tissue must be performed quickly, in order to prevent the analysis timepoint from adversely biasing the results.

Although recent advances in IHC, such as those in multiplexing and automation, have brought the technique a long way, inconsistencies in the preparation and assessment of the tissue can increase the chances of an inaccurate diagnosis [13-15]. In the context of breast cancer survival rates, the more likely a false negative result occurs, the more likely the cancer stage will deteriorate, which can dramatically impact the fate of those patients who do not receive a prompt diagnosis.

1.3 Objectives for Designing an Immunological Diagnostic Tool Able to Address Voids from Immunohistochemistry

The scope of this thesis work was to graft gold nanoparticles (AuNPs) with cancer-detecting antibodies via a polyethylene glycol (PEG) linker, a process known as biofunctionalization. This was to be optimized, in order to develop an immunoplasmonic (IP) tool, or a plasmon-generating formulation for immunological applications, in order to visualize *ex vivo* breast cancer cells under a dark-field microscope. Here, the visualization of cancer cells relies upon back-scattering by the AuNPs bound to them. This would allow for these IP-AuNPs to be compared with the conventional diagnostic test for breast cancer tissue samples, IHC. The difference between the two techniques is illustrated in Figure 1-2:

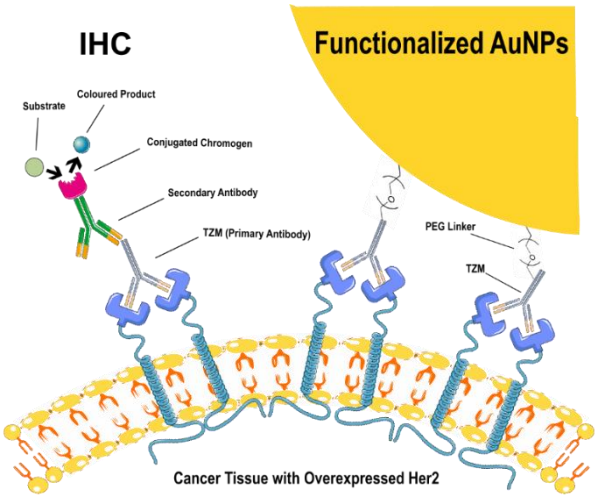

Figure 1-2 Schematic comparing IHC (*left*) with biofunctionalized IP-AuNPs (*right*) for detecting breast cancer tissue. Image inspired by work of Ciaurriz et. al, 2017 [16] .

AuNPs have been chosen for various reasons as the material of interest for designing a novel diagnostic tool for cancer. Most importantly, their intrinsic optical properties of absorption and scattering, as well as their photostability, make them superior to many other luminescent materials, including the conventional fluorophores used in IHC [17]. These intrinsic optical properties can be exploited by cancer researchers, in order to increase the sensitivity of localizing cancer cells that may normally fall out of the limit of detection of IHC [18]. For example, larger AuNPs above 50 nm have proven to be valuable for various imaging applications, such as dark-field microscopy, due to their advantageous scattering properties, which has allowed them to visualize small molecules and cells with a high resolution [19]. In contrast, the photostability of AuNPs can provide researchers with a reliable, consistent signal due to scattering that will not degrade over time, as AuNPs resist photobleaching [20].

The process of grafting cancer-detecting antibodies to gold nanoparticle AuNPs is known as biofunctionalization (i.e. conferring biologically functional properties to AuNPs), and will be henceforth referred to as such for the remainder of this thesis. The chosen antibodies for biofunctionalization are Trastuzumab (TZM), also commercialized as Herceptin®. TZM is an antibody conventionally used to treat breast cancer, and based on current knowledge in the field, has seen limited use in diagnostic tests. TZM has been selected for two reasons as the antibody of interest for this biofunctionalization: (1) it recognizes and targets the Her2 receptor overexpressed

in 25-30% of breast cancer types [21], and (2) it is easy to produce in mammalian cells, which are required to produce any humanized antibodies (such as TZM) that are glycosylated [22].

In order to test the diagnostic power of biofunctionalized AuNPs, two breast cancer cell lines have been selected. These cancer cell lines are MDA-MB-453, which overexpresses Her2 and is considered the positive control for breast cancer, and MDA-MB-231, which expresses basal levels of Her2 and is considered the negative control for breast cancer [23]. It is worth pointing out that basal levels of Her2 are always expressed in healthy breast tissue, due to this receptor belonging to a family of receptors (epidermal growth factor or EGF) required for maintenance and growth of epithelial cells. Therefore, the distinction between MDA-MB-453 and MDA-MB-231 lies in the expression levels of Her2, rather than the outright presence or lack thereof.

Given the scope of this thesis work, three sub-objectives stem from this general objective. The three sub-objectives represent the workflow of this Master's thesis, and their respective chapters in which they will be addressed are also listed. These sub-objectives are:

1. Explore and compare different strategies of biofunctionalization, including randomly oriented, semi-oriented and oriented grafting techniques, in order to develop and optimize robust and reproducible methods for functionalizing AuNPs with TZM (Chapter 3).
2. Develop and optimize characterization methods to assess both quantitatively and qualitatively each step of the process that functionalizes AuNPs with TZM (Chapter 3).
3. Apply TZM-biofunctionalized AuNPs to Her2 positive and negative cancer cell lines (MDA-MB-453 and MDA-MB-231, respectively) in order to evaluate their ability to visualize and detect cancer cells, while comparing this diagnostic tool in parallel to IHC (Chapter 3).

CHAPTER 2 LITERATURE REVIEW

2.1 Immunohistochemistry (IHC)

To be concise with content already discussed in Chapter 1, an overview of the current challenges faced by breast cancer researchers when using IHC as a diagnostic technique is provided in Table 2-1. For the reader who wishes to learn more about other visualization tools for imaging cancer cells, they are invited to consult Appendix M.

Table 2-1 Overview of challenges of IHC as a diagnostic technique for breast cancer

Challenge	Reason(s)	Consequence(s) (not necessarily aligned with each reason)
1. Non-specific adsorption of antibodies	a. Variations in blocking agent efficiencies, as well as durations of protein blocking and staining steps [9] b. Inappropriate selection and application of primary and secondary antibodies to tissue sample [24] c. Variations in tissue thickness [25]	i. Appearance of more aberrant antigens ii. Decreased signal-to-noise ratio (SNR) iii. Increased likelihood of false negatives
2. Photobleaching of fluorophores	a. Interference from the surrounding environment of the chromogen [26] b. Variations in chromogen selected [27]	i. Influence on time at which measurement is taken post-staining ii. Inability to use old tissue samples as a benchmark
3. Interobserver variability	a. Lack of standardization of experimental preparation of tissue [28] b. Lack of standardization of threshold point for positive test result [10] c. Level of experience of examiner [11]	i. Lack of reproducible results ii. Analysis of results susceptible to human error
4. Antigen loss	a. Variations in extraction procedure and time prior to fixation [29] b. Method and duration of fixation [30] c. Tissue storage conditions [31] d. Solubilization / Diffusion during extraction and epitope retrieval [32]	i. Decreased sensitivity ii. Appearance of more aberrant antigens

2.2 Gold Nanoparticle Visualization of Cancer Cells

The field of nanotechnology has exploded in interest in the last 20 years, with nanoparticles being a focal point of research. Nanoparticles (NPs) are a diverse class of formulations at the nanometre (nm) scale and can be comprised of various material, including metallic gold (Au). AuNPs have drawn interest in biotechnological and biomedical applications [17]. Their physical and optical can be harnessed for applications in therapeutics[2], diagnostics and theranostics [33]. The physical and optical properties of AuNPs are provided in the next two sections, which will rationalize why these NPs were chosen for this IP application.

2.2.1. Optical Properties of Gold Nanoparticles

AuNPs possess free electrons at their surfaces that can collectively oscillate upon irradiation. These oscillations are called plasmons, and when the natural frequency mode corresponds to the irradiating field frequency, plasmon resonance occurs [34, 35]. In particular, surface plasmon resonance (SPR) occurs when this phenomenon originates at the surface of metallic nanostructures, thereby conferring them with intrinsic optical properties [34, 36]. In the case of metallic NPs, whose sizes are considered to be much smaller than incident wavelengths in the ultraviolet to visible (UV-VIS) range of the electromagnetic (EM) spectrum (200 to 800 nm), the dynamics of interactions between incident light and the metal change [34, 36]. Here, incident wavelengths can penetrate the metal, causing polarization of conducting electrons. Thus, plasmon oscillations can occur across the entire volume of the NP, although in a localized manner, rather than in a propagating or interactive manner [37]. These localized patches of oscillating plasmons are called localized surface plasmons (LSPs), and can be shown in Figure 2-1:

[2] Therapeutic treatments involving AuNPs include induction of hyperthermia in cancer cells, as well as drug delivery.

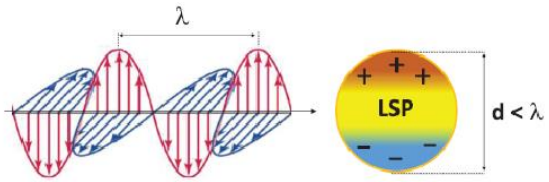

Figure 2-1 Schematic representation of the interactions between incident light (λ) and a spherical NP whose size (d) is small enough to generate LSPs. Image reproduced from Amendola et. al [37].

This polarization of plasmons across the entire surface of AuNPs renders the optical properties of AuNPs very sensitive to their immediate environments [38]. As a result, the SPR wavelength peak about which the overall NP plasmons oscillate is susceptible to small changes in its microenvironments, and can be shifted according to changes at the metallic surface: liquid interface [39]. Various properties of nanoformulations can influence the position of this SPR peak, including their: (1) size, (2) material composition and (3) geometry [40, 41]:

(1) The larger the size of the NP, the longer the SPR peak wavelength. For example, according to the NP manufacturer Nanopartz's website, 50 nm AuNPs have an SPR peak at 531 nm, while the peaks for 70 nm and 100 nm AuNPs are located at 542 and 569 nm, respectively [42].

(2) For material composition, silver will skew the real part of the extinction coefficient function towards higher values and thus LSPs at a higher energy [43]. Therefore, gold-silver alloys will have an SPR peak at a lower wavelength than their equivalent size gold counterparts.

(3) Geometry can change the anisotropy of the NPs resulting in LSPs across its entire volume, and multiple SPR peaks [44]. For example, nanorods have a second SPR peak that appears in the near-infrared (NIR) region of the EM spectrum, due to excitation along the longitudinal axis of the nanorods (Figure 2-2) [39]. This is unlike small, spherical AuNPs (of less than 50 nm), which only possess one SPR peak. Hence, the presence of asymmetry in the NP, that would deviate it from a traditional spherical shape, can shift the position of the SPR peak towards longer wavelengths. One could deduce that for spherical AuNPs, irregularities along their curved surfaces due to deformities could also shift their SPR peaks towards longer wavelengths.

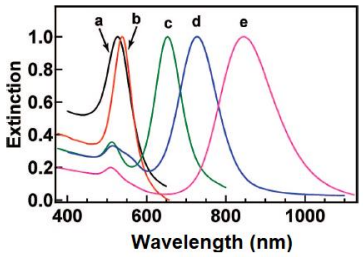

Figure 2-2 Spectra of different types of AuNPs: a) 15 nm nanospheres, b) 40 nm nanocubes, c-e) nanorods with aspect ratios of 2.4, 3.4 and 4.6, respectively. Image taken from Chen et. al [39].

The last factor influencing the position of the SPR peak is the presence of molecules attached to the surface of AuNPs. Molecules like PEG can shield incident irradiation and decrease the effective diameter of plasmons across the NP volume, which causes a shift towards longer wavelengths [45, 46]. Furthermore, differences in the density and molecular weight (MW) of these adsorbed molecules shift the plasmon peak towards longer wavelengths as their lowest unoccupied molecular orbital (LUMO) energies differ from AuNPs and couple with the plasmon conduction band, causing the width and energy of this band to decrease [47, 48]. A monolayer of PEG covering the surfaces of AuNPs will thus cause a redshift of the SPR peak.

Other optical properties include absorption and scattering, as both will contribute to the appearance of AuNPs in visible light. The overall extinction coefficient (ε) cross-section, or effective area that is excited by incident light, is the result of summing the absorption and scattering terms. AuNPs have a strong absorption cross-section extinction coefficient due to SPR. Absorption is considered a non-radiative effect as the energy of incident photons can be dissipated into the AuNPs in the form of heat, while scattering is considered a radiative effect [20]. The weighted sum of the non-radiative and radiative components of the overall extinction coefficient will determine how much AuNPs absorb or scatter light, respectively [49]. While absorption predominates at smaller AuNP sizes, scattering prevails above diameters of 70 nm up to 100 nm, as an extrinsic size effect will broaden the absorption spectrum and cause a redshift [34, 50]. This extrinsic size effect means that SPR wavelengths can be modulated in response to changes in size.

Mie theory describes how both absorption and scattering contribute to the shapes of AuNP UV-VIS absorbance spectra. When incident light reaches homogenous, spherical AuNPs, light waves at both their surfaces and internally can be approximated as planar waves that fit the sphere's

radius [51, 52]. The incident and internal electric fields of these planar waves are expanded to fit a multipole field with mathematically derived expansion coefficients. This multipole field behaves normally provided that the waves are internal or at the surfaces of the AuNPs. Beyond the radii of the AuNPs, this approximation fails, and the waves behave as if they were spheres, which can be macroscopically attributed to the scattering of incident light by the AuNPs [51, 52]. When applying this approximation to larger NPs, this multipole field expansion converges at higher orders, resulting in a greater contribution to the scattering term [53]. Consequently, one can observe the difference between smaller and larger NPs in their UV-VIS absorbance spectra, where the SPR peak broadens as size increases, due to the increased contribution of scattering (Figure 2-3). It is worth noting in this figure that the near-ultraviolet (NUV) tail preceding the SPR peak corresponds to the interband region of AuNPs, where single electrons are excited within the conduction band, creating a hole in the deeper lying d-band [54].

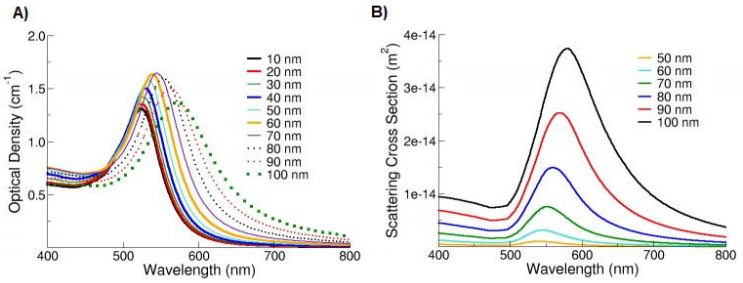

Figure 2-3 Effects of AuNP Size on A) shape of SPR peak and B) weight contribution of scattering to peak. Images reproduced from nanoComposix [55].

Due to the strong weight contribution from scattering to the extinction coefficient of AuNPs at larger sizes, AuNPs with diameters between 50 and 100 nm have drawn research interest in cancer diagnostics, as they can be easily detected by a commercial microscope under dark-field illumination [56-58]. Alongside their superior photostability, AuNPs in this size range are ideal candidates for cancer imaging. As scattering increases with size, 100 nm AuNPs will scatter light more strongly than 50 nm AuNPs, and thus be more easily detectable in dark-field microscopy. For this reason, AuNPs with a diameter of 100 nm have been chosen as the scaffold for this thesis work.

2.2.2. Physical Properties of Gold Nanoparticles

Synthesis of AuNPs represents the first step required to confer them with their favourable optical properties. Traditionally, AuNPs have been synthesized by the Turkevich method, where sodium citrate is used as a reducing agent [59]. However, due to the presence of citrate, this method has a limitation of preventing growth of AuNPs larger than 20 nm [60]. For example, larger AuNPs are more difficult to synthesize, as the growth rates of particles across the population vary dramatically according to their sizes, with larger particles growing more slowly than smaller ones [61]. Consequently, there can be dispersion in the final sizes of AuNPs. This can be observed in a UV-VIS spectrum as the SPR peak of these dispersed AuNPs will broaden more when compared to ones that have grown more uniformly, which will show a narrower peak. For this reason, researchers have opted to develop other synthesis strategies to obtain larger AuNPs with finer size dispersions. One of these strategies is the seeded growth method, which proceeds in a stepwise manner with smaller NPs serving as intermediates, referred to as seeds [60, 61]. By allowing the entire population of NPs to collectively grow towards each intermediate size, there is a better control on the final size dispersion of larger NPs. Given some of the challenges related to synthesizing AuNPs and controlling their dispersion, many researchers elect to acquire AuNPs from commercial sources, in order to accelerate their research on functionalized AuNPs [61].

In terms of stabilizing and storing AuNPs, the **sodium citrate** used to synthesize them also serves as a **capping agent for stabilizing** the assembled spheres, resulting in formation of a monolayer [17, 62]. Despite the presence of citrate, this gold-citrate bond is moderately weak and citrate ions **can be easily displaced**, especially when exposed to high ionic strength solutions [63]. Therefore, it is recommended to store AuNPs in **low salt solutions**, such as deionized water, in order to store citrate-capped AuNPs over the long-term. One issue related to AuNP destabilization (ex: under high salt) is aggregation, which results in a flattening and large redshift of their UV-VIS spectra, as displayed in Figure 2-4. This aggregation can usually be observed by a change in the colour of the AuNP solution towards a blueish tint or a complete loss of colour, which indicates irreversible aggregation [64, 65]. For this reason, AuNP stabilization is an important concern to address throughout their experimental use, during either synthesis, grafting of biomolecules onto their surfaces, or application to cells and/or tissues for detection [66]. For aggregation, it is important to distinguish it from dispersion, with the former arising due to agglomeration of

destabilized AuNPs, and the latter occurring due an irregular size distribution from either synthesis or functionalization. This difference between dispersion and aggregation is apparent in Figure 2-4:

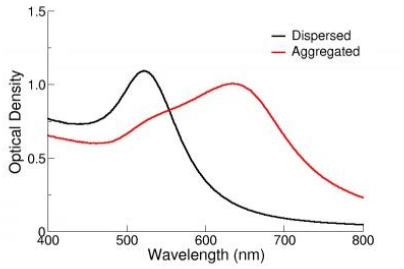

Figure 2-4 Comparison between the UV-VIS spectra of dispersed and aggregated AuNPs. Image reproduced from nanoComposix [55].

By synthesizing and stabilizing AuNPs, their physical properties can be exploited by researchers to improve their utility as a cancer diagnostic tool. First, IP-AuNPs can be turned into a multiplexed tool by employing AuNPs of different sizes, shapes and composition (the latter via silver-gold alloys), for which each type would be functionalized with a different antibody [67]. By employing a variety of different IP-AuNPs, each type can be resolved visually, such as by colour, or by the position of its SPR peak. Therefore, multiple cancer antigens could be screened for at once in a histological setting. In contrast, the large surface areas of AuNPs can be used as scaffolds to enhance the avidity and selectivity of antibody-antigen binding as more antibodies can be grafted onto the same AuNP surface. This is unlike IHC for breast cancer, where these interactions are limited to two antibodies per Her2 receptor (Figure 2-5) [68]. Finally, when functionalized nanocages are employed, AuNPs can also serve as drug delivery vectors by housing drugs and releasing them upon binding to their targets [69]. This provides them with duality for cancer diagnostics and treatment, with applications in the growing field of theranostics. For these reasons, the range of applications of IP-AuNPs are hot topics in research.

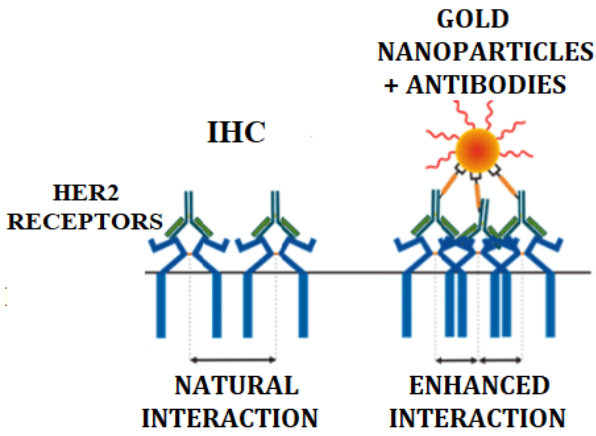

Figure 2-5 Difference in TZM avidity for Her2 receptors between IHC (*left*) and functionalized AuNPs (*right*), highlighting the potential increase in avidity resulting from functionalization. Concept of increased avidity of functionalized AuNP conjugates has been demonstrated in past literature [70, 71].

AuNPs can be diverse in both their shapes and sizes. In Figure 2-6 we can observe the sheer diversity of NPs that can be synthesized for various applications [33].

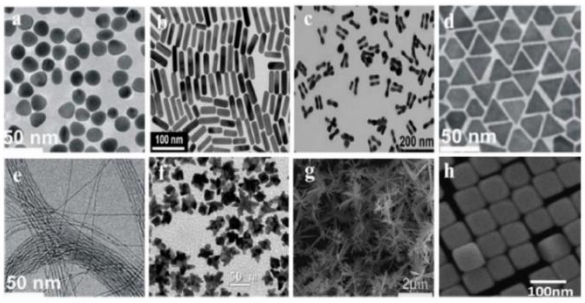

Figure 2-6 Diversity of AuNP shapes and sizes: a) nanospheres, b) nanorods, c) nanodumbbells, d) triangular nanoprisms, e) nanowires, f) nanostars, g) nanodendrites, h) nanocubes. Image reproduced from Elahi et. al [33].

Nanorods, for example, are interesting for therapeutics, due to their strong absorbance in the NIR, which can be useful for *in vivo* studies [72, 73].[3] Nanocages also share many of the same applications as nanorods, and are interesting from both therapeutic and theranostic standpoints, due

[3] The NIR has a range between 650 and 1350 nm, and is the region where light penetration of tissue is the greatest.

to their ability to act as a drug delivery vector, and strongly absorb and scatter light for detection [74]. In contrast, nanospheres and nanocubes are interesting for diagnostics and biosensing, due to their scattering [75, 76]. For this thesis work, nanospheres have been elected as the scaffold for these IP-AuNPs, instead of other formulations such as nanorods or nanocubes. This is due to their simplicity in synthesis, their lower cost, and their well-studied physical and optical properties [77].

2.3 Functionalization of Gold Nanoparticles with Biological Molecules

Biofunctionalization is the process of transforming NPs into biologically active nanoformulations, by conjugating biomolecules onto their surfaces. The reasons for AuNP biofunctionalization are varied, and entail: (1) conferring them with biological properties, (2) improving their colloidal stability, (3) improving their half-life in the human body by decreasing their renal clearance (i.e. improving their stealth to excretion), or (4) targeting cells and/or tissues in a specific manner [78].

Various terms will be introduced for the sake of clarity in later sections when these terms will be used again. A description of this vocabulary is provided in a list below in the same sequence as the experimental methods of this thesis. To provide visual context, Figure 2-7 shows an overview of these terms and their interrelatedness:

1) **PEGylation:** the process of covering the AuNP surface with polyethylene glycol (PEG), usually carried out with two types of PEG, namely: i) **heteromonofunctional PEG,** which contains only one **functional group**, and **heterobifunctional PEG,** which contains **two different functional groups**. **Thiol (SH) groups** are added to each end of these two forms of PEG, in order to provide a chemical handle for binding to the **AuNP** surface.

2) **Antibody Conjugation:** the process of covalently bonding **cancer-targeting antibodies** to a **PEG linker** already decorated onto the surface of AuNPs as heterobifunctional PEG. The exposed functional group serves as a chemical handle for attachment to the antibodies. The **bioactive antigen-binding region** is the area of interest for recognition and detection of cancer cells, and is ideally left untouched following conjugation.

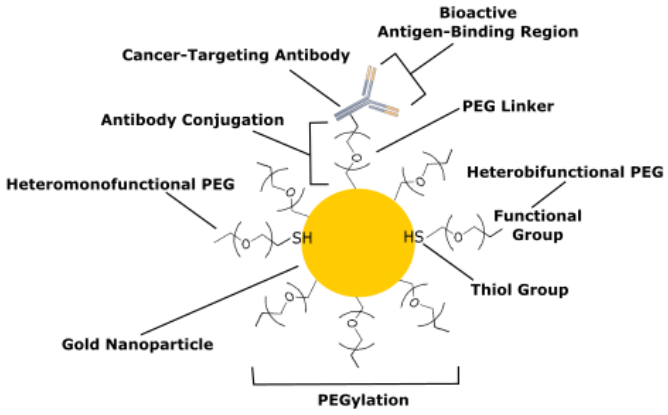

Figure 2-7 Overview of the vocabulary employed to introduce the biofunctionalization of AuNPs with PEG and cancer-targeting antibodies.

In physiological media that are comprised of complex fluids with various salts, proteins and other biomolecules that could potentially adsorb to exposed surfaces, it is imperative that AuNPs are stabilized, in order to retain their physical and optical properties. The mechanism of aggregation of AuNPs is not well-understood, with some insight suggesting that there is an equilibrium shift between individual AuNPs and aggregates [79]. Aggregation of AuNPs is likely a cooperative process, and thus, the more that aggregates are formed, the more complete aggregation of the entire population of AuNPs occurs [80]. For this reason, AuNP stabilization remains one of the most important challenges for researchers to optimize throughout the process of biofunctionalization.

2.3.1. Decoration of Gold Nanoparticles with Polyethylene Glycol (PEGylation)

PEG is a polymeric chain of C_2H_4O ether repeats (Figure 2-8). It is amphiphilic and has numerous applications in the medical and industrial fields. Varying chain length repeats are possible giving them MWs on the order of magnitude of thousands of Daltons (Da). Given the need to cover the surfaces of AuNPs to prevent their aggregation, PEG is usually selected as the stabilizing molecule for AuNPs under physiological conditions, where they are confronted with solutions of high ionic strength [78, 81]. When stored in low ionic strength solutions, AuNPs tend to stay apart due to electrostatic repulsion. However, this repulsion is overcome by high ionic strength solutions due to salt screening, resulting in aggregation of AuNPs [82]. PEG therefore imparts AuNPs with a packed monolayer that covers their surfaces, contributing to both steric and

hydrophobic stabilization. It has been more widely accepted that steric effects caused by packing of their chains are the most effective way in which PEG stabilizes AuNPs, as it helps prevent salt permeation across this layer [82-87]. A hydrophobic effect conferred by PEG packing is very much akin to how the cell membrane repels simple diffusion of ions.

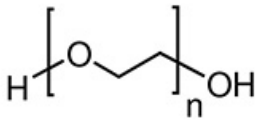

Figure 2-8 Structure of PEG. Image reproduced from Sigma Aldrich [88].

PEGylation of AuNPs occurs by taking advantage of **free thiol** (SH) groups chemically added to the ends of PEG chains. The strength of the Au-SH bond is between 40 and 50 kilocalories per mole (kcal/mol) [89, 90]. As SH groups show the **strongest affinity** for gold, and the bond formed between them is **stronger** than the one formed with citrate ions capping its surface, PEG molecules with free thiols can **easily displace citrate** ions, without triggering aggregation of AuNPs [91, 92].

To adequately shield PEGylated AuNPs from high concentrations of salt present in physiological media (on the order of magnitude of mM), a minimal density of thiolated PEG is required to adequately cover the surface so that lipophilic shielding effects can be ensured. A few estimations of this minimal density per nm^2 of AuNP surface have been performed by past research and have shown that a minimum of three thiolated PEG molecules per nm^2 of AuNP surface is required [93, 94]. When applying a PEGylation strategy to larger AuNPs, the same calculation of PEG density per surface area needs to be considered. Larger AuNPs tend to have more surface defects and heterogeneities than their smaller counterparts, as their synthesis and dispersion are not as easily controlled , meaning that the surfaces of these spheres are not smooth, but rather contain hills and valleys [95]. This means that in certain spots along their surfaces, a larger density of PEG may be required, as the binding affinities of thiolated PEG molecules can be altered in these spots, resulting in their diffusion away from these surface defects [96]. These surface defects can also impact the minimum concentration of PEG required to ensure adequate surface coverage, as their presence increases the surface area of AuNPs. These irregularities present in larger AuNPs can

pose many challenges for efficient PEGylation, as well as characterization [62]. Figure 2-9 shows this phenomenon of AuNP surface defects and their related PEGylation challenges.

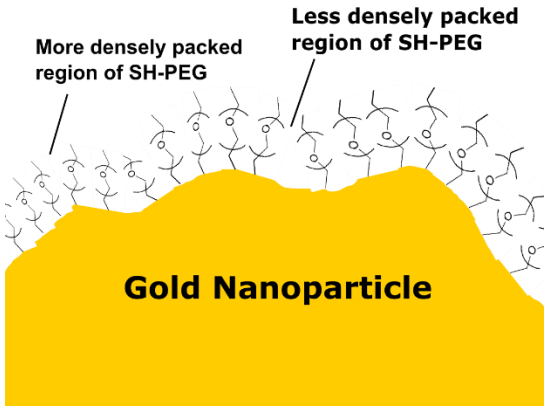

Figure 2-9 Schematic showing how surface defects hamper the PEGylation efficiency of AuNPs by varying the densities of PEG able to pack along irregular surfaces, such as hills and valleys.

Heterobifunctional PEG molecules can be manufactured to incorporate a SH group at one end for binding to AuNPs, and a reactive functional group on the other end, allowing for PEG to serve a role in bioconjugation, such as binding to antibodies [97]. PEGylation of AuNPs thus accomplishes two goals: (1) stabilize AuNPs to prepare them for physiological conditions experienced in biomedical applications, (2) serve as an intermediate link for conjugation to biomolecules. While antibodies could be simply adsorbed onto the surfaces of AuNPs via electrostatic interactions, without using PEG, this adsorption can randomly orient antibodies and decrease their biological activity, and even trigger aggregation of AuNPs [98]. For this reason, PEG is an important linker molecule needed to control the conjugation chemistry and orientation of antibodies over AuNPs, while also stabilizing them. Table 2-2 shows the sheer diversity of heterobifunctional PEG that could be used as a linker for bioconjugating antibodies to AuNPs.

Table 2-2 Example of commercially available, heterobifunctional PEG containing a SH group at one end. List of PEG drawn from several vendors labelled as: 1 – Nanocs, 2 – Sigma-Aldrich, 3 – JenKem, 4 – Creative PEGWorks, 5 – Polyscience, 6 – Pure PEG, 7 – Boc Sciences [99].

Name	Vendor(s)	Functional Groups	Reactivity of Non-Thiol End
Aldehyde PEG Thiol		-CHO, -SH	Diamines, Hydrazides, Hydroxyls, Phenolates
Amine PEG Thiol	1–7	-NH_2, -SH	Anhydrides, NHS Esters, Phenolates
Biotin PEG Thiol	1, 3	-biotin, -SH	Streptavidin
Carboxyl PEG Thiol	1, 2, 4, 5, 7	-COOH, -SH	Diamines and Diimides, NHS Esters
Hydrazide PEG Thiol	1, 4	-(C=O)N_2H_4, -SH	Aldehydes, NHS Esters
Hydroxyl PEG Thiol	3, 6, 7	-OH, -SH	Acylating and Alkylating Agents, Aldehydes
N-Hydroxysuccinimide PEG Thiol	1	-NHS, -SH	Amines, Hydrazides
Succinimidyl Propionate PEG Thiol	3, 7	-SPA, -SH	Amines, Hydrazides

To ensure sufficient coverage of the surfaces of AuNPs, and an adequate density of reactive functional groups exposed, most PEGylation strategies recommend using a mixture of both **heteromonofunctional PEG** containing a SH group able to bind to the Au surface (methoxy-PEG-thiol) and **heterobifunctional PEG** containing a SH group at one end and a functional group on the other end that serves as a chemical handle for bioconjugation.

2.3.2. Characterization of PEGylation

Various techniques are used to characterize both qualitatively and quantitatively the PEGylation efficiency. These techniques evaluate: (1) the size of the PEG-decorated AuNPs, (2) their surface charge, (3) the number of all PEG molecules attached to their surfaces, (4) the number of heterobifunctional PEG molecules attached.

The first way to evaluate PEGylated AuNPs looks at approximating their size and dispersion. The following information can be provided:

(i) **Average size** of PEGylated AuNPs, which can be compared to bare AuNPs of known sizes.

(ii) **Average dispersion** of PEGylated NPs, which can provide insight on any aggregation that may have occurred during PEGylation.

One technique employed to measure changes in size and dispersion is dynamic light scattering (DLS). DLS analyzes incident light scattered by NPs by measuring their Brownian motion on the receiving end of this scattered light [100]. This motion depends on the hydrodynamic size of NPs, as well as the viscosity and temperature of the solvent in which the NPs are suspended [101]. NPs of varying shapes and sizes are capable of scattering light. **The larger a NP** is, the **more efficiently it can scatter** light (Section 2.2.1). Thus, via appropriate calibration, and by knowing the refractive index of the material, the size of a NP can be estimated [102]. It is worth noting that this size information is not absolute, but rather relative, and should be compared with internal references of the same material that are suspended in the same solution, such as bare AuNPs [100].

By measuring size, DLS measurements can also provide information on the dispersion and aggregation of NPs. There is a correlation between **the full width at half-maximum** (FWHM) of the peaks measured by DLS and the **extent of dispersion** of AuNPs. The greater the dispersion, the greater the size distribution of that NP (Section 2.2.2). Consequently, the extent of dispersion could hint at the aggregation state of functionalized AuNPs, with wider peaks indicating aggregation, while narrower peaks are desirable as they suggest a better control of functionalization [103]. By comparing to an internal reference standard of the same material suspended in the same solution, FWHM can estimate the extent of aggregation relative to a control. The second and more obvious indicator of aggregation is the sudden appearance of a second peak at any size greater than the size of the bare AuNPs. This would occur when larger agglomerates are formed, whose Rayleigh scattering properties vary considerably from individual NPs and smaller NP aggregates, due to a **sixth power dependence** of scattering on size (d), as seen in Equation 1 [104]:

$$\sigma_s = \frac{2\pi^5}{3}\frac{d^6}{\lambda^4}\left(\frac{n^2-1}{n^2+2}\right)^2$$

Equation 1 Rayleigh scattering cross-section of particles, where *d=diameter, λ=wavelength, n=refractive index*. Equation taken from Siegel and Howell [105].

Despite the power of DLS in measuring the size and dispersion of AuNPs, it has one shortcoming that must be considered. When factoring in the six power dependence of size on scattering (Equation 1), a size bias can introduced by averaging across all NPs, including

aggregates and individual particles, resulting in a z-value being generated that does not necessarily reflect on the true state of the population of NPs. For this reason, it is recommended to consult the polydispersion index (PDI) so as to get a more accurate illustration of the make-up of the population of NPs on the basis of their dispersion in size [100].

Another technique employed for analyzing PEGylated AuNPs is measuring their surface Zeta Potential (ZP). ZP is the electric potential of colloidal AuNPs as they move across an electric field, and reflects on the potential difference between the electric double layer of mobile particles and the amount of solution surrounding them along their slipping plane [106]. In essence, it corresponds to the **surface charge** of AuNPs [107]. In this thesis work, AuNPs are normally negatively charged, due to the gain in electrons upon reduction of gold cations. Hence, positively charged ions in solution will be drawn towards them. PEGylation can thus shield the negatively charged surface, as gold atoms present in the NPs will be re-oxidized to gold cations when they form a dative bond with negatively charged sulfide groups from the thiolated PEG molecules [108]. Consequently, PEGylation will make AuNPs **less negative**. By comparing PEGylated AuNPs to an internal reference of bare AuNPs, one can correlate the change in ZP with the extent of PEG covering the surfaces of AuNPs. Logically, this correlation means that a **more efficient** PEGylation would decrease the negatively charged surfaces of AuNPs by a greater amount.

The next way to characterize PEGylated AuNPs is by UV-VIS spectroscopy. Here, the average size of the PEGylated AuNPs can be approximated by fitting their UV-VIS spectra to the Mie theory-predicted spectra for nanospheres [109]. As was seen in Section 2.2.1, the **position of the SPR peak** of AuNPs is susceptible to **changes in their microenvironments**. PEGylation can partially shield the effective diameter of LSPs in AuNPs, and cause a **redshift of the SPR peak** [47, 48]. Additionally, the **width of the SPR peak** is related to the **dispersion of the AuNPs**, and thus, the FWHM of this peak can be related to the size distribution of AuNPs, and estimate the degree of aggregation. Finally, the concentration of PEGylated AuNPs can be measured by evaluating their spectra and comparing them to bare AuNPs of known concentrations [110].

The concentration of heterobifunctional PEG bound to the surfaces of AuNPs can also be measured. Here, specific tests targeting the reactive functional groups present on heterobifunctional PEG are employed to approximate the number of exposed, reactive PEG molecules. For example, the concentration of hydrazides or amines can be measured by reacting PEGylated AuNPs with

trinitrobenzenesulfonic acid (TNBS), which recognizes and reacts with these functional groups in a colorimetric assay [111]. Similarly, the concentration of biotinylated PEG molecules grafted onto AuNPs can be quantified by employing fluorophore 4'-hydroxyazobenzene-2-carboxylic acid (HABA), which competes with streptavidin for biotin [112]. In addition, to quantify the number of PEG molecules bound to AuNPs, Hsieh et. al [113] generated anti-PEG bioparticles combined with anti-PEG antibodies for a quantitative enzyme-linked immunosorbent assay (ELISA).

Finally, to evaluate the successful clean-up of excess, unbound thiolated PEG molecules, an Ellman's test can be done, which uses the colorimetric reagent 5,5'-dithio-bis-(2-nitrobenzoic acid) (DTNB) to measure the concentration of free thiols [114]. However, this test can only be conducted under **one condition** where **thiolated PEG molecules must be in their reduced formed,** as opposed to oxidized form where they form disulfide bridges with each other. Adapting this assay to characterize PEGylation, a decrease in the colorimetric response of DTNB reacted with excess PEG in the supernatants can indicate a better PEGylation, but drawing any definitive conclusions is difficult as this response could also be due to increased oxidation of thiolated PEG molecules. In contrast, an Ellman's test can be conducted on thiolated PEG molecules bound to AuNPs to provide a more direct quantification, and requires dissolving AuNPs in aqua regia [115].

2.3.3. Conjugation of PEGylated Gold Nanoparticles to Antibodies

Before introducing antibody conjugation strategies, an explanation of the structure of antibodies is needed. A typical antibody is shown in Figure 2-11. Antibodies are Y-shaped molecules comprised of **four peptide chains** named the **heavy** and **light chains (two each)**, which refer to their respective MWs. Their arrangement makes the antibody molecule symmetrical. The heavy chains span the length of the Y, while the light chains are located on the branches of the Y. These peptide chains are linked by **inter-chain disulfide bridges**, of which there are **four**. **Two** are found in the **middle region** where the heavy chains bend, while the **other two** join the heavy and light chains. This middle region is called the **hinge region**. The region where only the heavy chain can be found is the fragment-crystallizable region, or **Fc region**, while the region where both chains can be found is the fragment antigen-binding region, or **Fab region** for short. The Fab region confers antibodies with the ability to specifically recognize and bind to antigen receptors, while the

Fc region is conserved across all antibodies of the same immunoglobulin family. In contrast, the Fc region has one unique feature, which is that it is post-translationally **glycosylated.**

There are many approaches to conjugating antibodies to AuNPs. Conjugating antibodies to AuNPs can be accomplished by adsorbing them directly onto the surfaces of AuNPs, or indirectly conjugating them to a reactive functional group (to form a covalent bond) on a PEG linker bound to AuNPs [116]. Only covalent conjugation strategies involving PEG as a linker will be discussed. Irrespective of the conjugation strategy, challenges with the chemistry include reaction yields, non-specific adsorption (NSA), aggregation of either AuNPs or antibodies, purification, and the orientation and activity of the Fab region [62, 117-121]. It is especially important that the **biological activity of antibodies is conserved by keeping the Fab region unimpaired**, so that their affinity for their antigens is not adversely affected [121-124]. Each approach has its pros and cons, which should be taken into account when optimizing the conjugation strategy, in the interest of finding the right balance between the yield of antibody conjugation products and their biological activity [125]. An overview of possible antibody conjugation strategies is shown in Figure 2-10:

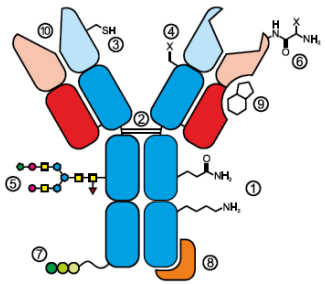

Figure 2-10 Antibody conjugation strategies: (1) natural amino acids, (2) disulfide bridges, (3) engineered cysteines, (4) non-natural amino acids, (5) glycosylated region, (6) N-termini of heavy and light chains, (7) engineered tags, (8) strong non-covalent interactions via Fc binding domains, (9) nucleotide binding site, (10) receptor-binding region. Image taken from Dennler et. al [125].

The main strategies explored in this thesis work for **covalently conjugating antibodies** to PEGylated AuNPs can be categorized into three overarching approaches. Each of these orients differently the antibodies with respect to the AuNPs: **(1) a randomly oriented approach**, which involves functional groups distributed throughout the antibody, **(2) a semi-oriented approach**, which targets the two disulfide bridges of the hinge region, and **(3) an oriented approach**, which

targets either the sugar chains located in the Fc region or amino acids artificially overexpressed in this region. Differences between these three approaches are shown in Figure 2-11:

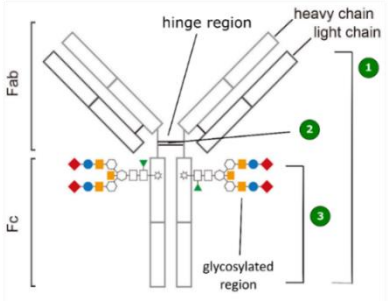

Figure 2-11 Schematic of the three main approaches explored in this Master's thesis for covalent conjugation of antibodies: (1) randomly oriented, (2) semi-oriented, (3) oriented.

a) Randomly Oriented Approach

The first approach targets any region of the antibody that could act as an anchoring point to a reactive PEG linker. For this approach, researchers usually take advantage of the abundant amine (NH_2) groups present in antibodies. These amine groups normally come from lysine residues, or from the N-termini of the heavy or light chains. Each immunoglobulin G (IgG) (the antibody family for TZM) contains roughly 80 lysine residues that are potential attachment points [126]. Hence, any conjugation chemistry that targets these lysine residues will generate a large heterogeneity of products, potentially altering the physicochemical properties of these antibodies to their antigens or partner molecules that can interact with their Fc regions [127, 128]. **As these lysine residues are randomly located** throughout the IgG backbone, conjugation could result in a **random orientation and their activity potentially altered**. Most solvent-accessible lysine residues are located in the CH_2 domain[4] of the Fc region though, which decreases this randomness [129].

One functional group used to realize this conjugation strategy is called N-hydroxysuccinimide (NHS). **NHS functional groups react with nucleophiles**, such as free amine groups, to generate stable amide bonds (Figure 2-12) [98]. These NHS groups can be introduced by either PEG linkers on their end chains, or by converting PEG linkers with an end chain carboxyl

[4] Fc domain adjacent to the hinge region of antibodies

(COOH) functional group into an NHS group by reacting them with NHS and 1-ethyl-3-(3-dimethylaminopropyl)carbodiimide (EDC) (Figure 2-12). NHS/EDC chemistry is a well-studied and popular conjugation chemistry technique, and has advantages being efficient and generating stable products by forming amide bonds [98]. An overview of NHS/EDC chemistry and their ensuing reaction with amine groups present in antibodies is shown in Figure 2-12.

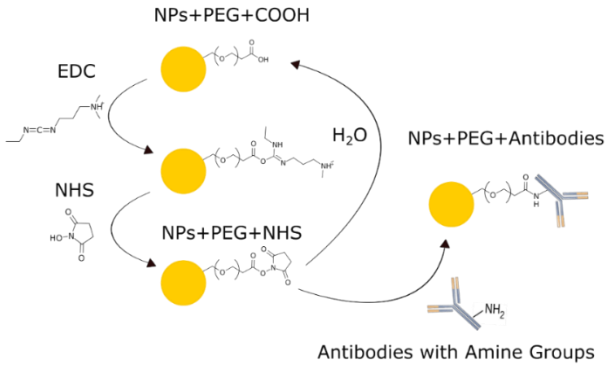

Figure 2-12 Schematic of the randomly oriented approach, whereby NHS/EDC chemistry is employed to conjugate PEGylated AuNPs to antibodies via their amine groups.

NHS/EDC chemistry has been widely used to biofunctionalize AuNPs with antibodies. For example, two studies synthesized either 6 or 10 nm AuNPs with exposed carboxyl and alcohol groups provided by a thiolated fatty acid, before conjugating them to monoclonal antibodies via NHS/EDC [130, 131]. On the contrary, Loo et. al [132] reacted monoclonal antibodies with a heterobifunctional linker with an NHS group on one end, before conjugating them to gold nanoshells. Wilson et. al [133] chose a similar strategy to this previous one, except that gold nanospheres replaced gold nanoshells.

Despite the widespread use of NHS groups to biofunctionalize AuNPs, this conjugation strategy has some drawbacks. First, NHS groups have a half-life of a few hours under physiological conditions, and are **susceptible to hydrolysis** over time, even if EDC is employed to reactivate the NHS groups [97, 134]. This can deplete the number of reactive NHS groups available in solution. Therefore, optimizing this conjugation approach requires quickly reacting any NHS-containing PEG molecules, in order to generate higher yields from this strategy.

Furthermore, NHS groups are not selective to just amine groups, as they **can react with stronger nucleophiles** present in the IgG backbone [134, 135]. This primarily concerns serine,

threonine and tyrosine residues who have hydroxyl (OH) groups that are exposed and accessible from the IgG backbone. Thus, a larger heterogeneity of bioconjugate products can be generated, due to a lack of control over the specificity of this reaction. One way to circumvent these concerns about NHS selectivity is to alter the reaction pH. Under more neutral and alkaline pH conditions, NHS groups will preferably react with lysine residues over other amino acids, although some serine and tyrosine residues may inevitably react with NHS esters [134-137].

Other concerns related to reacting NHS groups is the formation of cross-linked AuNPs conjugated to the same antibody [135]. As their kinetics are well-known, these groups will quickly react with any accessible nucleophile or amine group, and cross-linking can arise when the ratio of antibodies to available NHS groups is skewed in favour of NHS, resulting in antibodies being the limiting reagent, and multiple NHS groups reacting in excess with the same antibody. Avoiding cross-linking of AuNPs can prove to be a challenge with this conjugation strategy, as any cross-linked AuNPs can lead to the generation of clusters, potentially causing aggregation. For this reason, it is recommended to react antibodies in excess to the number of available NHS groups, in order to minimize the extent of cross-linking [138].

b) Semi-Oriented Aproach

The second approach relies on targeting SH groups of the disulfide bridges that link the heavy and light chains of antibodies. Several functional groups chemically added to PEG can target these exposed thiols, including maleimide (Mal), as depicted in Figure 2-13 [97]. Unlike the randomly oriented approach, this will be considered a semi-oriented approach as the number of cysteine residues in the IgG backbone is much less than the number of lysine residues targeted by NHS ester groups, and these cysteine residues are **more uniformly distributed** in specific regions of IgG molecules, particularly in their **hinge regions**. For each IgG, there are 16 cysteine pairs that form disulfide bridges, with 4 of these inter-chain and the remaining 12 being intra-chain [126]. Usually though the 4 inter-chain disulfide bridges are targeted by conjugation strategies, as they are more solvent accessible than the intra-chain disulfide bridges [139].

This approaches requires the **reduction of disulfide bridges** in order for the SH groups to be exposed (Figure 2-13). This must also be done in a controlled fashion to preserve the overall integrity and biological activity of the antibodies. Several reducing agents can target these disulfide

bridges, two of them being β-mercaptoethanol (BME) and dithiothreitol (DTT). There are some notable drawbacks to using these two reagents. First, DTT can lead to cross-linking of antibodies or intramolecular antibody reactions, as it contains two reactive SH groups that can reduce two subsequent disulfide bridges [126]. BME, on the other hand, is considered a strong reducing agent and its reactivity cannot be as easily controlled, which can lead to a heterogeneity of reduced antibody products [140]. For these reasons, milder reducing agents that more selectively target the inter-chain disulfide bridges of the hinge region of IgG molecules are desired.

One milder reducing agent that has been successfully employed for reducing the inter-chain disulfide bridges of the hinge region of IgG is tris(2-carboxyethyl)phosphine hydrochloride (TCEP). Advantages of TCEP include it lacking SH groups that could participate in intramolecular reactions, being water-soluble and stable under physiological conditions, and working over a wide pH range [141]. TCEP typically generates half-antibody fragments whose intrachain disulfide bridges remain untouched, as depicted below in Figure 2-13 [141-143]. Thus, these half-antibody-generated products keep the Fc and Fab regions intact. Although half-antibody fragments are not seen under physiological conditions, this method has demonstrated that disulfide bridge reduction does not impair the ability of these half-antibody fragments to bind to their antigens [144]. In fact, it has even been shown that this conjugation method can improve the sensitivity of biosensing assays [142]. Moreover, by lowering the pH of the reaction, this method can improve the yield of half-antibody fragments, which demonstrates the high selectivity imparted by TCEP [144].

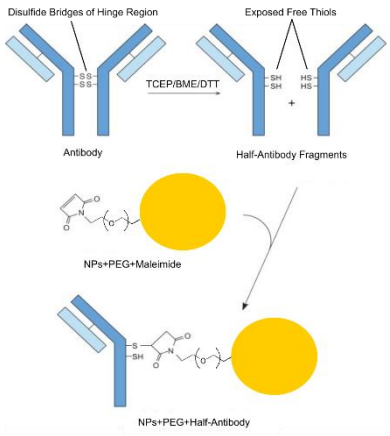

Figure 2-13 Schematic of the semi-oriented approach, assuming covalent conjugation to maleimide-exposed, PEGylated AuNPs that can react with exposed free thiols.

This conjugation strategy has been successfully employed before. Chen et. al [145] reduced antibodies in excess to TCEP, before conjugating them to a drug. In comparison, Strachan et. al [146] employed TCEP to reduce antibodies while preserving their biological activity, before conjugating them to biotin for a chromatography application. Lastly, Groysbeck et. al [147] reduced antibodies by TCEP, before conjugating them to DTNB-transformed AuNPs, which could then react with the reduced disulfide bridges of the hinge region of these antibodies, in a similar fashion to how DTNB works in an Ellman assay to detect free thiols. However, it is worth noting that this group did not use a PEG linker to span between the AuNPs and the half-antibody fragments. Based on current knowledge of the literature, TCEP reduction of antibodies for the purposes of conjugation to PEGylated AuNPs has never been published.

One challenge related to this conjugation approach includes low reaction yields due to the limited number of disulfide bridges that can react, with only two interchain bridges at the hinge region of each IgG being targeted [139, 148, 149]. However, optimizing the reaction has been shown to improve this yield [144]. On the flip side, employing TCEP could be beneficial by reducing the heterogeneity of conjugation products. Thus, researchers should ideally find a balance between optimizing yields and minimizing product heterogeneities in their conjugation strategies.

c) Oriented Aproach

The last approach revolves around **targeting the Fc region** of antibodies (Figure 2-11). By targeting this region, the antigen-binding Fab region remains untouched, reducing the risks of impairing the activity of the antibodies. To carry out this oriented approach, there are a few options:

(1) Engineer overexpressed, reactive amino acids like cysteine into the Fc region, to react with SH-targeting functional groups on PEG linkers [125]. Some drawbacks include: (i) the high costs of genetic engineering and production of recombinant glycosylated antibodies, and (ii) antibody aggregation due to disulfide bridges forming between cysteine residues [150, 151].

(2) Incorporate a tag into the Fc region that can be targeted by an enzyme that can add a chemical or biological handle, such as biotin, for attachment to other mediator molecules like streptavidin [125]. This strategy has high costs associated with: (i) genetic engineering and production of recombinant glycosylated antibodies, and (ii) enzymatic processing of the Fc region tag [125].

For economical and practical reasons, more cost-effective strategies for targeting the Fc region of antibodies have been sought out. Most often, the **sugar moieties** that are post-translationally added to human antibodies in their **Fc regions** can be targeted. Glycosylation of antibodies plays many roles in the body, including modulating the activity of other proteins as an effector, and participating in specific immune responses [152, 153]. Normally, monoclonal antibodies have two oligosaccharide chains following glycosylation, one for each side of the IgG molecule. To target these chains, antibodies are oxidized by adding sodium periodate ($NaIO_4$) in excess, which targets sialic acid moieties in these oligosaccharide chains, yielding aldehydes that can in turn react with amines or hydrazides, the latter preferred due to antibody cross-links less likely forming [125, 154, 155]. Thus, PEG molecules with either amine or hydrazide functional groups can react with oxidized antibodies to form stable amide or hydrazone bonds, respectively. An overview of this chemistry is shown in Figure 2-14:

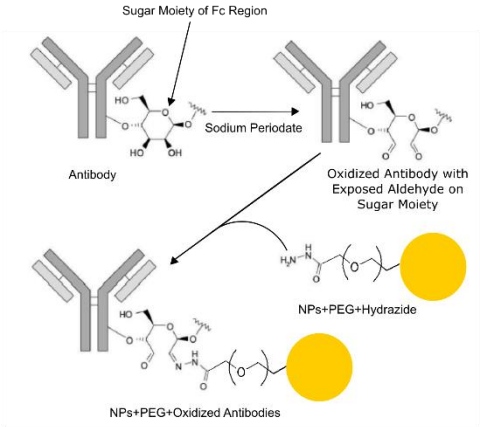

Figure 2-14 Schematic of periodate oxidation of glycosylated antibodies and their ensuing conjugation to hydrazide-exposed, PEGylated AuNPs. Image adapted from Hermanson et. al [97].

Previous research has demonstrated the oriented approach as a viable conjugation strategy. Kumar et. al [156] showed that they could target the glycosylated region of monoclonal antibodies via periodate oxidation, before conjugating them to hydrazide-PEG-thiol (Hyd-PEG-SH), and subsequently decorating these conjugates onto 20 nm AuNPs. Their protocol showed that the process of oxidizing antibodies is very fast, and if kept to a short incubation time under milder conditions, it can produce a high yield of oxidized antibodies. In comparison, Kubota et. al [157] adopted the same conjugation strategy as this previous work, except this time they generated 50

nm AuNPs conjugated to TZM. Finally, Zhou et. al [158] further controlled the oxidation process via glycoengineering by enzymatically transforming glycan residues into sialic acids, which are more selectively targeted by periodate oxidation than other carbohydrate moieties. By doing this, they were able to generate site-specific oxidized antibodies which were then conjugated to a drug. Despite the findings from these studies, none were performed on larger AuNPs, and none explored into further depth the effects of oxidation on the affinities of antibodies to their antigen receptors.

One of the major challenges with this strategy is **controlling the oxidation conditions.** Periodate oxidation is considered a harsh treatment that can lead to overoxidation of the glycosylated regions and impact the biological activity of these regions, or provoke the formation of cross-links between antibodies through their glycosylated chains, triggering their aggregation [159]. In addition, periodate oxidation has been shown to target certain amino acids, notably tyrosine, tryptophan, cysteine, methionine and serine [155].[5] If this oxidation of amino acid residues were to occur in the Fab region, this could negatively impact the affinities of antibodies to their receptors. For these reasons, researchers have explored the optimization of milder oxidation conditions, noting that control over temperature, incubation time, pH, periodate concentration and molar ratio to antibodies can minimize the extent of undesirable side effects due to oxidation [160].

2.3.4. Characterization of Antibodies Conjugated to PEGylated AuNPs

In order to evaluate the success of conjugating antibodies to PEGylated AuNPs, a characterization by qualitative and quantitative means is needed. The common goal of both set-ups is to evaluate the biological activity of antibodies grafted to AuNPs.

a) Quantitative Assays for Characterizing Antibody-Functionalized AuNPs

The first type of assay that can be conducted is an ELISA. Van der Heide and Russell [161] evaluated their functionalized AuNPs of 16 nm by incubating HRP-labelled antigens with them, and found a concentration in the range of nM translating to 1 to 35 antibodies per NP. One advantage with ELISA assays is its low limit of detection (pM), which allows for a larger range of

[5] Tyrosine and serine have -OH groups, tryptophan has indole rings, and methionine and cysteine have sulfur groups

bound antibody concentrations to be determined [162]. For larger AuNPs that have lower concentrations than smaller NPs, an ELISA could be more suitable due to its higher sensitivity.

Another way to quantify functionalized AuNPs is to compare absorbance of the supernatants before and after each step of their preparation and relating these values to concentrations by knowing the right extinction coefficient. One group performed a Bradford assay on the supernatants before and after functionalization and purification [163]. However, there are notable limitations with the Bradford assay, including its low sensitivity which may prevent it from accurately measuring concentration values or detecting any differences between each step [164].

Finally, the number of antibodies bound to AuNPs can be estimated by analyzing the UV-VIS spectra of bare and functionalized AuNPs. Mustafaoglu et. al [165] analyzed these spectra pre- and post-functionalization, and identified any shifts in the location and shape of the SPR peak, providing them with a validation of antibodies bound to AuNPs. This was followed by a DLS characterization of their functionalized AuNPs versus bare AuNPs. However, it is worth mentioning that their AuNPs were about the same size as their antibodies, which allowed them to easily measure a doubling in their size upon functionalization. In the case of larger AuNPs however, any increases in their radii upon functionalization attributable to grafting antibodies are harder to detect, especially if the AuNPs dwarf the antibodies in size. For this reason, DLS measurements need to be interpreted cautiously, as it is subjected to errors that are strongly influenced by factors such as concentration, solvent, temperature and aggregation [101].

b) Characterization of the Bioactivity of Antibody-Functionalized AuNPs

Overall, **characterization of functionalized AuNPs**, with respect to the **quantification of the number of bound and active antibodies**, can be challenging and represents the largest gap in knowledge in this research area. First, Tripathi and Driskell [166] have pointed out the challenge of discerning between loaded and active antibodies. For loaded antibodies, some assays fail to detect their activity as readings simply measure a higher loader density, which may not be indicative of their biological activity. On the other hand, active antibodies bound to AuNPs may actually be at much lower concentrations than inactive antibodies, due to either a low conjugation yield or NSA that may have impaired the activity of other bound antibodies. Thus, it is important that the limitations of these characterization techniques be noted in terms of their interpretative

power, and should be instead used to validate the presence of active loaded antibodies, until more sensitive and specific techniques for quantitative purposes have been developed [166].

c) Application of Antibody-Functionalized AuNPs to Cells for their Characterization

As the previous two sections have shown, characterization methods evaluating both the quantity and activity of antibodies functionalized onto AuNPs can be challenging. Therefore, **the best way to assess the success of a functionalization strategy** is to apply the antibody-AuNP conjugates to their target cells, for the purposes of visualizing them under a microscope.

Several works have shown the power of AuNPs as a visualization tool for imaging cells. Research on dark-field microscopy has shown that AuNPs incubated with cells can produce a bright signal on a dark background at a 5-fold order of magnitude higher than conventional fluorophores [167]. This owes to the scattering properties of larger AuNPs of greater than 50 nm. Consequently, many applications involving functionalized AuNPs have spun off from this observation, including measuring their cellular uptake [168], monitoring attachment of viral particles to cells [169], and measuring interactions between partner biomolecules with SPR thanks to shifts in the interparticle distance between NPs [170].

Applications of dark-field microscopy have been extended to the visualization of cancer cells incubated with functionalized AuNPs. Qian et. al [171] showed that angled dark-field illumination systems incorporated into a conventional inverted light microscope allowed for bioconjugated AuNPs incubated with cancer cells to be imaged, where the AuNPs acted as contrast agents. They were able to detect cellular uptake of these AuNPs by selectively conjugating peptides that would target specific organelles. Another research group chemically conjugated EGF antibodies to 17 nm AuNPs, which were then used to target and detect cancer cells under a dark-field microscope [172]. Surprisingly, the AuNPs were much smaller than larger spherical AuNPs known to scatter light more effectively under dark-field condition. Thus, this demonstrated that smaller AuNPs do scatter light to a certain degree and can still provide contrast under dark-field illumination. Nonetheless, larger AuNPs will still provide a better contrast from the background than these smaller AuNPs, for reasons previously discussed in Section 2.2.1.

CHAPTER 3 CHEMICAL CONJUGATION OF POLYETHYLENE GLYCOL AND ANTIBODIES TO GOLD NANOPARTICLES

Preamble Explaining the Outline to Chapter 3:

This chapter will explore the different chemical and analytical strategies to biofunctionalize and characterize AuNPs conjugated to heterobifunctional PEG linkers and antibodies, and visualize them with cancer cells under a microscope. This chapter constitutes the research work conducted in this thesis, and will tackle Objectives 1, 2 and 3 outlined in Section 1.3. As a reminder, these objectives are:

1. Explore and compare different strategies of biofunctionalization, including randomly oriented, semi-oriented and oriented grafting techniques, in order to develop and optimize robust and reproducible methods for functionalizing AuNPs with TZM.
2. Develop and optimize characterization methods to assess both quantitatively and qualitatively each step of the process that functionalizes AuNPs with TZM.
3. Apply TZM-biofunctionalized AuNPs to Her2 positive and negative cancer cell lines (MDA-MB-453 and MDA-MB-231, respectively) in order to evaluate their ability to visualize and detect cancer cells, while comparing in parallel this diagnostic tool to IHC.

The outline of this chapter and the thought process of this structure is as follows:

3.1. Methods and Materials for Characterization of Biofunctionalized AuNPs: this section will introduce the materials used to carry out biofunctionalization, including the various forms of PEG and antibodies used. It will then go over the different characterization techniques employed to analyze each step of biofunctionalizing AuNPs with antibodies.

3.2. PEGylation of AuNPs: this section will present and discuss results collected from the decoration of AuNPs with PEG and their characterization. This will discuss the first step of biofunctionalization, namely covering the surface of AuNPs with mono- and bifunctional PEG.

3.3. Randomly Oriented Strategy for Antibody Conjugation: this section will cover the most important results obtained from the first biofunctionalization strategy targeting in a non-oriented manner amine groups in antibodies.

3.4. Semi-Oriented Strategy for Antibody Conjugation: this section will review the most important results acquired from the second biofunctionalization strategy targeting the hinge region disulfide bridges of antibodies.

3.5. Oriented Strategy for Antibody Conjugation: this section will go over the last strategy for biofunctionalization targeting the oxidized Fc region of antibodies.

3.6. Comparison Between Antibody Conjugation Strategies: this section will compare each biofunctionalization strategy explored during this thesis work based on the results from the above sections. Further characterization of biofunctionalized AuNP samples prepared via each strategy, and their application to cells, will also be discussed.

Please note that in the interest of brevity, this chapter will focus on key techniques and results employed during this thesis work, rather than go over in detail the methods used to come to these results. For the reader who wishes to delve further into these details, they can consult the appendices, whose respective references will be highlighted in each section of this chapter.

3.1 Materials and Methods for Characterization of Biofunctionalized Gold Nanoparticles

This section will review the materials and most important techniques used to characterize each step of the biofunctionalization of AuNPs with PEG and antibodies.

3.1.1. Materials for Biofunctionalization

Note: details on this section regarding their purchase, preparation and storage are in Appendix A.

a) Source of AuNPs

Spherical AuNPs with a diameter of 100 nm, dispersed in Milli-Q water (MQ) and capped with sodium citrate were consistently used. This diameter was selected due to its optimal scattering properties for this particular diagnostic application, as was discussed in Section 2.2.1. The concentration of AuNPs corresponded to 4.96×10^9 NPs/mL, or 8.30 pM.

b) Sources of PEG

Various forms of PEG (mono- and bifunctional) were employed in this thesis work to carry out each biofunctionalization strategy. They are outlined below:

Table 3-1 Overview of different PEG molecules used during this Master's thesis project. Biofunctionalization strategies are labelled as follows: (1) random, (2) semi-oriented, (3) oriented.

Full Name	Short Form	Length (kDa)	Functional Groups	Strategy(-ies)
methoxy-PEG-Thiol	mPEG-SH	5	Thiol	1, 2, 3
N-Hydroxysuccinimide-PEG-Thiol	NHS-PEG-SH	5	NHS, Thiol	1, 2
Boc-Hydrazine-PEG-Thiol	Hyd-PEG-SH	5	Hydrazide (protected), Thiol	3

An Ellman's test was performed on PEG aliquots to measure their free thiol concentration (2 mM).

c) Source of Antibodies

The antibodies used for this thesis were Trastuzumab (TZM), and were chosen as they could target the antigen of interest in breast cancer, Her2. Freezer stock aliquots of 27 μM were used. **To keep language clear in this thesis**, the terms antibodies and TZM will be used interchangeably.

3.1.2. Characterization Methods for Biofunctionalization

The general objectives of the various characterization techniques employed during this thesis were to: **a) evaluate the state of the functionalized system** after each step, and b**) assess its stability**. A table below summarizes these different characterization techniques and their specific goals, and provides their respective appendix reference:

Table 3-2 Overview of the techniques used to characterize the biofunctionalization of AuNPs.

Name	Biofunctionalization Goal(s)	Stability Goal(s)	Appendix Reference
Dynamic Light Scattering (DLS)	• Measure changes in size after each step	• Monitor changes in dispersion/ aggregation	B
Zeta Potential (ZP)	• Measure changes in surface charge after each step	• Irrelevant	B

UV-VIS Absorbance	• Measure shift in SPR peak wavelength • Measure changes in concentration of AuNPs by comparing to reference standard of bare NPs	• Measure changes in SPR peak width (FWHM) to track destabilization • Measure losses of AuNPs from SPR peak amplitude	C
Ellman's Test	• Quantify free thiol concentration of dissolved AuNPs or PEG in solution	• Irrelevant	D
Enzyme-Linked Immunosorbent Assay (ELISA)	• Indirectly quantify the concentration of antibodies on AuNPs by measuring their washed supernatants	• Irrelevant	J
NanoOrange™ Assay	• Directly quantify the concentration of antibodies on AuNPs	• Irrelevant	K
Incubation with Cancer Cell Lines	• Measure the attachment of biofunctionalized AuNPs to cancer cells to determine their biological activity	• Irrelevant	L

Note that following acquisition of all results in this thesis work, data analysis was performed on sample measurements obtained in triplicate (for three separate runs). Student's t-tests were performed on these triplicates to identify statistically significant differences, **which were present when the *p*-value was less than 0.05 and/or 0.01.**

3.2 PEGylation of Gold Nanoparticles

Note: details on the methods employed to prepare PEGylated AuNPs can be found in Appendix E.

The goal of PEGylation of AuNPs was to: **(1) cover their surfaces** with a molecule (PEG) that **conferred them with stability** against physiological conditions (preventing their aggregation), and **(2) decorate them with mono- and bifunctional molecules**, the latter acting as a linker for antibody conjugation. Here, extensive characterization will assess the PEGylation of AuNPs and compare **two forms** of PEG employed to decorate the surfaces of AuNPs, namely: (1)

monofunctional mPEG-SH, as well as bifunctional (2) NHS-PEG-SH.[6] These forms of PEG and their respective biofunctionalization strategies were discussed in Section 3.1.1. To carry out PEGylation, PEG was incubated with AuNPs at a total final concentration of 10 μM, with **varying percentages** of NHS-PEG-SH, while adjusting the concentration of mPEG-SH accordingly. **Details on the methods** used to prepare these PEGylated AuNPs are in Appendix E. Upon preparation of PEGylated AuNP samples, characterization was performed by **a) DLS** and **b) ZP.**

3.2.1. Characterization of the Decoration of Gold Nanoparticles with PEG

a) DLS Measurements

Upon PEGylating AuNPs with varying percent compositions of mPEG-SH and NHS-PEG-SH (samples summarized in Table 3-3), DLS measurements that would measure the average hydrodynamic diameter (z-value) and dispersion of the samples were obtained. This would allow for an estimation of the approximate increase in size of the AuNPs upon PEGylation, as well as identify any signs of aggregation or clustering between PEGylated AuNPs. The rationale behind testing different percent compositions of each form of PEG was to see whether a particular percentage of NHS groups would result in a better yield when conjugated to antibodies, while also providing optimal stability. The results for DLS measurements can be seen in Figure 3-1:

Table 3-3 Overview of different samples tested for DLS characterization of PEGylated AuNPs.

Sample	Percent Composition mPEG-SH (%)	Percent Composition NHS-PEG-SH (%)
Bare AuNPs (Control)	None	None
AuNPs+PEG	100	0
AuNPs+PEG-NHS 3%	97	3
AuNPs+PEG-NHS 10%	90	10
AuNPs+PEG-NHS 30%	70	30

[6] Bifunctional Hyd-PEG-SH only had stability assays done on it. Its results can be seen in Appendix I, Section IV.

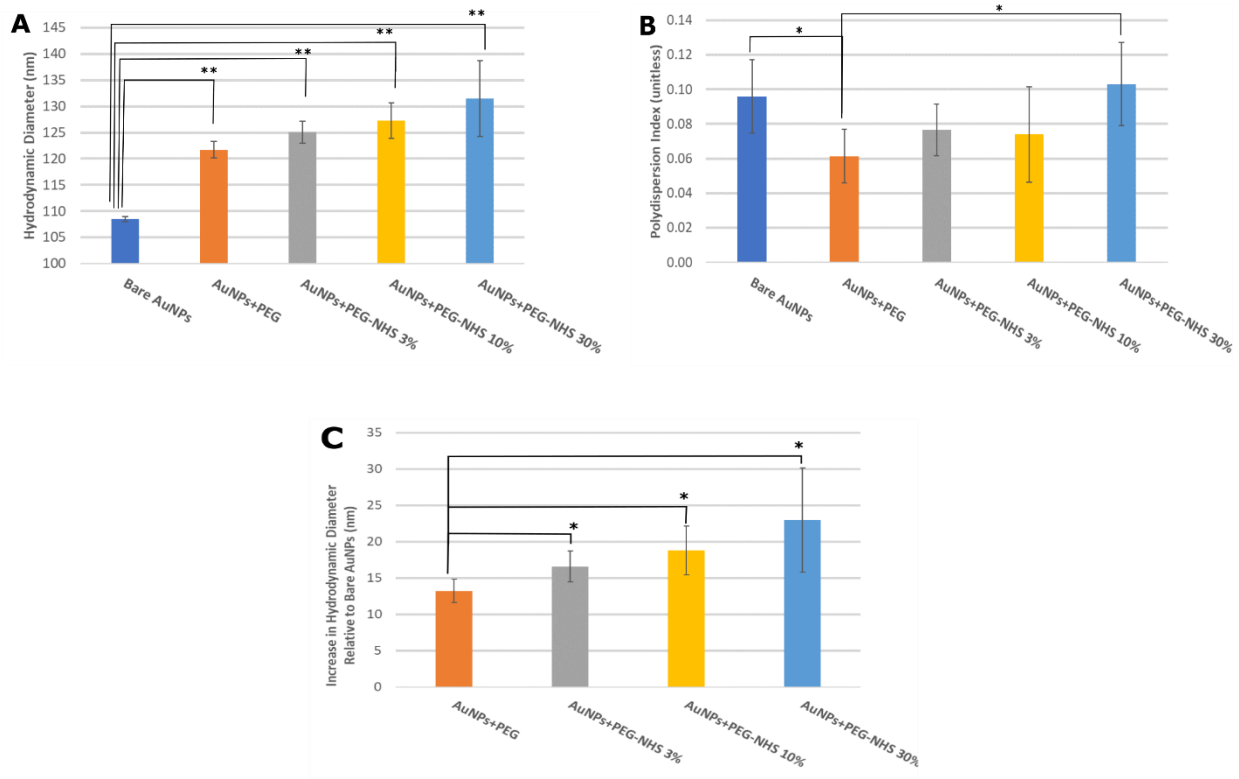

Figure 3-1 Effect of NHS- and methoxy-PEGylation (m-PEGylation) on (A) hydrodynamic diameter, (B) dispersion of AuNPs compared to bare AuNPs, and (C) size increase relative to bare AuNPs. Values represent averages of three replicates and error bars show their standard deviation. Asterisks * and ** indicate statistically significant differences of $p<0.05$ and 0.01, respectively, and brackets compare the two samples for which this difference is significant.

Interesting observations can be seen when examining the results for the DLS characterization. **First, there is a significant increase in size compared to bare AuNPs for all percentages of m- and NHS-PEGylated AuNPs when compared to bare AuNPs** (p=0.002**,** 0.003, 0.005 and 0.009 for PEG, 3% NHS, 10% NHS and 30% NHS, respectively), suggesting that the 5 kDa-long chain of PEG is enough to introduce a detectable increase in the size of AuNPs (Figure 3-1 A). Furthermore, based on the dispersion results in Figure 3-1 B, **the dispersion of PEG, 3% NHS and 10% NHS AuNPs is slightly reduced** when compared to bare AuNPs (Figure 3-1 B). Although this decrease could suggest that PEG confers a stabilizing effect to bare AuNPs, it is important to note that the polydispersion index (PDI) values are around 0.1 and below, which according to the literature, would correspond to monodisperse AuNPs [173, 174].

In addition, **Figure 3-1 C shows noticeable differences between NHS- and m-PEGylated AuNPs.** For all percent compositions of NHS-PEGylated AuNPs, there is a significant increase in their size when compared to m-PEGylated AuNPs (p=0.03, 0.04 and 0.04 for 3% NHS, 10% NHS and 30% NHS, respectively). Given the low PDI values in Figure 3-1 B, this could suggest that NHS-groups are slightly larger than methoxy-groups in term of their hydrodynamic diameter. Given that there is a sixth power dependence (Equation 1 in Section 2.3.2) between the hydrodynamic diameter and the scattering term that is detected by the DLS machine, this slight variation in size between NHS and methoxy-groups could explain their differences [105]. Thus, it would be logical to conclude that as the initial percent composition of NHS-PEG-SH increased, more molecules of this heterobifunctional PEG could bind to the surfaces of AuNPs thereby increasing their hydrodynamic size, when compared to lower percent compositions.

These initial results showed that different make-ups of PEGylated AuNPs could be differentiated. However, a technique with a higher sensitivity for size, such as transmission electron microscopy (TEM), could further resolve samples [175, 176].

b) ZP Measurements

Similarly, ZP measurements were obtained for the same samples characterized by DLS**. It is important to note that for all ZP measurements conducted during this thesis work, the same solvent was used, namely MQ with 5 mM NaCl.** This solvent was consistently used for ZP measurements to ensure that comparisons could be made between samples, as the salt concentration can influence the conductivity and surface charge of ZP-measured samples [173, 177]. For these initial ZP measurements, changes in the surface charge of PEGylated AuNPs relative to bare AuNPs were measured., to provide information on the coverage of AuNP surfaces. A similar rationale behind testing different percent compositions of each form of PEG was also adopted, in order to determine which percentage would result in the most distinguishable change in surface charge upon conjugating antibodies. ZP results can be seen in Figure 3-2:

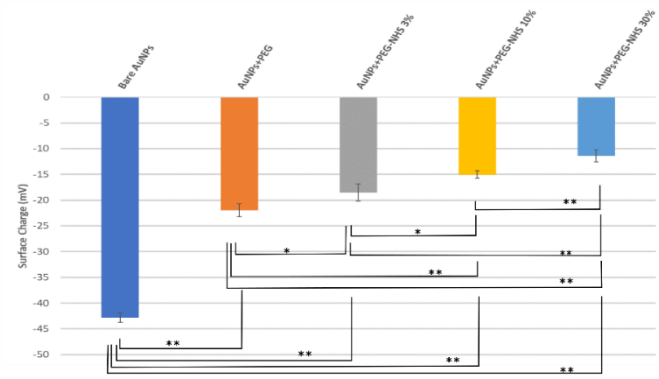

Figure 3-2 Effect of NHS- and m-PEGylation on ZP (surface charge) of AuNPs, compared to control of bare AuNPs. Abbreviations of samples are the same as those measured for DLS. Values represent averages of three replicates and error bars show standard deviation. Asterisks * and ** indicate statistically significant difference at $p<0.05$ and 0.05, respectively, and brackets compare the two samples for which this difference is significant.

Interesting trends can be observed regarding changes in the surface charges of both m- and NHS-PEGylated AuNPs. Unsurprisingly, there was a significant increase in positive charge (or decrease in negative charge) across the entire set of PEGylated AuNPs when compared to bare AuNPs ($p=1\text{x}10^{-5}$, $1\text{x}10^{-4}$, $1\text{x}10^{-6}$, and $2\text{x}10^{-6}$ for PEG, 3% NHS, 10% NHS, and 30% NHS, respectively) (Figure 3-2). PEG likely has a shielding effect on negatively charged bare AuNPs, thereby reducing the extent by which the ZP machine detects this negative charge. These results are consistent with the literature [178]. This would validate that these PEGylated AuNP samples have thus been covered with a layer of PEG, although the extent of this coverage is unknown.

Moreover, significant differences between m-PEGylated AuNPs and NHS-PEGylated AuNPs of different percent compositions can be noted ($p=0.02$, 0.002 and 0.000 2 for 3% NHS, 10% NHS and 30% NHS, respectively), with the smallest increase in positive charge being for 3% NHS-PEGylated AuNPs, and the largest increase being for 30% NHS-PEGylated AuNPs (Figure 3-2). In fact, a positive trend between the percent composition of NHS and the increase in positive charge can be clearly seen, with there even being significant differences between different percent compositions of NHS-PEGylated AuNPs ($p=0.02$ for 3% NHS vs. 10% NHS, 0.002 for 3% NHS vs. 30%, and 0.009 for 10% NHS vs. 30%) (Figure 3-2). These results would suggest that different percent compositions of NHS-PEGylated AuNPs can be distinguished via ZP. It also implies that

a greater percentage of NHS-groups can contribute to an overall increase in the surface charge of PEGylated AuNPs. These findings are curious, as NHS groups have a neutral charge [97]. In this case, it would most likely suggest that NHS groups result in the screening of negative charge that can normally interact with PEG and AuNPs, essentially causing a partial neutralization, and therefore, an apparent increase in the positive charge of NHS-PEGylated AuNPs. Screening of negative charge along the surfaces of, bare and PEGylated AuNPs has been well characterized and understood in the literature, although an extensive characterization of the effect of NHS groups on the resultant ZP of PEGylated AuNPs has not been found [179].

3.2.2. Stability of PEGylated Gold Nanoparticles

Note: Details on the methods for this section can be found in Appendix F.

The goal of the stability assays conducted at each step of the functionalization process, whether it followed PEGylation of AuNPs, or conjugation of antibodies to PEGylated AuNPs, was to **monitor changes in their UV-VIS absorbance spectr**a, in order to **identify conditions** and **timepoints** at which samples began to **destabilize and aggregate**. In order to track destabilization, various elements were extracted from the UV-VIS absorbance spectra measured at each timepoint of the assay, and attention was drawn towards the: **a) relative amplitudes** and **b) widths (FWHM)** of the SPR peak of each sample. In order to clarify these different spectral elements extracted and analyzed, Figure 3-3 highlights them:

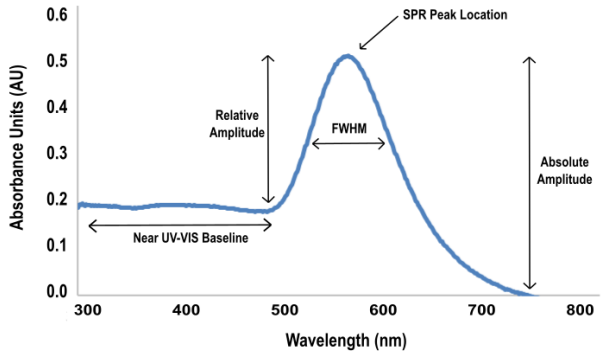

Figure 3-3 Illustration of a typical 100 nm AuNP UV-VIS absorbance spectra and its various elements extracted and analyzed from the stability assays.

To generate time course stability curves for each sample, and account for variations between samples, the **relative amplitudes and widths were normalized**. This was accomplished by: (1) **extracting the relevant spectral elements** from the raw absorbance values (following the method in Appendix F), (2) dividing that extracted element at each timepoint by the **value extracted at the initial timepoint**, in order to obtain either a percentage or percent change (for relative amplitudes and widths, respectively) and (3) dividing that percent value at each timepoint by the **equivalent timepoint-calculated percent value for the positive control** of bare AuNPs.

Note that for these stability assays, AuNP samples were either: (1) **pre-washed with fresh citrate (800 µM, pH 7)**, or (2) **left in the storage conditions of the manufacturer (3 mM, pH 7) which would be considered unwashed**. This washing step was done before PEGylation, and was implemented to assess whether replacing the manufacturer's older citrate capping the stored AuNPs with fresh citrate could result in gains in stability.

The **two main conditions** compared for assessing the stability of PEGylated AuNPs were **the presence and absence of salt**. Phosphate-buffered saline (PBS) was chosen in order to mimic physiological conditions of high salt, to which these functionalized AuNPs would be ultimately exposed to in their clinical applications. High salt can provoke aggregation of AuNPs due to interference with the surface charge of neighbouring AuNPs that would normally experience electrostatic repulsion from each other [86, 180-182]. Thus, each PEGylation strategy would be evaluated on the extent of its coverage of AuNPs and ability to stabilize them against physiological conditions. On the other hand, Milli-Q (MQ) represents a condition of no salt, a condition that has been well reported as stable for AuNPs either capped with citrate or PEGylated [182]. Finally, to compare stability results to benchmarks of either stable or aggregated AuNPs, a positive control of bare AuNPs in MQ or a negative control of bare AuNPs in PBS, respectively, were also tested.

To outline the various conditions tested on PEGylated AuNP samples during these stability assays, an overview is provided in Table 3-4. Results for both normalized percent values of AuNPs remaining (extracted from relative amplitudes) and percent change in widths of SPR peaks (extracted from FWHM) can be found in Figure 3-4, Figure 3-5 and Figure 3-6 for controls, PEGylated samples and NHS-PEGylated samples, respectively.

Table 3-4 List of monofunctional methoxy- and bifunctional NHS-PEGylated AuNP samples and their respective conditions tested during the stability assay.

Sample	Citrate Washed (W) / Normal or Unwashed (N)	PEG Composition	Final Solvent (MQ / PBS)
(+)-N	Unwashed	None	MQ
(+)-W	Washed	None	MQ
(-)	Washed	None	PBS
PEG-N-MQ	Unwashed	100% mPEG-SH	MQ
PEG-W-MQ	Washed	100% mPEG-SH	MQ
PEG-N-PBS	Unwashed	100% mPEG-SH	PBS
PEG-W-PBS	Washed	100% mPEG-SH	PBS
NHS-N-MQ	Unwashed	10% NHS-PEG-SH, 90% mPEG-SH	MQ
NHS-W-MQ	Washed	10% NHS-PEG-SH, 90% mPEG-SH	MQ
NHS-N-PBS	Unwashed	10% NHS-PEG-SH, 90% mPEG-SH	PBS
NHS-W-PBS	Washed	10% NHS-PEG-SH, 90% mPEG-SH	PBS

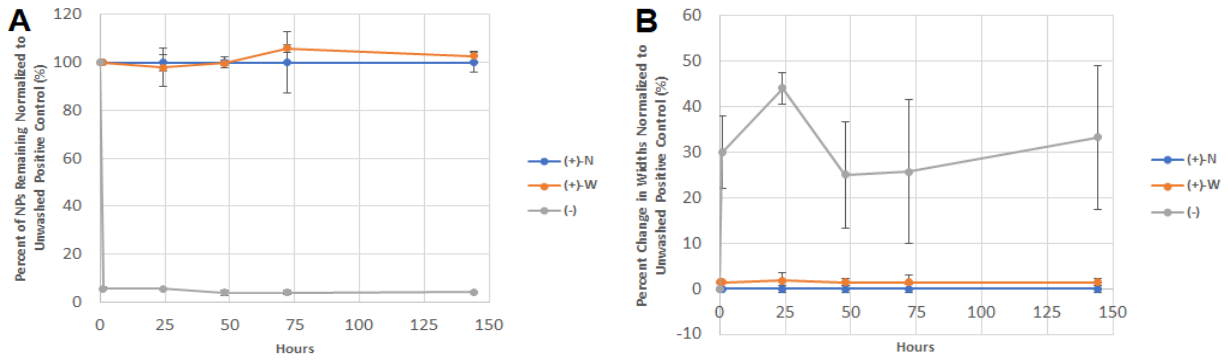

Figure 3-4 Stability curves for controls: (A) normalized percentage of AuNPs remaining, calculated from relative amplitudes of their SPR peaks, and (B) normalized percent change in FWHM of AuNP SPR peaks. Values represent averages of six replicates from two repeats of this experiment (2x3 data points), and error bars show standard deviation. Symbols in legend are depicted as: (+) – positive control, (-) – negative control, N – unwashed, W – washed.

The control curves for stability displayed above in Figure 3-4 show several important features:

In Figure 3-4 A, the y-axis shows the percent of AuNPs remaining normalized[7] to the unwashed positive control, while the x-axis shows the hours elapsed. The negative control shows complete instability, as its percent normalized value drops close to zero within the first 24 hours, which would be indicative of the SPR peak amplitude flattening. The instability of the negative control would suggest that the exposure of bare AuNPs to PBS results in a fast destabilization. On the other hand, the curves of the positive controls establish the benchmark for complete stability, with their curves practically flat for the duration of the assay, which would be indicative of their SPR peak amplitude values staying consistent. Interestingly, the washed positive control slightly outperforms the unwashed positive control, which could hint at some extra stabilization conferred by the replacement of citrate during the pre-PEGylation washing step.

In Figure 3-4 B, the y-axis shows the percent change in the widths[8] normalized to the unwashed positive control, while the x-axis shows the hours elapsed. Regarding the negative control, one can clearly observe the effect of PBS on bare AuNPs, as the percent change in width of its SPR peak increases considerably, which would be indicative of an increase in dispersion over time resulting from aggregation of AuNPs. Once again, most increases in widths of the negative control occurred in the first 24 hours of exposing bare AuNPs to PBS, which is consistent with the conclusion drawn from Figure 3-4 A indicating a fast destabilization. In contrast, the positive control shows stability as the percent change in widths of its SPR peaks remain constant, which would indicate their dispersion remaining consistent over time. This time however, unlike the case in Figure 3-4 A, the washed positive control has a slightly larger increase in the width of its SPR peaks. This could likely be attributed to the extra washing step, where the centrifugation step used to replace the manufacturer's citrate may have provoked partial aggregation of bare AuNPs.

[7] Calculated from normalizing relative amplitudes, see Appendix F-III for more details.

[8] Calculated from normalizing percent change in widths of SPR peaks, see Appendix F-III for more details.

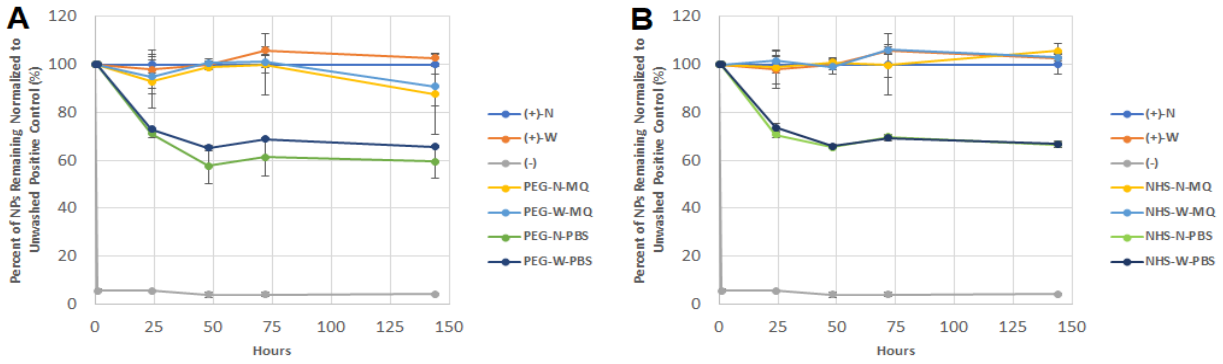

Figure 3-5 Stability curves extracted from the relative amplitudes and percent-normalized to the positive control of unwashed, bare AuNPs, for either: (A) 100% mPEG-SH and (B) 10% NHS-PEG-SH and 90% mPEG-SH. Values represent averages of six replicates from two repeats of this experiment (2x3 data points), and error bars represent standard deviation. Symbols in legend are depicted as: (+) – positive control, (-) – negative control, N – unwashed, W – washed, PEG – mPEG-AuNPs, NHS – NHS-PEG-AuNPs, MQ – Milli-Q incubation, PBS – PBS incubation.

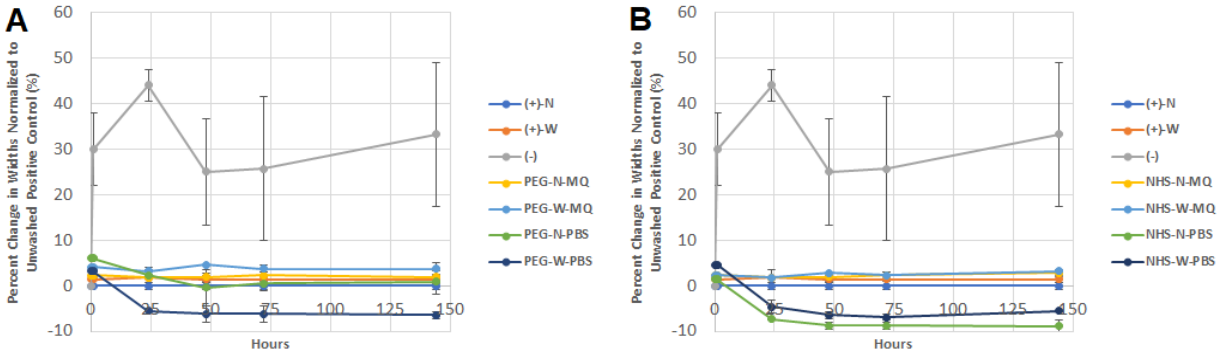

Figure 3-6 Stability curves extracted from the FWHM and percent-normalized to the positive control of unwashed, bare AuNPs, for either: (A) 100% mPEG-SH and (B) 10% NHS-PEG-SH and 90% mPEG-SH. Values represent averages of six replicates from two repeats of this experiment (2x3 data points), and error bars represent standard deviation. Symbols in legend are depicted as: (+) – positive control, (-) – negative control, N – unwashed, W – washed, PEG – mPEG-AuNPs, NHS – NHS-PEG-AuNPs, MQ – Milli-Q incubation, PBS – PBS incubation.

The above two figures (Figure 3-5 and Figure 3-6) show interesting general trends:

For Figure 3-5, most loss of PEGylated AuNPs (whether they were containing mPEG-SH or a mixture of mPEG-SH and NHS-PEG-SH) in PBS appeared to arise in the first 48 hours of the

experiment, after which point fluctuations in the percentages of PEGylated AuNPs remaining were minimal. This would suggest that the initial exposure of the PEGylated AuNPs to the high salt concentration of PBS may have caused aggregation of some AuNPs due to a screening of their charge, thereby reducing the degree of electrostatic repulsion that would normally keep these individual AuNPs apart. Thus, it would be logical to conclude that an increased exposure to salt would result in more aggregation and an ensuing decrease in the number of individual AuNPs contributing to the SPR peak amplitude, and a decrease in their percent normalized curves. This explanation would be consistent with the literature whereby the phenomenon of salt-screening of AuNPs can result in their clustering and/or aggregation [179] .

For Figure 3-6, similar trends were seen for the percent changes in widths of the PEGylated AuNPs in the first 48 hours of the experiment, where samples re-suspended in PBS saw their absorbance peaks widen initially, after which point this widening ceased. These observations could also be explained by salt screening as was seen in Figure 3-6 A. The minimal fluctuations in percent widths after 48 hours would suggest a stabilization of the PEGylated AuNP samples.

Regarding both figures, differences between the stability curves of mPEG-SH AuNP samples and NHS-PEG-SH AuNP samples appear to be minimal for both percent remaining and percent change in width. The order of magnitude of difference between mPEG-SH samples and NHS-PEG-SH containing samples both re-suspended in MQ is almost negligible, suggesting little destabilization of PEGylated AuNPs occurs even at a final composition of 10% NHS groups.

Interestingly, NHS-PEGylated AuNPs saw their widths of their SPR peaks decrease relative to the positive control, and by a greater extent than AuNPs containing solely mPEG-SH (Figure 3-6). There may have been a greater loss of larger AuNP aggregates (resulting from salt screening) for the NHS-PEGylated samples, that could have narrowed the widths of the spectra by decreasing their dispersion. A possible explanation for the destabilization of NHS-PEGylated AuNP samples relative to m-PEGylated AuNP samples is that the introduction of NHS groups decreased the extent of PEG-corona formation around AuNPs. In the literature, it is known that mPEG-SH confers protection to the surfaces of bare AuNPs via steric stabilization [85]. By having more NHS groups introduced into this PEG monolayer covering bare AuNPs, this corona would not be 100% comprised of mPEG-SH, and thus NHS-PEGylated AuNPs would be more vulnerable to being lost due to their destabilization. This decrease in the extent of corona formation resulting from NHS-

PEGylation would also be consistent with the salt screening explanation from the literature [179]. As a result, non-specific adsorption (NSA) of aggregated NHS-PEGylated AuNPs against the walls of the 96-well plate may have decreased the number of NHS-PEGylated AuNPs measured by the spectrophotometer when absorbance measurements were being taken.

3.3 Randomly Oriented Strategy for Antibody Conjugation

Note: Further details on the methods used for this strategy can be found in Appendix G.

This section will examine the results obtained from characterizing biofunctionalized AuNPs prepared by a randomly oriented strategy, before reviewing results obtained from stability assays (designed very similarly to the stability assays in Section 3.2.2). This strategy for antibody conjugation to PEGylated AuNPs served to take advantage of the naturally occurring amine groups in the antibodies, by using NHS/EDC chemistry. An overview of the general sequence of steps employed to prepare biofunctionalized AuNPs via the randomly oriented strategy can be summarized as follows (a schematic to show this methodology can also be seen in Figure 3-7):

(1) Preparation of NHS- and m-PEGylated AuNPs of varying percent compositions

(2) Reactivation of hydrolyzed NHS groups via the addition of EDC (a) and NHS (b)

(3) Grafting of antibodies to re-activated NHS-PEGylated AuNPs

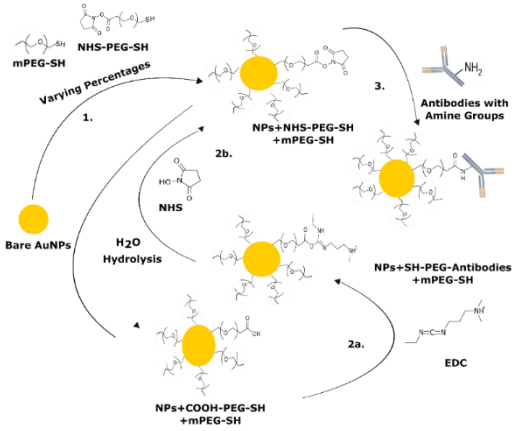

Figure 3-7 Schematic showing a stepwise overview of the chemistry employed to biofunctionalize AuNPs via a randomly oriented strategy.

3.3.1. Characterization of Antibody Conjugation

a) DLS Measurements

Similar to the previous characterization of NHS-PEGylated AuNPs, measurements were obtained for antibody-conjugated, NHS-PEGylated AuNPs. However, before these biofunctionalized samples could be characterized via DLS measurements, controls of m-PEGylated AuNPs put into contact with antibodies via physical adsorption were prepared. These controls served to evaluate the extent of NSA that could arise between m-PEGylated AuNPs and antibodies, as physical adsorption between these two was initially observed, despite the fact that methoxy-groups exposed from PEGylated AuNPs are not able to covalently conjugate to antibodies.

Thus, to test for physical adsorption between AuNPs and PEG, preparation of controls put into contact with antibodies occurred **in two different solvents, either PBS or PBS+Tween-20 (0.5% v/v)**. PBS was chosen as a solvent as it mimics the physiological conditions that these final biofunctionalized AuNP samples would be exposed to when added to cells. PBS is also a solvent that can increase the half-life of antibodies compared to other solvents, such as MQ, by preserving their quaternary structure, keeping them stable for a longer period of time (albeit they will still end up aggregating over time) [183]. In contrast, the addition of Tween-20 served to reduce the extent of NSA of antibodies against the walls of the tubes used to prepare the biofunctionalized AuNP samples. The ability of Tween-20 to reduce NSA of proteins is well-known in the literature [184]. It is posited that the loss of antibody-conjugated, PEGylated AuNPs can be reduced in the presence of Tween-20. An overview of the controls tested is provided in Table 3-5. Results for the DLS characterization of m-PEGylated AuNP controls, showing their evolution in size and dispersion following PEGylation on Day 1 to following addition of antibodies and their re-suspension in the final incubation solvent on Day 2 (**denoted as "solvent change"**), can be seen in Figure 3-8:

Table 3-5 Overview of different samples tested for DLS characterization of m-PEGylated AuNPs put into contact with antibodies.

Sample	Percent Composition PEG	Incubation Solvent	Antibodies
AuNPs+PEG (PBS)	100% mPEG-SH	PBS	No
AuNPs+PEG (PBS+Tween-20)	100% mPEG-SH	PBS+Tween-20	No

AuNPs+PEG+TZM (PBS)	100% mPEG-SH	PBS	Yes
AuNPs+PEG+TZM (PBS+Tween-20)	100% mPEG-SH	PBS+Tween-20	Yes

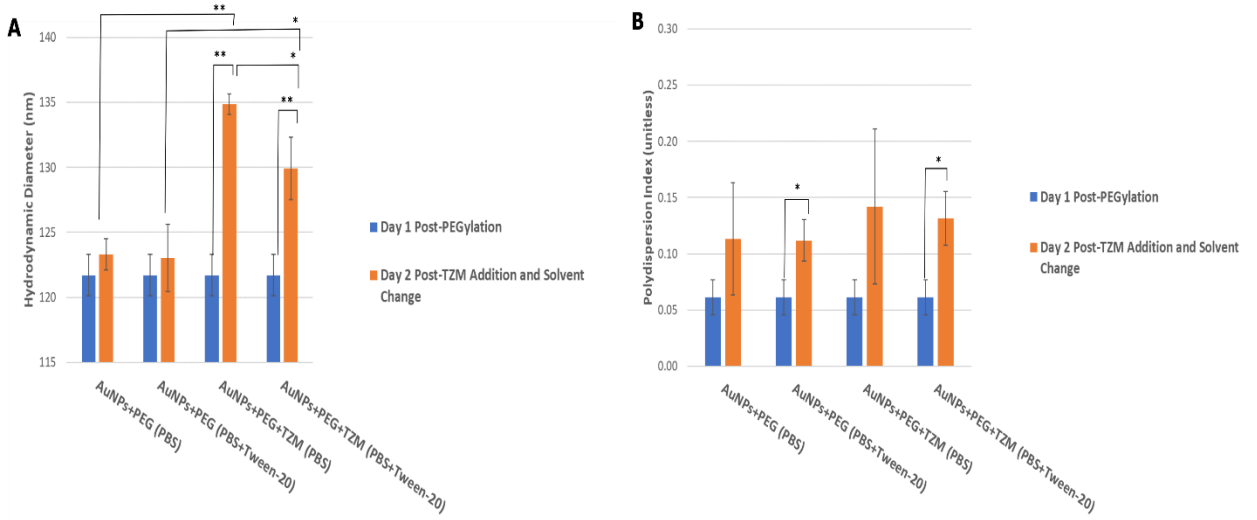

Figure 3-8 DLS results for m-PEGylated AuNP controls: (A) change in size pre- and post-addition of antibodies, (B) change in dispersion pre- and post-addition of antibodies. Values represent averages of three replicates and error bars show standard deviation. Asterisks * and ** indicate statistically significant differences at $p<0.05$ and 0.01, respectively, and brackets compare the two samples for which there is a statistically significant difference.

In Figure 3-8 A, significant increases in the size of m-PEGylated AuNPs were seen upon incubating them with antibodies, compared to their PEGylated counterparts ($p=0.004$ for PEG-TZM+PBS vs. PEG+PBS and 0.01 for PEG-TZM+Tween-20 vs. PEG+Tween-20), regardless of the incubation solvent. This shows that despite the PEGylation (and no exposed reactive functional groups from m-PEG), NSA of antibodies to PEGylated AuNPs still occurs. This suggests that there may be a partial formation of a corona between m-PEGylated AuNPs and antibodies, which would agree with the literature that NSA between protein and PEGylated AuNPs **cannot be completely reduced,** although PEG plays a role in reducing the extent of this adsorption [185-187].

However, by considering the results in Figure 3-8 B, it appears that this NSA of antibodies onto m-PEGylated AuNPs does not greatly impact the final dispersion of the AuNPs, with their PDIs still between 0.1 and 0.15, which is considered monodisperse according to the literature [174]. Albeit these antibody-adsorbed PEGylated AuNPs showed a statistically

significant increase in dispersion from their antibody-absent counterparts, this increase could likely be attributed to the formation of AuNP-antibody clusters that slightly skew the dispersion profile of AuNPs measured. Considering that DLS samples the entire population of AuNPs and calculates an average dispersion and size based on this population, these clusters could be outliers that have an impact on these values due to the sixth power dependence of DLS scattering signal on size [100].

In terms of comparing PBS against PBS+Tween-20, Tween-20 slightly reduces the size of antibodies adsorbed to m-PEGylated AuNPs, with a statistically significant difference between it and antibodies adsorbed to m-PEGylated AuNPs in PBS (p=0.02) (Figure 3-8 A). This suggests that Tween-20 can partially mitigate the extent of undesired NSA, although not completely minimize it, as there is still a significant increase in size from m-PEGylated AuNPs incubated on their own with PBS+Tween-20 (p=0.01). The effectiveness of Tween-20 in reducing NSA, albeit not completely, is thus shown [184]. Issues related to the effectiveness of the PEGylation (i.e. insufficient density of PEG covering the surfaces of AuNPs) or the molar ratio of antibodies to AuNPs (i.e. possible saturation of antibodies above the PEG monolayer covering AuNPs) could explain the extent of NSA observed. Despite efforts made in this thesis work to reduce NSA by adding Tween-20 to the incubation solvent between antibodies and PEGylated AuNPs, NSA of antibodies cannot be completely eliminated.

Following the DLS characterization of these controls, DLS characterization of functionalized AuNP samples prepared via the randomly oriented strategy was carried out. **It is important to note that based on the results from the controls experiment (Figure 3-8), PBS+Tween-20 (0.5% v/v) was chosen as the final incubation solvent** when adding antibodies to the various PEGylated AuNP samples and controls, as this solvent was determined to be the most effective in reducing the extent of NSA. Hereon for the remainder of this thesis work (unless stated otherwise explicitly), PBS+Tween-20 was the final solvent in which PEGylated AuNP samples were re-suspended in prior to incubating them with antibodies.

DLS measurements performed for samples prepared by the randomly oriented strategy would hopefully differentiate between varying percent compositions of NHS-PEG-SH on the basis of their size and dispersion, while being compared to m-PEGylated controls. At the same time, controls of blocked NHS groups were prepared by reacting ethanolamine with NHS-PEGylated AuNPs, so that NSA between deactivated NHS-PEGylated AuNPs and antibodies could be

examined. Ethanolamine is an effective blocking agent for NHS-groups that hydrolyzes them to carboxyl groups, preventing them from covalently reacting with antibodies [188].

It is worth noting that the ratio of antibodies relative to theoretically active NHS groups exposed from PEGylated AuNPs (8, 30 or 80 nM for 3%, 10% and 30% NHS-PEG-SH, respectively) [9] was held consistent at 10:1. This excess of antibodies was chosen so as to minimize cross-linking that could occur at lower concentrations of antibodies, whereby diffusion could limit the number of antibodies in close proximity of NHS-PEGylated AuNPs, resulting in multiple AuNPs reacting with the same antibody [97]. Previous research has reacted antibodies in a molar excess with PEGylated AuNPs, and hence a similar excess was justified for this functionalization, so as to minimize the extent of any cross-linking [165].

As for the m-PEGylated AuNP control put into contact with antibodies, the same concentration used for 10% NHS was arbitrarily chosen here (same concentration in Figure 3-8), as this corresponded to the middle of the range of different antibody concentrations incubated with NHS-PEGylated AuNPs. The results for this DLS characterization of samples prepared by the randomly oriented strategy, showing their evolution from Day 1 of the experiment following PEGylation to Day 2 following re-suspension in PBS+Tween-20 (**denoted as "solvent change"**) and antibody incubation, can be seen in Figure 3-9. A table summarizing the different samples characterized by DLS measurements is also provided in Table 3-6:

Table 3-6 Overview of different samples tested for DLS characterization of antibody-conjugated, NHS-PEGylated AuNPs.

Sample	**Percent Composition PEG**	**Final Incubation Solvent**	**Presence / Absence of Antibodies**
AuNPs+PEG	100% mPEG-SH	PBS+Tween-20	No
AuNPs+PEG+TZM	100% mPEG-SH	PBS+Tween-20	Yes
AuNPs+PEG-NHS 3% Blocked+TZM	3% NHS-PEG-SH, 97% mPEG-SH	PBS+Tween-20	Yes
AuNPs+PEG-NHS 30% Blocked+TZM	30% NHS-PEG-SH, 70% mPEG-SH	PBS+Tween-20	Yes

[9] The calculation of the number of theoretical NHS groups can be seen in Appendix G-II.

AuNPs+PEG-NHS 3%+TZM	3% NHS-PEG-SH, 97% mPEG-SH	PBS+Tween-20	Yes
AuNPs+PEG-NHS 10%+TZM	10% NHS-PEG-SH, 90% mPEG-SH	PBS+Tween-20	Yes
AuNPs+PEG-NHS 30%+TZM	30% NHS-PEG-SH, 70% mPEG-SH	PBS+Tween-20	Yes

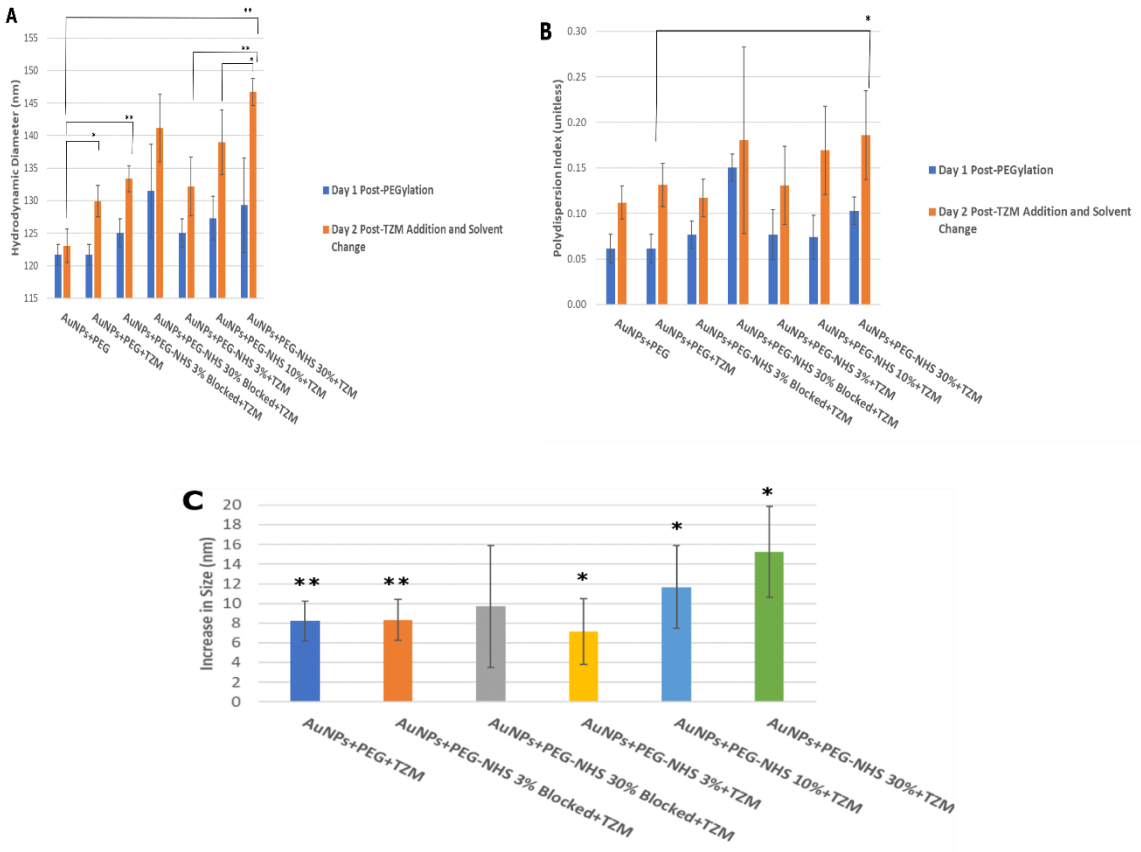

Figure 3-9 Randomly oriented strategy DLS results for: (A) change in size pre- and post-addition of antibodies and re-suspension in PBS+Tween-20, (B) change in dispersion pre- and post-addition of antibodies and re-suspension in PBS+Tween-20, and (C) overall change in size for functionalized AuNPs subtracting post-PEGylation size (pre-block for controls) from post-antibody addition size. Values represent averages of three replicates, and error bars show standard deviation. Asterisks * and ** in (A) and (B) indicate statistically significant differences at $p<0.05$ and 0.01, respectively, and brackets compare the two samples for which there is a statistically significant difference. For (C), # and ^ depict statistically significant differences at $p<0.05$ and 0.01, respectively comparing subtracted size post-PEGylation to final size post-antibody addition.

To unpack the results from the DLS characterization of antibody-conjugated, NHS-PEGylated AuNPs, samples and controls of a similar make-up will be compared one after the other:

(1) **PEG+TZM vs. PEG-NHS+TZM AuNPs:** only a significant increase in size and dispersion was observed between 30% NHS-PEGylated AuNPs conjugated to antibodies and antibodies adsorbed to m-PEGylated AuNPs (p=0.04) (Figure 3-9 A), with the increase in the dispersion being moderate and in the realm of monodisperse AuNPs (PDI<0.2) (Figure 3-9 B). This suggests that the highest percentage of NHS groups exposed from PEGylated AuNPs could generate a high enough yield of grafted antibodies detected by the DLS machine, and that the grafting was controlled as the dispersion is low. For 10% and 3% NHS-PEGylated AuNPs, there is a slight increase in the size and dispersion when compared to antibodies adsorbed to m-PEGylated AuNPs, but these differences are not significant (Figure 3-9 A and B). Thus, at lower concentrations of NHS groups, the yield of grafted antibodies is likely lower than for the highest percent composition of 30%, possibly due to diffusion that could predominate at lower concentrations of active NHS groups. The slight increases in size between antibodies adsorbed to m-PEGylated AuNPs versus NHS-PEGylated AuNPs bound to antibodies (either attached or adsorbed) show however, that antibodies can change their hydrodynamic diameter due to a possible outwardly orientation of the antibodies (Figure 3-9 A). The slight increases in dispersion between NHS- and m-PEGylated AuNPs incubated with antibodies could be due to variations in the yields of antibodies bound to individual AuNPs (Figure 3-9 B).

(2) **PEG-NHS Blocked+TZM vs. PEG-NHS+TZM AuNPs:** minimal differences in size and dispersion between the two for both 3% and 30% NHS (Figure 3-9 A and Figure 3-9 B). This suggests that despite blocking the NHS groups of these PEGylated AuNPs, some background NSA of antibodies still occurred. It is unlikely that there are still stray active NHS groups for the blocked samples, as ethanolamine blocked these and is considered a harsh treatment that can very quickly deactivate NHS groups via hydrolysis [97, 188].

(3) **Set of Different PEG-NHS+TZM AuNPs:** significant increases in size, with a partial increase in dispersion, when comparing results on Day 2 post-antibody-conjugation to results on Day 1 post-PEGylation (p=0.03, 0.01, and 0.03 for 3%, 10% and 10% NHS, respectively) (Figure 3-9 C). This suggests that antibodies can increase the overall size of PEGylated AuNPs. In contrast, there are some statistically significant increases in size (p=0.003 for 3% NHS vs. 30% NHS

and 0.02 for 10% NHS vs. 30% NHS), with minimal variance in dispersion, between NHS-PEGylated AuNPs of different percent compositions (Figure 3-9 A and B). Here, the percent composition of NHS-PEG-SH can be likely played with to acquire a better yield of antibodies conjugated to PEGylated AuNPs. To be cautious however, it is likely that NSA could be changing their size and dispersion, due to the minimal differences between the blocked NHS-PEGylated and m-PEGylated controls, and their respective NHS-PEGylated counterparts.

b) ZP Measurements

Similar to the DLS measurements for controls, ZP measurements were obtained for m-PEGylated AuNP controls put into contact with antibodies, which served to characterize NSA and evaluate any differences between incubation solvents (PBS versus PBS+Tween-20) for antibodies and m-PEGylated AuNPs. Samples prepared by the conditions in Table 3-5 had their changes in surface charge pre- and post-addition of antibodies (and re-suspension in their respective solvent, denoted as solvent change) measured. This characterization can be seen in Figure 3-10:

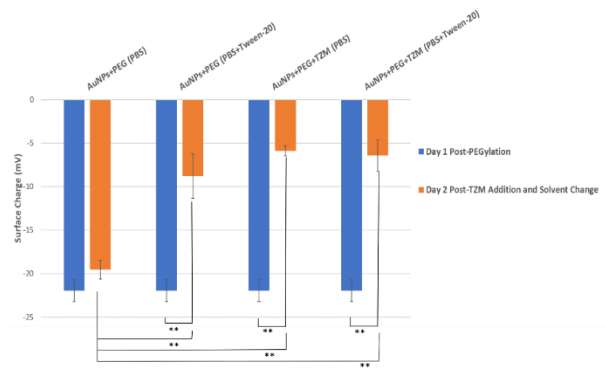

Figure 3-10 ZP results pre- and post-addition of antibodies to m-PEGylated controls in PBS or PBS+Tween-20. Samples are abbreviated as previously during DLS characterization. Values represent averages of three replicates and error bars show standard deviation. Asterisks * and ** indicate statistically significant differences at $p<0.05$ and 0.01, respectively, and brackets compare the two samples for which there is a statistically significant difference.

ZP results for the m-PEGylated AuNP controls incubated with antibodies show that **despite adding Tween-20, positive charge still increases** when compared to m-PEGylated AuNP samples incubated with antibodies in PBS (Figure 3-10). It is worth mentioning that the antibodies chosen

for this thesis work are positively charged at the physiological pH employed for their incubation with AuNPs, and thus antibodies should skew the trend in surface charge of PEGylated AuNPs once they chemically conjugate or physically adsorb [189]. However, by adding Tween-20 to m-PEGylated AuNPs in the absence of antibodies, there is a roughly equal gain in positive charge compared to the antibody-adsorbed samples (Figure 3-10). Given the significant increases from Day 1 to Day 2 for both samples re-suspended in PBS+Tween-20 (p=0.002 for PEG+Tween-20 and 0.004 for PEG-TZM+Tween-20), Tween-20 likely impacts the surface charge of these AuNPs (Figure 3-10). Furthermore, significant increases in positive charge for both Tween-20 incubated samples (in the absence or presence of antibodies), when compared to m-PEGylated AuNPs in PBS (p=0.002 for PEG-TZM+PBS and 0.006 for PEG-TZM+Tween-20), demonstrate the effect of Tween-20 on PEGylated AuNPs (Figure 3-10). This impact of Tween-20 on the decrease in negative charge of PEGylated AuNPs may suggest screening of this charge normally present in m-PEGylated AuNPs, although this phenomenon would need to be further explored to confirm this hypothesis. Previous research showed that surfactants like Tween-20 can reduce the negative charge of bare AuNPs, although it is worth noting that these AuNPs did not contain PEG [190].

Based on the results involving the m-PEGylated AuNP controls, further characterization via ZP measurements was performed on the same samples prepared in Table 3-6, in order to evaluate changes in the surface charge of antibody-conjugated, NHS-PEGylated samples before and after the addition of antibodies, and their final re-suspension in PBS+Tween-20. The same controls were also selected in order to evaluate NSA. The results of this characterization can be seen in Figure 3-11:

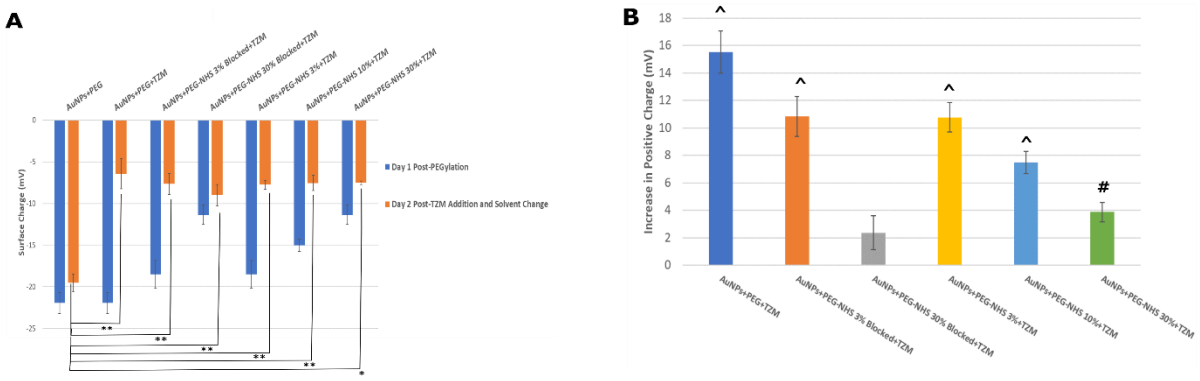

Figure 3-11 Randomly oriented strategy ZP results for: (A) change in surface charge pre- and post-addition of antibodies, and (B) overall change in surface charge for functionalized AuNPs subtracting post-PEGylation size (pre-block for controls) from post-antibody addition size. Samples are abbreviated as previously during DLS characterization. Values represent averages of three replicates and error bars represent show standard deviation. Asterisks * and ** in (A) indicate statistically significant differences at $p<0.05$ and 0.01, respectively, and brackets compare the two samples for which there is a statistically significant difference. For (B), # and ^ depict statistically significant differences at $p<0.05$ and 0.01, respectively comparing subtracted surface charge post-PEGylation to final surface charge post-antibody addition.

Regarding ZP measurements, the following interpretations can be made:

(1) **PEG+TZM vs. PEG-NHS+TZM AuNPs:** Differences in the surface charge of these various NHS-PEGylated AuNPs are minimal when compared to the control of antibodies adsorbed to m-PEGylated AuNPs, which could be attributed to the lingering presence of Tween-20 in the solvent used to measure the ZP of these samples (MQ plus 5 mM NaCl) (Figure 3-11 A). It is possible that there are remnants of Tween-20 from the solvent employed to incubate antibodies with PEGylated AuNP samples. Despite thoroughly washing these antibody-grafted samples with MQ, Tween-20 may have intercalated or adsorbed with either the bare AuNPs or PEG monolayer, although this hypothesis remains untested and more work would need to be done to explore how Tween-20 can impact the ZP of antibody-bound, PEGylated AuNP samples.

(2) **PEG-NHS Blocked vs. PEG-NHS+TZM AuNPs:** for the same reasons discussed in (1) little conclusions can be drawn between these samples on the basis of their ZP measurements.

(3) **Set of Different PEG-NHS+TZM AuNPs:** for the same reasons discussed in (1) little conclusions can be drawn between these samples on the basis of their ZP measurements.

Regarding overall changes in surface charge between Day 1 and 2 of the experiment, either following PEGylation or the addition of antibodies, respectively, the control of antibodies adsorbed to m-PEGylated AuNPs had the largest overall increase in their surface charge, when compared to NHS-PEGylated samples conjugated to antibodies (Figure 3-11 B). Although few interpretations can be drawn due to the likely interference from Tween-20 screening their charge (resulting in difficulties resolving between samples), there is a trend of a decrease in the amount of charge gained from PEGylation as the initial percent composition of NHS-PEG-SH increases (Figure 3-11 B), which suggests that NHS-PEG-SH may be able to counteract any effects of Tween-20 on surface charge, although this hypothesis remains untested.

3.3.2. Stability of Antibody-Conjugated, PEGylated Gold Nanoparticles

Similar to before in Section 3.2.2, a stability assay was set-up to monitor changes in the number of stable AuNPs and the widths of their peaks, in order to assess their stability, after adding antibodies to m- or NHS-PEGylated. Like before, bare AuNPs were pre-washed with citrate, before undergoing the same steps shown in Figure 3-7 (details on these methods can be found in Appendix F). Different conditions of PBS, PBS+Tween-20 and MQ were also tested, in order to determine the optimal solvent for incubating antibodies with PEGylated AuNPs, and subsequently storing them. Changes in the relative amplitudes and FWHM of the UV-VIS absorbance-measured SPR peaks were measured in order to track changes in the stability of samples tested under different conditions. **It is important to note that the first timepoint for UV-VIS absorbance measurements occurred after an overnight incubation between antibodies and PEGylated AuNP samples**, which deviates from when these first measurements were made for the stability assays involving PEGylated AuNP samples without antibodies. A summary of the different samples and their conditions is provided in Table 3-7. The results for the amplitude and width stability curves can also be seen in Figure 3-12.

Table 3-7 List of monofunctional m- and bifunctional NHS-PEGylated AuNP samples incubated with antibodies, with their respective conditions tested during the stability assay.

Sample	PEG Composition	Solvent	Presence / Absence of Antibodies (TZM)
(+)	None	MQ	None
(-)	None	PBS	None
PEG+PBS	100% mPEG-SH	PBS	None
PEG+Tween-20	100% mPEG-SH	PBS+Tween-20	None
PEG+TZM+PBS	100% mPEG-SH	PBS	Yes
PEG+TZM+Tween-20	100% mPEG-SH	PBS+Tween-20	Yes
PEG+TZM+MQ	100% mPEG-SH	MQ	Yes
NHS+PBS	10% NHS-PEG-SH, 90% mPEG-SH	PBS	None
NHS+TZM+PBS	10% NHS-PEG-SH, 90% mPEG-SH	PBS	Yes
NHS+TZM+Tween-20	10% NHS-PEG-SH, 90% mPEG-SH	PBS+Tween-20	Yes
NHS+TZM+MQ	10% NHS-PEG-SH, 90% mPEG-SH	MQ	Yes

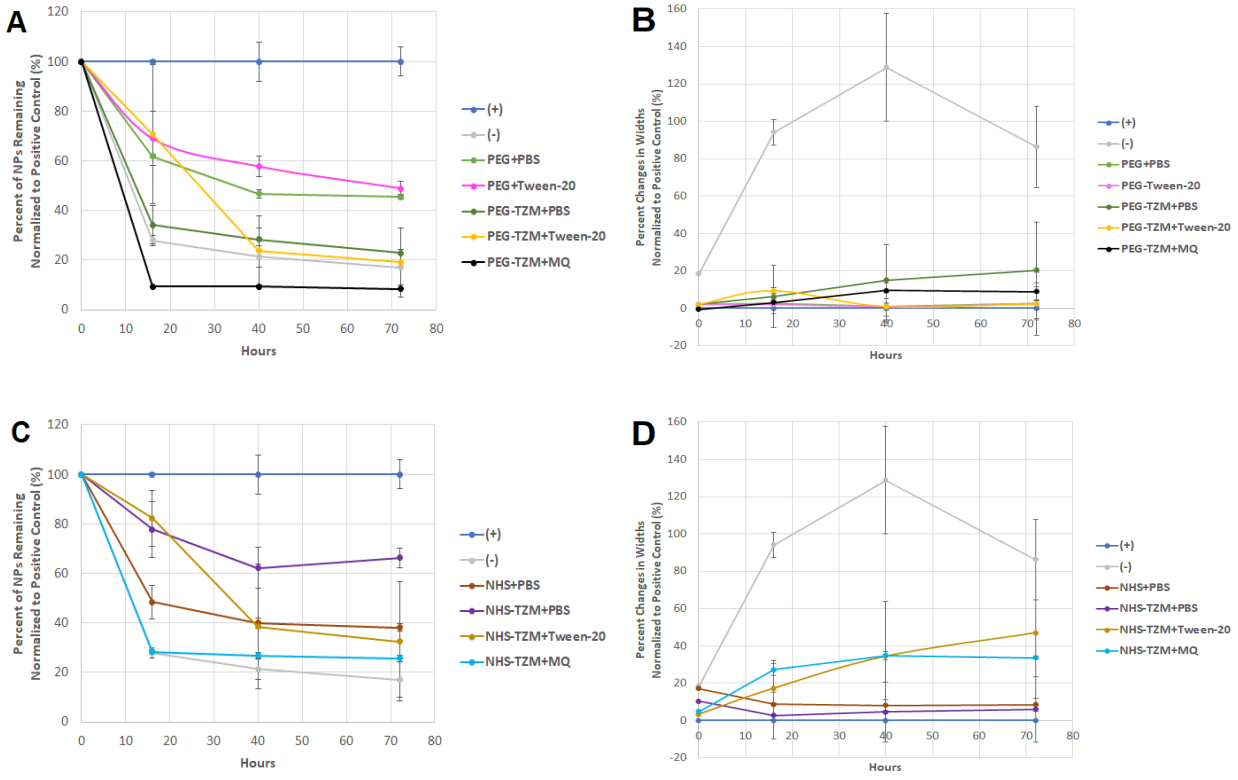

Figure 3-12 Stability curves of NHS- and m-PEGylated AuNPs bound (conjugated or adsorbed) to antibodies for: (A) normalized percentages of TZM-mPEG-AuNPs remaining relative to positive control, as calculated from the relative amplitudes of SPR peaks, (B) normalized percent changes in FWHM of TZM-mPEG-AuNP SPR peaks relative to positive control, (C) normalized

percentages of TZM-NHS-PEG-AuNPs remaining relative to positive control, as calculated from the relative amplitudes of SPR peaks, and (D) normalized percent changes in FWHM of TZM-NHS-PEG-AuNP SPR peaks relative to positive control. Values represent averages of six replicates from two repeats of this experiment (2x3 replicates each), and error bars show standard deviation. Symbols in legend are depicted as: (+) – positive control, (-) – negative control, N – unwashed, W – washed, PEG – mPEG-AuNPs, NHS – NHS-PEG-AuNPs, MQ – Milli-Q incubation, PBS – PBS incubation, Tween-20 – PBS+Tween-20 incubation.

For Figure 3-12 A and C, MQ results in a greater loss of both m- and NHS-PEGylated AuNP samples incubated with antibodies, respectively, in terms of normalized percentage of AuNPs remaining, as the curves of PEG+TZM+MQ and NHS+TZM+MQ are around the same level as the negative control. In contrast, the addition of PBS, and even more so PBS+Tween-20, to antibody-incubated samples appeared to reduce the loss of these samples, when compared to MQ, as the curves for PEG+TZM+Tween-20 and NHS+TZM+Tween-20 are higher in terms of normalized percentages of AuNPs remaining, when compared to their counterpart AuNP samples incubated in MQ (Figure 3-12 A and C). The higher values of the relative-amplitude normalized curves of the samples incubated in Tween-20 can be likely explained by the fact that Tween-20 reduces NSA of protein and thus helps to reduce the amount AuNP:antibody conjugates lost upon adsorption to the walls of the 96-well plate, which would decrease the loss in the SPR relative amplitude value measured [191]. In fact, previous work has shown that Tween-20 can improve not only the stability and preservation of bare AuNPs, but even more so PEGylated AuNPs, when they are allowed to come into contact with biomolecules such as antibodies [192].

In contrast, the normalized percent loss of NHS-PEGylated AuNPs conjugated to antibodies was less prominent than for unconjugated, NHS-PEGylated AuNPs (Figure 3-12 C). A similar conclusion as was drawn in Section 3.2.2 can be made here, by explaining that the initial exposure of the NHS-PEGylated AuNPs to the high salt of PBS may have caused aggregation of these AuNPs due to charge screening, which reduced electrostatic repulsion between individual AuNPs [179]. As a result, the SPR relative amplitude value measured for these NHS-PEGylated AuNPs may have dropped due to NSA of AuNPs against the walls of the 96-well plate (which would have increased their loss). Once antibodies were added to these NHS-PEGylated AuNPs, non-specific interactions between these antibody-conjugated, NHS-PEGylated AuNPs and the walls of the 96-

well plate may have been reduced (although this hypothesis remains untested and unexplained by the literature), which would have improved the SPR relative amplitude value measured.

For Figure 3-12 B and D, the most considerable changes in the state of aggregation of the conjugated system occurred for NHS-PEGylated AuNPs in MQ, with up to a 40% gain in the width of their absorbance peaks. For these antibody-conjugated, NHS-PEGylated AuNPs incubated in MQ, it suggests that there more aggregation and/or dispersion may have occurred in this solvent, which corroborates the conclusions in the amplitude curves (Figure 3-12 C). On the other hand, Tween-20, while initially stabilizing antibody-conjugated, NHS-PEGylated AuNPs, later results in an increase in the widths of their peaks the longer the storage time, which suggests some partial dispersion and/or aggregation (Figure 3-12 D). Despite an exhaustive literature review, there is no explanation for the widening of the SPR peaks of NHS+TZM+Tween-20 over time. This would partially contradict the literature suggesting that the stability of PEGylated AuNPs, when put into contact with biomolecules such as antibodies, is enhanced in the presence of Tween-20 [192].

In contrast, antibody-adsorbed, m-PEGylated AuNPs in MQ, as well as antibody-conjugated, NHS-PEGylated AuNPs in PBS, show similar degrees of increase in their widths in Figure 3-12 B and D, which is consistent with the findings of the amplitude curves in Figure 3-12 A and C, as well as observations in the laboratory when this experiment was conducted, when their wells became clearer in colour and resembled the negative control. According to the literature, a change or loss in the colour of AuNP solutions is a sign of aggregation [64, 65]. Finally, the percent change in width curves of antibodies adsorbed to m-PEGylated AuNPs in Figure 3-12 B are smaller than the changes observed for their relative amplitude, percent normalized curves in Figure 3-12 A, with an approximate 10% increase in the widths of their peaks, compared to a 10% recovery, respectively. This could hint at more NSA of these antibody-adsorbed, m-PEGylated samples, which would have decreased the SPR amplitude value measured by the spectrophotometer.

Regardless of how aggregation or loss of antibody-conjugated, NHS-PEGylated AuNPs arose, the most important conclusions from these two figures are that PBS+Tween-20 should be the chosen as the solvent for conjugating antibodies to NHS-PEGylated AuNPs, while PBS should be chosen as the solvent for storage, so that any aggregation and dispersion caused by the long-term storage of antibody-conjugated, NHS-PEGylated AuNPs in PBS+Tween-20 is minimized.

3.4 Semi-Oriented Strategy for Antibody Conjugation

Note: Further details on the methods used for this strategy can be found in Appendix H.

This section will examine the results obtained from characterizing biofunctionalized AuNPs prepared by the semi-oriented strategy, before reviewing results acquired from stability assays. This strategy was adapted from the work of Makaraviciute and Ramanaviciene (2013) [155] to this system of PEGylated AuNPs. This strategy focused on targeting the hinge region disulfide bridges of TZM antibodies via TCEP reduction to reduce them into half-antibody fragments, before conjugating them to PEGylated AuNPs. By targeting this region, risks of impairing the activity of the receptor-binding Fab region of antibodies were minimized. To realize this strategy, the following steps were carried out and are shown in Figure 3-13:

(1) NHS-PEGylated AuNPs with active NHS groups were prepared in the same way as in the randomly oriented strategy

(2) The reagent N-ε-maleimidocaproic acid hydrazide (EMCH) was used to transform the active NHS groups into maleimide (Mal) groups. These Mal groups can target free, exposed thiols located on the reduced antibodies (transformed PEG denoted as Mal-PEG-SH).

(3) (a) TCEP-reduced antibodies were prepared and characterized, before (b) incubating them with Mal-transformed PEGylated AuNPs.

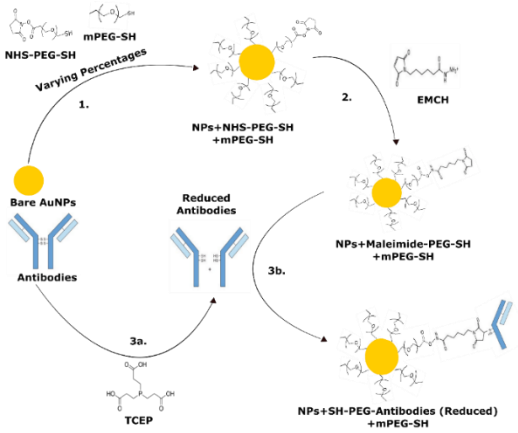

Figure 3-13 Schematic showing a stepwise overview of the chemistry employed to biofunctionalize AuNPs via a semi-oriented strategy.

3.4.1 Characterization of Antibody Conjugation

a) DLS Measurements

Antibody-conjugated, Mal-PEGylated (Mal-PEG-SH) AuNPs were prepared for this strategy, and were then characterized by DLS measurements. For controls, Mal-PEGylated AuNPs in the absence of reduced antibodies were measured, and 30% Mal-PEGylated AuNPs had their Mal groups blocked by adding cysteine, before putting them into contact with non-reduced antibodies. Finally, Mal-PEGylated AuNPs of varying compositions were incubated with non-reduced antibodies**. Similar to before, prior to incubating antibodies with PEGylated AuNP samples and controls, a solvent change occurred by re-suspending them in PBS+Tween-20** (same solvent seen in Section 3.3.1). A summary of the samples and controls tested is provided in Table 3-8. The results of this DLS characterization can be seen in Figure 3-14:

Table 3-8 Overview of different samples tested for DLS characterization of antibody-conjugated, Mal-PEGylated AuNPs.

Sample	Composition of PEG	Type of Antibodies
AuNPs+PEG	100% mPEG-SH	None
AuNPs+PEG+TZM	100% mPEG-SH	Non-Reduced
AuNPs+PEG-Mal 3%	3% Mal-PEG-SH, 97% mPEG-SH	None
AuNPs+PEG-Mal 10%	10% Mal-PEG-SH, 90% mPEG-SH	None
AuNPs+PEG-Mal 30%	30% Mal-PEG-SH, 70% mPEG-SH	None
AuNPs+PEG-Mal 30% Blocked+TZM Non-Red	30% Mal-PEG-SH, 70% mPEG-SH	Non-Reduced
AuNPs+PEG-Mal 3%+TZM Non-Red	3% Mal-PEG-SH, 97% mPEG-SH	Non-Reduced
AuNPs+PEG-Mal 10%+TZM Non-Red	10% Mal-PEG-SH, 90% mPEG-SH	Non-Reduced
AuNPs+PEG-Mal 30%+TZM Non-Red	30% Mal-PEG-SH, 70% mPEG-SH	Non-Reduced
AuNPs+PEG-Mal 3%+TZM Red	3% Mal-PEG-SH, 97% mPEG-SH	Reduced
AuNPs+PEG-Mal 10%+TZM Red	10% Mal-PEG-SH, 90% mPEG-SH	Reduced
AuNPs+PEG-Mal 30%+TZM Red	30% Mal-PEG-SH, 70% mPEG-SH	Reduced

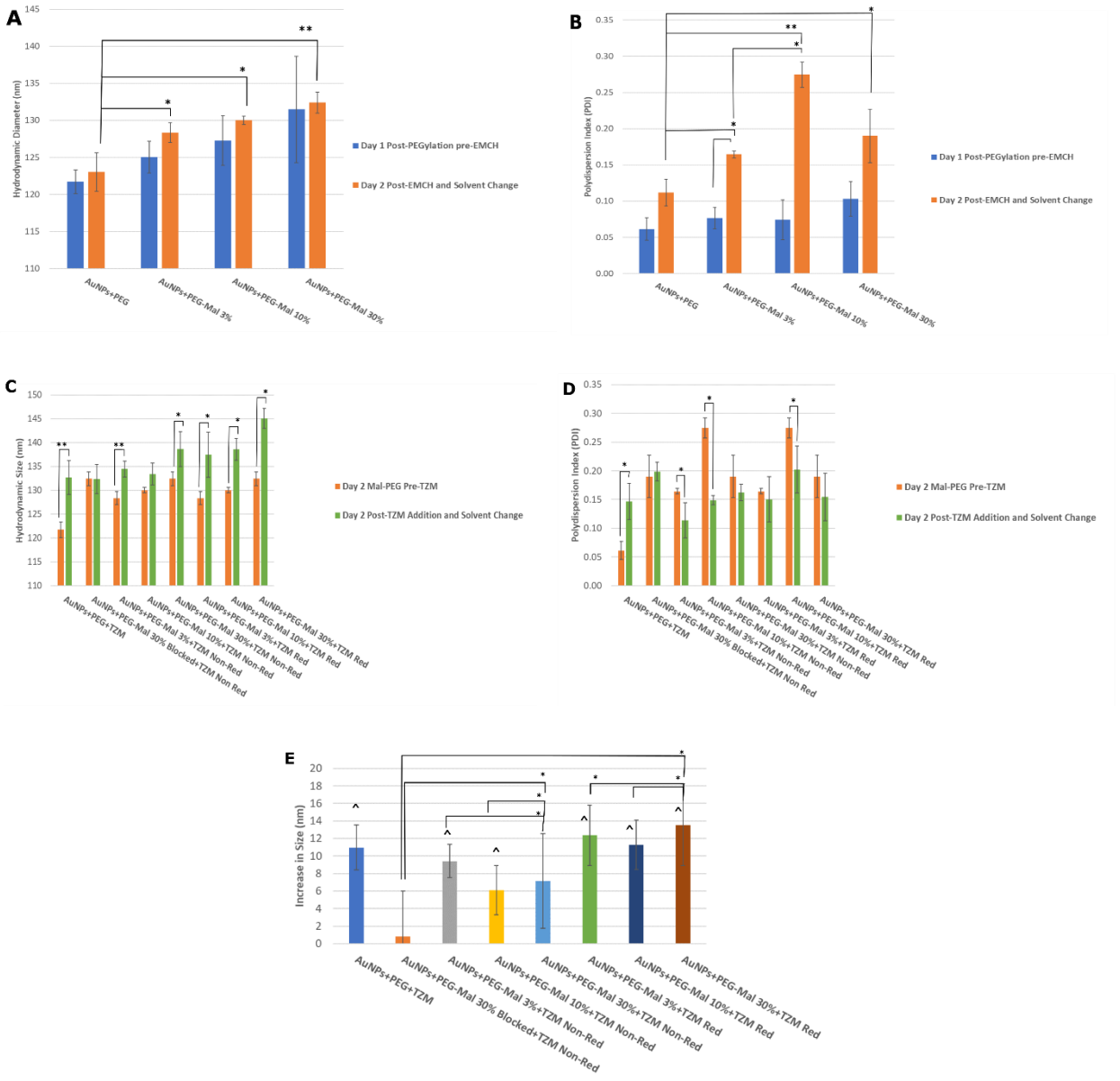

Figure 3-14 Semi-oriented strategy DLS results for: (A) change in size pre- and post-EMCH reaction, (B) change in dispersion pre- and post-EMCH reaction, (C) change in size of EMCH-transformed AuNPs pre- and post-addition of antibodies, (D) change in dispersion of EMCH-transformed AuNPs pre- and post-addition of antibodies, and (E) overall change in size for functionalized AuNPs subtracting post-PEGylation size (pre-EMCH reaction) from post-antibody addition size. All sub-figures have controls of methoxy- and/or Mal-PEGylated AuNPs. Values represent averages of three replicates and error bars show standard deviation. Asterisks * and ** in (A–E) indicate statistically significant differences at p<0.05 and 0.01, respectively, and brackets

compare the two samples for which there is a statistically significant difference. For (E), ^ depicts statistically significant increases ($p<0.01$) comparing subtracted size post-PEGylation (pre-EMCH reaction) to final size post-antibody addition, and brackets compare final sizes (in C), rather than increases.

To analyze the results from the DLS characterization of antibody-conjugated, Mal-PEGylated AuNPs, samples and controls of a similar make-up will be compared one after the other:

(1) **PEG+TZM vs. PEG-Mal+TZM (non-reduced and reduced) AuNPs:** generally there were no statistically significant increases in size following the addition of antibodies to Mal-PEGylated AuNPs, when compared to m-PEGylated controls, although there is still a noticeable increase in their size (**Figure 3-14 C and E**). This suggests that the EMCH linker used to introduce the Mal groups to NHS-PEGylated AuNPs increased the size of the AuNPs, albeit by a small amount. In comparison, there were minimal differences in dispersion between Mal-PEGylated AuNPs put into contact with antibodies (reduced or non-reduced) versus the m-PEGylated controls, with all of these samples showing PDI values on the order of magnitude of 0.2, which would suggest monodisperse AuNPs (**Figure 3-14 D**).

(2) **PEG-Mal (no antibodies) vs. PEG-Mal+TZM (non-reduced and reduced) AuNPs:** regardless of which antibody was added to Mal-PEGylated AuNPs, significant increases in size were reported for **all of these Mal-PEGylated AuNP samples** ($p=0.03$ for Mal 3% vs. Mal 3% TZM-Non Red, 0.04 for Mal 3% vs. Mal 3% TZM-Red, 0.006 for Mal 10% vs. Mal 10% TZM-Red, 0.04 for Mal 30% vs. Mal 30% TZM-Non Red, 0.04 for Mal 30% vs. Mal 30% TZM-Red), **except for 10% Mal-PEGylated AuNPs** incubated with non-reduced antibodies (**Figure 3-14 C**). As ethanolamine was added to the Mal-transformed PEGylated AuNPs to block any NHS groups that did not react with EMCH, these consistent increases in size, even in the presence of non-reduced antibodies, could suggest two things. **First, partial NSA** between PEG and non-reduced antibodies may have occurred, similar to before when characterizing by DLS randomly oriented-prepared functionalized AuNPs (Figure 3-9). **Second, a partial opening of the hinge region disulfide bridges** of intact non-reduced antibodies may have occurred (due to an equilibrium exchange releasing free thiols), which could have temporarily exposed SH groups from hinge region, allowing Mal groups on PEGylated AuNPs to react with them. There is a partial equilibrium between oxidized disulfide

bridges and free thiols, which can be altered by their microenvironment, such as pH [193]. In contrast, the PDI values of 3%, 10% and 30% Mal-PEGylated AuNPs in the absence of antibodies were significantly reduced (by a significant degree for two samples, namely $p=0.03$ for 10% Mal vs. 10% Mal TZM-Non Red and 0.04 for 10% Mal vs. 10% Mal TZM) once reduced or non-reduced antibodies were added to them (**Figure 3-14 D**). This suggests NSA of Mal-transformed PEGylated AuNPs to the walls of the polystyrene tubes (used for incubation) via hydrophobic interactions mediated by either the Mal groups or the EMCH linker. Hydrophobic interactions between biomolecules and labware has been shown in research, where Goebel-Stengel et. al (2012) [194] demonstrated the need to choose the right labware to work with more hydrophobic biomolecules that can more readily adsorb to polystyrene.

(3) **PEG-Mal Blocked+TZM (non-reduced) vs. PEG-Mal+TZM (non-reduced and reduced) AuNPs:** significant difference in size were reported for 30% Mal-PEGylated AuNPs conjugated to either reduced or non-reduced antibodies ($p=0.04$ and 0.03, respectively), when compared to antibodies adsorbed to cysteine-blocked 30% Mal-PEGylated AuNPs (**Figure 3-14 E**). This shows that cysteine was adequate for blocking Mal groups, and confirms that antibodies (non-reduced or reduced) could only have adsorbed to PEG or covalently conjugated to Mal groups via their reduced disulfide bridges, hence confirming what was discussed in (2).

(4) **PEG-Mal+TZM Non-Reduced vs. PEG-Mal+TZM Reduced AuNPs:** as was discussed in (2), minimal variations in size were observed between PEGylation and post-addition of antibodies (**Figure 3-14 E**). Despite the possible equilibrium exchange between oxidized disulfide bridges and reduced free thiols leading to covalent conjugation of non-reduced antibodies to Mal-PEGylated AuNPs, it appears that the increases in size of Mal-PEGylated AuNPs conjugated to reduced antibodies are slightly higher (**Figure 3-14 C**). The differences in resultant size between reduced and non-reduced antibodies conjugated to Mal-PEGylated AuNPs are logical given their huge difference in reduced antibody concentrations.

(5) **Set of PEG-Mal+TZM Non-Reduced AuNPs:** minimal differences in size and dispersion were observed after putting non-reduced antibodies into contact with 3% or 10% Mal-PEGylated AuNPs (**Figure 3-14 E**). This suggests either a saturation in the yield of conjugated antibodies at 3% Mal-PEGylated AuNPs, or a roughly equal contribution to the overall size change of AuNP samples from both NSA and covalent conjugation via partial reduction of non-

reduced antibodies. In comparison, 30% Mal-PEGylated AuNPs put into contact with non-reduced antibodies saw a significant difference in their overall size change when compared to both 3% and 10% Mal-PEGylated AuNPs (p=0.04 and 0.04, respectively) (**Figure 3-14 E**). This could suggest more NSA, or more covalent conjugation via partial reduction, both of them resulting in a higher yield.

(6) **Set of PEG-Mal+TZM Reduced AuNPs:** statistically significant increases in size were observed between 30% Mal-PEGylated AuNPs and 3% or 10% Mal-PEGylated AuNPs (p=0.04 and 0.01, respectively) (**Figure 3-14 E**). These significant differences at 30% maleimide follow the trend seen in (5) for non-reduced antibodies, and could be explained by more NSA or covalent conjugation of antibodies. However, given the statistically significant increase for 3% Mal-PEGylated AuNPs conjugated to reduced antibodies between PEGylation and addition of antibodies (p=0.001) (**Figure 3-14 E**), it is possible that a saturation in yield (based on size increase) may already have occurred at this lower percent composition of Mal.

b) ZP Measurements

To characterize the changes in surface charge of antibody-conjugated, Mal-PEGylated AuNPs, ZP measurements were obtained for the same set of samples previously prepared for DLS characterization. The results of this characterization can be seen in Figure 3-15:

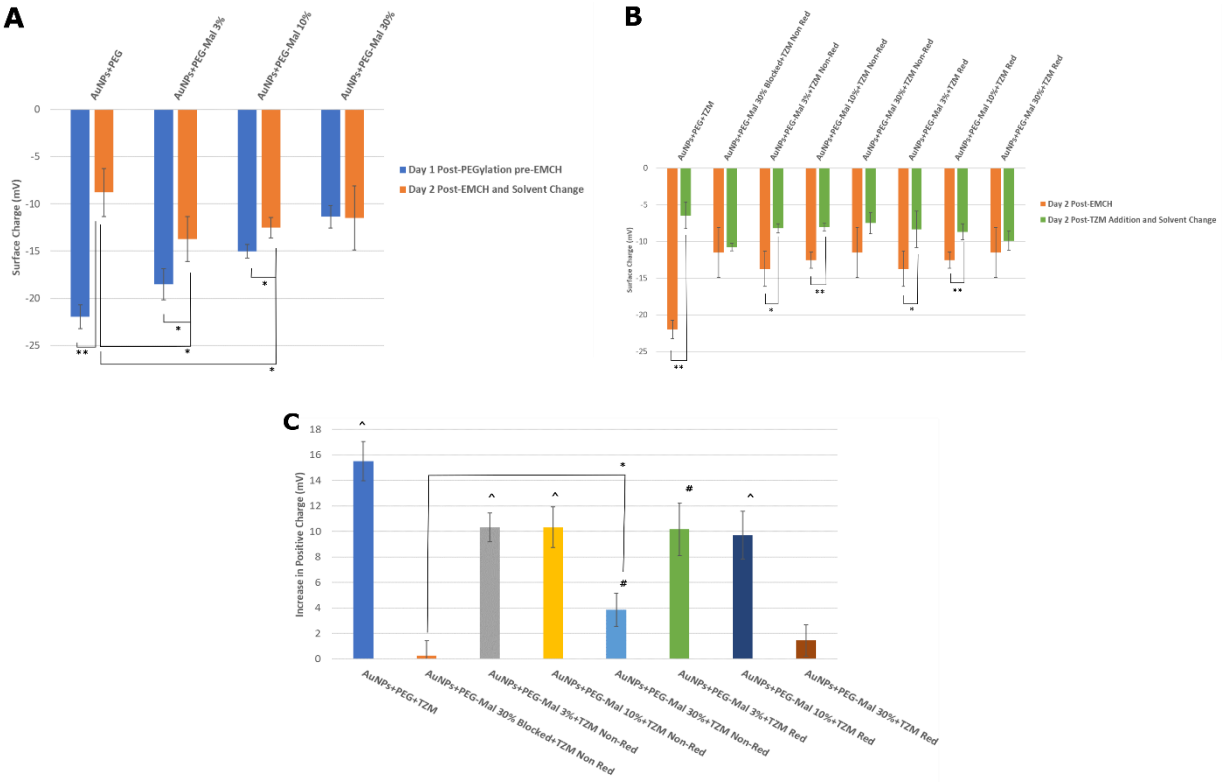

Figure 3-15 Semi-oriented strategy ZP results for: (A) change in surface charge pre- and post-EMCH reaction, (B) change in surface charge of EMCH-transformed AuNPs pre- and post-addition of antibodies, (C) overall change in surface charge for functionalized AuNPs between post-PEGylation (pre-EMCH) and post-addition of antibodies. Controls of methoxy- and/or Mal-PEGylated AuNPs are included. Samples are labelled as previously. Values represent averages of three replicates and error bars show deviation. Asterisks * and ** in (A–C) indicate statistically significant differences at p<0.05 and 0.01, respectively, and brackets compare the two samples for which the difference is significant. For (C), # and ^ depict statistically significant increases (p<0.05 and 0.01, respectively) comparing subtracted surface charge post-PEGylation (pre-EMCH reaction) to final surface charge post-antibody addition.

To analyze the results from the ZP characterization of antibody-conjugated, Mal-PEGylated AuNPs, samples and controls of a similar make-up will be compared one after the other:

(1) **PEG+TZM vs. PEG-Mal+TZM (reduce AuNPs:** No statistically significant differences in surface charge were observed between these two (**Figure 3-15 A and C**). Knowing the effect of Tween-20 on screening the ZP of PEGylated AuNP samples in the presence of antibodies

(as discussed in Section 3.3.1 b)), minimal conclusions can be drawn here as it is difficult to discern between different samples on the basis of surface charge.

(2) **PEG-Mal (no antibodies) vs. PEG-Mal+TZM (non-reduced and reduced) AuNPs:** for both percent compositions of 3 and 10% Mal, there are statistically significant increases in positive charge upon conjugating either non-reduced or reduced antibodies to them (p=0.03 for 3% Mal vs. 3% Mal+TZM Non-Red, 0.04 for 3% Mal vs. 3% Mal+TZM Red, 0.004 for 10% Mal vs. 10% Mal+TZM Non-Red, and 0.006 for 10% Mal vs. 10% Mal+TZM Red) (**Figure 3-15 B**). However, knowing the effect of Tween-20, and based on the lack of differences in surface charge for 3 and 10% Mal-PEGylated samples conjugated to reduced or non-reduced antibodies (**Figure 3-15 B**), minimal conclusions can be drawn here.

(3) **PEG-Mal Blocked+TZM (non-reduced) vs. PEG-Mal+TZM (non-reduced and reduced) AuNPs:** only significant increase in positive charge was seen for 30% Mal-PEGylated AuNPs incubated with non-reduced antibodies relative to cysteine-blocked 30% Mal-PEGylated AuNPs (p=0.02), but few conclusions can be drawn here, as Tween-20 likely screened the surface charge of Mal-PEGylated AuNPs incubated with antibodies (**Figure 3-15 C)**.

(4) **PEG-Mal+TZM Non-Reduced vs. PEG-Mal+TZM Reduced AuNPs:** same conclusions drawn in (1).

(5) **Set of PEG-Mal+TZM Non-Reduced AuNPs:** same conclusions drawn in (1).

(6) **Set of PEG-Mal+TZM Reduced AuNPs:** same conclusions drawn in (1).

3.4.2 Stability of Antibody-Conjugated, PEGylated Gold Nanoparticles

A stability assay similar to the one conducted for the randomly oriented strategy was also set up to evaluate the stability of antibody-conjugated, PEGylated AuNPs prepared via the semi-oriented strategy. These results can be seen in Figure 3-16. Based on the results of DLS and ZP characterization, 30% Mal-PEGylated AuNPs were chosen. MQ was also not tested as an incubation buffer for addition of antibodies to PEGylated AuNPs, and this decision was made based on the results of the stability assays for the randomly oriented strategy (Section 3.3.2). An overview of the samples and conditions tested is provided in Table 3-10:

Table 3-9 List of monofunctional methoxy- and bifunctional Mal-PEGylated AuNP samples incubated with their respective antibodies, alongside controls and incubation conditions tested during the stability assay. Please note that all samples were washed with citrate prior to PEGylation.

Sample	PEG Composition	Solvent	Type of Antibody
(+)	None	MQ	None
(-)	None	PBS	None
PEG+PBS	100% mPEG-SH	PBS	None
PEG+Tween-20	100% mPEG-SH	PBS+Tween-20	None
PEG+TZM+PBS	100% mPEG-SH	PBS	Non-Reduced
PEG+TZM+Tween-20	100% mPEG-SH	PBS+Tween-20	Non-Reduced
Mal+TZM+PBS	30% Mal-PEG-SH, 70% mPEG-SH	PBS	Reduced
Mal+TZM+Tween-20	30% Mal-PEG-SH, 70% mPEG-SH	PBS+Tween-20	Reduced

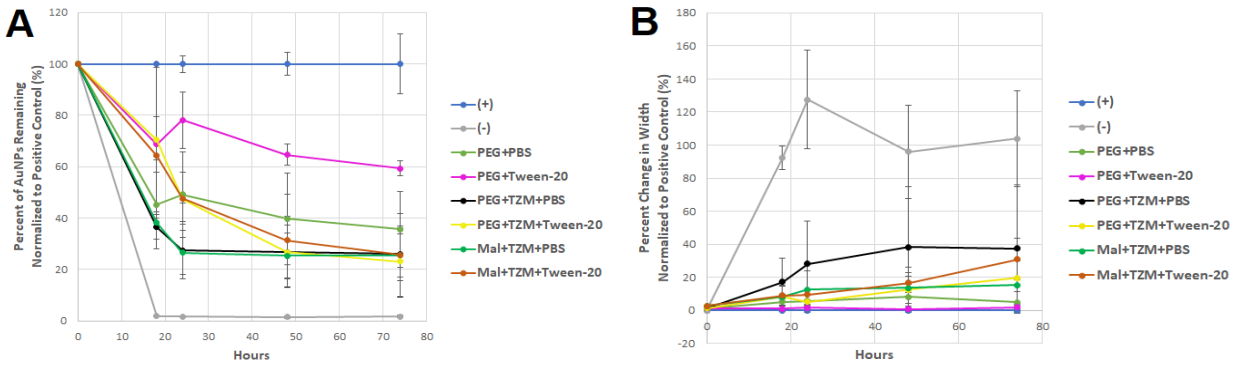

Figure 3-16 Stability curves of Mal- and m-PEGylated AuNPs conjugated to antibodies for: (A) normalized percentage of AuNPs remaining calculated from the relative amplitudes of their SPR peaks, and (B) normalized percent change in FWHM of AuNP SPR peaks. Values represent averages of six replicates from two repeats (2x3 replicates), and error bars show standard deviation.

Based on the results from these stability assays, the following observations can be made:

(1) **Amplitude Curves in Figure 3-16 A:** for all three samples (PEG, PEG+TZM, Mal+TZM) incubated in PBS+Tween-20, there is a noticeable increase in the number of AuNPs retained in the first 24 hours of the experiment, when compared to the same three samples incubated in just PBS. This suggests that Tween-20 helped reduced AuNP loss resulting from NSA against the walls of both the plasticware used to prepare these samples, as well as the walls of the 96-

well plate used for the absorbance measurements. Tween-20 stabilized AuNP:antibody conjugates in solution, preventing aggregates from forming against the walls of this labware.

(2) **Width Curves in Figure 3-16 B:** there is a larger initial increase in the widths of the SPR peaks of the three samples (especially PEG+TZM) incubated in just PBS compared to the same set incubated in PBS+Tween-20. This observation could likely be explained by the same reason suggested in (1). However, over time there is a considerable increase in the widths of PEG+TZM and Mal+TZM incubated in PBS+Tween-20, similar to what was seen in Section 3.3.2. This may suggest that prolonged exposure of these AuNPs to Tween-20 in the presence of antibodies could have caused their aggregation. One explanation, besides Tween-20 interacting with the AuNPs, is antibody aggregation from Tween-20 could have resulted in a downstream chain of events causing further aggregation of AuNPs. As Tween-20 did not affect the dispersion of PEGylated AuNPs in the absence of antibodies, this latter explanation would be more logical. Therefore, it would be advisable to avoid prolonged storage of antibody-conjugated, PEGylated AuNPs incubated in Tween-20 following their incubation reaction.

3.5 Oriented Strategy for Antibody Conjugation

Note: Further details on the methods used for this strategy can be found in Appendix I.

This section will examine the oriented strategy. An overview of the procedure employed to PEGylate AuNPs, prepare them for antibody conjugation, and conjugate them to oxidized antibodies is shown in Figure 3-17. This strategy targeted the sugar moieties of the Fc region of antibodies for functionalizing PEGylated AuNPs. This approached looked to selectively target the Fc region, in order to minimize the risks of the conjugation strategy impairing the activity of the Fab region. To realize this strategy, the following steps were carried out:

(1) Boc-hydrazine-PEGylated (Hyd-PEG-SH) AuNPs were prepared similarly to previous PEGylation protocols

(2) Boc-groups removed by acid deprotection to expose hydrazide groups

(3) (a) Periodate oxidation of glycosylated region of antibodies followed by (b) their conjugation to hydrazide-PEGylated AuNPs

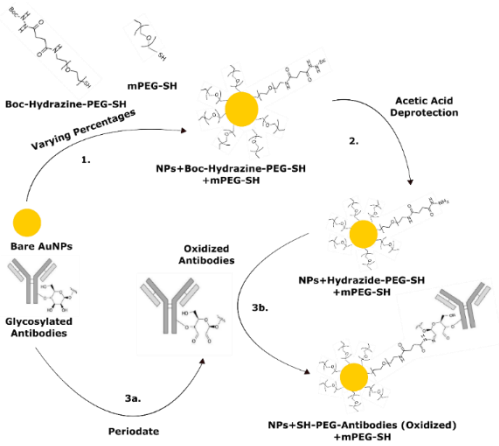

Figure 3-17 Schematic showing a stepwise overview of the chemistry employed to biofunctionalize AuNPs via an oriented strategy.

For this strategy, preliminary results obtained from characterizing oxidized antibodies will be solely discussed. Due to time constraints, as well as several concerns related to the oxidation of antibodies (which will be discussed in more detail in this section), the final conjugation of oxidized antibodies to hydrazide-PEGylated AuNPs was not explored.

3.5.1. Oxidation of Antibodies

To oxidize antibodies, periodate was used to target the glycosylated region of the antibodies, by following a procedure similar to that conducted by and Kumar et. al (2008), as well as Hermanson (2013) [156]. Due to concerns of over-oxidizing this region (as was discussed in Section 2.3.3 c)) resulting in cross-linking between antibodies, only mild conditions were employed (10 mM, room temperature, 30 min incubation). Following oxidation, antibodies were purified by size-exclusion chromatography (SEC), to: (1) characterize the number of stable oxidized antibodies retained, (2) separate excess, unreacted periodate on the basis of differences in size between salt and antibodies. They were then re-concentrated, and further characterized.

3.5.2. Characterization of Oxidized Antibodies

Oxidized antibodies were characterized by four different techniques: (1) absorbance 280 nm (A280) measurements from the SEC chromatograms, (2) A280 measurements following their

re-concentration, (3) Purpald® assay measuring the number of free aldehydes generated from their oxidation, and (4) SPR sensorgrams measuring the affinity for their receptor Her2.

a) Chromatograms of Oxidized Antibodies Compared to Standards

The reason for characterizing oxidized antibodies as they eluted from the SEC column was to identify any losses of antibodies by quantifying their eluted concentration via integration of their A280 peaks (compared to a standard curve of non-oxidized antibodies), in order to compare with the starting concentration used for periodate oxidation. The overlayed chromatograms of oxidized antibodies compared to these standards can be seen in Figure 3-18:

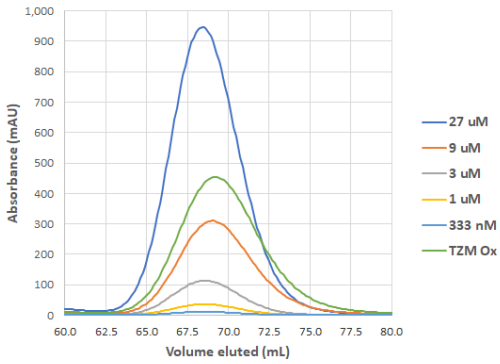

Figure 3-18 Chromatograms (A280 curves) of collected fractions for TZM standards and oxidized TZM (prepared at 27 μM) that eluted from the SEC column.

It is worth noting that a starting concentration of 27 μM was employed for periodate oxidation. Thus, based on Figure 3-18, there is already a reduction in the height of the A280 peak for oxidized antibodies compared to their non-oxidized counterpart. As it would be implausible to suggest that nearly half of these antibodies were lost over during their oxidation and purification, it would be more sensible to suggest that other factors could explain the drop in the A280 peak height of oxidized antibodies compared to their non-oxidized counterpart.

b) UV-VIS Absorbance Measurement of Re-Concentrated Oxidized Antibodies

To further characterize these oxidized antibodies, re-concentration of the SEC-eluted fraction collected was performed by centrifuging the eluate, and measuring the absorbance spectra of the re-concentrated retentate (compared to a standard). As SEC dilutes protein samples as they pass through the column, this step served to backcheck with the A280 chromatograms to look for

similar observations seen in a), and provide another data point for measuring and comparing between the two [195]. The results of these absorbance spectra can be seen in Figure 3-19:

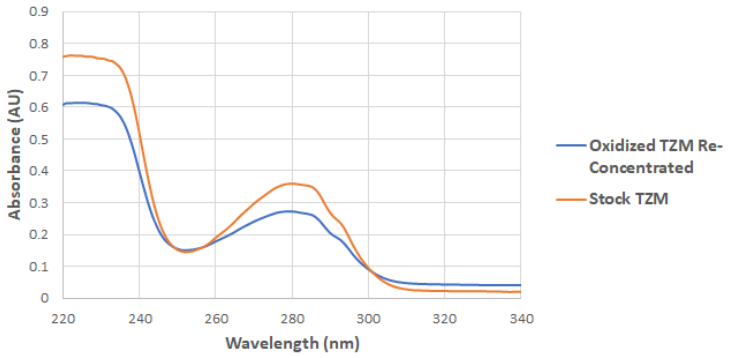

Figure 3-19 UV-VIS absorbance curves of oxidized TZM SEC fraction re-concentrated with an Amicon™ centrifuge filter (30 kDa MWCO), and compared to stock TZM (27 μM).

Based on a reduction in the peak height of the spectra of oxidized antibodies, a similar observation to A280 SEC chromatograms can be made (Figure 3-19). This suggests that other factors, such as the harshness of the oxidation conditions employed, may have resulted in a reduction in the height of the spectra of oxidized antibodies. In fact, literature has shown that under periodate oxidation conditions, factors such as concentration, length of reaction and ratio of periodate to antibodies can result in an over oxidation of antibodies, by not only targeting the sugar moieties of the glycosylated region, but also amino acid residues susceptible to oxidation, such as serine, threonine and tyrosine [155]. It is particularly oxidation of tyrosine residues that could explain the drop in the heights of the A280 peaks. Although this would imply that not as many antibodies have been lost as previously presumed, there is a possibility that the biological activity of these oxidized antibodies has been reduced due to an impairment of amino acid residues that could be responsible for binding to the receptor of this antibody.

Compiling the concentrations of oxidized antibodies calculated by: (1) A280 chromatogram peak height, (2) A280 chromatogram peak integration, and (3) A280 of re-concentrated fraction, the concentration of oxidized antibodies retained was calculated in Table 3-10:

Table 3-10 Concentrations of oxidized TZM recovered calculated either by: (A) linear regression analysis of integrated chromatograms from TZM standard curves in Appendix I (Figure 5-6),

following injection and elution from SEC column, and (B) UV-VIS A280 measurement following re-concentration of the SEC fraction collected.

Method	Concentration (μM)
Standard Curve Height	13.0
Standard Curve Area under the Curve	15.1
UV-VIS Absorbance of Re-Concentrated Fraction	20.3
Average:	16.1
Percent Yield Relative to Stock TZM:	60%

c) Purpald Assay to Quantify Oxidized Antibodies

Purpald®'s reagent (4-amino-3-hydrazino-5-mercapto-1,2,4-triazole) is a reagent that forms a purple colour upon reacting with free aldehydes. It can react with oxidized antibodies containing free aldehydes, in order to provide a quantification of the number of oxidized sugars per antibody. A protocol outlined by Quesenberry and Lee (1996) was used for this assay [196].

Unfortunately, due to several issues related to this procedure, desirable results were not acquired for this assay to be able to accurately quantify the number of oxidized sugars per antibody following periodate oxidation. First, due to concerns over the toxicity of the formaldehyde standard employed in this assay by Quesenberry and Lee [196], benzaldehyde was chosen instead, and behaved sub-optimally, likely due to precipitation between it and Purpald®'s reagent. It is worth noting that both structures have aromatic rings, which could likely explain their precipitation due to the formation of π-π interactions with each another. A decrease in the solubility of aromatic complexes formed via π-π interactions (in certain solvents) and its interference with spectrophotometric measurements, have been previously noted by other researchers, and could thus partially explain the issues related to using benzaldehyde with Purpald®'s reagent [197]. Although acetaldehyde was then chosen as a standard to replace benzaldehyde, Purpald®'s reagent did not react readily with the oxidized antibodies, suggesting that either further modifications to the procedure would be needed, in order to optimize its reaction kinetics, or a better reagent for detecting free aldehydes from oxidized antibodies would be needed [198]. Contrary to what was noted by Kumar et. al (2008) [156], who also employed a Purpald® assay to quantify oxidized antibodies, the reagent reacted very slowly (>24h) with oxidized antibodies. Due to time constraints

with the remainder of this thesis work, alternative strategies for quantifying the number of oxidized sugars per antibody, or troubleshooting the existing protocol, were never attempted.

d) SPR Sensorgrams to Evaluate Activity of Oxidized Antibodies

Considering the results from the chromatograms and absorbance measurements of oxidized antibodies, concerns were raised over a decrease in activity resulting from periodate-targeting of amino acid residues. Thus, to quantify any changes in activity of oxidized antibodies, SPR was chosen to evaluate the binding affinity between oxidized antibodies (TZM) and their receptor, Her2, and compare them with non-oxidized antibody standards. Closely following a procedure outlined in Analytical and Bioanalytical Chemistry (2018) [199], oxidized antibodies were injected over a layer of Her2 receptors immobilized to a dextran-covered gold surface, and the response change upon binding allowed for an estimation of the activity of oxidized antibodies to be compared with non-oxidized antibody standards. Between each injection, antibodies were dissociated from the receptors by adding 10 mM glycine-HCl (pH 1.5). Oxidized antibodies were also tested at different concentrations in order to take into account any diffusive effects that could impact the binding affinity between oxidized antibodies and Her2, as well as to provide more data points for the sake of averaging. The results from this experiment can be seen in Figure 3-20:

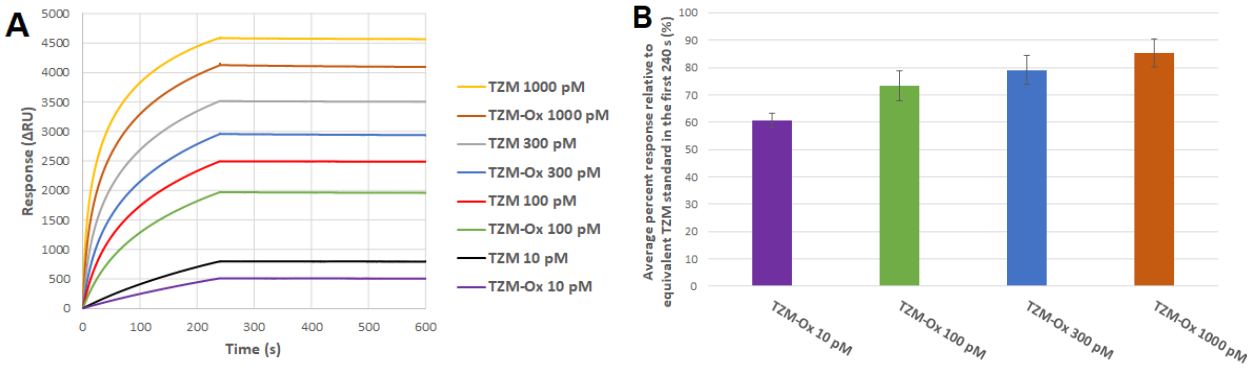

Figure 3-20 (A) Sensorgrams of antibody standards vs. oxidized antibodies and (B) percent response of oxidized antibodies retained relative to equivalent antibody standard, based on the first 240 s of injection, for SPR experiment injecting antibodies onto Her2 receptors immobilized on a dextran-covered gold surface. Curves in (A) represent average of three separate measurements, with error bars omitted for clarity. Bars in (B) represent average of 2400 data points in 240 s interval, and error bars represent standard deviation of these data points.

Based on the sensorgrams in Figure 3-20 A and the percent response of oxidized antibodies relative to antibody standards in Figure 3-20 B, there appears to be a slight reduction in the binding affinity between oxidized antibodies and their receptor, at least in terms of initial binding kinetics. Based on the linear response in the first 100 s for oxidized and standard antibodies at 10 pM in Figure 3-20 A, the activity of these oxidized antibodies is roughly 60% of standard antibodies, based on Figure 3-20 B, as its response is more proportional to the antibody concentration bound to Her2. Linear responses for SPR can be more easily observed at lower concentrations of analyte being injected above a surface, as diffusion will limit the rate at which antibodies bind to Her2, thereby preventing the surface from being saturated too quickly and generating a non-linear response [200, 201]. Regardless of a precise determination of the binding affinity constant, it appears that periodate oxidation impacted the binding affinity of oxidized antibodies for their receptors. This would be most likely explained by the same factors previously discussed regarding the chromatograms and UV-VIS absorbance spectra. It is most probable that the periodate oxidation conditions employed were not as mild as had been conceived, as harsh conditions can impact the biological activity of antibodies [202].

3.6 Comparison Between Antibody Conjugation Strategies

Four techniques, namely: (1) UV-VIS absorbance spectra measurements, (2) indirect quantification of number of antibodies per AuNP, (3) direct quantification of number of antibodies per AuNP, and (4) quantification of number of functionalized AuNPs per cancer cell, served to compare between the randomly oriented and semi-oriented strategies, while evaluating in parallel NSA of antibodies to m-PEGylated AuNPs. These four respective techniques will be discussed in the same order as above for this section.

3.6.1. Functionalized AuNP Concentrations Measured via UV-VIS Absorbance

Following preparation of either antibody-conjugated, heterobifunctional PEGylated AuNPs or antibodies adsorbed to m-PEGylated AuNPs, their UV-VIS absorbance spectra were acquired and compared to controls of bare AuNPs and m-PEGylated AuNPs, in order to estimate their concentrations by comparing their peak heights to one another. The results of these measurements can be seen in Figure 3-21:

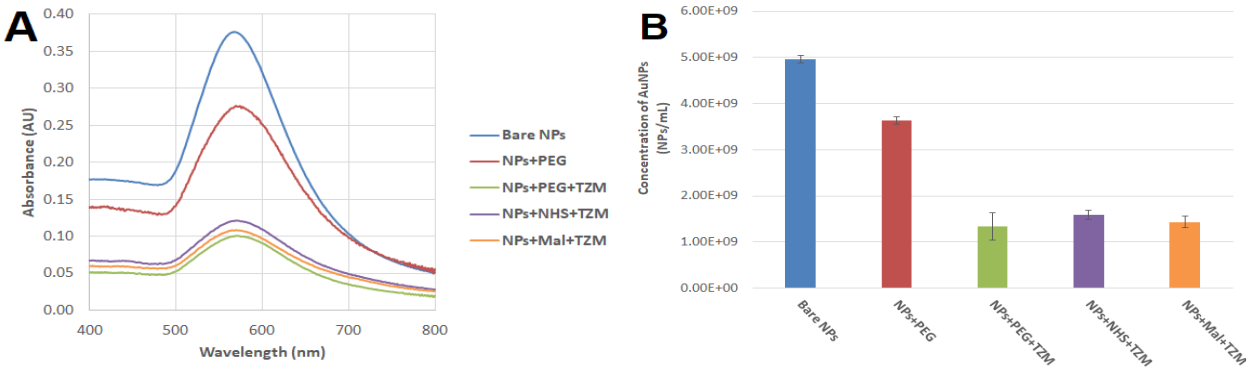

Figure 3-21 Characterization of the number of antibody-functionalized AuNPs recovered following incubation with antibodies based on their: (A) UV-VIS absorbance spectra and (B) calculated concentrations extracted from their SPR peak maxima and divided relative to a reference standard of bare AuNPs. Abbreviations mean the following: PEG – 100% mPEG-SH, NHS – 30% NHS-PEG-SH and 70% mPEG-SH, Mal – 30% Mal-PEG-SH and 70% mPEG-SH, TZM – incubation with 800 nM TZM antibodies (non-reduced or reduced). Concentration and curve values represent average of three replicates, and error bars represent standard deviation. Standard deviations for UV-VIS absorbance curves are omitted for clarity.

Moreover, these absorbance results were used to calculate the concentrations of biofunctionalized AuNPs by comparing their SPR peak values to the standard of bare AuNPs, which provided a yield and allowed for losses of biofunctionalized AuNPs (from all the steps required to prepare them) to be quantified. This SPR peak value-calculated concentration was also used to **estimate the number of theoretically available PEG functional groups** (NHS or maleimide) that could covalently conjugate with non-reduced or reduced antibodies, based on the two formulas shown in Equation 2 and Equation 3. Note that the ratio of PEG molecules per NP surface area was assumed to be 1 PEG per nm^2 (based on literature), and was thus fixed at 31 416 PEG molecules per AuNP, which corresponds to the surface area of 100 nm AuNPs [93].

$$C_{FG}\ (nM) = \frac{\left(\#\frac{PEG}{NP}\right) * \left(C\frac{NPs}{mL}\right) * 1000 * 10^9 * (\%\ HBF\ PEG)}{N_A}$$

Equation 2 Formula employed to estimate the number of theoretically available PEG functional groups (NHS or maleimide) on the surfaces of (concentration-measured) PEGylated 100 nm

AuNPs. Acronyms mean: *FG – functional groups, C – concentration, HBF – heterobifunctional, N_A – Avogadro's number.*

3.6.2. Indirect Quantification of Functionalized NPs via ELISA

Note: Further details on the methods used for this technique can be found in Appendix J.

An ELISA was performed on the supernatants withdrawn from washed antibody-conjugated, PEGylated AuNPs. Antibody-conjugated, PEGylated AuNPs at an initial percentage of 30% NHS-PEG-SH were prepared by both the randomly oriented and semi-oriented strategies, and were compared to m-PEGylated AuNPs non-specifically adsorbed to antibodies. Incubation buffers of PBS with or without Tween-20 were also compared in order to evaluate the extent of NSA of antibodies to AuNPs under both conditions. This assay allowed for the concentration of excess free antibodies remaining in the supernatant to be calculated, and compared with the starting incubation concentrations of antibodies. **This thus provided an indirect quantification** of the total number of antibodies bound per AuNP (whether conjugated or non-specifically adsorbed) to be determined. At the same time, based on the estimated concentration of functional groups able to covalently conjugate with antibodies in these biofunctionalized AuNPs (based on Equation 2), the extent of covalent conjugation of antibodies to AuNPs could be calculated via Equation 3, **by assuming each antibody could only covalently conjugate to one functional group**. This estimation of covalent conjugation of antibodies to biofunctionalized AuNPs allowed for a ratio to non-specifically adsorbed antibodies (calculated by subtracting estimated number of covalently conjugated antibodies from total number measured by ELISA) to be determined. The results of this indirect quantification via ELISA can be seen in Figure 3-22 and Figure 3-23, respectively:

$$\#\ Covalently\ Conjugated\ TZM\ per\ AuNP = \frac{C_{FG}\ * 10^{-9} * N_A}{(C\ of\ Func\ NPs/mL) * 1000}$$

Equation 3 Formula employed to calculate number of covalently conjugated antibodies per AuNP, based on Equation 2-calculated concentration of functional groups available, and SPR peak-measured concentration of biofunctionalized AuNPs. Acronyms mean: *C – concentration, FG – functional groups, N_A – Avogadro's number, Func – biofunctionalized.*

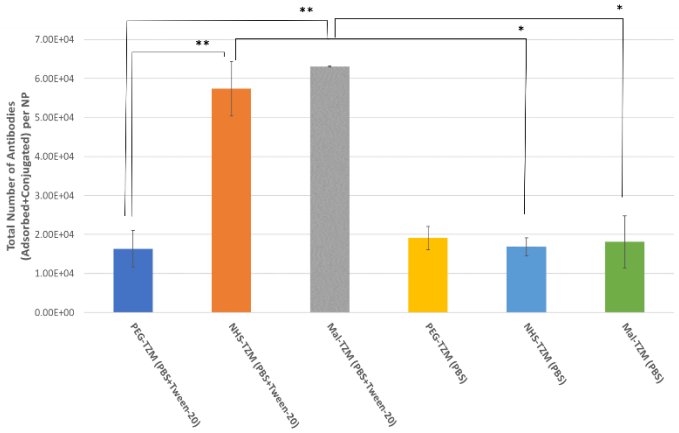

Figure 3-22 Indirectly calculated number of antibodies conjugated and/or adsorbed to various functionalized and PEGylated AuNPs, as obtained through ELISA assays performed on the supernatants collected from functionalized samples incubated overnight. Averages represent triplicates, and error bars represent standard deviation. Asterisks * and ** indicate statistically significant differences at $p<0.05$ and 0.01, respectively, and brackets compare the two samples for which there is a statistically significant difference.

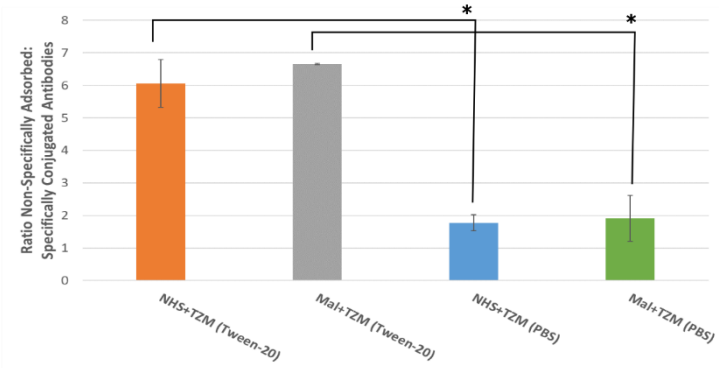

Figure 3-23 Estimated ratio of non-specifically adsorbed antibodies to conjugated antibodies based on ELISA-mediated indirect quantification of total number of immobilized antibodies on antibody-functionalized, PEGylated AuNPs. Averages represent triplicates, and error bars represent standard deviation. Asterisk * indicates a statistically significant difference at $p<0.05$ and brackets compare the two samples for which there is a statistically significant difference.

Regarding Figure 3-22, the presence of Tween-20 in PBS for incubating antibodies with either NHS- or maleimide-PEGylated AuNPs had a statistically significant effect on the number of

antibodies bound to AuNPs (p=0.04 for NHS-TZM+Tween-20 vs. NHS-TZM+PBS and 0.03 for Mal-TZM+Tween-20 vs. Mal-TZM+PBS). Thus, the presence of Tween-20 in the incubation solvent could have resulted in a reduced loss of antibodies due to NSA with the labware used to incubate them with PEGylated AuNPs. Hence, a greater retention of antibodies that could have interacted with the PEGylated AuNPs would have resulted in a higher yield of antibodies per AuNP (as per the indirect calculations) based on a lower ELISA-measured signal from the supernatants. In comparison, **the lower indirectly calculated numbers of antibodies per AuNP for the three samples in PBS in the absence of Tween-20** (PEG+TZM, NHS+TM and Mal+TZM) would suggest a greater loss of antibodies from solution during incubation with AuNPs, due to NSA against the labware (Figure 3-22). Hydrophobic interactions between antibodies and polystyrene (the material of which the labware is comprised) have been demonstrated in previous studies, and thus the lower indirectly calculated ratios of antibodies per AuNPs (i.e. higher ELISA signal for supernatants) in PBS lacking Tween-20 are explainable [203].

For the set of samples incubated in PBS+Tween-20, significant differences in the number of antibodies per AuNP were reported between Mal+TZM and PEG+TZM (p=0.001), as well as NHS+TZM and PEG+TZM (p=0.009) (Figure 3-22). In this case, the addition of Tween-20 to the incubation solvent used to conjugate antibodies to m-PEGylated AuNPs therefore likely reduced the extent of NSA of antibodies to them. Alongside the significant differences between the Mal+TZM samples in the presence or absence of Tween-20 (p=0.03) and the NHS+TZM samples in the presence of absence of Tween-20 (p=0.04), this demonstrates the advantage of using Tween-20 to incubate antibodies with PEGylated AuNPs, as there are no detectable differences (via this indirect ELISA assay) between any of samples incubated in PBS without Tween-20 (Figure 3-22).

In contrast, Figure 3-23 highlights similar differences between biofunctionalized samples Mal+TZM and NHS+TZM incubated in the presence and absence of Tween-20 observed in Figure 3-22. Given that Figure 3-23 displays a theoretical estimation of the degree of NSA relative to covalent conjugation, based on Equation 2 and Equation 3, it is important to note the limitations of this method in distinguishing between non-specifically adsorbed and covalently conjugated antibodies, as an assumption was made that only one antibody could react with each available functional group (when it could have reacted with two neighbouring functional groups on the same AuNP or on separate AuNPs). Nevertheless, the same trend of PBS+Tween-20 improving the yield

of all antibodies (adsorbed and conjugated) bound to PEGylated AuNPs holds true, which would have likely skewed the adsorbed values towards higher numbers, due to a saturation of covalent conjugation sites. Given the order of magnitude of the total number of bound antibodies per AuNP indirectly calculated from the ELISA measurements of the supernatants (Figure 3-22), these higher skewed values of physically adsorbed antibodies are unsurprising.

For maleimide-PEGylated AuNPs conjugated to reduced antibodies, it is important to note that the presence of reduced half-antibody fragments in the ELISA assay may have skewed the results in favour of a higher indirect quantification of the number of immobilized antibodies. This is because the designed ELISA assay relied upon a sandwich of capture and detection antibodies lying underneath and above the antibodies recovered from the supernatants of samples. As half-antibody fragments contain one less Fc region to interact with other antibodies (antibodies interact with each other via this region), the affinity of reduced antibodies to both the capture and detection antibodies may have been reduced, resulting in a lower absorbance measurement for their respective supernatants, and thus an abnormally higher-calculated concentration of AuNP-bound antibodies indirectly quantified. An antibody with a lower binding affinity to either the capture or detection antibody is known in ELISA to reduce the signal generated, and for this reason higher affinity antibodies are preferred [204]. Although a reduced antibody standard curve was generated in order to improve the accuracy of characterizing functionalized AuNPs prepared via the semi-oriented strategy (see Appendix J-II), it had a minimal impact on the final calculated ratios of antibodies either non-specifically adsorbed to specifically conjugated to AuNPs.

3.6.3. Direct Quantification of Functionalized NPs via NanoOrange Assay

Note: Further details on the methods used for this technique can be found in Appendix K.

Based on the indirect quantification results, a more direct quantification assay was opted for in order to better estimate the number of antibodies bound to AuNPs. For this direct quantification assay, the colorimetric dye NanoOrange™ was chosen. A procedure described by Filbrun and Driskell was closely followed to carry out this assay [205]. Prepared antibody-functionalized AuNPs (incubated in PBS+Tween-20) were dissolved with potassium iodide (KI) and iodine (I_2), which helped to liberate antibodies immobilized onto the surfaces of these AuNPs.

This dye could then couple with free antibodies and generate a colorimetric signal based on fluorescence. The results of this quantification are shown in Figure 3-24:

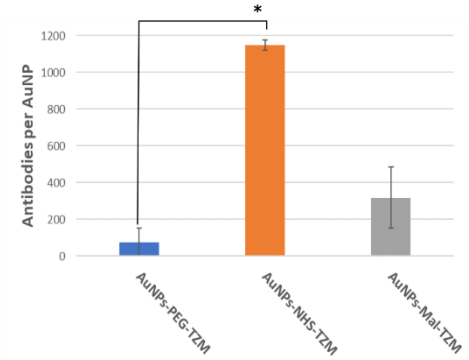

Figure 3-24 NanoOrange™ results quantifying the number of antibodies bound to AuNPs via: (1) adsorption onto m-PEGylated AuNPs, (2) conjugation to 30% NHS-PEGylated AuNPs, and (3) conjugation to 30% maleimide-PEGylated AuNPs Values represent averages of three samples each measured in triplicate on a 96-well plate (3x3 data points), and error bars show standard deviation. Asterisk * indicates a statistically significant difference at $p<0.05$ and brackets compare the two samples for which there is a statistically significant difference.

Interesting observations can be drawn from this assay. First, it appears that the randomly oriented strategy with NHS-PEGylated AuNPs had a higher yield of antibodies detected by the NanoOrange™ dye, when compared to the semi-oriented strategy with Mal-PEGylated AuNPs (Figure 3-24). Given that NHS groups can freely react with any amine group located on each antibody, these results are not surprising [126]. As Mal groups are restricted to reacting with the limited number of free thiols exposed from the hinge region of reduced antibodies, a lower yield of antibodies able to successfully conjugate to these groups is more likely [139]. Furthermore, re-oxidation of reduced half-antibody fragments may also pose a problem by reducing the number of reduced antibodies that could covalently bond to Mal groups, thereby further reducing the yield of antibodies functionalized to AuNPs via this semi-oriented strategy [144].

Despite these results for the two biofunctionalization strategies, it is worth noting that there was one deviation from the procedure described by Filbrun and Driskell [205]. Due to limitations with access to a fluorimeter, the fluorescence of the NanoOrange™-stained functionalized AuNPs was not measured, but instead two absorbance measurements were acquired at both the excitation

and emission wavelengths suggested by Filbrun and Driskell [205]. As AuNPs strongly absorb at both of these wavelengths (see reference spectra in Figure 3-21), fluorescence measurements would allow for the overlapping UV-VIS absorbance spectra of AuNPs and NanoOrange™ dye to be deconvoluted, as the emission spectra resulting from AuNP-dye complexes would only be measured by applying an emission wavelength filter, instead of measuring both AuNP and NanoOrange™ absorbance spectra at both wavelengths. In terms of mathematical processing of this spectral data, fluorescence measurements would thus be much simpler to analyze.

3.6.4. Quantification of Number of Functionalized NPs Bound to Cancer Cells

Note: Further details on the methods used for this technique can be found in Appendix L.

In order to evaluate the biological activity of these functionalized AuNPs, their ability to bind to cancer cells was tested by **incubating them with fixed cells, and visualizing them under a microscope by back-scattering**. This protocol was adapted from co-supervisor Michel Meunier's group, where AuNPs attached to cells were counted as bright white spheres hovering above demarcated cells (images are provided in Appendix L) [206]. **It is important to note that the same initial ratio of AuNPs incubated with cells, as well as the total number of cells, was held constant**. This was to prevent variables like diffusion from introducing any discrepancies in the results, and thus ensure that each functionalization strategy could be compared head-to-head.

Once again, antibodies adsorbed to m-PEGylated AuNPs were also prepared to compare their ability to bind to cancer cells. A control of bare AuNPs which are known to bind to cells in high numbers due to NSA [207], and a control of m-PEGylated AuNPs in the absence of antibodies (to assess a successful PEGylation), were both tested. Finally, functionalized AuNP samples were tested for their ability to bind to two different breast cancer cell lines, namely MDA-MB-231 and MDA-MB-453 (or 231 and 453 for short, respectively). These two respective cell lines are cited in the literature as expressing basal and enhanced levels of the Her2 receptor which is recognized and targeted by the antibodies bound to AuNPs (TZM) [23]. For the sake of simplicity, 231 and 453 will be designated as Her2 (-) and Her2 (+), respectively. The results of this AuNP:cell incubation experiment and the counting of AuNPs attached to cells can be seen in Figure 3-25:

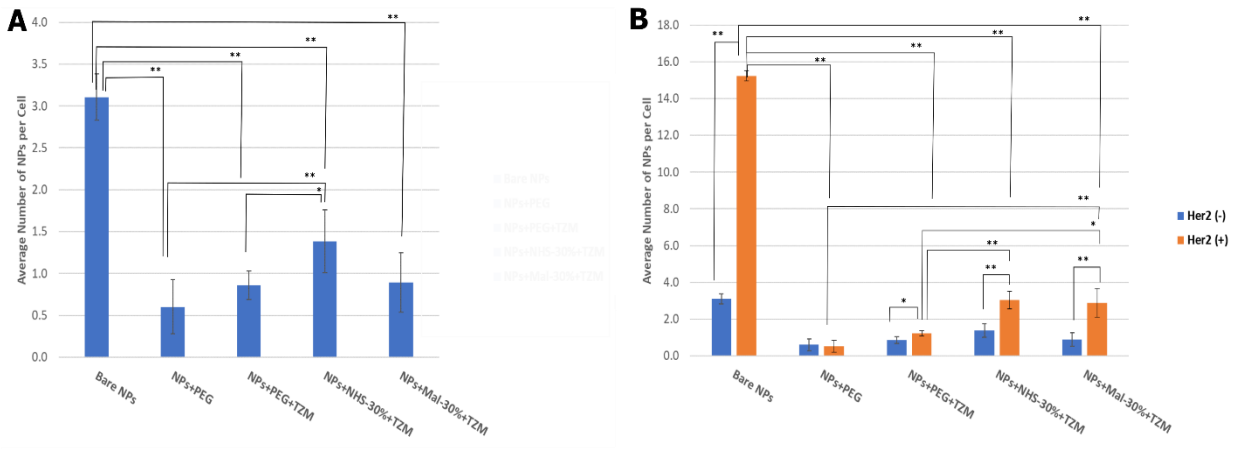

Figure 3-25 Average number of AuNPs bound per cancer cell for: (A) Her2 (-) (MDA-MB-231), and (B) Her2 (-) vs. Her2 (+) (MDA-MB-453). Averages represent two repeats of same experiment, each with a sample size of 30 imaged cells, and error bars indicate standard deviation. Asterisks * and ** indicate statistically significant differences at $p<0.05$ and 0.01, respectively, and square brackets compare the two samples for which there is a statistically significant difference.

Regarding controls, bare AuNPs unsurprisingly bind at a higher level to both Her2 (-) and (+) cancer cell lines, which indicates a lack of specificity between these AuNPs and cells, while the control of m-PEGylated AuNPs shows a nearly complete lack of binding between AuNPs and cells (Figure 3-25 A and B). The high binding of bare AuNPs to cells is consistent with the literature [207]. The lack of binding between m-PEGylated AuNPs and cells would be indicative of the protective effect of PEG against NSA of AuNPs to cells [185].

Regarding samples in Figure 3-25 A, biofunctionalized AuNPs prepared by the randomly oriented strategy (NHS-PEGylated) show a slightly increased ability to bind to the Her2 (-) cell line when compared to functionalized AuNPs prepared by the semi-oriented strategy (Mal-PEGylated). This observation is consistent with the results from the NanoOrange™ assay (Figure 3-24), indicating that there are likely more antibodies bound to NHS-PEGylated AuNPs than Mal-PEGylated AuNPs. The significant differences between covalently conjugated NHS+TZM or non-specifically adsorbed PEG+TZM ($p=0.02$) also suggest that there is a higher yield of biologically active antibodies bound to these biofunctionalized AuNPs (as previously shown in Figure 3-24). As Her2 (-) cell line is not a true Her2 negative control (as it expresses basal levels of it), the fact that there are noticeable differences at basal levels of Her2 expression between NHS-PEGylated

AuNPs and their two other antibody-bound PEGylated counterparts is promising for the potential applicability of these functionalized AuNPs to clinical settings involving breast cancer tissue [23].

In contrast, Figure 3-25 B shows significant differences in binding between Her2 (-) and Her2 (+) for all three antibody-bound PEGylated AuNP samples (p=0.02, 0.006 and 0.005 for PEG+TZM, NHS+TZM and Mal+TZM, respectively), with the largest differences being for covalently conjugated NHS- and Mal-PEGylated AuNPs, versus physically adsorbed m-PEGylated AuNPs. This is unsurprising given knowledge about the expression profiles of the Her2 (-) and (+) cell lines [23]. These antibody-conjugated, PEGylated AuNP samples prepared by the randomly oriented and semi-oriented strategies also show significant increases in their abilities to bind to the Her2 (+) cell line when compared to antibodies adsorbed to m-PEGylated AuNPs (p=0.003 and 0.01, respectively) (Figure 3-25 B). This observation would likely confirm that there is a higher yield of biologically active antibodies bound to PEGylated AuNPs prepared by these two strategies.

In contrast, the antibody functionalization strategies for AuNPs showed no differences in their ability to bind to the Her2 (+) cell line (Figure 3-25 B). However, when compared to the control of bare AuNPs, these two biofunctionalized AuNPs showed significant improvements in binding to the Her2 (+) cell line more specifically (p=5x10^{-5} for Mal+TZM vs. bare AuNPs and 2x10^{-4} for NHS+TZM vs. bare AuNPs), which indicates a greater control in specificity in binding to Her2. In addition, after considering the 4-fold higher yield of antibodies via the non-oriented strategy versus the semi-oriented strategy in the NanoOrange™ assay (Figure 3-24), **these similar levels of binding to cancer cells** for both functionalization strategies show that **both succeeded in yielding a similar number of biologically active AuNPs.**

To reiterate, the low binding between cells and m-PEGylated AuNPs without antibodies show that the PEGylation reduced NSA between AuNPs and cells. In contrast, significant differences for the Her2 (+) cell line between m-PEGylated AuNPs bound to antibodies and these two biofunctionalized AuNPs (p=0.01 for Mal+TZM vs. PEG+TZM and 0.003 for NHS+TZM vs. Mal+TZM) show an improved sensitivity compared to simply attaching PEGylated AuNPs to cells (Figure 3-25 B). This is promising in terms of potential applicability of these functionalized AuNPs to a clinical setting, where not only specificity in binding will be critical, in order to provide the most accurate diagnosis of breast cancer by these Her2-targeting AuNPs, but sensitivity in generating a signal that could be resolved from background noise such as autofluorescence [9] .

CHAPTER 4 GENERAL DISCUSSION

A general discussion of the major findings and takeaways from this thesis work will be provided, while drawing from the literature to make comparisons and justify the novelty of this work. Finally, an evaluation of the original thesis objectives in Chapter 1 will be provided.

4.1. Summary of Important Results

During this thesis work, two covalent conjugation strategies (randomly oriented and semi-oriented) for functionalizing AuNPs with cancer-detecting antibodies were explored in detail and optimized. A summary comparing these two types of antibody-bound, PEGylated AuNPs is provided in Table 4-1. This will provide a head-to-head comparison between these two on the basis of: (1) orientation of bound antibodies, (2) relative difficulty level for preparation, (3) length of time required for preparation, (4) optimal initial percent composition of heterobifunctional PEG according to characterization results, (5) relative stability, and (6) relative efficacy in terms of yield and activity according to quantification and cell experiment results.

Table 4-1 Overview of the two biofunctionalization strategies explored with a relative comparison of different parameters.

	NHS-PEGylated	**Maleimide-PEGylated**
Antibody orientation	Random via covalent conjugation	Semi-oriented via covalent conjugation
Relative difficulty level (number of steps)	Simple	Slightly harder
Preparation time	≈ 34 h	≈ 36 h
Optimal percentage	30% (Figure 3-9)	3% (Figure 3-14)
Relative stability	For incubation: PBS+Tween-20 For storage: PBS (Figure 3-12)	For incubation: PBS+Tween-20 For storage: PBS (Figure 3-16)
Relative efficacy (Figure 3-21 for yield, Figure 3-25 for activity)	Slightly higher yield; High activity	Slightly lower yield; High activity

During this thesis work, several takeaways resulted from this research. **First, non-specific adsorption was identified as a key challenge** in generating stable, well-characterizable functionalized AuNPs that were discernable from each other, as was shown during the DLS and ZP characterization of the controls of antibodies adsorbed to m-PEGylated AuNPs (Figure 3-8 and

Figure 3-10). Despite efforts to employ Tween-20, this NSA of antibodies could not be avoided, although it was reduced by a large extent once antibodies were incubated with PEGylated AuNPs during the conjugation steps (Figure 3-9 and Figure 3-14). However, these levels of non-specifically adsorbed antibodies seemed to have minimal impact on the final biological activity of the functionalized AuNPs (Figure 3-25). Stability assays also showed the advantages of employing Tween-20, and these experiments showed consistently that it could improve the stability of functionalized AuNPs (Figure 3-12 and Figure 3-16). Thus, for this particular application, it does not appear that the presence of non-specifically adsorbed antibodies on functionalized AuNPs is a pressing concern in terms of their biological activity and short-term stability.

In addition, **development of the randomly oriented strategy** showed that parameters influencing the activity and stability of biofunctionalized AuNPs could be controlled for during their preparation. These parameters included the initial percent composition of NHS-PEG-SH, which increased the size of the AuNPs (Figure 3-9), and selecting the optimal incubation solvent (by adding Tween-20) for antibodies, which minimized NSA of antibodies to labware or AuNPs (Figure 3-12). Additionally, employing a longer period of PEGylation with a higher concentration of PEG (Section 3.2) ensured that PEG could stabilize AuNPs and protect them against aggregation and/or NSA to labware (Figure 3-5 and Figure 3-6). Other details, like a re-activation step for NHS groups (Figure 3-7), also refined their development. By controlling all of these factors impacting the stability and biological activity of these functionalized AuNPs, their specificity in binding to cancer cells was improved (Figure 3-25). Although their yield decreased as per their UV-VIS absorbance spectra (Figure 3-21), this sacrifice of AuNPs (due to steps required to prepare them such as washing) for gains in their activity shows the importance of controlling the development of these nanoformulations. For breast cancer diagnostic applications, it is important to produce formulations that are stable, well-characterized and possess higher specificity [208]. Progress here thus is a good sign moving forward.

In comparison, **the semi-oriented strategy** was also optimized. To further develop these biofunctionalized AuNPs from re-activated NHS-PEGylated AuNPs, similar results were achieved in both stability and minimizing NSA (Figure 3-16), while improving their biological activity (Figure 3-25). Various parameters were optimized to achieve these results. First, Tween-20 was again identified as optimal for reducing NSA (Figure 3-16). Moreover, the initial percent

composition of NHS-PEGylated AuNPs transformed into Mal-PEGylated AuNPs could be lowered to 3%, as the resultant size of reduced antibodies per PEGylated AuNP ended up being higher at this percentage, indicating saturation of antibodies on AuNPs at higher percent compositions (Figure 3-14). There was even a yield of non-reduced antibodies that could graft to PEGylated AuNPs (albeit lower than reduced antibodies) at each percent composition (Figure 3-14). This observation hints at an alternate avenue for developing functionalized AuNPs that would be cost-effective and attractive from a commercial standpoint, as it would not require the purchase of the TCEP gel used to reduce antibodies (Appendix H-II). Although the yield of these functionalized AuNPs decreased as per UV-VIS absorbance results (Figure 3-21), no considerable losses in both stability (Figure 3-16) and specificity in biological activity (Figure 3-25) were detected. These results show that researchers should be controlling the development of biofunctionalized AuNPs. By optimizing the activity of antibodies functionalized to AuNPs to enhance their specificity and sensitivity, researchers can improve the clinical applicability of these nanoformulations [209].

Overall, the **functionalized AuNPs prepared via both strategies were successful in terms of their efficacy and stability**, while also being relatively easy to prepare. While it is worth noting that the stability of these functionalized AuNPs is short-term (<24h), as per the stability assays (Figure 3-12 and Figure 3-16), in the context of this particular application, these functionalized AuNPs could be prepared the day before their use, and applied to cells immediately after their preparation. Despite this constraint, yields of antibodies per AuNP for both strategies were high, as per the ELISA assays, showing that the chemistry was successful (Figure 3-22). In addition, their ability to bind to cancer cells in a specific manner, and improve sensitivity compared to m-PEGylated AuNPs, shows their promise as a clinical application for diagnosing breast cancer (Figure 3-25). As AuNPs are a popular material for diagnostic applications, this thesis work should help provide fundamental research related to developing them in a controlled manner [210].

4.2. Comparison to Literature

Functionalizing AuNPs with antibodies, whether it be for diagnostic or therapeutic end goals, is not a novel idea in research. However, this thesis work advances the field of AuNP functionalization in four key ways, namely:

(1) Optimizing the biofunctionalization of larger AuNPs of 100 nm here, while past research has focused on smaller AuNPs whose surface properties are better understood and who can more easily be covered with PEG to confer protective steric effects against aggregation and NSA of biomolecules such as antibodies [98, 211, 212].

(2) Providing a more in-depth characterization of the physical and chemical properties of biofunctionalized AuNPs, which allowed for their effects on yield and biological activity to be established. In contrast, past literature did not explore as exhaustively these inherent properties for each functionalization strategy, and instead focused on applications of biofunctionalized AuNPs by comparing different strategies head-to-head [78, 213, 214].

(3) Minimizing NSA of antibodies to AuNPs by optimizing the PEGylation and incubation conditions, and showing how this can adversely impact biological activity and yield of antibodies per AuNP (Figure 3-22, Figure 3-24 and Figure 3-25). In comparison, past literature has studied the physical adsorption of antibodies against AuNPs (without PEG) via electrostatic interactions, and showed that the biological activity for their particular application was not adversely impacted [116, 213, 215]. This contradiction suggests the need to carefully examine the goals of the biofunctionalization strategy and whether a greater yield of active antibodies can be achieved via physical adsorption, especially when AuNPs are PEGylated. For example, in the context of this thesis, the biological activity of functionalized AuNPs with covalently conjugated antibodies was greatly enhanced when compared to physically adsorbed antibodies (Figure 3-25).

(4) Improving existing procedures from a collaborator's lab (Pr. Michel Meunier's group) for developing antibody-functionalized AuNPs (100 nm), by extending the procedure time, minimizing NSA by introducing Tween-20 to the incubation solvent for conjugating antibodies, and controlling the chemistry by carrying out PEGylation before antibody conjugation [133, 216]. In addition, a new strategy, the semi-oriented targeting of the hinge region of antibodies, was also introduced and presents an alternative way to produce biofunctionalized AuNPs that can simultaneously rival the other strategy (randomly oriented) (Figure 3-25). Despite an exhaustive literature review, the semi-oriented strategy for functionalizing PEGylated AuNPs with antibodies has never been done before.

4.3. Evaluation of Thesis Objectives

To review the main objectives of this thesis work outlined in Chapter 1, and provide a commentary on the success of this work in achieving these objectives, they are highlighted below:

1. Explore and compare different strategies of biofunctionalization, including randomly oriented, semi-oriented and oriented grafting techniques, in order to develop and optimize robust and reproducible methods for functionalizing AuNPs with TZM – **this objective was explored for two strategies, but not fully developed for the oriented strategy.**
2. Develop and optimize characterization methods to assess both quantitatively and qualitatively each step of the process that functionalizes AuNPs with TZM – **this objective was achieved for both the randomly oriented and semi-oriented strategies.**
3. Apply TZM-biofunctionalized AuNPs to Her2 positive and negative cancer cell lines (MDA-MB-453 and MDA-MB-231, respectively) in order to evaluate their ability to visualize and detect cancer cells, while comparing in parallel this diagnostic tool to IHC – **this objective was achieved with fixed cancer cell lines, but due to constraints related to the pandemic and accessing the appropriate facility to conduct this work, a parallel comparison with IHC was not achieved.**

CHAPTER 5 CONCLUSIONS AND RECOMMENDATIONS

Overall, this thesis work has made encouraging progress in the field of biofunctionalizing AuNPs. A list of recommendations for future directions in this research field will be explained in detail below, along with a rationale. This will be followed by some concluding remarks.

5.1. Recommendations

(1) **Further characterization of antibodies bound to AuNPs**:

A preliminary characterization of antibodies bound to functionalized AuNPs was performed in this thesis work, by both indirect and direct absorbance-based methods. While the NanoOrange™ assay can be a developed into a fluorescence-based measurement, the biological activity of bound antibodies still needs to be explored. This would require a more extensive characterization of them by measuring their Fab region binding affinity towards Her2 receptors. Although the cell experiments suggest some success with regards to the biological activity of these functionalized AuNPs, questions remain about quantifying their biological activity towards their receptors. It is plausible that the binding affinity of many of these antibodies towards Her2 was impaired, either due to the orientation of their Fab regions, or conformational changes. Tripathi and Driskell [166] discussed the importance of characterizing the activity of antibodies bound to functionalized AuNPs, ass many techniques do not distinguish between loaded and active antibodies

Several techniques could characterize the biological activity of antibodies bound to functionalized AuNPs. One is side-illumination, and examines shifts in the SPR peak as molecules approach the surfaces of AuNPs and light is scattered. As the SPR of AuNPs is largely influenced by their microenvironment, side-illumination takes advantage of the intrinsic optical properties of AuNP to provide a more extensive characterization of all molecules bound to the surfaces of functionalized AuNPs. This could allow for antibodies above a layer of PEG to be characterized (by measuring their plasmon shift when their receptor is injected above), while also evaluating the PEGylation. Side-illumination can also scan through more focal planes of cells bound to functionalized AuNPs, which can overcome some of the limitations of the AuNP:cell incubation experiment tested in this thesis work that was limited to one focal plane scan. This technique is still

novel however, and is being currently developed by co-supervisor Michel Meunier's group, who previously worked on a similar technology to image AuNPs bound to cancer cells [206].

Alternative spectrophotometric techniques to the NanoOrange™ and ELISA assays in this thesis could also quantify the activity of bound antibodies on functionalized AuNPs. Previous work by Tripathi and Driskell [166] injected horseradish peroxidase (HRP) over top of antibodies conjugated to AuNPs, and examined their binding characteristics due to Fc region-based interactions. There are still questions though with regards to the activity of the Fab region of bound antibodies. One interesting alternative would be to chemically conjugate HRP to Her2 receptors, and examine the ensuing absorbance signal. One challenge with this technique is that AuNPs strongly absorb in the same part of the UV-VIS region as HRP. Thus, deconvoluting these two spectra would need to be done in order to resolve any spectral differences.

(2) Further development of oriented strategy and controlling the oxidation of antibodies:

Although the oriented strategy for functionalizing AuNPs with antibodies was briefly attempted in characterizing oxidized antibodies, the procedure that would conjugate oxidized antibodies to AuNPs was never realized. Due to concerns over the impaired activity of periodate-oxidized antibodies, this strategy was abandoned. Although previous work has been done with this strategy, by both a research group in Texas, and the more recent work by Master's student Audrey Nsamela, questions still remain regarding control of the oxidation conditions to preserve the biological activity of bound antibodies [156, 216]. Additionally, issues with the Purpald assay for quantifying oxidized antibodies need to be troubleshooted.

(3) Applying functionalized AuNPs to more complex biological systems, such as tissues:

Ultimately, these functionalized AuNPs will be applied to more complex cellular systems such as tissues, where these formulations will be compared with IHC, an important diagnostic technique for breast cancer. As these cellular environments have their own challenges, (previously discussed in Section 2.1), the specificity and sensitivity of these functionalized AuNPs will be put to the test when applied to these environments. As the end goal is to accurately imitate *in vivo* and *ex vivo* conditions for diagnosing cancer, further work in this field will need to be pursued.

5.2. Concluding Remarks

Overall, this thesis work explored the optimization of chemical and physical conditions required to functionalize AuNPs with antibodies by two covalent conjugation strategies, while comparing them to non-specifically adsorbed antibodies. Differences between the two strategies were noted in terms of yield, activity, stability, and reproducibility, thanks to an in-depth characterization of each step of their functionalization. Although further work still needs to be pursued with regards to characterizing the activity of these bound antibodies, as well as ultimately applying these formulations to more complex biological systems, this thesis work should hopefully pave the way for future breakthroughs in the field of nanotechnology-based cancer diagnostics.

REFERENCES

1 Society, C.C.: 'Canadian Cancer Statistics 2018', in Editor (Ed.)^(Eds.): 'Book Canadian Cancer Statistics 2018' (Canadian Cancer Society, 2018, edn.), pp.

2 https://www.cancer.ca/en/cancer-information/cancer-type/breast/statistics/?region=on, accessed April 9 2020

3 Fernandes, F., Brasil, L., and Guadagnin, R.: 'Mammography Techniques and Review' (IntechOpen, 2015. 2015)

4 Seely, J.M., and Alhassan, T.: 'Screening for breast cancer in 2018-what should we be doing today?', Curr Oncol, 2018, 25, (Suppl 1), pp. S115-S124

5 Boisserie-Lacroix, M., Hurtevent-Labrot, G., Ferron, S., Lippa, N., Bonnefoi, H., and Mac Grogan, G.: 'Correlation between imaging and molecular classification of breast cancers', Diagn Interv Imaging, 2013, 94, (11), pp. 1069-1080

6 Zaha, D.C.: 'Significance of immunohistochemistry in breast cancer', World J Clin Oncol, 2014, 5, (3), pp. 382-392

7 Warford, A., Akbar, H., and Riberio, D.: 'Antigen retrieval, blocking, detection and visualisation systems in immunohistochemistry: a review and practical evaluation of tyramide and rolling circle amplification systems', Methods, 2014, 70, (1), pp. 28-33

8 https://www.novusbio.com/products/breast-cancer-tissue-slide_s166w0, accessed May 25 2020

9 Kim, S.W., Roh, J., and Park, C.S.: 'Immunohistochemistry for Pathologists: Protocols, Pitfalls, and Tips', J Pathol Transl Med, 2016, 50, (6), pp. 411-418

10 Gown, A.M.: 'Current issues in ER and HER2 testing by IHC in breast cancer', Mod Pathol, 2008, 21 Suppl 2, pp. S8-S15

11 Thomson, T., Hayes, MM, Spinelli, JJ, Hilland, E, Sawrenko, C, Phillips, D, Dupuis, B, Parker, RL 'HER-2/neu in breast cancer: interobserver variability and performance of immunohistochemistry with 4 antibodies compared with fluorescent in situ hybridization.', Modern Pathology, 2001, 14, (11), pp. 1079-1086

12 Johnson, G.D., Davidson, R.S., McNamee, K.C., Russell, G., Goodwin, D., Holborow, E.J.: 'Fading of Immunofluorescence during Microscopy: a Study of the Phenomenon and its Remedy', Journal of Immunological Methods, 1982, 55, pp. 231-242

13 Surace M, D.K., Huntley A, Zhao W, Bagnall C, Brown C, Wang C, Roman K, Cann J, Lewis A, Steele K, Rebelatto M, Parra ER, Hoyt CC, Rodriguez-Canales J.: 'Automated Multiplex Immunofluorescence Panel for Immuno-oncology Studies on Formalin-fixed Carcinoma Tissue Specimens.', Journal of Visualized Experiments, 2019, (143)

14 Stack, E.C., Wang, C., Roman, K.A., and Hoyt, C.C.: 'Multiplexed immunohistochemistry, imaging, and quantitation: a review, with an assessment of Tyramide signal amplification, multispectral imaging and multiplex analysis', Methods, 2014, 70, (1), pp. 46-58

15 Furrer, D., Sanschagrin, F., Jacob, S., and Diorio, C.: 'Advantages and disadvantages of technologies for HER2 testing in breast cancer specimens', Am J Clin Pathol, 2015, 144, (5), pp. 686-703

16 Ciaurriz, P., Fernandez, F., Tellechea, E., Moran, J.F., and Asensio, A.C.: 'Comparison of four functionalization methods of gold nanoparticles for enhancing the enzyme-linked immunosorbent assay (ELISA)', Beilstein J. Nanotechnol., 2017, 8, (1), pp. 244-253

17 Yeh, Y.C., Creran, B., and Rotello, V.M.: 'Gold nanoparticles: preparation, properties, and applications in bionanotechnology', Nanoscale, 2012, 4, (6), pp. 1871-1880

18 Singh, P., Pandit, S., Mokkapati, V., Garg, A., Ravikumar, V., and Mijakovic, I.: 'Gold Nanoparticles in Diagnostics and Therapeutics for Human Cancer', Int J Mol Sci, 2018, 19, (7)

19 Jain, P.K., Huang, X.H., El-Sayed, I.H., and El-Sayed, M.A.: 'Noble Metals on the Nanoscale: Optical and Photothermal Properties and Some Applications in Imaging, Sensing, Biology, and Medicine', Accounts of Chemical Research, 2008, 41, (12), pp. 1578-1586

20 Huang, X., and El-Sayed, M.A.: 'Gold nanoparticles: Optical properties and implementations in cancer diagnosis and photothermal therapy', Journal of Advanced Research, 2010, 1, (1), pp. 13-28

21 Carlsson, J., Nordgren, H., Sjöström, J., Wester, K., Villman, K., Bengtsson, N.O., Ostenstad, B., Lundqvist, H., and Blomqvist, C.: 'HER2 expression in breast cancer primary tumours and corresponding metastases. Original data and literature review', British journal of cancer, 2004, 90, (12), pp. 2344-2348

22 Nahta, R., and Esteva, F.J.: 'Trastuzumab: triumphs and tribulations', Oncogene, 2007, 26, (25), pp. 3637-3643

23 Subik, K., Lee, J.F., Baxter, L., Strzepek, T., Costello, D., Crowley,P. Xing, L., Hung, M.C., Bonfiglio, T., Hicks, D.G., Tang, P.: 'The Expression Patterns of ER, PR, HER2, CK5/6, EGFR, Ki-67 and AR by Immunohistochemical Analysis in Breast Cancer Cell Lines', Breast Cancer (Auckland), 2010, 4, pp. 35-41

24 Ivell, R., Teerds, K., and Hoffman, G.E.: 'Proper Application of Antibodies for Immunohistochemical Detection: Antibody Crimes and How to Prevent Them', Endocrinology, 2014, 155, (3), pp. 676-687

25 McCampbell, A.S., Raghunathan, V., Tom-Moy, M., Workman, R.K., Haven, R., Ben-Dor, A., Rasmussen, O.F., Jacobsen, L., Lindberg, M., Yamada, N.A., and Schembri, C.: 'Tissue Thickness Effects on Immunohistochemical Staining Intensity Markers of Cancer', Applied Immunohistochemistry & Molecular Morphology, 2019, 27, (5), pp. 345-355

26 Gadd, J.C., Fujimoto, B.S., Bajjalieh, S.M., and Chiu, D.T.: 'Single-molecule fluorescence quantification with a photobleached internal standard', Anal Chem, 2012, 84, (24), pp. 10522-10525

27 Berlier, J.E., Rothe, A., Buller, G., Bradford, J., D.R., G., Filanoski, B.J., Telford, W.G., Yue, S., Liu, J.X., Cheung, C.Y., Chang, W., Hirsch, J.D., Beechem, J.M., and Haugland, R.P.: 'Quantitative comparison of long-wavelength Alexa Fluor dyes to Cy dyes: Fluorescence of the dyes and their bioconjugates', Journal of Histochemistry & Cytochemistry, 2003, 51, (12), pp. 1699-1712

28 Bussolati, G., and Leonardo, E.: 'Technical pitfalls potentially affecting diagnoses in immunohistochemistry', J Clin Pathol, 2008, 61, (11), pp. 1184-1192

29 Pekmezci, M., Szpaderska, A., Osipo, C., and Ersahin, C.: 'The Effect of Cold Ischemia Time and/or Formalin Fixation on Estrogen Receptor, Progesterone Receptor, and Human Epidermal Growth Factor Receptor-2 Results in Breast Carcinoma', Patholog Res Int, 2012, 2012, pp. 947041

30 Engel, K.B., and Moore, H.M.: 'Effects of Preanalytical Variables on the Detection of Proteins by Immunohistochemistry in Formalin-Fixed, Paraffin-Embedded Tissue': 'Archives of Pathology & Laboratory Medicine' (2011), pp. 537-543

31 Economou, M., Schöni, L., Hammer, C., J.A., G., Mueller, D.E., and Zlobec, I.: 'Proper paraffin slide storage is crucial for translational research projects involving immunohistochemistry stains', Clinical Translational Medicine, 2014, 3, (1)

32 Jones, W.T., Stockard, C.R., and Grizzle, W.E.: 'Effects of time and temperature during attachment of sections to microscope slides on immunohistochemical detection of antigens', Biotech Histochem, 2001, 76, (2), pp. 55-58

33 Elahi, N., Kamali, M., and Baghersad, M.H.: 'Recent biomedical applications of gold nanoparticles: A review', Talanta, 2018, 184, pp. 537-556

34 Maier, S.A.: 'Plasmonics: Fundamentals and Applications' (Springer, 2007. 2007)

35 Kittel, C.: 'Introduction to Solid State Physics' (Wiley, 2004. 2004)

36 Kreibig, U., and Vollmer, M.: 'Optical Properties of Metal Clusters' (Springer, 1995, 1 edn. 1995)

37 Amendola, V., Pilot, R., Frasconi, M., Marago, O.M., and Iati, M.A.: 'Surface plasmon resonance in gold nanoparticles: a review', J Phys Condens Matter, 2017, 29, (20), pp. 203002

38 Lee, K., and El-Sayed, M.A.: 'Gold and silver nanoparticles in sensing and imaging: Sensitivity of plasmon response to size, shape, and metal composition', Journal of Physical Chemistry B, 2006, 110, (39), pp. 19220-19225

39 Chen, H., Kou, X., Yang, Z., Ni, W., and Wang, J.: 'Shape- and Size-Dependent Refractive Index Sensitivity of Gold Nanoparticles', Langmuir, 2008, 24, (10), pp. 5233-5237

40 Haes, A.J., Haynes, C.L., McFarland, A.D., Schatz, G.C., Van Duyne, R.P., Zou, S.: 'Plasmonic Materials for Surface-Enhanced Sensing and Spectroscopy', MRS Bulletin, 2005, 30, (5), pp. 368-375

41 Xia, Y., and Halas, N.J.: 'Shape-Controlled Synthesis and Surface Plasmonic Properties of Metallic Nanostructures', MRS Bulletin, 2011, 30, (5), pp. 338-348

42 https://www.nanopartz.com/spherical_gold_nanoparticles.asp, accessed April 22 2020

43 Verbruggen, S.W., Keulemans, M., Martens, J.A., and Lenaerts, S.: 'Predicting the Surface Plasmon Resonance Wavelength of Gold–Silver Alloy Nanoparticles', The Journal of Physical Chemistry C, 2013, 117, (37), pp. 19142-19145

44 Harris, N., Ford, M.J., Mulvaney, P., and Cortie, M.B.: 'Tunable infrared absorption by metal nanoparticles: The case for gold rods and shells', Gold Bulletin, 2008, 41, pp. 5-14

45 Garcia, M.A.: 'Surface plasmons in metallic nanoparticles: fundamentals and applications', Journal of Physics D: Applied Physics, 2012, 45, (38)

46 Mayer, K.M., and Hafner, J.H.: 'Localized surface plasmon resonance sensors', Chem Rev, 2011, 111, (6), pp. 3828-3857

47 Zijlstra, P., Paulo, P.M., Yu, K., Xu, Q.H., and Orrit, M.: 'Chemical interface damping in single gold nanorods and its near elimination by tip-specific functionalization', Angew Chem Int Ed Engl, 2012, 51, (33), pp. 8352-8355

48 Aruda, K.O., Tagliazucchi, M., Sweeney, C.M., Hannah, D.C., Schatz, G.C., and Weiss, E.A.: 'Identification of parameters through which surface chemistry determines the lifetimes of hot electrons in small Au nanoparticles', Proc Natl Acad Sci U S A, 2013, 110, (11), pp. 4212-4217

49 Kats, M.A., Yu, N., Genevet, P., Gaburro, Z., and Capasso, F.: 'Effect of radiation damping on the spectral response of plasmonic components', Optics Express, 2011, 19, (22), pp. 21748-21753

50 Jain, P.K., Lee, K.S., El-Sayed, I.H., El-Sayed, M.A.: 'Calculated Absorption and Scattering Properties of Gold Nanoparticles of Different Size, Shape, and Composition: Applications in Biological Imaging and Biomedicine', Journal of Physical Chemistry, 2006, 110, (14), pp. 7238-7248

51 Mishchenko, M.I., Travis, L.D., and Lacis, A.A.: 'Scattering, Absorption and Emission of Light by Small Particles' (Cambridge University Press, 2002, 3rd edn. 2002)

52 Bohren, C.F., and Huffman, D.R.: 'Absorption and Scattering of Light by Small Particles' (Wiley, 1998. 1998)

53 Jones, P.H., Marago, O.M., and Volpe, G.: 'Optical Tweezers: Principles and Applications' (Cambridge University Press, 2015. 2015)

54 Derkachova, A., Kolwas, K., and Demchenko, I.: 'Dielectric Function for Gold in Plasmonics Applications: Size Dependence of Plasmon Resonance Frequencies and Damping Rates for Nanospheres', Plasmonics (Norwell, Mass.), 2016, 11, pp. 941-951

55 https://nanocomposix.com/pages/gold-nanoparticles-optical-properties, accessed April 23 2020

56 Orendorff, C.J., Sau, T.K., and Murphy, C.J.: 'Shape-dependent plasmon-resonant gold nanoparticles', Small, 2006, 2, (5), pp. 636-639

57 Boisselier, E., and Astruc, D.: 'Gold nanoparticles in nanomedicine: preparations, imaging, diagnostics, therapies and toxicity', Chem Soc Rev, 2009, 38, (6), pp. 1759-1782

58 Yang, C.-T., Xu, Y., Pourhassan-Moghaddam, M., Tran, D.P., Wu, L., Zhou, X., and Thierry, B.: 'Surface Plasmon Enhanced Light Scattering Biosensing: Size Dependence on the Gold Nanoparticle Tag', Sensors (Basel, Switzerland), 2019, 19, (2), pp. 323

59 Kimling, J., Maier, M., Okenve, B., Kotaidis, V., Ballot, H., Plech, A.: 'Turkevich Method for Gold Nanoparticle Synthesis Revisited', 2006, 2006, 110, (32), pp. Journal Physical Chemistry B

60 Zhao, P., Li, N., and Astruc, D.: 'State of the art in gold nanoparticle synthesis', Coordination Chemistry Reviews, 2013, 257, (3-4), pp. 638-665

61 Daruich De Souza, C., Ribeiro Nogueira, B., and Rostelato, M.E.C.M.: 'Review of the methodologies used in the synthesis gold nanoparticles by chemical reduction', Journal of Alloys and Compounds, 2019, 798, pp. 714-740

62 Sapsford, K.E., Algar, W.R., Berti, L., Gemmill, K.B., Casey, B.J., Oh, E., Stewart, M.H., and Medintz, I.L.: 'Functionalizing nanoparticles with biological molecules: developing chemistries that facilitate nanotechnology', Chem Rev, 2013, 113, (3), pp. 1904-2074

63 Aldewachi, H., Woodroofe, N., and Gardiner, P.: 'Study of the Stability of Functionalized Gold Nanoparticles for the Colorimetric Detection of Dipeptidyl Peptidase IV', Applied Sciences, 2018, 8, (12)

64 Shi, D., Sheng, F., Zhang, X., and Wang, G.: 'Gold nanoparticle aggregation: Colorimetric detection of the interactions between avidin and biotin', Talanta, 2018, 185, pp. 106-112

65 Zhao, W., Brook, M.A., and Li, Y.F.: 'Design of Gold Nanoparticle-Based Colorimetric Biosensing Assays', Chembiochem, 2008, 9, (15), pp. 2363-2371

66 Zhou, J., Ralston, J., Sedev, R., and Beattie, D.A.: 'Functionalized gold nanoparticles: synthesis, structure and colloid stability', J Colloid Interface Sci, 2009, 331, (2), pp. 251-262

67 Howes, P.D., Chandrawati, R., Stevens, M.M.: 'Colloidal nanoparticles as advanced biological sensors', Science, 2014, 346, (6205), pp. 1-53

68 Gajria, D., and Chandarlapaty, S.: 'HER2-amplified breast cancer: mechanisms of trastuzumab resistance and novel targeted therapies', Expert Rev Anticancer Ther, 2011, 11, (2), pp. 263-275

69 Pang, B., Yang, X., and Xia, Y.: 'Putting gold nanocages to work for optical imaging, controlled release and cancer theranostics', Nanomedicine (London, England), 2016, 11, (13), pp. 1715-1728

70 Ermini, M.L., Chadtová Song, X., Špringer, T., and Homola, J.: 'Peptide Functionalization of Gold Nanoparticles for the Detection of Carcinoembryonic Antigen in Blood Plasma via SPR-Based Biosensor', Front. Chem., 2019, 7, (40)

71 Li, S., Bouchy, S., Penninckx, S., Marega, R., Fichera, O., Gallez, B., Feron, O., Martinive, P., Heuskin, A.C., Michiels, C., and Lucas, S.: 'Antibody-functionalized gold nanoparticles as tumor-targeting radiosensitizers for proton therapy', Nanomedicine (Lond), 2019, 14, (3), pp. 317-333

72 Stone, J., Jackson, S., and Wright, D.: 'Biological applications of gold nanorods', Wiley Interdiscip Rev Nanomed Nanobiotechnol, 2011, 3, (1), pp. 100-109

73 Smith, A.M., Mancini, M.C., and Nie, S.: 'Second window for in vivo imaging', Nature Nanotechnology, 2009, 4, (11), pp. 710-711

74 Skrabalak, S.E., Chen, J., Sun, Y., Lu, X., Au, L., Cobley, C.M., and Xia, Y.: 'Gold nanocages: synthesis, properties, and applications', Acc Chem Res, 2008, 41, (12), pp. 1587-1595

75 Zhang, X.: 'Gold Nanoparticles: Recent Advances in the Biomedical Applications', Cell Biochem Biophys, 2015, 72, (3), pp. 771-775

76 Zeng, S., Yong, K.-T., Roy, I., Dinh, X.-Q., Yu, X., and Luan, F.: 'A Review on Functionalized Gold Nanoparticles for Biosensing Applications', Plasmonics, 2011, 6, (3), pp. 491-506

77 Menon, S., S, R., and S, V.K.: 'A review on biogenic synthesis of gold nanoparticles, characterization, and its applications', Resource-Efficient Technologies, 2017, 3, (4), pp. 516-527

78 Fratila, R.M., Mitchell, S.G., del Pino, P., Grazu, V., and de la Fuente, J.M.: 'Strategies for the biofunctionalization of gold and iron oxide nanoparticles', Langmuir, 2014, 30, (50), pp. 15057-15071

79 Neupane, S., Pan, Y., Takalkar, S., Bentz, K., Farmakes, J., Xu, Y., Chen, B., Liu, G., Qian, S.Y., and Yang, Z.: 'Probing the Aggregation Mechanism of Gold Nanoparticles Triggered by a Globular Protein', The Journal of Physical Chemistry C, 2017, 121, (2), pp. 1377-1386

80 Chegel, V., Rachkov, O., Lopatynskyi, A., Ishihara, S., Yanchuk, I., Nemoto, Y., Hill, J.P., and Ariga, K.: 'Gold Nanoparticles Aggregation: Drastic Effect of Cooperative Functionalities in a Single Molecular Conjugate', The Journal of Physical Chemistry C, 2012, 116, (4), pp. 2683-2690

81 Oh, E., Susumu, K., Mäkinen, A.J., Deschamps, J.R., Huston, A.L., and Medintz, I.L.: 'Colloidal Stability of Gold Nanoparticles Coated with Multithiol-Poly(ethylene glycol) Ligands: Importance of Structural Constraints of the Sulfur Anchoring Groups', The Journal of Physical Chemistry C, 2013, 117, (37), pp. 18947-18956

82 Laaksonen, T., Ahonen, P., Johans, C., and Kontturi, K.: 'Stability and electrostatics of mercaptoundecanoic acid-capped gold nanoparticles with varying counterion size', Chemphyschem, 2006, 7, (10), pp. 2143-2149

83 Sakura, T., Takahashi, T., Kataoka, K., and Nagasaki, Y.: 'One-pot preparation of mono-dispersed and physiologically stabilized gold colloid', Colloid and Polymer Science, 2005, 284, (1), pp. 97-101

84 Zareie, H.M., Boyer, C., Bulmus, V., Nateghi, E., Davis, T.P.: 'Temperature-Responsive Self-Assembled Monolayers of Oligo(ethylene glycol): Control of Biomolecular Recognition', ACS Nano, 2008, 2, (4), pp. 757-765

85 Suk, J.S., Xu, Q., Kim, N., Hanes, J., and Ensign, L.M.: 'PEGylation as a strategy for improving nanoparticle-based drug and gene delivery', Adv Drug Deliv Rev, 2016, 99, (Pt A), pp. 28-51

86 Manson, J., Kumar, D., Meenan, B.J., and Dixon, D.: 'Polyethylene glycol functionalized gold nanoparticles: the influence of capping density on stability in various media', Gold Bulletin, 2011, 44, (2), pp. 99-105

87 Daou, T.J., Li, L., Reiss, P., Josserand, V., Texier, I.: 'Effect of Poly(ethylene glycol) Length on the in Vivo Behavior of Coated Quantum Dots', Langmuir, 2009, 25, (5), pp. 3040-3044

88 https://www.sigmaaldrich.com/technical-documents/articles/materials-science/polyethylene-glycol-selection-guide.html, accessed May 8 2020

89 Nuzzo, R.G., Zegarski, B.R., and Dubois, L.H.: 'Fundamental studies of the chemisorption of organosulfur compounds on gold(111). Implications for molecular self-assembly on gold surfaces', J Am Chem Soc, 1987, 109, (3), pp. 733-740

90 Ulman, A.: ‘Formation and Structure of Self-Assembled Monolayers’, Chem Rev, 1996, 96, (4), pp. 1533-1554

91 Love, J.C., Estroff, L.A., Kriebel, J.K., Nuzzo, R.G., Whitesides, G.M.: ‘Self-assembled monolayers of thiolates on metals as a form of nanotechnology’, Chemical Reviews, 2005, 105, (4), pp. 1103-1169

92 Kanaras, A.G., Kamounah, F.S., Schaumburg, K., Kiely, C.J., and Brust, M.: ‘Thioalkylated tetraethylene glycol: a new ligand for water soluble monolayer protected gold clusters’, Chem Commun (Camb), 2002, (20), pp. 2294-2295

93 Rahme, K., Chen, L., Hobbs, R.G., Morris, M.A., O'Driscoll, C., and Holmes, J.D.: ‘PEGylated gold nanoparticles: polymer quantification as a function of PEG lengths and nanoparticle dimensions’, RSC Adv., 2013, 3, (17), pp. 6085-6094

94 Xia, X., Yang, M., Wang, Y., Zheng, Y., Li, Q., Chen, J., Xia, Y.: ‘Quantifying the Coverage Density of Poly(ethylene glycol) Chains on the Surface of Gold Nanostructures’, ACS Nano, 2012, 6, (1), pp. 512-522

95 Kimura, K., Takashima, S.: ‘Molecular Approach to the Surface Potential Estimate of Thiolate-Modified Gold Nanoparticles’, Journal Physical Chemistry B, 2002, 106, pp. 7260-7266

96 Hostetler, M.J., Templeton, A.C., Murray, R.W.: ‘Dynamics of Place-Exchange Reactions on Monolayer-Protected Gold Cluster Molecules’, Langmuir, 1999, 15, (3782-3789)

97 Hermanson, G.T.: ‘Bioconjugate Techniques’ (Academic Press, 2013. 2013)

98 Sperling, R.A., and Parak, W.J.: ‘Surface modification, functionalization and bioconjugation of colloidal inorganic nanoparticles’, Philos Trans A Math Phys Eng Sci, 2010, 368, (1915), pp. 1333-1383

99 http://www.nanocs.com/PEG.htm, accessed April 29 2020

100 Stetefeld, J., McKenna, S.A., and Patel, T.R.: ‘Dynamic light scattering: a practical guide and applications in biomedical sciences’, Biophys Rev, 2016, 8, (4), pp. 409-427

101 Harding, S.E., and Jumel, K.: ‘Light Scattering’, Current Protocols in Protein Science, 1998, 11, (1), pp. 7.8.1-7.8.14

102 Jans, H., Liu, X., Austin, L., Maes, G., Huo, Q.: ‘Dynamic Light Scattering as a Powerful Tool for Gold Nanoparticle Bioconjugation and Biomolecular Binding Studies’, Analytical Chemistry, 2009, 81, (22), pp. 9425-9432

103 Alexander, D.L., Maxim, P.N., Mikhail, K.A., Ekaterina, B.D., Vitaly, G.G., Alina, S.R., and Irina, P.A.: ‘Nano-biosensors based on dynamic light scattering’, in Editor (Ed.)^(Eds.): ‘Book Nano-biosensors based on dynamic light scattering’ (2019, edn.), pp.

104 Malm, A.V., and Corbett, J.C.W.: ‘Improved Dynamic Light Scattering using an adaptive and statistically driven time resolved treatment of correlation data’, Scientific Reports, 2019, 9, (1), pp. 13519

105 Siegel, R.W., and Howell, J.R.: ‘Thermal radiation heat transfer’ (Taylor & Francis, 2002. 2002)

106 Kaszuba, M., Corbett, J., Watson, F.M., and Jones, A.: ‘High-concentration zeta potential measurements using light-scattering techniques’, Philosophical transactions. Series A, Mathematical, physical, and engineering sciences, 2010, 368, (1927), pp. 4439-4451

107 Clogston, J.D., Patri, A.K.: ‘Zeta Potential Measurement’, in McNeil, S. (Ed.): ‘Characterization of Nanoparticles Intended for Drug Delivery. Methods in Molecular Biology (Methods and Protocols)’ (Humana Press, 2011)

108 Burgi, T.: ‘Properties of the gold-sulphur interface: from self-assembled monolayers to clusters’, Nanoscale, 2015, 7, (38), pp. 15553-15567

109 Amendola, V., Meneghetti, M.: ‘Size Evaluation of Gold Nanoparticles by UV-vis Spectroscopy’, Journal Physical Chemistry, 2009, 113, pp. 4277-4285

110 Haiss, W., Thanh, N., Aveyard, J., and Fernig, D.: ‘Determination of Size and Concentration of Gold Nanoparticles from UV-Vis Spectra’, Analytical Chemistry, 2007, 79, pp. 4215-4221

111 Cayot, P., and Tainturier, G.: ‘The quantification of protein amino groups by the trinitrobenzenesulfonic acid method: a reexamination’, Analytical Biochemistry, 1997, 249, (2), pp. 184-200

112 Batchelor, R.H., Sarkez, A., Cox, W.G., and Johnson, I.: ‘Fluorometric assay for quantitation of biotin covalently attached to proteins and nucleic acids’, Biotechniques, 2007, 43, (4), pp. 503-507

113 Hsieh, Y.-C., Cheng, T.-C., Wang, H.-E., Li, J.-J., Lin, W.-W., Huang, C.-C., Chuang, C.-H., Wang, Y.-T., Wang, J.-Y., Roffler, S.R., Chuang, K.-H., and Cheng, T.-L.: ‘Using anti-poly(ethylene glycol) bioparticles for the quantitation of PEGylated nanoparticles’, Scientific Reports, 2016, 6, (1), pp. 39119

114 Winther, J.R., and Thorpe, C.: ‘Quantification of thiols and disulfides’, Biochim Biophys Acta, 2014, 1840, (2), pp. 838-846

115 Chen, H., Paholak, H., Ito, M., Sansanaphongpricha, K., Qian, W., Che, Y., and Sun, D.: ‘'Living' PEGylation on gold nanoparticles to optimize cancer cell uptake by controlling targeting ligand and charge densities’, Nanotechnology, 2013, 24, (35), pp. 355101-355101

116 Jazayeri, M.H., Amani, H., Pourfatollah, A.A., Pazoki-Toroudi, H., and Sedighimoghaddam, B.: ‘Various methods of gold nanoparticles (GNPs) conjugation to antibodies’, Sensing and Bio-Sensing Research, 2016, 9, pp. 17-22

117 Sapsford, K.E., Tyner, K.M., Dair, B.J., Deschamps, J.R., and Medintz, I.L.: ‘Analyzing nanomaterial bioconjugates: a review of current and emerging purification and characterization techniques’, Anal Chem, 2011, 83, (12), pp. 4453-4488

118 Algar, W.R., Prasuhn, D.E., Stewart, M.H., Jennings, T.L., Blanco-Canosa, J.B., Dawson, P.E., and Medintz, I.L.: ‘The controlled display of biomolecules on nanoparticles: a challenge suited to bioorthogonal chemistry’, Bioconjug Chem, 2011, 22, (5), pp. 825-858

119 Mullen, D.G., and Banaszak Holl, M.M.: ‘Heterogeneous ligand-nanoparticle distributions: a major obstacle to scientific understanding and commercial translation’, Acc Chem Res, 2011, 44, (11), pp. 1135-1145

120 Medintz, I.: ‘Universal Tools for Biomolecular Attachment to Surfaces’, Nature Materials, 2006, 5, pp. 842

121 Nel, A.E., Madler, L., Velegol, D., Xia, T., Hoek, E.M., Somasundaran, P., Klaessig, F., Castranova, V., and Thompson, M.: ‘Understanding biophysicochemical interactions at the nano-bio interface’, Nature Materials, 2009, 8, (7), pp. 543-557

122 Aubin-Tam, M.E., and Hamad-Schifferli, K.: ‘Structure and function of nanoparticle-protein conjugates’, Biomed Mater, 2008, 3, (3), pp. 034001

123 Lynch, I., Cedervall, T., Lundqvist, M., Cabaleiro-Lago, C., Linse, S., and Dawson, K.A.: ‘The nanoparticle-protein complex as a biological entity; a complex fluids and surface science challenge for the 21st century’, Adv Colloid Interface Sci, 2007, 134-135, pp. 167-174

124 Park, S., and Hamad-Schifferli, K.: ‘Nanoscale interfaces to biology’, Curr Opin Chem Biol, 2010, 14, (5), pp. 616-622

125 Dennler, P., Fischer, E., and Schibli, R.: ‘Antibody Conjugates: From Heterogeneous Populations to Defined Reagents’, Antibodies, 2015, 4, (3), pp. 197-224

126 McCombs, J.R., and Owen, S.C.: ‘Antibody drug conjugates: design and selection of linker, payload and conjugation chemistry’, AAPS J, 2015, 17, (2), pp. 339-351

127 Boylan, N.J., Zhou, W., Proos, R.J., Tolbert, T.J., Wolfe, J.L., and Laurence, J.S.: ‘Conjugation site heterogeneity causes variable electrostatic properties in Fc conjugates’, Bioconjug Chem, 2013, 24, (6), pp. 1008-1016

128 Acchione, M., Kwon, H., Jochheim, C.M., and Atkins, W.M.: ‘Impact of linker and conjugation chemistry on antigen binding, Fc receptor binding and thermal stability of model antibody-drug conjugates’, MAbs, 2012, 4, (3), pp. 362-372

129 Wakankar, A.D., Feeney, M.B., River, J., Chen, Y., Kim, M., Sharma, V.K., and Wang, Y.J.: ‘Physicochemical Stability of the Antibody-Drug Conjugate Trastuzumab-DM1: Changes due to Modification and Conjugation Processes’, Bioconjugate Chemistry, 2010, 21, pp. 1588-1595

130 Di Pasqua, A.J., Mishler, R.E., Ship, Y.-L., Dabrowiak, J.C., and Asefa, T.: ‘Preparation of antibody-conjugated gold nanoparticles’, Materials Letters, 2009, 63, (21), pp. 1876-1879

131 Singh, V., Nair, S.P., and Aradhyam, G.K.: ‘Chemistry of conjugation to gold nanoparticles affects G-protein activity differently’, J Nanobiotechnology, 2013, 11, pp. 7

132 Loo, C., Hirsch, L., Lee, M.H., Chang, E., West, J., Halas, N.J., and Drezek, R.A.: ‘Gold nanoshell bioconjugates for molecular imaging in live cells’, Optics Letters, 2005, 30, (9), pp. 1012-1014

133 Wilson, A., Mazzaferri, J., Bergeron, E., Patskovsky, S., Marcoux-Valiquette, P., Costantino, S., Sapieha, P., and Meunier, M.: ‘In Vivo Laser-Mediated Retinal Ganglion Cell Optoporation Using KV1.1 Conjugated Gold Nanoparticles’, Nano Letters, 2018, 18

134 Koniev, O., and Wagner, A.: ‘Developments and recent advancements in the field of endogenous amino acid selective bond forming reactions for bioconjugation’, Chem Soc Rev, 2015, 44, (15), pp. 5495-5551

135 Kalkhof, S., and Sinz, A.: ‘Chances and pitfalls of chemical cross-linking with amine-reactive N-hydroxysuccinimide esters’, Anal Bioanal Chem, 2008, 392, (1-2), pp. 305-312

136 Leavell, M.D., Novak, P., Behrens, C.R., Schoeniger, J.S., and Kruppa, G.H.: ‘Strategy for selective chemical cross-linking of tyrosine and lysine residues’, J Am Soc Mass Spectrom, 2004, 15, (11), pp. 1604-1611

137 Swaim, C.L., Smith, J.B., and Smith, D.L.: ‘Unexpected products from the reaction of the synthetic cross-linker 3,3'-dithiobis(sulfosuccinimidyl propionate), DTSSP with peptides’, J Am Soc Mass Spectrom, 2004, 15, (5), pp. 736-749

138 Leitner, A., Walzthoeni, T., Kahraman, A., Herzog, F., Rinner, O., Beck, M., and Aebersold, R.: ‘Probing native protein structures by chemical cross-linking, mass spectrometry, and bioinformatics’, Mol Cell Proteomics, 2010, 9, (8), pp. 1634-1649

139 Sun, M.M.C., Beam, K.S., Cerveny, C.G., Hamblet, K.J., Blackmore, R.S., Torgov, M.Y., Handley, F.G.M., Ihle, N.C., Senter, P.D., and Alley, S.C.: ‘Reduction-Alkylation Strategies for the Modification of Specific Monoclonal Antibody Disulfides’, Bioconjugate Chemistry, 2005

140 Brocchini, S., Godwin, A., Balan, S., Choi, J.W., Zloh, M., and Shaunak, S.: ‘Disulfide bridge based PEGylation of proteins’, Adv Drug Deliv Rev, 2008, 60, (1), pp. 3-12

141 Cherkaoui, S., Bettinger, T., Hauwel, M., Navetat, S., Allemann, E., and Schneider, M.: ‘Tracking of antibody reduction fragments by capillary gel electrophoresis during the coupling to microparticles surface’, J Pharm Biomed Anal, 2010, 53, (2), pp. 172-178

142 Sharma, H., and Mutharasan, R.: ‘Half antibody fragments improve biosensor sensitivity without loss of selectivity’, Anal Chem, 2013, 85, (4), pp. 2472-2477

143 Trilling, A.K., Beekwilder, J., and Zuilhof, H.: ‘Antibody orientation on biosensor surfaces: a minireview’, Analyst, 2013, 138, (6), pp. 1619-1627

144 Makaraviciute, A., Jackson, C.D., Millner, P.A., and Ramanaviciene, A.: ‘Considerations in producing preferentially reduced half-antibody fragments’, J Immunol Methods, 2016, 429, pp. 50-56

145 Chen, T., Su, D., Gruenhagen, J., Gu, C., Li, Y., Yehl, P., Chetwyn, N.P., and Medley, C.D.: ‘Chemical de-conjugation for investigating the stability of small molecule drugs in antibody-drug conjugates’, J Pharm Biomed Anal, 2016, 117, pp. 304-310

146 Strachan, E., Mallia, A.K., Cox, J.M., Antharavally, B., Desai, S., Sykaluk, L., O'Sullivan, V., and Bell, P.A.: ‘Solid-phase biotinylation of antibodies’, J Mol Recognit, 2004, 17, (3), pp. 268-276

147 Groysbeck, N., Stoessel, A., Donzeau, M., da Silva, E.C., Lehmann, M., Strub, J.M., Cianferani, S., Dembele, K., and Zuber, G.: ‘Synthesis and biological evaluation of 2.4 nm thiolate-protected gold nanoparticles conjugated to Cetuximab for targeting glioblastoma cancer cells via the EGFR’, Nanotechnology, 2019, 30, (18), pp. 184005

148 Doronina, S.O., Toki, B.E., Torgov, M.Y., Mendelsohn, B.A., Cerveny, C.G., Chace, D.F., DeBlanc, R.L., Gearing, R.P., Bovee, T.D., Siegall, C.B., Francisco, J.A., Wahl, A.F., Meyer, D.L., and Senter, P.D.: ‘Development of potent monoclonal antibody auristatin conjugates for cancer therapy’, Nature Biotechnology, 2003, 21, (7), pp. 778-784

149 Lazar, A.C., Wang, L., Blattler, W.A., Amphlett, G., Lambert, J.M., and Zhang, W.: 'Analysis of the composition of immunoconjugates using size-exclusion chromatography coupled to mass spectrometry', Rapid Commun Mass Spectrom, 2005, 19, (13), pp. 1806-1814

150 Caron, P.C., Laird, W., Co, M.S., Avdalovic, N.M., Queen, C., and Scheinberg, D.A.: 'Engineered humanized dimeric forms of IgG are more effective antibodies', J Exp Med, 1992, 176, pp. 1191-1195

151 Shopes, B.: 'A genetically engineered human IgG with limited flexibility fully initiates cytolysis via complement', Mol Immunol, 1993, 30, pp. 603-609

152 Alter, G., Ottenhoff, T.H.M., and Joosten, S.A.: 'Antibody glycosylation in inflammation, disease and vaccination', Seminars in Immunology, 2018, 39, pp. 102-110

153 Jefferis, R.: 'Recombinant antibody therapeutics: the impact of glycosylation on mechanisms of action', Trends Pharmacol Sci, 2009, 30, (7), pp. 356-362

154 Adak, A.K., Li, B.Y., Huang, L.D., Lin, T.W., Chang, T.C., Hwang, K.C., and Lin, C.C.: 'Fabrication of antibody microarrays by light-induced covalent and oriented immobilization', ACS Appl Mater Interfaces, 2014, 6, (13), pp. 10452-10460

155 Makaraviciute, A., and Ramanaviciene, A.: 'Site-directed antibody immobilization techniques for immunosensors', Biosens Bioelectron, 2013, 50, pp. 460-471

156 Kumar, S., Aaron, J., and Sokolov, K.: 'Directional conjugation of antibodies to nanoparticles for synthesis of multiplexed optical contrast agents with both delivery and targeting moieties', Nat Protoc, 2008, 3, (2), pp. 314-320

157 Kubota, T., Kuroda, S., Kanaya, N., Morihiro, T., Aoyama, K., Kakiuchi, Y., Kikuchi, S., Nishizaki, M., Kagawa, S., Tazawa, H., and Fujiwara, T.: 'HER2-targeted gold nanoparticles potentially overcome resistance to trastuzumab in gastric cancer', Nanomedicine, 2018, 14, (6), pp. 1919-1929

158 Zhou, Q., Stefano, J.E., Manning, C., Kyazike, J., Chen, B., Gianolio, D.A., Park, A., Busch, M., Bird, J., Zheng, X., Simonds-Mannes, H., Kim, J., Gregory, R.C., Miller, R.J., Brondyk, W.H., Dhal, P.K., and Pan, C.Q.: 'Site-specific antibody-drug conjugation through glycoengineering', Bioconjug Chem, 2014, 25, (3), pp. 510-520

159 Hudson, B.G., and Barker, R.: 'The Overoxidation of Carbohydrates with Sodium Metaperiodate', Journal Organic Chemistry, 1967, 32, pp. 2101-2109

160 Wolfe, C.A.C., and Hage, D.S.: 'Studies on the Rate and Control of Antibody Oxidation by Periodate', Analytical Biochemistry, 1995, 231, pp. 123-130

161 van der Heide, S., and Russell, D.A.: 'Optimisation of immuno-gold nanoparticle complexes for antigen detection', J Colloid Interface Sci, 2016, 471, pp. 127-135

162 Zhang, S., Garcia-D'Angeli, A., Brennan, J.P., and Huo, Q.: 'Predicting detection limits of enzyme-linked immunosorbent assay (ELISA) and bioanalytical techniques in general', Analyst, 2014, 139, (2), pp. 439-445

163 Puertas, S., Batalla, P., Moros, M., Polo, E., del Pino, P., Guisan, J.M., Grazu, V., and de la Fuente, J.M.: 'Taking Advantage of Unspecific Interactions to Produce Highly Active Magnetic Nanoparticle-Antibody Conjugates', ACS Nano, 2011, 5, (6), pp. 4521-4528

164 Ernst, O., and Zor, T.: 'Linearization of the bradford protein assay', J Vis Exp, 2010, (38), pp. 1918

165 Mustafaoglu, N., Kiziltepe, T., and Bilgicer, B.: 'Site-specific conjugation of an antibody on a gold nanoparticle surface for one-step diagnosis of prostate specific antigen with dynamic light scattering', Nanoscale, 2017, 9, (25), pp. 8684-8694

166 Tripathi, K., and Driskell, J.D.: 'Quantifying Bound and Active Antibodies Conjugated to Gold Nanoparticles: A Comprehensive and Robust Approach To Evaluate Immobilization Chemistry', ACS Omega, 2018, 3, (7), pp. 8253-8259

167 Wu, Y., Ali, M.R.K., Chen, K.C., Fang, N., and El-Sayed, M.A.: 'Gold nanoparticles in biological optical imaging', Nano Today, 2019, 24, pp. 120-140

168 Rosman, C., Pierrat, S., Henkel, A., Tarantola, M., Schneider, D., Sunnick, E., Janshoff, A., and Sonnichsen, C.: 'A new approach to assess gold nanoparticle uptake by mammalian cells: combining optical dark-field and transmission electron microscopy', Small, 2012, 8, (23), pp. 3683-3690

169 Wan, X.-Y., Zheng, L.-L., Gao, P.-F., Yang, X.-X., Li, C.-M., Li, Y.F., and Huang, C.Z.: 'Real-Time Light Scattering Tracking of Gold Nanoparticles- bioconjugated Respiratory Syncytial Virus Infecting HEp-2 Cells', Scientific Reports, 2014, 4, (1), pp. 4529

170 Rong, G., Wang, H., Skewis, L.R., and Reinhard, B.M.: 'Resolving Sub-Diffraction Limit Encounters in Nanoparticle Tracking Using Live Cell Plasmon Coupling Microscopy', Nano Letters, 2008, 8, (10), pp. 3386-3393

171 Wei, Q., Xiaohua, H., Bin, K., and Mostafa, A.E.-S.: 'Dark-field light scattering imaging of living cancer cell component from birth through division using bioconjugated gold nanoprobes', Journal of Biomedical Optics, 2010, 15, (4), pp. 1-9

172 Gao, J., Huang, X.Y., Liu, H., Zan, F., and Ren, J.C.: 'Colloidal Stability of Gold Nanoparticles Modified with Thiol Compounds: Bioconjugation and Application in Cancer Cell Imaging', Langmuir, 2012, 28, (9), pp. 4464-4471

173 Bhattacharjee, S.: 'DLS and zeta potential - What they are and what they are not?', J Control Release, 2016, 235, pp. 337-351

174 Clayton, K.N., Salameh, J.W., Wereley, S.T., and Kinzer-Ursem, T.L.: 'Physical characterization of nanoparticle size and surface modification using particle scattering diffusometry', Biomicrofluidics, 2016, 10, (5), pp. 054107

175 Khlebtsov, B.N., and Khlebtsov, N.G.: 'On the measurement of gold nanoparticle sizes by the dynamic light scattering method', Colloid Journal, 2011, 73, (1), pp. 118-127

176 Tomaszewska, E., Soliwoda, K., Kadziola, K., Tkacz-Szczesna, B., Celichowski, G., Cichomski, M., Szmaja, W., and Grobelny, J.: 'Detection Limits of DLS and UV-Vis Spectroscopy in Characterization of Polydisperse Nanoparticles Colloids', Journal of Nanomaterials, 2013, 2013, pp. 313081

177 Nobbmann, U.: 'Zeta potential in salt solution (or any other ions)', in Editor (Ed.)^(Eds.): 'Book Zeta potential in salt solution (or any other ions)' (Malvern Panalytical, 2018, edn.), pp.

178 Xu, Q., Ensign, L.M., Boylan, N.J., Schön, A., Gong, X., Yang, J.-C., Lamb, N.W., Cai, S., Yu, T., Freire, E., and Hanes, J.: 'Impact of Surface Polyethylene Glycol (PEG) Density on

Biodegradable Nanoparticle Transport in Mucus ex Vivo and Distribution in Vivo', ACS Nano, 2015, 9, (9), pp. 9217-9227

179 Pfeiffer, C., Rehbock, C., Hühn, D., Carrillo-Carrion, C., de Aberasturi, D.J., Merk, V., Barcikowski, S., and Parak, W.J.: 'Interaction of colloidal nanoparticles with their local environment: the (ionic) nanoenvironment around nanoparticles is different from bulk and determines the physico-chemical properties of the nanoparticles', Journal of the Royal Society, Interface, 2014, 11, (96), pp. 20130931-20130931

180 Pamies, R., Cifre, J.G.H., Espín, V.F., Collado-González, M., Baños, F.G.D., and de la Torre, J.G.: 'Aggregation behaviour of gold nanoparticles in saline aqueous media', J. Nanopart. Res., 2014, 16, (4)

181 Moore, T.L., Rodriguez-Lorenzo, L., Hirsch, V., Balog, S., Urban, D., Jud, C., Rothen-Rutishauser, B., Lattuada, M., and Petri-Fink, A.: 'Nanoparticle colloidal stability in cell culture media and impact on cellular interactions', Chem Soc Rev, 2015, 44, (17), pp. 6287-6305

182 Barreto, Â., Luis, L.G., Girão, A.V., Trindade, T., Soares, A.M.V.M., and Oliveira, M.: 'Behavior of colloidal gold nanoparticles in different ionic strength media', J. Nanopart. Res., 2015, 17, (12), pp. 493

183 Johnson, M.: 'Antibody Storage and Antibody Shelf Life', MATER METHODS 2012, 2, (120)

184 Zhang, W., Ang, W.T., Xue, C.Y., and Yang, K.L.: 'Minimizing nonspecific protein adsorption in liquid crystal immunoassays by using surfactants', ACS Appl Mater Interfaces, 2011, 3, (9), pp. 3496-3500

185 Larson, T.A., Joshi, P.P., and Sokolov, K.: 'Preventing protein adsorption and macrophage uptake of gold nanoparticles via a hydrophobic shield', ACS nano, 2012, 6, (10), pp. 9182-9190

186 Li, B., and Lane, L.A.: 'Probing the biological obstacles of nanomedicine with gold nanoparticles', Wiley Interdiscip Rev Nanomed Nanobiotechnol, 2019, 11, (3), pp. e1542

187 Lichtenberg, J.Y., Ling, Y., and Kim, S.: 'Non-Specific Adsorption Reduction Methods in Biosensing', Sensors (Basel, Switzerland), 2019, 19, (11), pp. 2488

188 Frederix, F., Bonroy, K., Reekmans, G., Laureyn, W., Campitelli, A., Abramov, M.A., Dehaen, W., and Maes, G.: 'Reduced nonspecific adsorption on covalently immobilized protein surfaces using poly(ethylene oxide) containing blocking agents', Journal of Biochemical and Biophysical Methods, 2004, 58, (1), pp. 67-74

189 Lee, J., Kang, H.A., Bae, J.S., Kim, K.D., Lee, K.H., Lim, K.J., Choo, M.J., and Chang, S.J.: 'Evaluation of analytical similarity between trastuzumab biosimilar CT-P6 and reference product using statistical analyses', mAbs, 2018, 10, (4), pp. 547-571

190 Shih, Y.-C., Ke, C.-Y., Yu, C.-J., Lu, C.-Y., and Tseng, W.-L.: 'Combined Tween 20-Stabilized Gold Nanoparticles and Reduced Graphite Oxide–Fe3O4 Nanoparticle Composites for Rapid and Efficient Removal of Mercury Species from a Complex Matrix', ACS Appl. Mater. Interfaces, 2014, 6, (20), pp. 17437-17445

191 Liberelle, B., Merzouki, A., and De Crescenzo, G.: 'Immobilized carboxymethylated dextran coatings for enhanced ELISA', J Immunol Methods, 2013, 389, (1-2), pp. 38-44

192 Zhao, Y.Y., Wang, Z., Zhang, W., and Jiang, X.Y.: 'Adsorbed Tween 80 is unique in its ability to improve the stability of gold nanoparticles in solutions of biomolecules', Nanoscale, 2010, 2, (10), pp. 2114-2119

193 Winther, J.R., and Thorpe, C.: 'Quantification of thiols and disulfides', Biochimica et biophysica acta, 2014, 1840, (2), pp. 838-846

194 Goebel-Stengel, M., Stengel, A., Taché, Y., and Reeve, J.R., Jr.: 'The importance of using the optimal plasticware and glassware in studies involving peptides', Analytical biochemistry, 2011, 414, (1), pp. 38-46

195 Burgess, R.R.: 'A brief practical review of size exclusion chromatography: Rules of thumb, limitations, and troubleshooting', Protein Expression and Purification, 2018, 150, pp. 81-85

196 Quesenberry, M.C., and Lee, Y.C.: 'A Rapid Formaldehyde Assay Using Purpald Reagent: Application under Periodation Conditions', Analytical Biochemistry, 1996, 234, pp. 50-55

197 Shao, Y., Yin, G.-Z., Ren, X., Zhang, X., Wang, J., Guo, K., Li, X., Wesdemiotis, C., Zhang, W.-B., Yang, S., Zhu, M., and Sun, B.: 'Engineering π–π interactions for enhanced photoluminescent properties: unique discrete dimeric packing of perylene diimides', RSC Advances, 2017, 7, (11), pp. 6530-6537

198 Anthon, G.E., and Barrett, D.M.: 'Comparison of Three Colorimetric Reagents in the Determination of Methanol with Alcohol Oxidase. Application to the Assay of Pectin Methylesterase', J. Agric. Food Chem., 2004, 52, pp. 3749-3753

199 Lakayan, D., Haselberg, R., Gahoual, R., Somsen, G.W., and Kool, J.: 'Affinity profiling of monoclonal antibody and antibody-drug-conjugate preparations by coupled liquid chromatography-surface plasmon resonance biosensing', Anal Bioanal Chem, 2018, 410, (30), pp. 7837-7848

200 Merwe, P.A.: 'Surface plasmon resonance', in Editor (Ed.)^(Eds.): 'Book Surface plasmon resonance' (2002, edn.), pp.

201 Schasfoort, R.B.M.: 'Chapter 1 Introduction to Surface Plasmon Resonance': 'Handbook of Surface Plasmon Resonance (2)' (The Royal Society of Chemistry, 2017), pp. 1-26

202 Abraham, R., Moller, D., Gabel, D., Senter, P., Hellström, I., and Hellström, K.E.: 'The influence of periodate oxidation on monoclonal antibody avidity and immunoreactivity', J Immunol Methods, 1991, 144, (1), pp. 77-86

203 Zhang, Z., Orski, S., Woys, A.M., Yuan, G., Zarraga, I.E., Wagner, N.J., and Liu, Y.: 'Adsorption of polysorbate 20 and proteins on hydrophobic polystyrene surfaces studied by neutron reflectometry', Colloids Surf B Biointerfaces, 2018, 168, pp. 94-102

204 Liang, M., Klakamp, S.L., Funelas, C., Lu, H., Lam, B., Herl, C., Umble, A., Drake, A.W., Pak, M., Ageyeva, N., Pasumarthi, R., and Roskos, L.K.: 'Detection of high- and low-affinity antibodies against a human monoclonal antibody using various technology platforms', Assay Drug Dev Technol, 2007, 5, (5), pp. 655-662

205 Filbrun, S.L., and Driskell, J.D.: 'A fluorescence-based method to directly quantify antibodies immobilized on gold nanoparticles', Analyst, 2016, 141, (12), pp. 3851-3857

206 Patskovsky, S., Bergeron, E., Rioux, D., and Meunier, M.: 'Wide-field hyperspectral 3D imaging of functionalized gold nanoparticles targeting cancer cells by reflected light microscopy', J Biophotonics, 2015, 8, (5), pp. 401-407

207 Wang, P., Wang, X., Wang, L., Hou, X., Liu, W., and Chen, C.: 'Interaction of gold nanoparticles with proteins and cells', Science and technology of advanced materials, 2015, 16, (3), pp. 034610-034610

208 Zong, J.Y., Cobb, S.L., and Cameron, N.R.: 'Peptide-functionalized gold nanoparticles: versatile biomaterials for diagnostic and therapeutic applications', Biomater. Sci., 2017, 5, (5), pp. 872-886

209 Daraee, H., Eatemadi, A., Abbasi, E., Aval, S.F., Kouhi, M., and Akbarzadeh, A.: 'Application of gold nanoparticles in biomedical and drug delivery', Artif. Cell. Nanomed. Biotechnol., 2016, 44, (1), pp. 410-422

210 Singh, P., Pandit, S., Mokkapati, V., Garg, A., Ravikumar, V., and Mijakovic, I.: 'Gold Nanoparticles in Diagnostics and Therapeutics for Human Cancer', Int. J. Mol. Sci., 2018, 19, (7), pp. 16

211 Arnida, Janát-Amsbury, M.M., Ray, A., Peterson, C.M., and Ghandehari, H.: 'Geometry and surface characteristics of gold nanoparticles influence their biodistribution and uptake by macrophages', European journal of pharmaceutics and biopharmaceutics : official journal of Arbeitsgemeinschaft fur Pharmazeutische Verfahrenstechnik e.V, 2011, 77, (3), pp. 417-423

212 Erathodiyil, N., and Ying, J.Y.: 'Functionalization of Inorganic Nanoparticles for Bioimaging Applications', Accounts of Chemical Research, 2011, 44, (10), pp. 925-935

213 Ciaurriz, P., Fernandez, F., Tellechea, E., Moran, J.F., and Asensio, A.C.: 'Comparison of four functionalization methods of gold nanoparticles for enhancing the enzyme-linked immunosorbent assay (ELISA)', Beilstein J. Nanotechnol., 2017, 8, pp. 244-253

214 Del Pino, P., Yang, F., Pelaz, B., Zhang, Q., Kantner, K., Hartmann, R., Martinez de Baroja, N., Gallego, M., Moller, M., Manshian, B.B., Soenen, S.J., Riedel, R., Hampp, N., and Parak, W.J.: 'Basic Physicochemical Properties of Polyethylene Glycol Coated Gold Nanoparticles that Determine Their Interaction with Cells', Angew Chem Int Ed Engl, 2016, 55, (18), pp. 5483-5487

215 Goossens, J., Sein, H., Lu, S., Radwanska, M., Muyldermans, S., Sterckx, Y.G.J., and Magez, S.: 'Functionalization of gold nanoparticles with nanobodies through physical adsorption', Analytical Methods, 2017, 9, (23), pp. 3430-3440

216 Matombi, A.N.: 'Fonctionnalisation de nanoparticules plasmoniques pour le ciblage de cellules du cancer du sein *in vitro*', Polytechnique Montréal, 2019

217 Liberelle, B.D.C., G., Henry, O.: 'Cahier de laboratoire : production, purification et analyse de Rituximab', in Editor (Ed.)^(Eds.): 'Book Cahier de laboratoire : production, purification et analyse de Rituximab' (École Polytechnique, 2019, edn.), pp. 1-70

218 Sowa, Y., Steel, B.C., and Berry, R.M.: 'A simple backscattering microscope for fast tracking of biological molecules', Rev Sci Instrum, 2010, 81, (11), pp. 113704

219 Dixon, A.R., Bathany, C., Tsuei, M., White, J., Barald, K.F., and Takayama, S.: 'Recent developments in multiplexing techniques for immunohistochemistry', Expert Rev Mol Diagn, 2015, 15, (9), pp. 1171-1186

220 Parra, E.R.: ‘Novel Platflorms of Multiplexed Immunofluorescence for Study of Paraffin Tumor Tissues’, Journal Cancer Treatment Diagnosis, 2018, 2, (1), pp. 43-53

221 Schubert, W., Bonnekoh, B., Pommer, A.J., Philipsen, L., Bockelmann, R., Malykh, Y., Gollnick, H., Friedenberger, M., Bode, M., and Dress, A.W.: ‘Analyzing proteome topology and function by automated multidimensional fluorescence microscopy’, Nat Biotechnol, 2006, 24, (10), pp. 1270-1278

222 Glass, G., Papin, J.A., and Mandell, J.W.: ‘SIMPLE: a sequential immunoperoxidase labeling and erasing method’, J Histochem Cytochem, 2009, 57, (10), pp. 899-905

223 Levin, M., Kron, S.J., Schwartz, D., and Snyder, H.: ‘Abstract 3949: Rapid 5-marker multiplex phenotyping of breast cancer subtypes & tumor-infiltrating leukocytes “in situ” in FFPE sections’, American Association for Cancer Research, 2016, 76, (14)

224 Faget, L., and Hnasko, T.S.: ‘Tyramide Signal Amplification for Immunofluorescent Enhancement’, in Hnasko, R. (Ed.): ‘ELISA. Methods in Molecular Biology’ (Humana Press, 2015)

225 Kairdolf, B.A., Smith, A.M., Stokes, T.H., Wang, M.D., Young, A.N., and Nie, S.: ‘Semiconductor quantum dots for bioimaging and biodiagnostic applications’, Annu Rev Anal Chem (Palo Alto Calif), 2013, 6, pp. 143-162

226 Zrazhevskiy, P., True, L.D., and Gao, X.: ‘Multicolor multicycle molecular profiling with quantum dots for single-cell analysis’, Nat Protoc, 2013, 8, (10), pp. 1852-1869

227 Mansfield, J.R., Gossage, K.W., Hoyt, C.C., and Levenson, R.M.: ‘Autofluorescence removal, multiplexing, and automated analysis methods for in-vivo fluorescence imaging’, J Biomed Opt, 2005, 10, (4), pp. 41207

228 Yong, K.T., Law, W.C., Hu, R., Ye, L., Liu, L., Swihart, M.T., and Prasad, P.N.: ‘Nanotoxicity assessment of quantum dots: from cellular to primate studies’, Chem Soc Rev, 2013, 42, (3), pp. 1236-1250

229 Bilan, R., Fleury, F., Nabiev, I., and Sukhanova, A.: ‘Quantum Dot Surface Chemistry and Functionalization for Cell Targeting and Imaging’, Bioconjugate Chemistry, 2015, 26, (4), pp. 609-624

230 Matros, A., and Mock, H.-P.: ‘Mass Spectrometry Based Imaging Techniques for Spatially Resolved Analysis of Molecules’, Frontiers in Plant Science, 2013, 4, (89)

231 Rimm, D.L.: ‘What brown cannot do for you’, Nature Biotechnology, 2006, 24, (8), pp. 914-916

232 Dempsey, L.A.: ‘CyTOF analysis of anti-tumor responses’, Nat Immunol, 2017, 18, (3), pp. 254

233 Di Palma, S., and Bodenmiller, B.: ‘Unraveling cell populations in tumors by single-cell mass cytometry’, Current Opinion in Biotechnology, 2015, 31, pp. 122-129

234 Bendall, S.C., Simonds, E.F., Qiu, P., Amir el, A.D., Krutzik, P.O., Finck, R., Bruggner, R.V., Melamed, R., Trejo, A., Ornatsky, O.I., Balderas, R.S., Plevritis, S.K., Sachs, K., Pe'er, D., Tanner, S.D., and Nolan, G.P.: ‘Single-cell mass cytometry of differential immune and drug responses across a human hematopoietic continuum’, Science, 2011, 332, (6030), pp. 687-696

235 Yalcin, E.B., and de la Monte, S.M.: 'Review of matrix-assisted laser desorption ionization-imaging mass spectrometry for lipid biochemical histopathology', J Histochem Cytochem, 2015, 63, (10), pp. 762-771

APPENDIX A – MATERIALS

I. AuNP Product Information

AuNPs of a 100 nm diameter, dispersed in MQ water and capped with citrate, were ordered from Nanopartz®. The product number of the AuNPs was A11-100-CIT-DIH-1-100-CS. According to Nanopartz® data sheets, the concentration of the AuNPs at an optical density (OD) of 1 was $4.96x10^9$ NPs/mL, which corresponded to a molar concentration of 8.30 pM. With respect to its spectral data, these AuNPs showed an SPR peak at 569 nm, corresponding to a molar extinction coefficient of $1.21x10^{11}$ M^{-1} cm^{-1} at its maximal concentration. The decision to opt for commercially synthesized AuNPs was made by identifying that controlling their size distribution (when synthesizing them in the lab) would be a considerable challenge, and that manufacturer-synthesized AuNPs would boast a smaller size dispersion (for example, Nanopartz® claims that their 100 nm AuNPs have a dispersion of less than 4%). Moreover, turning our attention towards AuNP synthesis would ultimately fall out of the scope of the objectives of this Master's thesis in functionalizing AuNPs with antibodies.

II. PEG Product Information and Preparation of Stocks

An overview of the different heteromono- and bifunctional PEG molecules employed during the entirety of this Master's thesis project, as well as their sources, are highlighted below.

Table 5-1 Overview of different PEG molecules (heteromono- and bifunctional) used during this Master's thesis project.

Full Name	Short Form	Manufacturer	Product Number
methoxy-PEG-Thiol	mPEG-SH	JenKem®	A3029-1/M-SH-5000
methoxy-PEG-Thiol	mPEG-SH	Nanocs®	PG1-TH-5k
N-Hydroxysuccinimide-PEG-Thiol	NHS-PEG-SH	Nanocs®	PG2-NSTH-5k
Boc-Hydrazine-PEG-Thiol	Hyd-PEG-SH	Polyscience®	26220

Due to complications related to the use of mPEG-SH from Nanocs®, all experiments conducted after discovering this faulty stock of PEG employed mPEG-SH from JenKem®. The results that confirmed the faulty stock of PEG from Nanocs® can be seen in Appendix F.

Prior to their addition to AuNP samples, PEG freezer stocks were prepared at a concentration of 2 mM. To 1 mL of solvent, 10 mg of powder was weighed out and dissolved. MQ was used to dissolve mPEG-SH, while dimethyl sulfoxide (DMSO) was used to dissolve NHS-

PEG-SH and Hyd-PEG-SH. From these stock solutions, 50 μL aliquots were prepared, and unused aliquots were stored at -80°C. To quantify the concentration of free thiols present in the prepared stocks (for the purposes of calculating the amount of PEG to add to AuNP samples), an Ellman's test was performed (details on this assay can be found in Appendix D). The thiol concentrations determined from an Ellman's test are provided below (note that mPEG-SH from Nanocs® is not shown):

Table 5-2 Summary of concentrations of free thiols determined from an Ellman's test performed on each PEG stock.

Name	PEG Concentration (mM)	Free Thiol Concentration (mM)
mPEG-SH (JenKem®)	2	1.74
NHS-PEG-SH	2	1.64
Hyd-PEG-SH	2	1.84

III. Antibody Product Information and Preparation of Stocks

Aliquots of the selected antibody, Trastuzumab (TZM), were used for the entirety of this Master's research project. The decision to work with TZM was made based on the desired diagnostic application that would target the Her2 receptor overexpressed in some breast cancer cell lines. Additionally, these antibodies were easy to produce in mammalian cell lines such as CHO, as glycosylation could be better controlled.

These antibodies were produced and expressed in Chinese hamster ovary (CHO) cell lines and produced at the National Research Council of Canada-Mont Royal. A titer of 500 mg at a concentration of 4.04 mg/mL (approximately 27 μM) was acquired and antibodies were stored in PBS. From this titer 100 μL aliquots were prepared and stored at -80°C.

APPENDIX B – DYNAMIC LIGHT SCATTERING AND ZETA POTENTIAL

DLS and ZP measurements were acquired for each step of biofunctionalization of AuNPs. They were acquired following a wash of AuNP samples incubated with PEG, as well as after a wash of PEGylated AuNPs grafted to antibodies.

I. Protocol for Taking DLS Measurements

To measure the hydrodynamic radius of the PEGylated AuNP samples, DLS measurements were taken. These were performed on a Zetasize Malvern ZEN3600™ Instrument (from Malvern Panalytical, Inc.). To prepare the samples for DLS, and its subsequent ZP measurements on the same instrument, sodium chloride (NaCl) was added to the samples at a final concentration of 5 mM. Samples were injected into a folded capillary cell (Malvern Panalytical, Inc. DTS1070) with a 1 mL Luer-Lok™ syringe. Parameters were set as follows on the instrument prior to launching the standard operating procedure (SOP): (1) dispersant was MQ, (2) material was gold, (3) refractive index was 0.181, (4) number of scans was 15, (5) scans per second was 1, (6) number of replicates was three. To reuse the folded capillary cells between different samples, the samples were first carefully aspirated from the cells with a fresh syringe, before thoroughly flushing the cells with MQ to wash away any salt or gold residue, and drying them out with an air inlet. Finally, to compare the PEGylated AuNP samples to a standard size, DLS measurements were also taken for a control of bare, 100 nm AuNPs. Data acquired for analysis of samples and controls included the raw intensity measurements relative to the hydrodynamic size logarithmic scale, the Z-average size, the polydispersion index (PDI), and the PDI width. To illustrate the instrumental set-up required to obtain DLS measurements on the Zetasizer Malvern ZEN3600™, a figure is provided below:

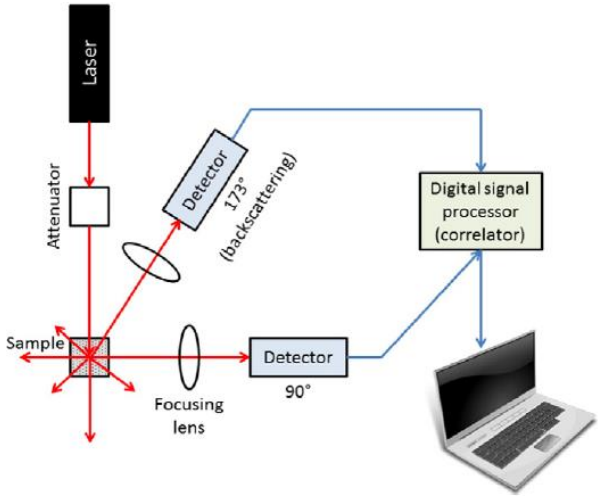

Figure 5-1 Schematic illustration depicting the instrumental set-up required for acquiring DLS measurements. Image reproduced from Bhattacharjee et. al, 2016 [173].

II. Protocol for Taking ZP Measurements

A similar set-up to DLS measurements (i.e. adding NaCl) was done to prepare the samples for ZP measurements on the same Zetasizer Malvern ZEN3600™ Instrument as previously This time, the only parameters that changed for the SOP were: (4) number of scans was 20, (5) scans per second was 2. Folded capillary cells were washed and dried the exact same way as for DLS, in order to reuse them for other samples. To compare the ZP measurements acquired for each sample, a control of bare, 100 nm AuNPs was used as a standard for the ZP surface charge. Data acquired for analysis of samples and controls included the ZP surface charge, the electrophoretic mobility (Mob) and the conductivity. A figure below provides a theoretical explanation to how the ZP surface charge is generated:

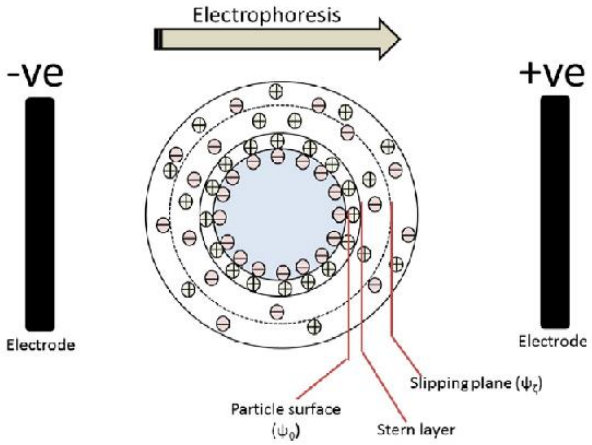

Figure 5-2 Schematic illustration depicting how the ZP surface charge is acquired. Image reproduced from Bhattacharjee et. al, 2016 [173].

APPENDIX C – UV-VIS ABSORBANCE

To prepare samples for UV-VIS absorbance measurements of the spectra of AuNP samples, 150 μL of each sample were pipetted in triplicate to the wells of a 96-well plate. Blanks corresponding to the solvents used to disperse the AuNPs, such as MQ or PBS, were also added to this plate. A control of bare, 100 nm AuNPs was also added. The plate was covered with plastic film in order to minimize evaporation during measurements. The plate was then placed inside a EPOCH™ Microplate Spectophotometer (from BioTek™). The SOP launched had the following parameters sets: (1) interval between scans – 1 nm, (2) range – 300 to 800 nm, (3) scanning speed – 4 nm/s. Upon acquisition of data, the raw absorbance values as a function of each wavelength were extracted for each sample, and the replicates of each sample and control were then averaged. The blank curves were then subtracted from each sample and control, and the data was plotted.

To determine the concentration of AuNP samples recovered after each step of functionalization, whether it was post-PEGylation or antibody incubation, the concentrations were calculated by dividing the peak absorbance value (absolute amplitude) of each sample by the peak absorbance value of the control of bare AuNPs. As the concentration of bare AuNPs was known based on the manufacturer's data sheets (4.96×10^9 NPs/mL), the concentrations of other AuNP samples were determined by multiplying the ratio between the peak absorbance values of sample:bare AuNPs by the concentration of bare AuNPs.

APPENDIX D – ELLMAN'S TEST

In order to quantify the number of free thiols present in PEG samples, Ellman's tests were conducted. First, a buffer of PBS containing ethylene diamine tetraacetic acid (EDTA) (100 mM phosphate and 1 mM EDTA) was prepared at a pH of 7.4. This buffer was used to dissolve Ellman's reagent (5,5'-Dithiobis-(2-Nitrobenzoic acid) or DTNB) at a concentration of 1 mg/mL (2.5 mM), as well as to dilute any thiol samples into the dynamic range of this assay (between 5 and 150 μM). A quenching solution of 0.5% (v/v) Tween-20 in MQ was also prepared.

For the assay, 60 μL of DTNB was added to 140 μL of sample (in triplicate) in PBS-EDTA buffer in a 96-well plate. A blank of 140 μL of PBS-EDTA buffer (in triplicate) was also incubated with the same volume of DTNB. Incubation was then allowed to proceed for 1 min, before the reaction was quenched by adding 10 μL of Tween-20. The absorbance was read on a Victor™ plate reader (from Perkin Elmer, Inc.) at 405 nm, and at 630 nm as a correction.

To process the data, first absorbance values at 630 nm were subtracted from the values at 405 nm. The averaged blank absorbance values were then subtracted from the samples. To calculate the concentration of free thiols, an approximation of 0.00963 absorbance units (AU) per μM of free thiol (an experimentally determined ratio previously found in the lab) was used, while also taking into account the D=1.5 dilution factor of the assay volume as well as any possible dilutions required to bring the sample into the dynamic range of the assay. Concentrations calculated for each sample were then averaged amongst its replicates, and standard deviations were calculated, prior to plotting the data.

APPENDIX E – PEGYLATION OF GOLD NANOPARTICLES

I. Calculation of PEG Concentrations and PEGylation Protocol

To calculate the minimal concentration of thiolated PEG that could completely cover the surface of AuNPs, the footprint of each thiolated PEG was approximated to be 3 molecules per nm^2 of AuNP surface. Based on a total surface area of 31 416 nm^2 for 100 nm spherical AuNPs at a concentration of $4.96x10^9$ NPs/mL, a minimal final concentration of 740 nM of free thiolated PEG was determined. In order to take into account the possibility of oxidation between PEG molecules, as well as diffusion effects, all of which could reduce the number of thiolated PEG molecules that could successfully bond to the gold surface, an excess concentration of 14x PEG relative to this minimal concentration was added to the samples. This excess concentration corresponded to 10 μM total PEG. To achieve varying percentages of heterobifunctional PEG, whether it was NHS-PEG-SH or Hyd-PEG-SH, the volumes from PEG freezer stock aliquots with a free thiol concentration of 2 mM were altered, while changing the volume of heteromonofunctional mPEG-SH accordingly. A summary of these freezer stock aliquot volumes required to achieve different compositions of each form of PEG is provided below.

Table 5-3 Overview of 2 mM thiolated PEG freezer stock aliquot volumes required per 600 μL of AuNPs, for PEGylating at different percentages of either NHS-PEG-SH or Hyd-PEG-SH (NHS and Hyd for short, respectively) relative to mPEG-SH, in order to achieve a final total thiolated PEG concentration of 10 μM.

Sample	**Form of PEG**	
	Volume of mPEG-SH (μL)	**Volume of NHS/Hyd-PEG-SH (μL)**
Control	3.0	N/A
3% NHS / Hyd	2.7	0.3
10% NHS / Hyd	2.4	0.6
30% NHS / Hyd	2.1	0.9

Upon addition of these respective volumes to AuNP samples, the mixtures were allowed to incubate at room temperature overnight for 16 hours on a shaker platform running at 100 rpm. Samples were covered with aluminium foil to protect them from light exposure.

II. Centrifugation and Washing Protocol for PEGylation and Antibody-Conjugation Strategies

Following incubation between PEG and AuNP samples, washing was carried out in order to remove excess, unbound PEG. First, they were centrifuged at 5 000xg for 5 min in a benchtop centrifuge, so as to pellet the AuNPs bound to PEG, and separate it from unbound PEG in the supernatant. While being careful not to disturb the pellets, 500 μL of supernatant was withdrawn per 600 μL of sample, and placed in a separate Eppendorf™ tube for further analysis by an Ellman's test (to quantify the number of thiolated PEG removed). Samples were re-suspended in 500 μL of MQ. Upon addition of MQ, samples were thoroughly mixed by first vortexing them at the highest speed, before sonicating them in a water bath at room temperature for brief 5 second intervals. This cycle of vortexing and sonicating was repeated until the walls of the sample tubes were completely clear from any AuNP adsorption (samples were held up to the light to ensure that the Eppendorf™ walls were completely transparent). This mixing step during re-suspension was important in ensuring that any losses of AuNPs due to NSA against the walls of the Eppendorf™ tubes would be minimized. After re-suspending and mixing the samples, the above sequence of steps for washing was repeated once more, and restoring the final volume to 600 μL.

As removal of AuNPs during their washing is unavoidable, losses were quantified by re-centrifuging the supernatants at 5 000xg for 5 min, in order to first validate qualitatively if a pellet was formed, before re-suspending the pellets and measuring the UV-VIS absorbance spectra of the supernatants.

APPENDIX F – STABILITY ASSAY DETAILS FOR EXPERIMENTAL SET-UP AND DATA ANALYSIS PROCEDURE

I. Set-Up of Assay and Differences from PEGylation and Antibody Conjugation Protocols

This Appendix will discuss the protocol employed to test and monitor the stability of both PEGylated and antibody-conjugated AuNPs, in order to determine the optimal conditions for storage. Several deviations from the traditional PEGylation protocol (see Appendix E) were introduced for this stability assay and will be discussed below:

(1) **Washing of AuNP samples with citrate:** all bare AuNP samples were washed with fresh 800 μM sodium citrate prior to PEGylation, by centrifuging them for 5 min at 5 000xg, withdrawing supernatant (and reserving it to quantify any losses of AuNPs), and re-suspending it in an equivalent volume of 800 μM sodium citrate, pH 7.

(2) **Re-suspension conditions for PEGylated AuNP samples:** AuNP samples were re-suspended in equivalent volumes of either PBS or MQ (i.e. replacing equivalent volume of supernatant with re-suspension solution), upon completion of the second centrifugation step for washing, in the case of stability assays with PEGylated AuNP samples. For stability assays involving antibody-conjugated, PEGylated AuNP samples, the solvents for re-suspension were either PBS, PBS+Tween-20 (0.5% v/v) or MQ.

(3) **Re-suspension conditions of antibody-conjugated, PEGylated AuNP samples:** following washing of PEGylated samples, **various treatments were performed** on the functional groups exposed from these samples, in order to **prepare them for conjugation** to antibodies by any of the three different strategies (further details on these treatments can be found in the Appendix section of each strategy). As a result, **it was important to uphold consistency in the solvents used** initially following re-suspension of washed PEGylated AuNP samples, and subsequently used to re-suspend samples following this treatment step (whether it be during a washing step or prior to conjugation). For example, a sample re-suspended initially in PBS following washing of PEGylated AuNPs would need to be consistently re-suspended in PBS for all remaining steps (treatment, conjugation and washing).

(4) **Preparation of positive and negative controls for stability**: citrate-washed, bare AuNPs in MQ were established as the **positive control** for stability, while citrate-washed, bare AuNPs re-suspended in PBS (after centrifuging for 5 min at 5 000xg and withdrawing supernatant) were set as the **negative control** for stability.

(5) **No further processing of the exposed functional groups** of PEGylated AuNPs was performed, so **only three variants of PEGylated AuNPs were tested,** either: (1) solely mPEG-SH, (2) mixture of mPEG-SH and Hyd-PEG-SH, or (3) a mixture of mPEG-SH and Hyd-PEG-SH.

Upon re-suspending PEGylated AuNP samples in their respective solvent (PBS, PBS+Tween-20, MQ) following the second centrifugation step in the standard PEGylation protocol, **timing for the assay began** (re-suspension of the negative control in PBS was also timed to line up with other samples re-suspended in their respective solvents). In the case of antibody-conjugated, PEGylated AuNP samples, however, **this initial time point began** when **antibodies were first added** to the treated PEGylated AuNP samples.

For all samples, they were added to a 96-well plate in triplicate by pipetting 150 μL into each well. **Blanks of MQ, PBS, PBS+Tween-20 and citrate** were also added to this plate (whose curves would be subtracted from their sample counterparts in order to account for differences between solvents). The plate was then covered with plastic film in order to **minimize losses** of AuNPs due to evaporation. The UV-VIS absorbance spectra were then acquired (following the same procedure in Appendix C), and the timepoint for each measurement **was noted and set relative** to initial timepoint of re-suspension. Summary tables outlining the different PEGylated AuNP samples, different antibody-conjugated, PEGylated AuNP samples, and controls tested with their respective conditions are provided below in Tables 5-5 and 5-6.

Table 5-4 List of heteromonofunctional mPEG-SH and heterobifunctional NHS-PEG-SH or Hyd-PEG-SH AuNP samples and their respective conditions tested during the stability assay. In the interest of simplicity, only mixed PEGylated AuNP samples with a 10% composition are included.

Sample	Type(s) of PEG	PBS / MQ Solvent
Positive Control	None	MQ
Negative Control	None	PBS
PEG+MQ	mPEG-SH	MQ

PEG+PBS	mPEG-SH	PBS
NHS+MQ	NHS-PEG-SH, mPEG-SH	MQ
NHS+PBS	NHS-PEG-SH, mPEG-SH	PBS
Hyd+MQ	Hyd-PEG-SH, mPEG-SH	MQ
Hyd+PBS	Hyd-PEG-SH, mPEG-SH	PBS

Table 5-5 List of heteromonofunctional mPEG-SH and heterobifunctional NHS-PEG-SH, Mal-PEG-SH or Hyd-PEG-SH AuNP samples adsorbed or conjugated to antibodies, and their respective conditions tested during the stability assay. In the interest of simplicity, mixed PEGylated AuNP samples of different percent compositions of each form of PEG are not included. Antibody conjugation approaches are numbered as follows: (1) randomly oriented, (2) semi-oriented, (3) oriented. Controls for all strategies are labelled as such.

Approach(es)	**Sample**	**Type(s) of PEG**	**PBS / MQ Solvent**	**Presence / Absence of Antibodies**
Control	Positive Control	None	MQ	None
Control	Negative Control	None	PBS	None
Control	PEG+PBS	mPEG-SH	PBS	None
Control	PEG+Tween-20	mPEG-SH	PBS+Tween-20	None
Control	PEG+TZM+PBS	mPEG-SH	PBS	Yes
Control	PEG+TZM+Tween-20	mPEG-SH	PBS+Tween-20	Yes
Control	PEG+TZM+MQ	mPEG-SH	MQ	Yes
1	NHS+PBS	NHS-PEG-SH, mPEG-SH	PBS	None
1	NHS+TZM+PBS	NHS-PEG-SH, mPEG-SH	PBS	Yes
1	Mal+TZM+Tween-20	NHS-PEG-SH, mPEG-SH	PBS+Tween-20	Yes
1	NHS+TZM+MQ	NHS-PEG-SH, mPEG-SH	MQ	Yes
2	Mal+PBS	Mal-PEG-SH, mPEG-SH	PBS	None
2	Mal+TZM+PBS	Mal-PEG-SH, mPEG-SH	PBS	Yes
2	Mal+TZM+Tween-20	Mal-PEG-SH, mPEG-SH	PBS+Tween-20	Yes

3	Hyd+PBS	Hyd-PEG-SH, mPEG-SH	PBS	None
3	Hyd+TZM+PBS	Mal-PEG-SH, mPEG-SH	PBS	Yes
3	Hyd+TZM+Tween-20	Mal-PEG-SH, mPEG-SH	PBS+Tween-20	Yes

II. Handling of Samples between Measurements on a Day-to-Day Basis

The stability of the AuNP samples was monitored over one week, with one UV-VIS absorbance spectra measurement taken every day. Between UV-VIS absorbance spectra measurements, the plate was stored at 4°C, and **a correction factor taking into account any potential loss** of AuNPs due to evaporation and loss from adsorption to plasticware (ex: pipette tips, walls of 96-well plate) was calculated by pipetting the volume of the blanks remaining in their wells.

As bare AuNPs have a tendency to **sediment** while being stored at lower temperatures (Figure 5-3), the wells containing the controls were gently pipetted up and down to re-suspend the AuNPs. Furthermore, **in order to take into account any losses of AuNPs** due to evaporation or NSA against the walls of the wells, the **volumes of the blanks** remaining in the wells were measured and used to approximate the percent loss of AuNPs. For example, if only 140 µL of blank was recovered at a certain timepoint, this volume would be divided by the initial volume of 150 µL in order to calculate a percent loss correction factor for all the other samples.

Figure 5-3 Example of AuNPs sedimented in the wells of a 96-well plate, in order to illustrate the importance of re-suspension of AuNPs between absorbance measurements over the course of the stability assays.

III. Data Analysis Procedure

i. Calculating Relative Amplitudes

To extract relative amplitudes, first the baseline of the near-UV (NUV) tail region preceding the SPR peak was averaged between 409 and 499 nm. This window for the baseline was selected as it was determined empirically that the SPR peak of the positive control would always begin shortly after 500 nm, and at wavelengths below 400 nm, the NUV tail region would begin to deviate from a flat curve, mostly due to non-radiative effects in AuNPs. After averaging the baselines of each sample (in triplicate), these were subtracted from each absorbance value of the SPR peak between 500 and 700 nm. Once again, this SPR peak window for the subtraction of each sample's baseline had been empirically determined from the spectra of the positive control. This subtraction would thus allow for the relative amplitude of the SPR peak to be identified for each sample. This procedure for extracting the relative amplitude was repeated in triplicate for each sample, before the relative amplitudes were averaged across all three replicates of each sample, and standard deviations were calculated.

ii. Calculating Full-Width at Half-Maximum (FWHM)

To extract FWHM, the non-averaged relative amplitudes previously determined were first divided by two to calculate their half-maxima. Next, the baseline-subtracted absorbance values in the same window of 500 to 700 nm were subtracted from each sample's half-maximum. This subtraction of the half-maxima would allow for the start and end points of the width of the baseline-subtracted SPR peak to be identified, based on at which points the half-maxima subtracted values would change sign. The FWHMs were then calculated from these start and end points for each sample (in triplicate), before averaging their widths and calculating their standard deviations.

iii. Further Processing of Spectral Elements

To further process acquired UV-VIS absorbance data of the AuNP samples:

(1) **A correction factor taking into account any losses of AuNPs** during their storage (either due to evaporation or NSA) was also determined. This was calculated by measuring the volumes of liquid remaining in the wells of the blanks, and comparing it to the starting volume of 150 μL, allowing for a **percent loss factor** to be calculated. As this percent loss

factor would decrease the baselines of the samples' UV-VIS absorbance spectra, it was applied to the relative amplitudes calculated in order to increase their values.

(2) **A normalization of the UV-VIS absorbance spectra of each sample** relative to the positive control's spectra was also calculated. To achieve this, the three elements extracted from each sample's UV-VIS absorbance spectra (SPR peak position, relative amplitude and FWHM) were converted into percentages by either: (i) **dividing the data value at the first measured time point** (not t=0) by the **positive control's value** or (ii) **fixing the data value** obtained at the **first measured time point to 100%,** and calculating percentages for all subsequent data values **relative to this value** at the first time point. The former was applied to the **two controls**, while the latter was applied to **each PEGylated AuNP sample**. Upon obtaining these percent values for all samples, the percentages were **normalized to the positive control** by dividing each percent value at a particular time point by the positive control's percent value. This would thus always set the positive control's percentage to 100%, and allow for a direct comparison of the stabilities of the negative control or PEGylated samples with the positive control.

(3) **Percent deviation of the percent values** was also calculated. This was done by simply subtracting the non-normalized percent values from the percent values of the positive control for the same timepoint, and then dividing this difference by the same percent value of the positive control.

APPENDIX G – RANDOMLY ORIENTED STRATEGY METHODS

I. Protocol for Re-Activating NHS Groups on NHS-PEGylated AuNPs

To account for any hydrolysis of the NHS groups of PEG that occurred during PEGylation or washing of AuNPs, reactivation of these groups was required, by adding NHS and EDC to the NHS-PEGylated AuNPs (dispersed in MQ), and letting them incubate.

To achieve re-activation of NHS groups, 50 μL each of EDC and NHS at stock concentrations of 400 and 100 mM, respectively (aliquots previously prepared and stored at -80°C), were added to 600 μL of hydrolyzed, NHS-PEGylated AuNP samples. EDC and NHS were thus incubated with the samples at a final concentration of 33 and 8.3 mM, respectively. Incubation was carried out for 15 min at room temperature on a shaker platform running at 100 rpm. To remove excess NHS and EDC, the samples underwent two washing cycles, where they were centrifuged at 5 000xg for 5 min, before 600 μL of their supernatants were withdrawn and the samples were re-suspended in 500 μL of MQ, restoring the final volume of the samples to their initial volume of 600 μL.

II. Calculations for Antibody Molar Excess Added to NHS-PEGylated AuNPs

Reactivated NHS-PEGylated AuNPs containing percentages of NHS-PEG-SH relative to mPEG-SH of either 3%, 10% or 30% were first prepared, and **re-suspended in PBS+Tween-20 0.5% v/v)** following **completion of the re-activation step**.[10] To minimize NHS-mediated cross-linking, a **10x molar excess** of antibodies relative to the theoretical concentration of NHS-PEGylated AuNPs was added. These theoretical concentrations were calculated to be 8, 30 and 80 nM for 3%, 10% and 30% NHS-PEG-SH initially added to the AuNP samples, respectively. These antibody concentrations for incubation would thus be 80, 300 and 800 nM, respectively. A table summarizing the volumes of antibody stocks added to samples is shown below in Table 5-6. Incubation was carried out overnight for 16 hours at room temperature on a shaker platform running at 100 rpm. At the same time, a methoxy-PEGylated AuNP sample in PBS+Tween-20 (0.5% v/v) was prepared, and **incubated with a molar excess of antibodies equivalent to the amount added**

[10] For stability assays, these re-activated NHS-PEGylated AuNPs were also re-suspended in MQ or PBS.

to the AuNP samples PEGylated with 10% NHS-PEG-SH, thus 300 nM. This sample would act as the control in order to evaluate the extent of NSA that could arise between PEG and antibodies. The next morning, the samples underwent centrifugation and washing to eliminate excess antibodies. The samples were stored at 4°C until further characterization.

Table 5-6 Volumes of -80°C freezer stock aliquots of TZM antibodies added to each re-activated NHS-PEGylated AuNP sample for the sake of the antibody-conjugation reaction.

Sample	**Incubation Concentration of TZM (nM)**	**Volume of TZM Aliquot (27 µM) to add to 600 µL of AuNP sample (µL)**
PEG (Control)	300	6.7
3% NHS	80	1.8
10% NHS	300	6.7
30% NHS	800	17.8

III. Centrifugation and Washing Protocol for Antibody-Conjugated, PEGylated AuNPs

The next morning, excess antibodies were removed by two centrifugation and washing cycles. Samples were centrifuged at 7 000xg for 5 min, 500 µL of supernatants were withdrawn, and pellets were re-suspended in PBS (to wash away any remaining Tween-20 from incubation)[11], to ensure that the initial volume of 600 µL was restored. At the conclusion of these two centrifugation and washing cycles, samples and controls were stored at 4°C until they were to be used for characterization or experiments involving cells.

[11] For the stability assays, samples were always re-suspended in their buffer of choice (PBS, MQ or PBS+Tween-20).

APPENDIX H – SEMI-ORIENTED STRATEGY METHODS

I. Protocol for Transforming NHS Groups on PEGylated AuNPs into Maleimide Groups

In order to be able to target the hinge region of reduced antibodies, re-activated NHS groups of PEGylated AuNPs (see Appendix G for reactivation protocol) had to be transformed into maleimide groups. This was performed by adding the reagent N-ε-maleimidocaproic acid hydrazide (EMCH), a heterobifunctional cross-linker capable of reacting with NHS groups via its hydrazide moiety, and introducing a maleimide functional group on its other end.

To 600 μL of re-activated NHS-PEGylated AuNPs with 10% NHS-PEG-SH, 6 μL of 100 10 mM N-ε-maleimidocaproic acid hydrazide (EMCH) in DMSO (stored at -20°C) was added, to achieve a final concentration of EMCH of 100 μM, which represented an amount far in excess to the concentration of NHS groups available at any initial percentage. Upon addition of EMCH to the AuNP samples, incubation was carried out for 30 min at room temperature on a shaker platform running at 100 rpm. To ensure that any stray, unreacted NHS groups would not react with the antibodies in a non-specific manner, these groups were then deactivated by adding 1 μL of 1 M ethanolamine, pH 7 to each sample. Deactivation of these NHS groups was then allowed to proceed for 15 min at room temperature. Following this step, excess EMCH and ethanolamine were before simultaneously removed by subjecting the samples to two washing cycles, where they were centrifuged at 5 000xg for 5 min, 500 μL of their supernatants were withdrawn and an equivalent volume of MQ was added to restore the original volume of each sample. Prior to addition of antibodies, samples were centrifuged once more at 5 000xg for 5 min, and the supernatant was replaced with PBS+Tween-20 (0.5% v/v).

II. Reduction of Antibodies

i. Protocol for Reducing Antibodies by TCEP

In order to successfully conjugate maleimide-PEGylated AuNPs to the hinge region of the antibodies, a tris(2-carboxyethyl)phosphine hydrochloride (TCEP) reduction of these antibodies had to be performed. A gel (ThermoScientific™ Pierce™ Immobilized TCEP Disulfide Reducing Gel, Product Number P177712) with an active concentration of 8 mM TCEP was used to reduce a

batch of 6.8 μM TZM in PBS with 10 mM EDTA. EDTA served the purpose of preventing re-oxidation of the thiol groups of antibodies once reduced.

By assuming that TCEP selectively targets the two disulfide bridges of antibodies found in their hinge region (as reported in the literature), upon diluting the antibodies down to 6.8 μM, a concentration of free thiols as high as 27 μM could be liberated once they were reduced by TCEP. As per the guidelines of the manufacturer of the TCEP gel, the optimal incubation time for 1 mg/mL of antibodies (6.8 μM) would be 1 hour.

Prior to incubation with antibodies, a slurry of the gel was washed to prepare it for incubation with the antibodies, by first vortexing 250 μL of it with 750 μL of PBS with 5 mM EDTA, before centrifuging the mixture at 1 000xg for 1 minute, discarding the supernatant, and re-suspending the pellet in an equivalent volume of PBS with 5 mM EDTA. This washing of the slurry was repeated twice more, before withdrawing 750 μL of supernatant a final time and adding 150 μL of 27 μM antibodies and 200 μL of PBS with 5 mM EDTA to the remaining 250 μL of washed slurry. This would bring the final volume for incubation up to 600 μL, and would thus dilute the antibodies down to 6.8 μM, the desired concentration for incubation. The mixture was vortexed, and incubation was allowed to proceed for 60 minutes at room temperature on a shaker platform running at 100 rpm. Upon concluding the incubation, the tube containing the mixture was centrifuged at 1 000xg for 1 minute, and as much of the supernatant was recovered (while recording the volume recovered). To calculate an average volume of supernatant recovered from the incubation, a second tube of washed slurry incubated with antibodies was prepared at the same time. This average volume was found to be roughly 600 μL, the same volume originally used for incubation between the slurry and antibodies.

ii. Characterization of Reduced Antibodies

After recovering the supernatant, **an Ellman test (Appendix D) was performed** on it in order to **quantify the concentration of reduced antibodies** with exposed thiol groups, making sure to take into account any dilutions that would arise during the prior incubation and washing steps (i.e. an initial dilution of 4 of freezer stock antibodies). After performing the above sequence of incubating and washing the antibody-slurry mixture in triplicate, an average free thiol concentration of 27 μM was measured for an incubation period of 60 min for 6.8 μM antibodies,

which corresponded to roughly 4 free thiols per antibody resulting from the TCEP reduction. It is worth noting that initially this incubation was also carried out for shorter and longer time intervals, in order to determine the optimal time point at which reduction of the disulfide bridges of the hinge region could be achieved. These results can be seen below in Figure 5-4. In order to calculate the ratio of free thiols per antibody upon reduction, a UV-VIS absorbance measurement at 280 nm was conducted, and an extinction coefficient of 1.47 L g^{-1} cm^{-1} was used to convert to mass concentration via Beer's Law [189]. To convert to molar concentrations, the average empirically-determined molecular weight of glycosylated TZM was used (150 kDa). This allowed for the molar concentration of free thiols detected by an Ellman's test to be divided by the measured concentration of reduced antibodies recovered from the TCEP gel.

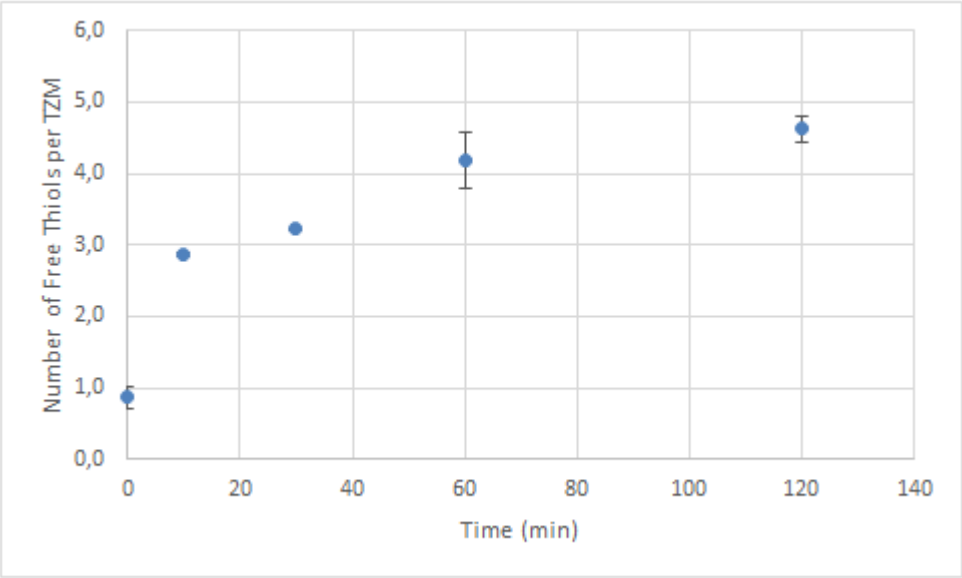

Figure 5-4 Number of free thiols per TZM over time, as measured from an Ellman's test of the supernatants collected from a TCEP-gel slurry at discrete time intervals. Values represent averages of three 96-well plate measurements per sample, and error bars represent standard deviation.

Finally, the performance of the TCEP gel over time was evaluated, in order to see whether re-using the gel between reduction experiments would negatively impact its ability to effectively reduce the gel. As it can be seen below in Figure 5-5, re-using the gel over time does result in a slight decrease in the efficacy of the gel in liberating free thiols from the hinge region of the antibodies, when the incubation time is held constant at 60 min.

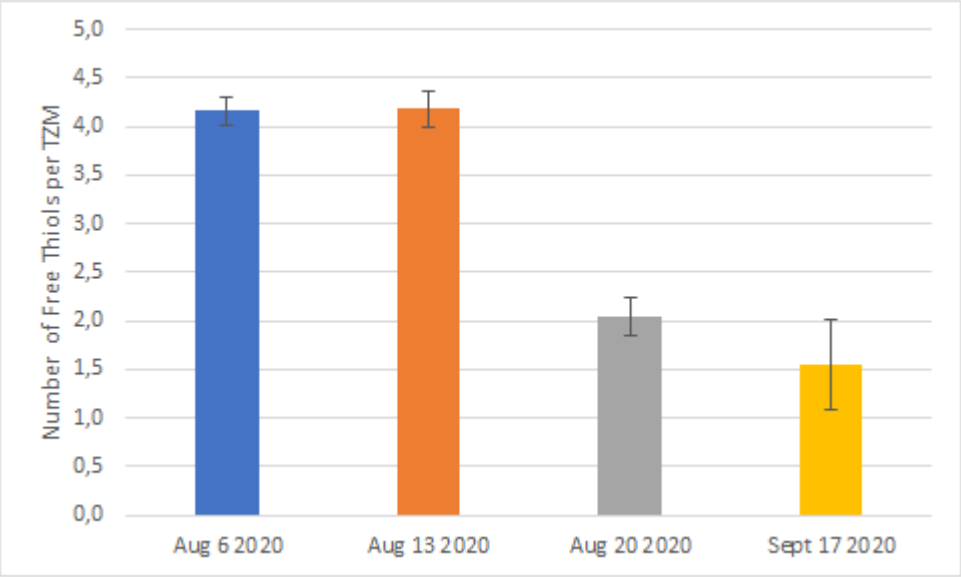

Figure 5-5 Performance of TCEP gel to reduced TZM antibodies over time, as determined by the number of free thiols per TZM detected based on an Ellman's test. Values represent averages of three 96-well plates measurements per sample, and error bars represent standard deviation.

III. Calculations for Reduced Antibody Molar Excess Added to Maleimide-PEGylated AuNPs

Maleimide-transformed PEGylated AuNPs were prepared, and were re-suspended in PBS+Tween-20 (0.5% v/v). A sample of methoxy-PEGylated AuNPs was also prepared and re-suspended in the same buffer. **In order to minimize** the extent of cross-linking between AuNPs, a 10x molar excess of antibodies was reacted relative to the **theoretically highest concentration of maleimide groups (either 8, 30 or 80 nM)** that could be yielded from NHS-PEGylated AuNPs initially prepared at either 3%, 10% or 30% NHS-PEG-SH. This antibody excess translated into the same incubation concentration seen for the randomly oriented strategy, thus either 80, 300 or 800 nM of reduced antibodies, respectively, were reacted with these maleimide-PEGylated AuNP samples. Methoxy-PEGylated AuNPs were reacted with the same incubation concentration of antibodies seen in the randomly oriented strategy (300 nM). An overnight incubation of 16 hours at room temperature on a shaker platform running at 100 rpm was then allowed to proceed, and the samples underwent two centrifugation and washing cycles in order to remove excess antibodies, once again following the same procedure as employed for the randomly oriented strategy.

APPENDIX I – ORIENTED STRATEGY METHODS

I. Protocol for Deprotecting Boc-Hydrazine Groups on PEGylated AuNPs to Expose Hydrazide Groups

Protected hydrazide groups of Boc-hydrazine-PEGylated AuNPs (prepared according to Appendix E) needed to be deprotected in order to expose the hydrazide groups that could react with oxidized antibody sugars. Although this step was never attempted, an acid work-up had been envisioned. Acetic acid was to be added to the washed Boc-hydrazine-PEGylated AuNP samples in order to achieve this.

To achieve this, 50 µL of 5% (v/v) acetic acid, pH 5 (874 mM) would be added to 600 µL of Boc-Hydrazine-PEGylated AuNP samples, to achieve a final concentration of acetate of 67 mM. Incubation would be carried out for 15 min at room temperature on a shaker platform running at 100 rpm. Excess acetate would be removed by two washing cycles, followed by centrifugation of the samples at 5 000xg for 5 min, withdrawal of 550 µL of supernatant, and re-suspension of the samples in 500 µL of PBS+Tween-20 (0.5% v/v) to restore the initial volume of 600 µL.

II. Oxidation of Antibodies

To carry out oxidation of the glycosylated region of the antibodies for allow for the Fc region to be selectively targeted by deprotected, hydrazide-PEGylated AuNPs , sodium periodate ($NaIO_4$) was used, which selectively targets hemiacetals and acetals present in the sugar chains, transforming them into aldehyde groups that can react with hydrazide groups. A batch of antibodies was oxidized by periodate, and then purified by size exclusion chromatography (SEC), and re-concentrated with Amicon® centrifuge filter tubes with a 30 kDa MWCO.

i. Protocol for Oxidizing Antibodies

First, a stock of 100 mM periodate was prepared in MQ and wrapped with aluminum foil to prevent exposure to the light, as periodate is light-sensitive. A stock solution of 100 mM sodium sulfite was also prepared in MQ. The sulfite solution would be responsible for quenching the oxidation reaction.

Oxidation of antibodies was carried out by reacting a 1 mL of the antibody freezer stock (at 27 µM) with 100 µL of 100 mM periodate, to obtain a final periodate concentration of 10 mM. The

aluminum foil-wrapped mixture was allowed to incubate for 30 minutes at room temperature on a shaker platform running at 100 rpm, at which point, a 2x molar excess of sulfite was added by adding 200 μL of 100 mM sulfite. The mixture was vortexed well to ensure complete quenching.

ii. Purification of Oxidized Antibodies

The oxidized antibodies were purified and separated from excess sulfite and periodate by resorting to size exclusion chromatography (SEC). For this, a Superde® 200 HiLoad® 16/600 column (GE Healthcare™) with a resin of cross-linked agarose and dextran[KE1] was chosen to separate and purify the mixture. The column was hooked up with tubing to a System Fast Protein Liquid Chromatography (FPLC) ÄKTA™ Explorer whose parameters could be controlled by an ÄKTA™ Explorer Unicorn software. The tubing lines were first equilibrated with MQ by setting the software to a flow rate of 5 mL/min and bypassing the column, allowing the lines to equilibrate for 5 min. The column was then equilibrated with MQ at a flow rate of 1.5 mL/min (by redirecting the tubing path to the column) until 0.25 column volume (CV) had flowed through. For this column, had a CV of 120 mL, this was equal to 30 mL. Next, the column was equilibrated with PBS at a flow rate of 1.5 mL/min until 2 CV had flowed through (equal to 240 mL).

The entirety of the oxidized antibody mixture (1.3 mL) was then aspirated with a fine-tip needle and injected through a separate valve connected to a loop on the System FPLC ÄKTA™ Explorer. The following parameters were set based on a previously established SOP for purifying TZM antibodies: (1) Column Position – 3, (2) Compensation Volume – 6 mL, (3) Pre-Injection Volume of Buffer – 3 mL, (4) Fractions – 0 (this was to ensure the fraction collector would not run), (5) Elution CV – 1 (i.e. 120 mL), (6) Flow Rate – 1.5 mL/min. The SOP was launched, and the sample was eluted via the column with PBS. At approximately 45 min after starting the run, TZM had been previously determined in the lab to exit the column, which corresponded to an elution volume centered around 68 mL at its peak. Absorbance at 280 nm (A280) was monitored on the display screen of the software. At the beginning of the A280 peak, the exit line was redirected from the waste towards a Falcon tube, and a 10 mL fraction corresponding to the antibodies was collected (this fraction volume of 10 mL had also been previously determined in the lab).

iii. Re-Concentration of Oxidized Antibodies

Upon collection of the fraction, the sample was re-concentrated in an Amicon™ ultra centrifugation tube with a 30 kDa MWCO, by centrifuging it at 3 000xg for 10 min. The volume of the retentate collected in the filter was measured, and was re-suspended in a volume of PBS allowing for the original volume of 1 mL of antibodies to be restored.

iv. Characterization of Oxidized Antibodies

Quantification of the total concentration of antibodies, as well as the concentration of oxidized antibodies, was carried out by three different characterization methods:

(1) Standard curve of antibodies injected and detected by the ÄKTA™ Explorer: the concentration of oxidized TZM antibodies purified by SEC and collected in the 10 mL fraction was measured by comparing the integrated area under the curve of its A280 peak to a series of standard TZM solutions of known concentrations. These standards were injected onto the column and were subjected to the exact same operating conditions for the column as previously described. A 10 mL fraction with its elution peak centered around 68 mL was once again collected. Standards in PBS at concentrations of 27, 9, 3, 1, 0.3 μM (injected in triplicate) were used to generate two standard curves of either integrated area vs. injected concentration or peak height vs. injected concentration. Integrated areas were acquired using the ÄKTA explorer software, whereby the same start and end points for the eluted peak were set to fix an elution peak with a baseline volume of 10 mL. This allowed for a line of best fit to be determined for the linear regression model, which was used to calculate the concentration of injected, oxidized TZM. The results of this standard curve can be seen below in Figure 5-6:

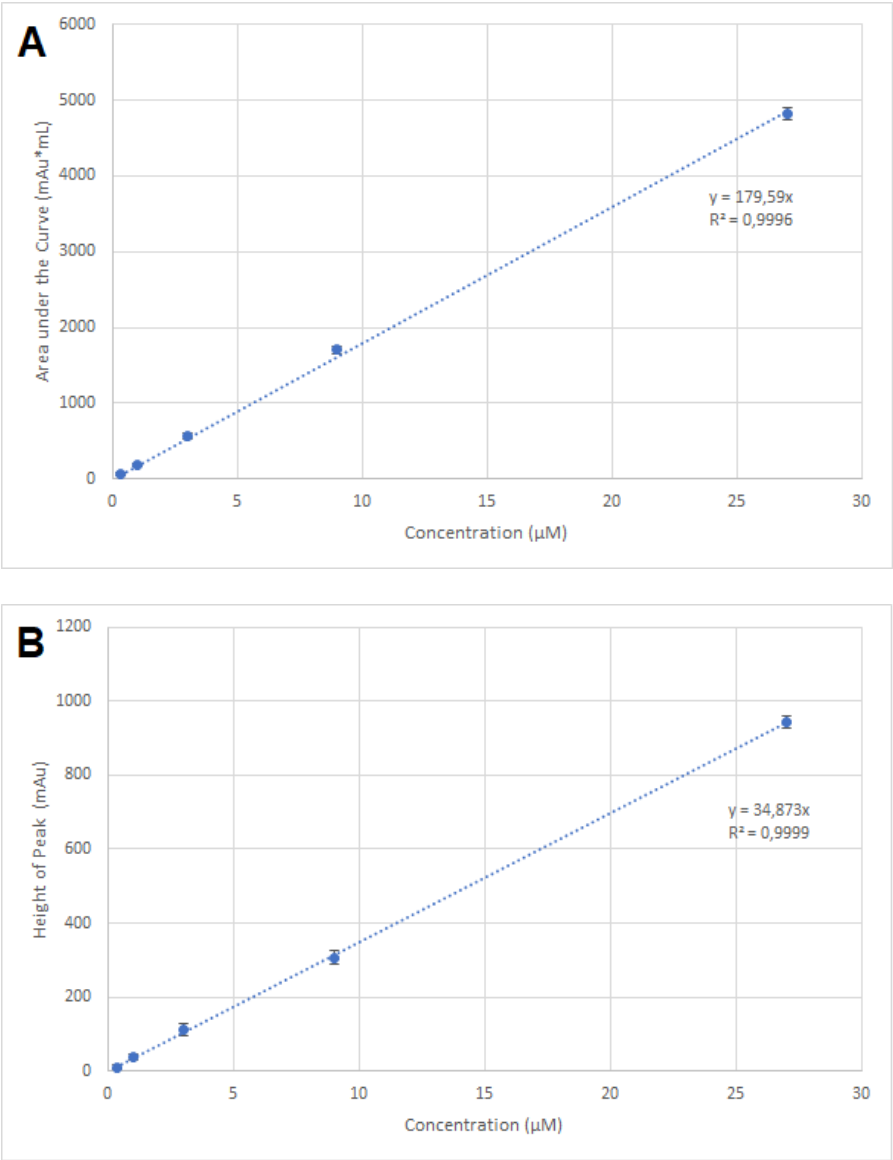

Figure 5-6 Standard curves of integrated chromatograms for: (A) area under the curve and (B) peak height for TZM standards injected onto SEC column and recovered at the same elution volume. Values represent average of two replicates, and error bars represent standard deviation.

(2) UV-VIS absorbance measurement at 280 nm for re-concentrated antibodies: re-concentrated antibodies were placed in a quartz cuvette for an A280 measurement, using PBS as a blank. Its concentration was determined via Beer's Law by using the mass extinction coefficient for TZM, which is 1.47 L g^{-1} cm^{-1} [189].

(3) Purpald® assay: the concentration of aldehyde groups yielded upon antibody oxidation was determined by carrying out a Purpald® assay. Although this protocol was never optimized, this was the protocol attempted by following that described by Quesenberry and Lee [196]. Due to concerns over the toxicity of formaldehyde, benzaldehyde was used instead. A 34.2 mM solution of Purpald's reagent, or 4-amino-3-hydrazino-5-mercapto-1,2,4-triazole (Sigma-Aldrich™, product number 162892), which preferentially reacts with free aldehydes, was prepared in 0.5 M sodium hydroxide (NaOH). Note that this solution was **always prepared fresh.** Standards of benzaldehyde (ACS grade, 99.5% from Sigma-Aldrich™, product number 402788) diluted in PBS were first prepared in parallel under the fume hood at concentrations of 300, 100, 30, 10, and 3 μM. For each standard and oxidized antibody sample, 100 μL (in triplicate) was first incubated for 10 min at 37°C. To each standard and sample, 100 μL of Purpald's reagent was added and the solution was vigorously vortexed and exposed to air between vortex cycles, to ensure adequate oxygenation. These mixtures were then incubated for 30 min at 37°C on a shaking platform running at 100 rpm, before adding the entire volume to the wells of a 96-well plate, and measuring their absorbance at 550 nm. The line of best fit was determined for the standard curve, and linear regression was used to calculate the concentration of oxidized antibodies.

(4) SPR assay: a procedure adapted from Analytical and Bioanalytical Chemistry (2018) was employed to characterize the binding affinity between oxidized TZM antibodies and their receptors Her2, compared to a series of TZM standards [199]. The experiments were performed on a Biacore™ instrument (GE Healthcare Life Sciences®). Briefly, recombinant human ErbB2/Her2 Fc chimera protein (R&D Systems, Novusbio) (Her2 receptor for short) as injected for 10 min at a flow rate of 10 μL/min at a concentration of 20 μg/mL in 10 mM sodium acetate (pH 4) onto a carboxymethyl dextran (CMD) hydrogel gold sensor chips (GE Healthcare) activated surface (equilibrated with immobilization buffer of 10 mM HEPES, 150 mM NaCl, 3 mM EDTA and 0.005% Tween-20 (v/v) for 10 min,). This CMD surface was activated by a 7 min injection with 0.4 M EDC and 0.1 M NHS. After immobilization of Her2 onto the activated CMD surface, remaining active NHS-esters were deactivated by adding 1 M ethanolamine (pH 8) two times for 7 min with 1 min buffer flow (with PBS) in between each injection.

Following this deactivation step, the surface was regenerated with a buffer of 10 mM glycine-HCl (pH 1.5), resulting in stripping of any non-covalently bound Her2 receptors. Following this loading and regeneration of the gold surface, standards of TZM (ranging from 10 to 1000 pM) in HEPES buffer (pH 7) were injected at 50 μL/min for 3 min over top of the Her2-loaded surface, and the ensuing relative response units (RU) were measured (baseline subtraction of prior measured RU from Her2 and NHS/EDC injection was also performed). This was followed by a dissociation step of 6 min to look for the formation of a stable plateau. In between each sample measurement, the surface was regenerated with the glycine buffer injected for 1 min. Similar to the standards of TZM, oxidized antibodies over the same range of concentrations in HEPES were also prepared, and subsequently injected onto the Her2-loaded surface following completion of the standard curve. All injections for each sample and standard were done in triplicate.

Data was analyzed by plotting the average change in response (ΔRU) vs. injection time for the 9 min duration over which sample or standard was injected. To calculate the percent affinity retained for the oxidized antibodies, each sample's respective time point RU value was divided by the equivalent TZM standard counterpart at the same time point, in order to generate a series of values of percent RU retained. These percent values were then averaged over the first 240 s (when the RU values of each curve peaked) to acquire a rough estimate of the percent activity of oxidized antibodies relative to their TZM standard counterparts.

III. Calculations for Oxidized Antibody Molar Excess Added to Hydrazide-PEGylated AuNPs

The protocol described in Hermanson was used to conjugate hydrazide-PEGylated AuNPs to oxidized antibodies [97]. Based on the determined concentration of re-concentrated, oxidized antibodies, a 10:1 molar excess of antibodies relative to the theoretically highest number of available hydrazide groups on PEGylated AuNPs was added. For compositions of 3, 10 and 30% Hyd-PEG-SH during the PEGylation of AuNPs with a total PEG concentration of 10 μM, this would correspond to maximal theoretical concentrations of 8, 30 and 80 nM, respectively. Hence, the same volumes used for the randomly oriented strategy (see Appendix G) were used to incubate

oxidized antibodies with their respective counterparts of deprotected, hydrazide-PEGylated AuNPs (re-suspended in PBS+Tween-20) at varying percent compositions of Hyd-PEG-SH. Incubation was then allowed to proceed overnight for 16 hours at room temperature on a shaker platform running at 100 rpm. The next morning, a ratio of 10 μL of 5 M sodium cyanoborohydride (NaCNBH) in 1 M NaOH (solution in this existing condition from Sigma-Aldrich™, product number 296945) per mL of reacted solution was added to the mixture under the fume hood. NaCNBH ensures that the hydrazone bond formed between the hydrazide groups and exposed aldehydes is stabilized. This mixture was allowed to react for 30 min at room temperature on a shaker platform running at 100 rpm. To quench the reaction by preventing any stray hydrazide groups from reacting, a ratio of 50 μL of 1 M ethanolamine, pH 9 (ACS grade, 99.0% from Sigma-Aldrich™, product number 398136) per mL of reacted solution was added to the mixture, and this mixture was then incubated for 30 min at room temperature once again.

Excess antibodies, ethanolamine and NaCNBH were removed from the reacted antibody-PEG-AuNP conjugates by two washing cycles, where the mixture was centrifuged for 5 min at 7 000xg, 550 μL of supernatant was withdrawn, and an equivalent volume of PBS was used to re-suspend the pellets and wash away any remaining Tween-20. At the conclusion of the second re-suspension, the samples were stored at 4°C until they were characterized or applied to cells.

IV. Stability Assays for Boc-Hydrazine and Methoxy-PEGylated AuNPs

As was previously seen for the stability assays involving NHS-PEGylated AuNPs, stability assays were also conducted for Boc-Hydrazine-PEGylated AuNPs compared to methoxy-PEGylated AuNPs, in order to evaluate their stability in MQ and PBS. The exact same procedure employed for preparing samples and extracting UV-VIS absorbance spectral elements were followed to analyze Boc-Hydrazine PEGylated AuNP samples prepared at an original percent composition of 10% Hyd-PEG-SH. The percent-normalized stability curves for both relative amplitudes and FWHM can be seen below:

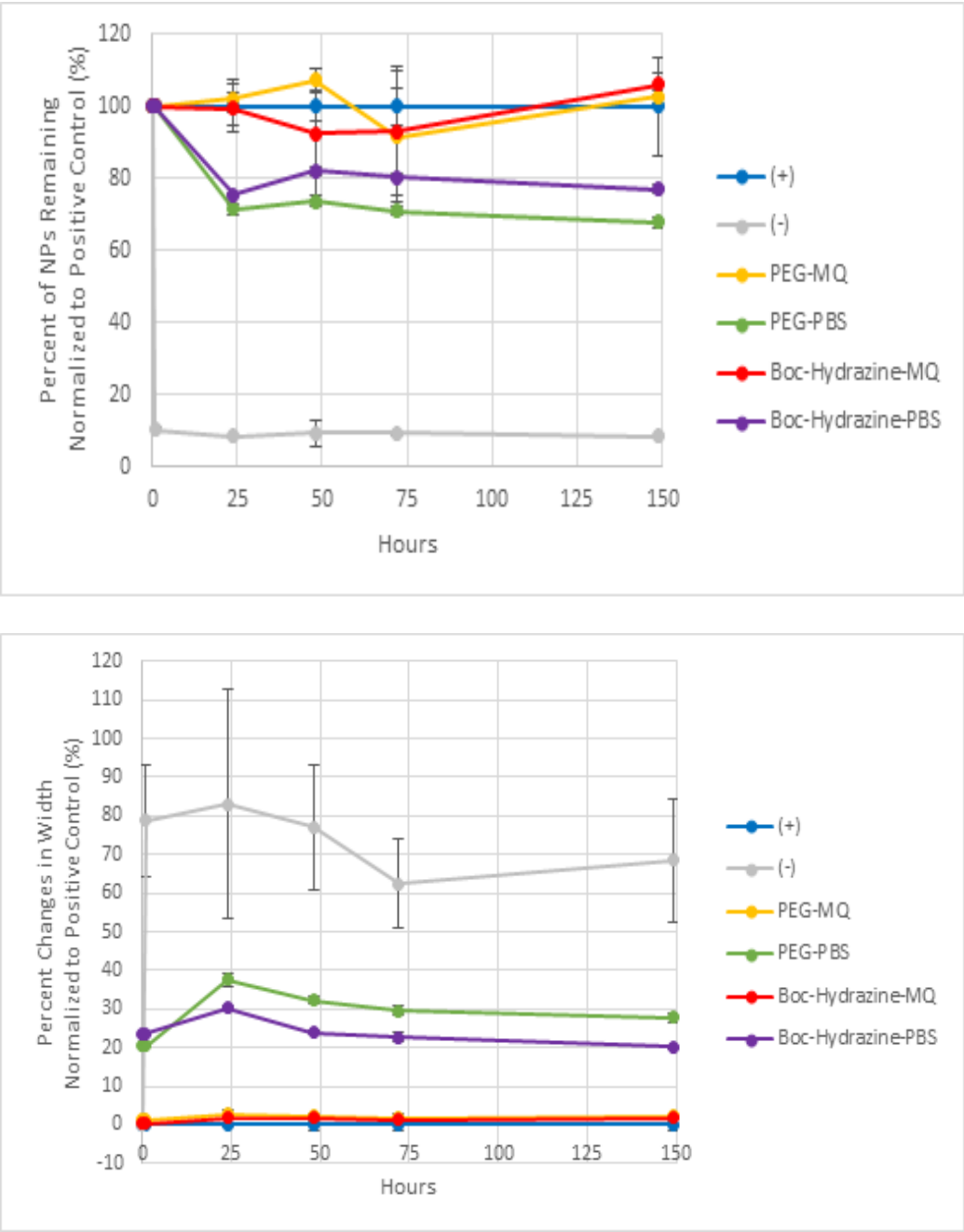

Figure 5-7 Stability curves of Boc-hydrazine- and methoxy-PEGylated AuNPs conjugated to antibodies for: (A) normalized percentage of AuNPs remaining, as calculated from the relative amplitudes of their SPR peaks, and (B) normalized percent change in FWHM of AuNP SPR peaks. Sample abbreviations are labelled as follows: (+) – positive control, (-) – negative control, PEG – mPEG-SH AuNPs, Boc-Hydrazine – 10:1 mPEG-SH:Hyd-PEG-SH AuNPs, MQ – re-suspended in MQ, PBS – re-suspended in PBS.

APPENDIX J – METHODS FOR INDIRECT QUANTIFICATION OF FUNCTIONALIZED ANTIBODIES

I. Set-Up of ELISA Assay

An ELISA sandwich assay was performed on the supernatants collected from the centrifuged, antibody-conjugated AuNP samples, in order to indirectly quantify the number of antibodies immobilized (either via NSA or molecular conjugation) onto the surfaces of the AuNP samples. These supernatants were collected in triplicate from the following antibody-incubated samples: AuNPs+PEG, AuNPs+PEG+TZM, AuNPs+NHS 30%+TZM and AuNPs+Mal 30%+TZM. These supernatants were stored at -20°C when they were not immediately used for this assay.

An ELISA protocol previously developed and optimized in the lab for the quantification of Rituximab was used as a guide for this protocol involving unbound TZM antibodies remaining in the supernatants [217]. Standards of unmodified TZM ranging from 0 to 50 ng/mL (0 constituting the blank), as well as reduced TZM ranging from 0 to 500 ng/mL, were prepared in PBS+Tween-20 (0.5% v/v). Considering the rather high concentrations of antibodies incubated with the PEGylated-AuNP samples (on the order of magnitude of 300 to 800 nM, or 45 to 120 μg/mL), the supernatants collected from methoxy-PEGylated, NHS-PEGylated and maleimide-PEGylated AuNP samples were diluted in PBS+Tween-20 by 1000-, 1500- and 150- fold, respectively, in order to get the supernatant antibody concentrations within the linear dynamic range of ELISA (10 pg/mL to 100 ng/mL). Note that the maleimide-PEGylated AuNP supernatants were not diluted as much as the other two samples, despite having the same starting antibody concentration for incubation. This was because after conducting the assay the first time, it was discovered that the maleimide-PEGylated AuNP supernatants generated a weak absorbance signal, which suggested poor affinity between the reduced antibodies and either the primary or detection antibodies. Given that these reduced antibodies were in fact half-antibody fragments, it is not surprising that the affinity for the Fc-region of these other antibodies was impacted.

Following this initial dilution of the PEGylated AuNP supernatants, one additional dilution of D=3 was done, in order to provide a set of two different dilutions that would both fall within the

linear dynamic range of ELISA, and thus allow for a more accurate concentration of free antibodies in the supernatant to be determined by averaging the absorbance values of the two dilutions.

All samples (at both dilutions) and standards were pipetted (100 μL each) in triplicate into the wells of a 96-well plate previously covered with primary antibodies (AffiniPure™ Goat Anti-Human IgG, 2 mg, Jackson ImmunoResearch® from Cedarlane®, product number 109-005-008) diluted to 8.8 μg/mL, and blocked with 1% (v/v) bovine serum albumin (BSA) in PBS. Primary antibodies (100 μL per well) had been previously incubated overnight to allow for adsorption to the walls of the plate. Following removal of excess, unbound antibodies remaining in the solution of each well (i.e. antibodies unbound to the walls of the plate), washing steps with PBS+Tween-20 (3 cycles, 150 μL per well) were carried out, prior to adding the next layer of either antibodies or BSA.

Incubation between supernatant antibodies and the blocked primary antibodies was carried out for 1 hour at room temperature on a shaking platform running at 100 rpm. Excess, unbound supernatant antibodies were then removed from the wells of the plate, washed with PBS+Tween-20 as before, prior to adding 100 μL per well of secondary antibodies (Peroxidase-conjugated AffiniPure™ Fragment Goat Anti-Human IgG, 2 mL, Jackson ImmunoResearch® from Cedarlane®, product number 109-035-003) diluted to 0.8 mg/mL. Incubation between secondary antibodies and the underlying layer of supernatant antibodies was carried out for 30 min at room temperature in the dark on a shaking platform running at 100 rpm. A final washing step (as before) was then performed after removing excess, unbound secondary antibodies, prior to adding 100 μL per well of the substrate for peroxidase, which was 3,3',5,5'-Tetramethylbenzidine (TMB) (Sigma-Aldrich™ product number T0440). This substrate was diluted by a factor of 2 from its stock solution. The substrate was allowed to react in the dark for 8 min. At this point, 50 μL per well of a stop solution of 1 M HCl was added to end the blue-colour generating reaction mediated by peroxidase. Absorbance measurements were then taken by a Victor™ plate reader (Perkin-Elmer, In.) at both 450 and 531 nm.

II. Data Analysis

Absorbance measurements at 531 nm were first subtracted from each sample's absorbance value measured at 450 nm. Triplicates were averaged for each sample and standard, before

subtracting the reference blank from each sample and standard in order to correct for any background absorbance. A standard curve was then plotted for both unmodified and reduced TZM, to generate two lines of best fit. These standard curves can be seen below in Figure 5-8:

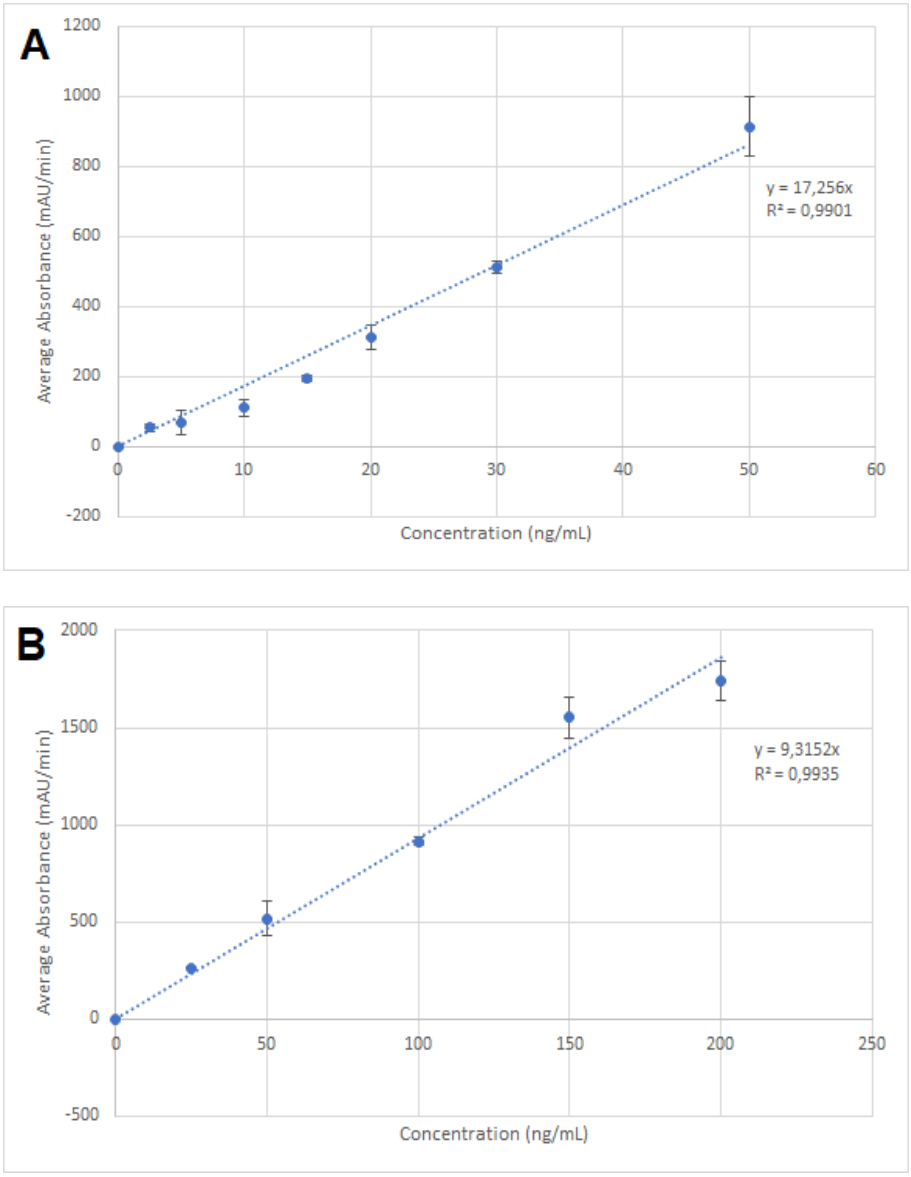

Figure 5-8 ELISA standard curves of: (A) unmodified TZM and (B) TCEP-reduced TZM used to perform linear regression analysis on supernatants of antibody-functionalized AuNP samples. Values represent average of three replicates, and error bars represent standard deviation.

To calculate the concentrations of antibodies residing in the supernatants of each sample, linear regression analysis was used to determine the diluted concentration for each sample's set of two dilutions. The appropriate dilution factors were then applied to calculate the actual antibody

supernatant concentration, before averaging between the two dilutions for each sample. Background absorbance values from PEGylated AuNPs lacking antibodies were then subtracted from each sample, in order to generate a corrected absorbance value. Finally, to indirectly calculate the concentration of immobilized antibodies on the AuNP samples, these measured and corrected supernatant absorbance values were subtracted from the starting concentrations used to incubate antibodies with each PEGylated-AuNP sample. A table summarizing these starting concentrations is shown below in Table 5-7. The indirectly calculated concentrations of antibodies immobilized onto each PEGylated AuNP sample can also be seen below in Figure 5-9.

Table 5-7 Overview of starting concentrations of antibodies (unmodified and reduced) used during incubation with PEGylated-AuNP samples.

Sample	**Incubation Concentration of Unmodified TZM (nM)**	**Incubation Concentration of Reduced TZM (nM)**
PEG (Negative Control)	N/A	N/A
PEG+TZM	300	N/A
30% NHS+TZM	800	N/A
30% Mal+TZM	N/A	800

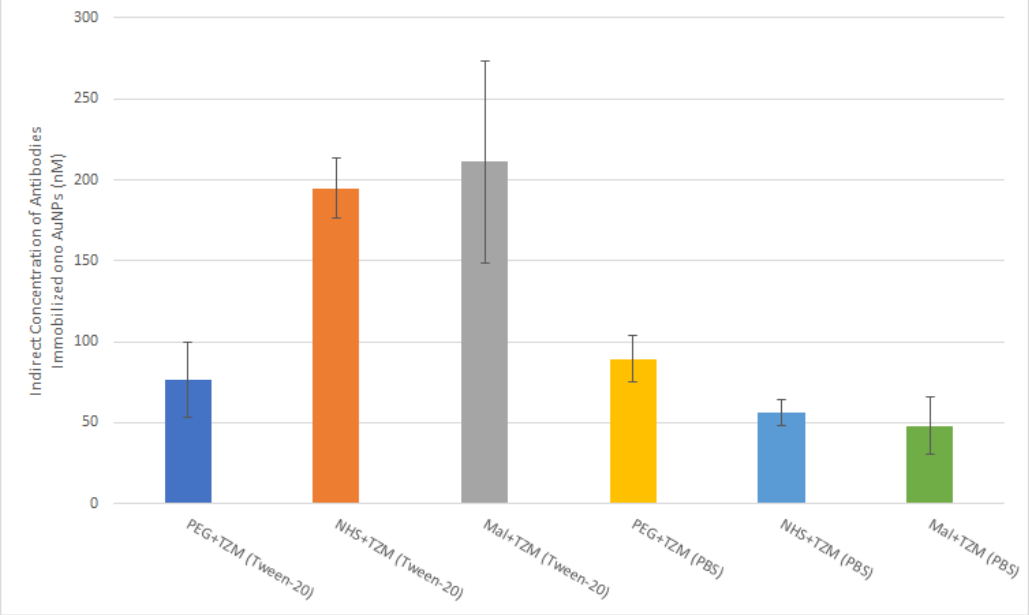

Figure 5-9 Concentrations of antibodies immobilized onto functionalized AuNPs, as obtained indirectly from the ELISA assays performed on the supernatants collected from functionalized AuNP samples incubated overnight. Concentrations determined via linear regression analysis of either unmodified or reduced TZM standard curves. Values represent averages of three samples acquired in triplicate, with each respective sample measured at two different dilution factors (3x2 data points), and error bars represent standard deviation.

Finally, to calculate the ratio of antibodies per PEGylated AuNP, these indirectly calculated immobilize antibody concentrations were compared to the calculated AuNP concentrations determined via UV-VIS absorbance (following the standard method by comparing their SPR peak values with bare AuNPs of a known concentration).

In contrast, to estimate the ratio of NSA to covalent conjugation, a few steps were used to process the data. First the number of active functional groups was calculated based on the AuNP concentration values, in order to estimate the number of covalently linked antibodies per AuNP. This value was then subtracted from the total number of antibodies per AuNP calculated above, allowing for a ratio between the extent of NSA versus covalent conjugation to be estimated.

APPENDIX K – METHODS FOR DIRECT QUANTIFICATION OF FUNCTIONALIZED ANTIBODIES

I. Set-Up of NanoOrange Assay

The procedure described by Filbrun and Driskell [205] was followed for preparation of samples and standards, and dissolving AuNP samples in potassium iodide (KI) / iodine (I_2). However, a few modifications to the procedure were introduced due to a lack of access to the appropriate equipment. First, instead of measuring the fluorescence of the NanoOrange dye (due to a lack of access to a fluorimeter), the absorbance of the samples was measured at the same two wavelengths described, namely 490 and 595 nm. Second, due to a lack of availability of an appropriate resin (in a desalting column) to remove excess KI / I_2 from dissolved AuNP samples, this excess was kept, and a correction factor was applied in order to take into account any absorbance from KI / I_2 that could interfere with analyzing the samples.

II. Data Analysis

To correct for these two modifications to the procedure, first the absorbance measurements at 490 nm were subtracted from the absorbance measurements obtained at 595 nm, which still allowed for some fluorescence to be detected, given that 490 nm was considered the excitation wavelength for the NanoOrange dye. Next, a blank of bare AuNPs lacking antibodies had its averaged absorbance values subtracted from each sample and standard, in order to calculate a reference absorbance value. This allowed for a standard curve to be generated from the bare AuNPs adsorbed to antibodies from a range of 0.6 nM to 60 nM, which was considered to fall within the linear dynamic range of the assay. However, upon plotting, a non-linear relationship between standard concentration and their reference absorbance value (rather a logarithmic relationship was seen), and thus a linear transformation was applied to the data by taking the reciprocal of both the standard concentrations and their reference absorbance values, in order to generate a linear line of best fit. The non-linear standard curve, as well as its linear transformation, can be seen below in Figure 5-10.

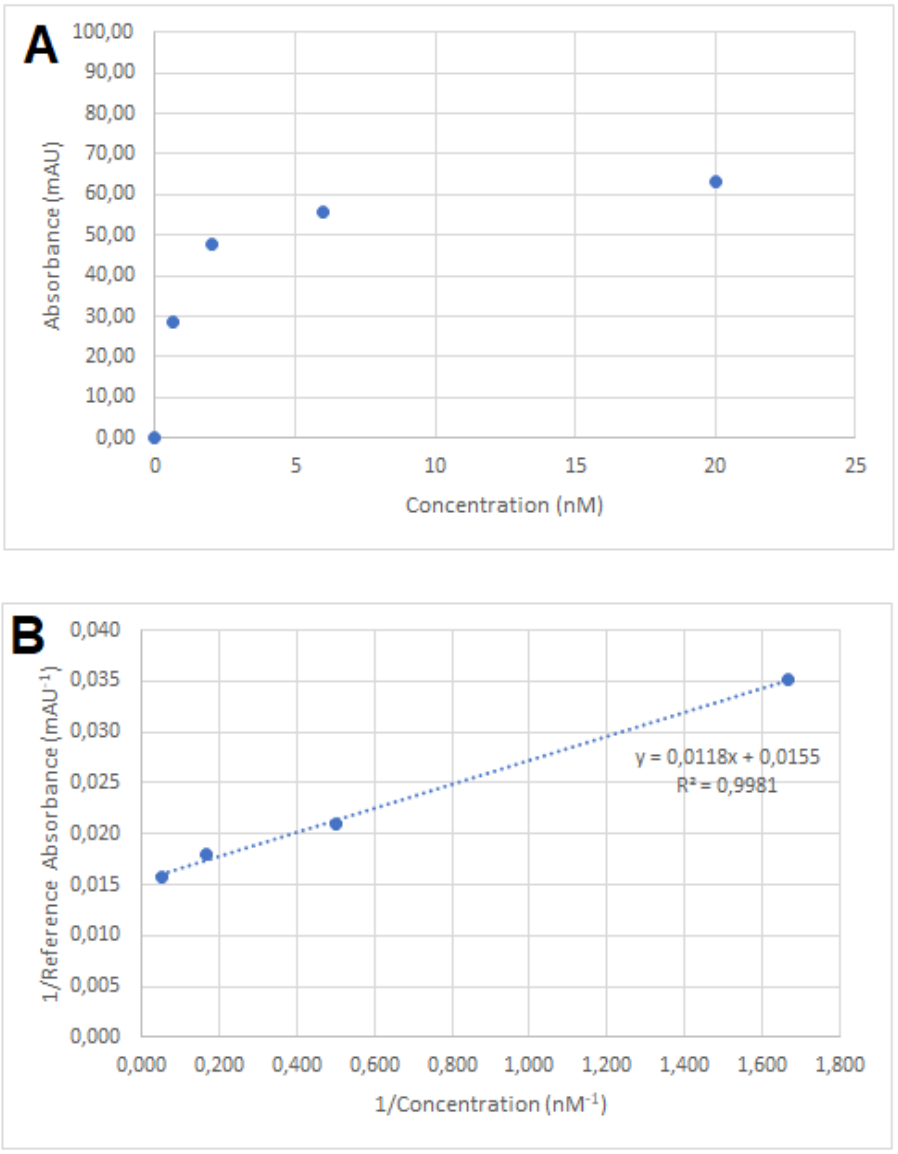

Figure 5-10 Antibody:AuNP standard curves for NanoOrange assay for: (A) untransformed data and (B) reciprocal transformation of data (the latter was used to calculate the concentrations of antibodies immobilized on functionalized AuNP samples). Values represent average of three replicates, and error bars represent standard deviation.

In order to calculate the concentration of immobilized antibodies on AuNP samples, a second correction factor was applied (for the same reasons as described above, to essentially correct for any background absorbance or interference from KI / I_2). A sample of PEGylated AuNPs lacking antibodies was used as a blank against the PEGylated AuNP samples containing antibodies. From each respective reference absorbance value (calculated following the same procedure used

for the standard curve), a reciprocal transformation was applied to each antibody-containing sample's absorbance value, as well as the PEGylated AuNP sample. Then, through linear regression analysis, the reciprocal concentration of antibodies was calculated, before subtracting the value calculated for PEGylated AuNPs lacking antibodies from each antibody-containing sample. The results of this linear regression analysis can be seen below in Figure 5-11:

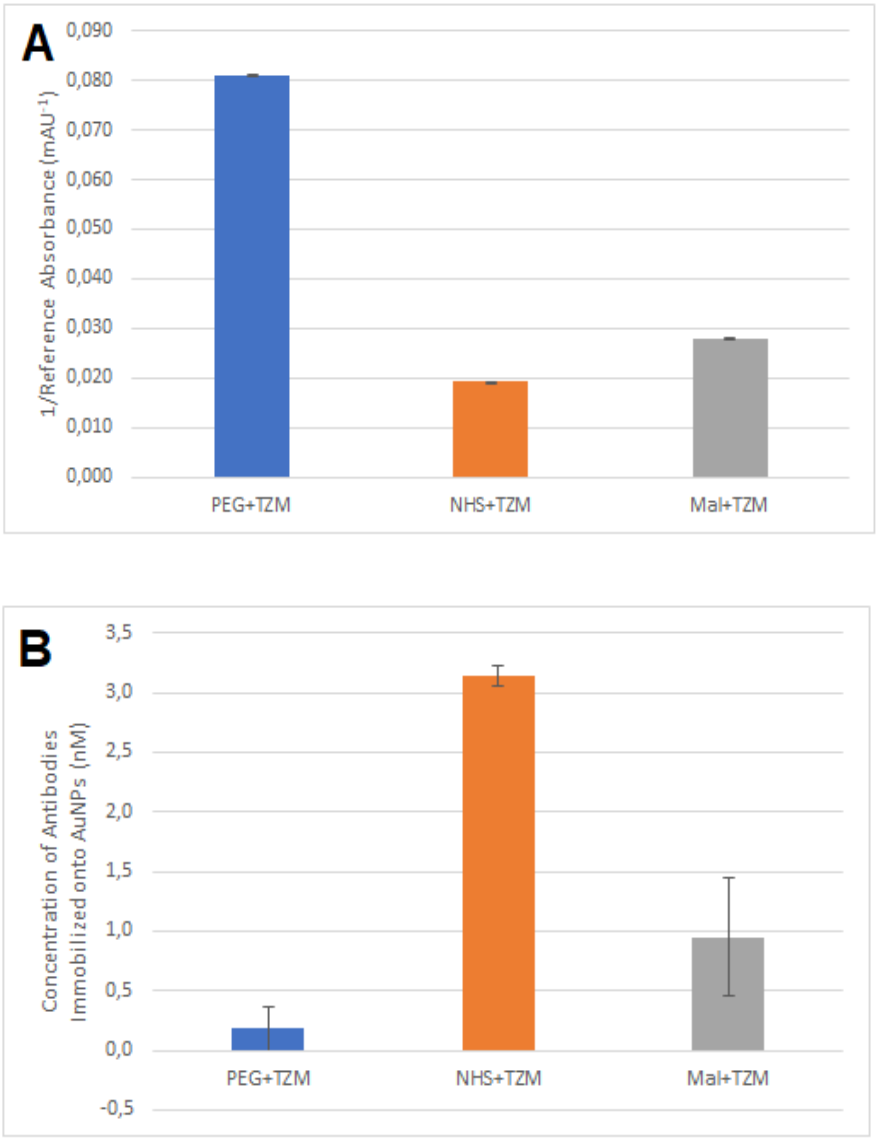

Figure 5-11 Determination of concentration of antibodies immobilized onto functionalized AuNP samples via the NanoOrange assay from: first (A) reciprocal transformation of reference absorbance data then (B) calculation of antibody concentrations via regression analysis of reciprocally-transformed standard curve (Figure 5-10 B). For the sake of simplicity, the antibody-

lacking PEGylated AuNP sample values are omitted and have already been subtracted from each antibody-containing sample. Values represent averages of three samples each measured on 96-well plate in triplicate (3x3 data points), and error bars represent standard deviation.

Finally, to calculate the number of antibodies immobilized onto each AuNP sample, the directly measured immobilized antibody concentrations were divided by the measured AuNP concentrations (following the same procedure of measuring the absorbance values of antibody-conjugated, PEGylated AuNP samples).

APPENDIX L – METHODS FOR QUANTIFICATION OF FUNTIONALIZED GOLD NANOPARTICLES BOUND TO CANCER CELLS

I. Cell Culturing and Fixation of Cancer Cell Lines

Frozen vials of cancer cell lines MDA-MB-231 and MDA-MB-453 were acquired from American Type Culture Collection (ATCC). According to the literature, these cell lines can be considered to express Her2 receptors at basal and enhanced levels [23]. Additionally, ATCC data sheets indicate that these cell lines are epithelial and adherent in nature, and were extracted from an adenocarcinoma tumour from breast tissue.

For the entirety of cell culturing, Dulbecco's Modified Eagle Medium (DMEM) supplemented was 10% (v/v) fetal bovine serum (FBS) and 1% (v/v) penicillin-streptomycin (PS) was chosen as the culture medium. The cell culturing procedure closely followed what was recommended by ATCC data sheets. Prior to using this culture medium with cells, it was always first pre-warmed for 30 min in a 37°C water bath.

To inoculate cells, the frozen vials were unthawed for 2 to 3 min in this same water bath, before decanting under a biosafety cabinet (BSC) the entirety of their volumes (1 mL each) in 9 mL of culture medium in a 15 mL conical centrifugal tube. The mixture was gently mixed via pipetting, before spinning down cells via centrifugation for 5 min at 200xg. The supernatant containing medium was carefully aspirated (without disturbing the cell pellets), before 10 mL of fresh culture medium was added to re-suspend the pellets. The entirety of this re-suspension mixture was then transferred to a T-75 flask and placed in a 37°C incubator supplemented with 5% carbon dioxide (CO_2). The cells were then allowed to grow for a couple of days, with periodic checks to monitor for any signs of contamination.

To maintain cells on a day-to-day basis (or as often as needed, even if that meant every two to three days), cells were passaged. All of the culture medium was removed from each T-75 flask, before replacing the contents with 5 mL of sterile PBS, in order to gently rinse the cells. This PBS was discarded, and then 1 to 2 mL of Trypsin was added, before placing the flasks in the 37°C incubator for 5 to 10 min. The goal of Trypsin was to detach cells that had adhered to the walls of the flask. To monitor for this detachment, the flasks were placed under a standard light microscope

to look for signs of cells floating in the Trypsin broth. Once cells had detached, 4 mL of fresh culture medium was added to each flask, and the cells were gently mixed via pipetting. The entirety of each flask was then placed in a 15 mL conical centrifugal tube, and centrifuged for 5 min at 200xg. Supernatant containing medium was carefully aspirated without disturbing the cell pellets, and replaced with 4 mL of fresh culture medium to re-suspend the pellets.

From this volume, 100 μL was withdrawn and used to count cells and assess their viability. To this, 50 μL of Trypan blue (which stains the nuclei of dead cells whose cell membranes are permeable to it) was added, and 10 μL was added to the chamber of a hemocytometer. Live and dead cells were then counted under a standard light microscope set to a 10x objective.

Based on these cell counts, an appropriate volume of seeded cells was added to 10 mL of fresh culture medium in a new T-75 flask. According to the ATCC data sheets, both of these cell lines have an approximate seeding density of 40 to 50 000 cells/cm^2. From experience with culturing these two cell lines, this meant adding roughly 1 mL of seeded cells to fresh culture medium each time a passage was done, if two to three passages per week were consistently done.

Cells were allowed to continue growing (passaging as often as needed), until a count of approximately 1 000 000 cells/mL was obtained. At this point, fixation of cells was done in order to ensure that cells would remain adherent. To 1 mL of cells, 4 mL of paraformaldehyde was added and the mixture was incubated for 5 min. The mixture was then centrifuged for 5 min at 200xg, before replacing the supernatant with 5 mL of fresh, sterile PBS. Two more washing cycles, each time replacing supernatant with PBS, were then done before the cells were stored at 4°C prior to being used for the experiment. A small volume of fixed cells was also withdrawn from this larger volume in order to count cells and calculate the appropriate volume of cells needed for the incubation experiment with AuNP samples (set to 150 000 cells per sample).

II. AuNP Sample and Cancer Cell Incubation Experiment

Functionalized AuNP samples were prepared following the same procedures described for the randomly oriented and semi-oriented strategies. The concentrations of these antibody-conjugated, PEGylated AuNP samples were calculated from measuring their UV-VIS absorbance spectra. Based on the measured cell counts, the number of cells for this experiment were set to 150 000, and a volume of AuNP samples allowing for a ratio of 500 NPs:cell to be obtained was

calculated. An example of the different samples tested for these incubation experiments, as well as their respective volumes incubated with each cell line, are shown below:

Table 5-8 Overview of latest AuNP:cell incubation experiment conducted between antibody-conjugated, PEGylated-AuNP samples and cancer cell lines MDA-MB-231 and MDA-MB-453 (abbreviated as 231 and 453), with the calculated volumes required to achieve 500 NPs:cell and 150 000 cells, respectively.

Sample Name	**Cancer Cell Line**	**Volume of Cells to Achieve 150 000 (µL)**	**AuNP Sample**	**AuNP Sample Concentration (NPs/mL)**	**AuNP Sample Volume to Achieve 500 NPs:Cell (µL)**
231-Bare AuNPs	231	138	Bare	4.96×10^9	15
231-PEG	231	138	PEG	4.07×10^9	18
231-PEG+TZM	231	138	PEG+TZM	2.79×10^9	27
231-NHS+TZM	231	138	NHS+TZM	2.01×10^9	37
231-Mal+TZM	231	138	Mal+TZM	1.59×10^9	47
453-Bare AuNPs	453	83	Bare	4.96×10^9	15
453-PEG	453	83	PEG	4.07×10^9	18
453-PEG+TZM	453	83	PEG+TZM	2.79×10^9	27
453-NHS+TZM	453	83	NHS+TZM	2.01×10^9	37
453-Mal+TZM	453	83	Mal+TZM	1.59×10^9	47

After adding the appropriate volumes of AuNP samples to each line cell in an Eppendorf tube, the mixtures were allowed to incubate at room temperature for 30 min on a shaker platform running at 100 rpm. At the conclusion of incubation, mixtures were spun down in a centrifuge for 5 min at 200xg, supernatants were carefully withdrawn, and 100 µL of PBS was added to re-suspend each cell:NP pellet.

III. Visualization of Cancer Cell:AuNP Mixtures Under a Microscope

To visualize the mixtures containing AuNP samples attached to each cancer cell line, a compound laser-transmission microscope (Ti Eclipse Nikon®) with a halogen lamp source (also from Nikon®) was relied upon to detect the back-scattering of AuNPs attached to cells under dark-field settings. In order to obtain the right optical configuration for this experiment, Petri dishes containing an optical centre consisting of a thin layer of glass (as opposed to plastic) were used to place each cell:AuNP mixture. This optical centre was chosen instead of using a standard plastic Petri dish as it would allow for the optical distance to be decreased, thus optimizing the extent of back scattering that could be detected by the camera of the transmission microscope.

This optical centre was first layered with 200 μL of 4% (v/v) Poly-L-Lysine (Sigma-Aldrich™) in PBS. Poly-L-Lysine is a polymer known for creating an adherent layer upon which cells can more easily attach, which prevents them from being stacked upon each other, but can be instead spread out along the Poly-L-Lysine surface. Once Poly-L-Lysine had been allowed to set on top of the optical centre for 30 min, 50 μL of each cell:AuNP sample was added to the centre of the plate above the Poly-L-Lysine layer.

Each Petri dish containing a cell:AuNP mixture was placed at the centre of the stage of the laser-transmission microscope above a 60x immersion oil objective (also from Nikon®). Immersion oil (Olympus®) was carefully added to this objective between each sample visualized. The objective was carefully rotated until it brushed the underside of the optical centre, creating an immersion oil:glass interface that would reduce the optical distance and allow for the extent of back scattering detected to be optimized. The fine knob focus was then adjusted while looking through the ocular lens (with the laser redirected via a beam splitter). A schematic showing this overall optical set-up required to visualize each cell:AuNP sample is shown below:

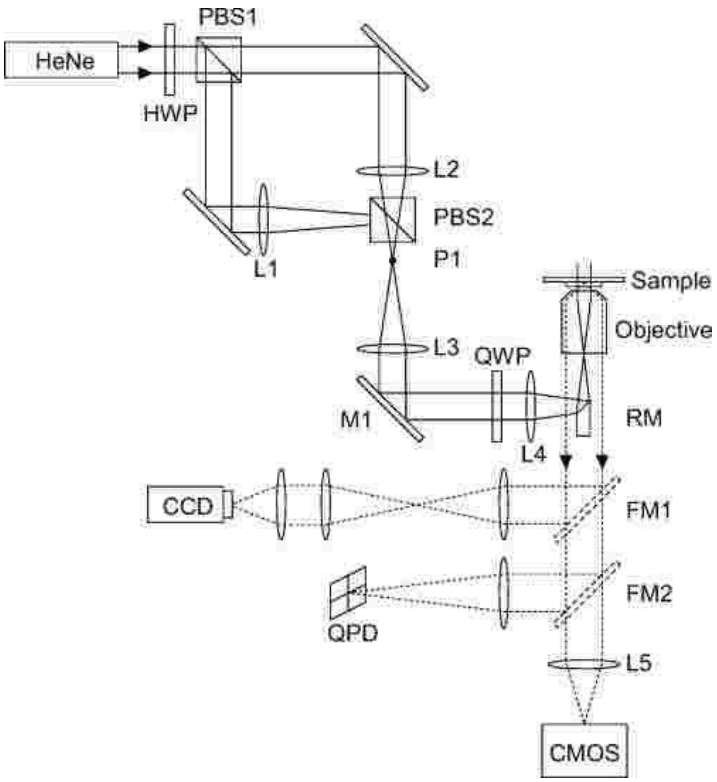

Figure 5-12 Schematic showing a similar optical set-up to the one used to image cells incubated with AuNPs via back scattering under a dark-field microscope. Note that the helium-neon lamp source is not the same as the halogen one used for this experiment, but the same principle for the rest of the set-up still applies. Elements of this optical set-up are abbreviated as follows: HWP – halfway plate to divide path into two, PBS1 and PBS2 – beam splitters 1 and 2, L1, L2 and L3 – focal lengths 1, 2 and 3 to collimate the beam, QWP – quarter-wave plate for circular polarization modulation, RM – small rod mirror used to focus light onto back focal plane of sample, CCD – camera used to take images and record videos, CMOS – sensor of high-speed camera (not used), QPD – quartz polarization device (not used). Image reproduced from Sowa et. al, 2010 [218].

The software used to visualize the cells was downloaded from proprietary software developed on LabView™. An optical camera (QIClick™ from QImaging in Surrey, BC, Canada) was used to record videos and capture images of each cell:AuNP sample. To scan through the entire range of the droplet of cells and AuNPs added to each Petri dish, a toggle was carefully adjusted to move between different fields of view, and ensure that no cells were being counted twice. Images or videos were thus acquired for each new field of view containing a fresh set of AuNPs attached to cells. To acquire either videos or images, a Z-scan within each separate field of view was

obtained by slowly adjusting the fine knob focus and either recording a video throughout the entire scan, or acquiring an image every time new NPs appeared on the software screen (appearing as bright, spherical white dots). An example of the images acquired through this Z-scan is shown below:

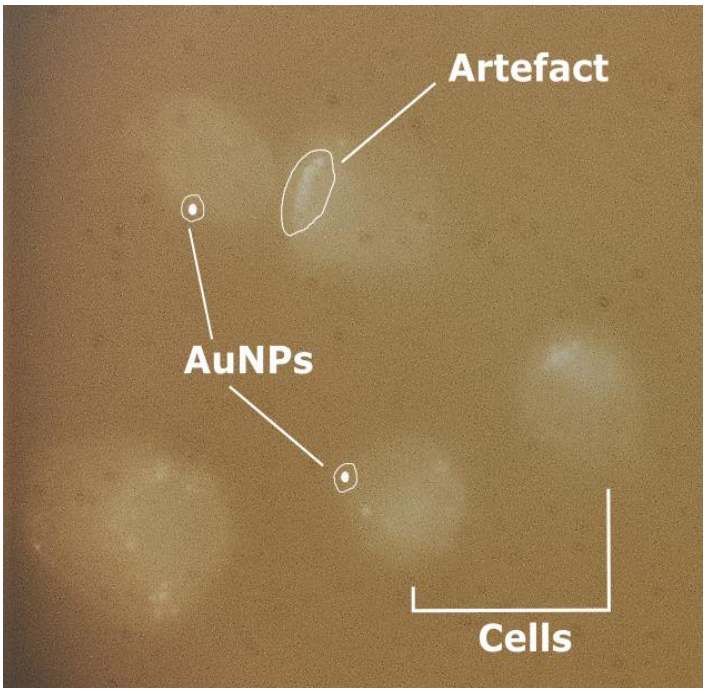

Figure 5-13 Example of image captured with optical camera while proceeding via Z-scan of one field of view containing AuNPs attached to cells. AuNPs are circled in white and highlighted as white dots, while an example of an artefact encountered during visualization is also shown.

IV. Counting of AuNPs Attached to Cancer Cells

Based on the images and videos acquired from the camera for each separate field of view, a simple procedure of counting AuNP samples attached to cells was carried out for each NP:cell mixture. Bright, spherical dots were considered as AuNPs while blurry, smeared images were considered as artefacts. The number of AuNPs per cell were counted across each Z-scan for each cell within one single field of view, before averaging amongst all of the cells in this particular field of view, and proceeding to the next field of view, where the same counting procedure was repeated for a new set of AuNPs attached to cells. The entirety of all separate fields of views and their respective averaged number of AuNPs per cell were then pooled and averaged, and standard deviations were then calculated. The data was then graphed, whereby the averaged pooled number

of AuNPs per cell was plotted against each sample, and T-tests at both significance levels of $p<0.05$ and 0.01 were conducted to identify any statistically significant differences between samples.

APPENDIX M – REVIEW OF MULTIPLEXING FOR IMAGING CANCER CELLS

Ultimately one of the goals of researchers designing biofunctionalized immunoplasmonic AuNPs is to be able to decorate different types of nanoparticles (NPs) with an array of antibodies, with each NP containing a different antibody. This would allow for multiple cancer biomarkers and/or antigens to be recognized and targeted simultaneously, while using different types of NPs to resolve, such as by colour, the visualized cells and/or tissue. This process of using different formulations of the same material to generate an assay with multiple, simultaneous functions is referred to as multiplexing.

The advantage of multiplexed IHC techniques is the enhanced ability to detect more than one cancer biomarker and/or antigen within the same assay set up, which can increase the power of IHC cancer diagnostics by allowing more antibody-antigen pairs to be screened, potentially lowering the chances of a false negative result [14]. Multiplexed IHC techniques even have the power to assess different tissues simultaneously [219]. Multiplexed IHC techniques can be roughly divided into three categories, namely: (1) differential staining techniques, (2) signal amplification techniques, and (3) mass spectrometry imaging techniques [220]. All of these are compatible with and can be streamlined into traditional IHC platforms.

Differential staining techniques (1) incorporate steps of photobleaching and subsequent staining to be able to target multiple antigens within the same assay set up, by proceeding in a stepwise manner with each antibody-antigen pair that is to be screened. These techniques include multiepitope-ligand cartography (MLC) [221] and sequential immunoperoxidase labelling and erasing (SIMPLE) [222]. Limitations to these techniques include, the time-consuming nature of the photobleaching and staining steps (mostly due to the stepwise experimental set up), (being limited to a small field of view that prevents examining the greater tissue area, and complicated image reconstruction algorithms required to overlay each stained image [220].

Signal amplification techniques (2) typically serve a purpose in targeting low-abundance biomarkers by either enhancing the fluorescent signal or replacing it with an internally generated luminescent signal. These techniques include modified-hapten based technologies [223], tyramide signal amplification platforms [224], and quantum dots (QDs) [225]. QDs are interesting as they have excellent photostability, possess narrow absorbance and emission spectra, and have well-

studied, intrinsic optical properties that can overcome issues related to background fluorescence from tissues in traditional IHC [226, 227]. However, their toxicity is well-known as they are typically comprised of heavy metals that are not biocompatible, which therefore prevents their use in *in vivo* settings [228]. Additionally, QDs are extremely small (less than 10 nm in diameter) which can present challenges with regards to optimizing their biofunctionalization with antibodies for immunological diagnostic purposes [229].

Finally, mass spectrometry (3) can be streamlined into IHC set-ups has attracted research interest. Here, mass spectrometry can target in a multiplexed setting different chemical compositions, such as various antibody-antigen pairs, from specific regions of tissue, and iteratively scan across the entire tissue, in order to evaluate the spatial distribution of these compositions resolved by mass [230]. By resolving by mass each localized region containing a specific antibody-antigen pair, any background noise resulting from non-specific interactions in that same area is practically eliminated, as its signal is distinguishable from specific interactions on the basis of mass [231, 232]. To achieve further specificity of antibody-antigen pairings, Di Palma and Bodenmiller [233] demonstrated that mass spectrometry can be combined with flow cytometry to allow for targeted channeling of each desired interaction, while reducing the effects of NSA due to spillover. Despite the promise of mass spectrometry in IHC applications, its limitations include slow acquisition time for data, the loss of tissue architecture upon its vaporization, and the inability to quantitatively compare signals from different antibody-antigen pairs due to their varying degrees of ionization [234, 235].